Title
Engineering non-photosynthetic carbon fixation pathways for the production of small molecule targets

Author
Gallagher, Joseph John

Publication Date
2017

Peer reviewed|Thesis/dissertation

Engineering non-photosynthetic carbon fixation pathways for the production of small molecule targets

By

Joseph John Gallagher

A dissertation submitted in partial satisfaction of the

requirements for the degree of

Doctor of Philosophy

in

Molecular & Cell Biology

in the

Graduate Division

of the

University of California, Berkeley

Committee in charge:

Professor Michelle C. Y. Chang, Chair
Professor Christopher Chang
Professor David Savage
Professor Anastasios Melis

Spring 2017

Engineering non-photosynthetic carbon fixation pathways for the production of small molecule targets

by Joseph John Gallagher

Abstract

Engineering non-photosynthetic carbon fixation pathways for the production of small molecule targets

by

Joseph John Gallagher

Doctor of Philosophy in Molecular & Cell Biology

University of California, Berkeley

Professor Michelle C. Y. Chang, Chair

The development of sustainable synthesis methods for societally important chemical products which serve as fuels, industrial feedstocks and materials is a pressing global challenge. Many of these target molecules are currently produced from fossil fuel-derived starting materials, which is problematic due both to the impending exhaustion of these resources and the dire environmental consequences of unrestrained carbon dioxide release into the atmosphere. An attractive alternative is using carbon dioxide along with sustainable energy sources for the production of these chemical targets. This thesis explores the development of multiple sustainable synthesis platforms based on interfacing inorganic materials, which function well for solar energy capture and charge transfer, with autotrophic microorganisms, which serve as biocatalysts, able to fix carbon dioxide into value-added products using the energy provided by the inorganic components.

An initial approach focused on the development of a hybrid bioinorganic device in which sustainable electrical and/or solar input drove production of hydrogen gas from water splitting using biocompatible inorganic catalysts. The hydrogen was then used by autotrphic microorganisms as a source of reducing equivalents for conversion of CO_2 to the value-added chemical product methane. Employing platinum or a newly synthesized earth-abundant substitute, α-NiS, as biocompatible hydrogen evolution reaction (HER) electrocatalysts and *Methanosarcina barkeri* as a biocatalyst for CO_2 fixation, robust and efficient electrochemical CO_2 to CH_4 conversion was demonstrated at up to 86% overall Faradaic efficiency for ≥7 d. Introduction of indium phosphide photocathodes and titanium dioxide photoanodes afforded a fully solar-driven system for methane generation from water and CO_2, establishing that compatible inorganic and biological components can synergistically couple light-harvesting and catalytic functions for solar-to-chemical conversion.

A second device attempted to mimic the biosynthetic process of natural photosynthesis, where solar energy powers the reduction of CO_2 to common biochemical building blocks, which are subsequently used for the synthesis of the complex mixture of molecular products that form biomass. The artificial photosynthesis system described here functions via a similar two-step process: A biocompatible high-surface-area silicon nanowire array harvests light energy to provide reducing equivalents to the obligately anaerobic acetogen, *Sporomusa ovata*, for the photoelectrochemical production of acetic acid with low overpotential ($\eta < 200$ mV), high Faradaic efficiency (up to 90%), and long-term stability (up to 200 h). The resulting acetate (~6 g/L) can

be activated to acetyl coenzyme A (acetyl-CoA) by strains of genetically engineered *Escherichia coli* and used as a building block for a variety of value-added chemicals, such as *n*-butanol, polyhydroxybutyrate (PHB) polymer, and three different isoprenoid natural products. Due to the local chemical environment within the nanowire array, the systems was also shown to perform well under aerobic conditions (21% O_2), allowing the cultivation of an obligate anaerobe using oxygen-containing gas feedstocks for growth. This system demonstrated the power of interfacing biocompatible solid-state nanodevices with living systems in order to create programmable platforms for chemical synthesis entirely powered by sunlight.

Informed by the successes of the previous systems, a next generation device was envisioned in which the autotrophic microorganism, which was interfaced with the biocompatible inorganic components, is directly engineered to produce value-added products, offering the simplicity of a single organism system with the product scope of co-culture platforms. Towards this goal methods for metabolic engineering of *Methanococcus maripaludis*, a methanogenic archaea, have been developed. These efforts have chiefly focused on achieving robust expression of multienzyme heterologous pathways, a goal complicated by the incompletely understood translational machinery in this organism. For optimization the 3-hydroxybutyrate pathway was used, which results in production of a monomer unit, which can be polymerized into the bioplastic PHB. Robust expression of the full 3-hydroxybutyrate biosynthetic pathway was achieved using a strong *Methanosarcina barkeri* promoter. Activity of all pathway enzymes was demonstrated in cell lysates; however, no product formation was observed. It is currently hypothesized that this is due to a lack of appropriate redox cofactors, specifically NADH. The NADH pool observed in *M. maripaludis* was found only to be 3% of that observed in *E. coli*. Current efforts are underway to enlarge this cofactor pool and incorporate it into the redox metabolism of the organism.

This work has demonstrated the power of hybrid biological-inorganic devices for the sustainable synthesis of value-added products. Systems have been developed that are fueled using sustainable sources of electric current or directly by illumination. A variety of product has been produced, both native products as well as more complex products, using a co-culture system. Efforts are ongoing to develop metabolic engineering tools for the unique class of organisms amenable to integration with inorganic materials. These engineering efforts will pave the way for future simplified devices with expanded product scopes.

Table of Contents

Table of Contents i
List of Figures and Tables iii
List of Abbreviations vi
Acknowledgments vii

Chapter 1: Introduction

1.1 Introduction 2
1.2 Metabolic engineering in heterotrophic systems 2
1.3 Engineering cyanobacteria and algae 3
1.4 Hybrid biological-inorganic devices 5
1.5 Thesis organization 11
1.6 References 12

Chapter 2: A hybrid bioinorganic approach to solar to chemical conversion

2.1 Introduction 20
2.2 Materials and methods 22
2.3 Results and discussion 32
2.4 Conclusions 42
2.5 References 43

Chapter 3: Nanowire-bacteria hybrids for unassisted solar carbon dioxide fixation to value-added chemicals

3.1 Introduction 51
3.2 Materials and methods 53
3.3 Results and discussion 62
3.4 Conclusions 74
3.5 References 75

Chapter 4: Engineering *Methanococcus maripaludis* for the production of multi-carbon products from carbon dioxide

4.1 Introduction 80

4.2 Materials and methods 81

4.3 Results and discussion 92

4.4 Conclusions and future directions 108

4.5 References 108

Conclusions and future directions

115

Appendix 1: Primers and gBlocks

117

List of Figures and Tables

Chapter 1

Figure 1.1 *Sustainable chemical synthesis using engineered heterotrophic chassis* 4

Figure 1.2 *Cyanobacterial production of value-added chemicals* 6

Figure 1.3 *Methods of interfacing inorganic and biological components in hybrid devices* 9

Figure 1.4 *Acetogen and methanogen metabolism* 10

Chapter 2

Figure 2.1 *General scheme depicting a hybrid bioinorganic approach to solar-to-chemical conversion.* 21

Figure 2.2 *Electrolysis cell photographs* 25

Figure 2.3 *GC calibration curve for H_2 and CH_4 quantification* 27

Figure 2.4 *Electrocatalytic reduction of carbon dioxide to methane with a hybrid platinum/M. barkeri platform* 33

Figure 2.5 *High-resolution mass spectra of headspace gases after electrolysis under $^{12}CO_2$ or $^{13}CO_2$ atmospheres* 34

Figure 2.6 *Synthesis and characterization of a biocompatible, earth-abundant HER catalyst for use in hybrid bioinorganic systems for solar-to-chemical conversion* 36

Figure 2.7 *TEM characterization of α-NiS nanoparticles* 36

Figure 2.8 *Thermogravimetric analysis of α-NiS catalyst* 37

Table 2.1 *Comparison of various first row transition metal HER catalysts at neutral pH* 37

Figure 2.9 *Faradaic efficiencies for H_2 generation for electrolysis, photoassisted electrolysis, and unassisted water splitting with Pt, α-NiS/C, n^+/p-Si/NiMo, and p-InP/Pt cathodes* 38

Figure 2.10 *Representative galvanostatic and potentiostatic traces for (photo)electrochemical and photochemical experiments with a M. barkeri culture* 39

Figure 2.11 *Galvanostatic experiment (2.5 mA) with α-NiS/C cathode* 40

Figure 2.12 *Photoelectrochemical and unassisted solar-driven conversion of carbon dioxide to methane with hybrid bioinorganic catalysts* 41

Figure 2.13 *Evaluation of microbial light toxicity* 42

Chapter 3

Figure 3.1 *Schematic of a general artificial photosynthesis approach* 52
Figure 3.2 *Electrochemical and photoelectrochemical (PEC) setup* 53
Figure 3.3 *Oxygen depletion capacity of nanowire and planar electrodes* 59
Table 3.1 *Plasmids and primers used in this study* 61
Figure 3.4 *Unassisted solar-powered acetate production from the nanowire-bacteria hybrid device* 64
Figure 3.5 *Electrochemical CO_2 reduction using the nanowire-bacteria hybrid electrode* 65
Figure 3.6 *Stable performance of the nanowire-bacteria hybrid photocathode for solar CO_2 reduction* 66
Figure 3.7 *Isotope labeling experiment for CO_2-fixation with nanowire-bacteria hybrids* 66
Figure 3.8 *Enhanced oxygen tolerance for nanowire-bacteria hybrids* 69
Figure 3.9 *E. coli growth in minimal media with acetate as the sole carbon source.* 70
Figure 3.10 *Butanol production from acetate under different aeration conditions* 71
Figure 3.11 *Synthetic enzymatic pathways for the biosynthesis of target organic compounds* 72
Table 3.2 *Biocatalytic production of diverse organic compounds using genetically engineered E. coli* 73
Figure 3.12 *Production of target organic molecules with genetically engineered E. coli strains* 73
Figure 3.13 *Butanol production and acetate consumption under different media conditions* 74

Chapter 4

Figure 4.1 *Genetic engineering strategies for M. maripaludis* 93
Figure 4.2 *Characteriziation of the adhE-expressing M. maripaludis strains* 95
Figure 4.3 *Purification of adhE from M. maripaludis* 95
Figure 4.4 *3HB biosynthetic pathway* 98
Figure 4.5 *Summary of constructs used in this study* 99

Figure 4.6. *Representative Western blot of protein expression from preliminary construct designs* 100
Figure 4.7 *Quantitative real-time PCR analysis of 3HB pathway expression* 100
Figure 4.8 *Expression of the full 3HB pathway in M. maripaludis* 101
Figure 4.9 *Expression of hbd and tesB in M. maripaludis* 101
Figure 4.10 *Cell lysate activity assays for 3HB pathway enzymes* 102
Figure 4.11 *M. maripaludis NAD^+ biosynthesis pathway* 103
Figure 4.12 *Quantification of NAD^+ and NADH pools in M. maripaludis and E. coli* 104
Figure 4.13 *Analysis of the transcript abundance of the M. maripaludis NAD^+ biosynthetic pathway enzymes* 104
Figure 4.14 *Characterization of a M. maripaludis strain overexpressing portions of the NAD^+ biosynthetic pathway* 105
Figure 4.15 *Dysregulation of the nitrogenase gene cluster* 107

List of Abbreviations

3HB	3-hydroxybutyrate
ATP	adenosine triphosphate
CoA	coenzyme A
CoM	coenzyme M
HER	hydrogen evolution reaction
NAD^+	nicotinamide adenine dinucleotide, oxidized
NADH	nicotinamide adenine dinucleotide, reduced
OD_{600nm}	optical density at 600 nm
PCR	polymerase chain reaction
PHA	polyhydroxyalkanoate
PHB	polyhydroxybutyrate
RHE	reversible hydrogen electrode
SHE	standard hydrogen electrode

Acknowledgments

I would like to take a moment to acknowledge all of the people who have helped me throughout my graduate school journey. This process would have been impossible without your support.

First, I would like to thank Michelle Chang for her mentorship and guidance, which have been instrumental in my development as a scientist. I have also really appreciated the freedom you have given me to pursue a project that is in many ways quite different than the other areas of study in our lab. I cannot imagine learning everything I have without this experience.

In that same vein, I have to thank my collaborators, Eva Nichols and Chong Liu, for not only being wonderful to work with, but for taking time to teach me so much about electrochemistry and photochemistry. I also have to thank Hans Carlson, who got me started growing anaerobes, and Harini Kaluarachchi, who helped me to set up the anaerobic glovebox that has been instrumental to so many experiments during my time in graduate school.

Additionally, I would like to thank all the members of the Chang Lab who I have had the privilege of working with. While I am thankful for all of your technical experimental advice and insightful research discussions, the thing I appreciate most is that you all have made our lab a great place to come to work to everyday. It is wonderful to do science in a friendly, helpful and supportive environment.

I would also like to thank the members of my thesis committee, Chris Chang, Dave Savage and Anastasios Melis, for helpful research discussions and creative project suggestions.

During my time in graduate school I have had the pleasure of working with a number of rotation students, Jorge Marchand, Kersh Thevasundaram, Justin Lopez, and Jack Desmarias. I appreciate all of your hard work and all the contributions you have made to my projects.

Finally, I have to thank all of the family and friends who have been so supportive during this time. You have been there to buoy my spirits during the most challenging moments and to celebrate with me during times of success. I cannot express how much I appreciate this or how much this has helped me to be successful inside the lab. Thank you.

Chapter 1: *Introduction*

1.1. Introduction

With finite fossil fuel reserves, which are slated for exhaustion in the next 100 years, serving not only as an important energy source but also as a feedstock for the synthesis of a wide variety of industrially important chemicals, and with a greater understanding of the environmental impacts of current manufacturing practices, the development of methods for the sustainable synthesis of chemical products for use as fuels, pharmaceuticals and materials has become a pressing scientific challenge of global importance [*1*]. Much progress has been made toward this goal using microorganisms as biological catalysts for the synthesis of complex value-added target molecules from simple starting materials. Initial work in this area was done using heterotrophic model organisms, such as *Escherichia coli* and yeast to convert sugars into myriad target compounds [*2, 3*]. While simple sugars can be produced from sustainable agriculture systems, the scales needed to replace current petroleum-based manufacturing raise the specter of competition with food crops for arable land [*4*]. To build a truly sustainable system, efforts are ongoing to fuel these systems using waste plant biomass or biomass generated from plants that can grow in marginal agriculture zones, areas unsuitable for the cultivation of food crops [*5, 6*]. To circumvent the technically challenging process of extracting simple sugars from the structural polysaccharides found in plant biomass, others have attempted a more direct coupling of target molecule synthesis to the carbon fixation and energy capture of photosynthesis by directly engineering cyanobacteria and algae with heterologous pathways [*7*]. Still others have attempted to replace the biological photosynthetic apparatus with inorganic components by constructing hybrid biological-inorganic devices, which couple inorganic catalysts or electrodes to the metabolism of non-photosynthetic carbon-fixing microorganisms for the production of target molecules from carbon dioxide [*8*]. These devices fall into two categories, those that seek to directly mimic photosynthesis using solar-powered electrode systems for the creation of stand-alone photosynthetic devices, and those that rely on electrocatalysts, which must be powered using externally applied current. The latter can be interfaced with any source of green electricity, greatly expanding potential energy sources available for biosynthesis.

Here we will review progress that has been made using each of these distinct methods of sustainable synthesis in order to frame the work that follows on the development of biological-inorganic hybrid systems for the production of value-added chemicals from carbon dioxide.

1.2. Metabolic engineering in heterotrophic systems

Since its inception, one area of focus within the field of synthetic biology has been using microorganisms as platforms for chemical synthesis [*9, 10*]. Early designs focused on engineering heterotrophic model systems using transcriptional and translation control of heterologous pathways. These relied on tuning expression using native and heterologous promoters as well as modulating translation through the use of native and engineered ribosome binding sites (RBS) [*3*]. Later designs have employed complex genetic logic circuits, RNA level regulatory elements such as riboswitches and antisense RNAs, as wells as compartmentalization of heterologous reaction pathways and protein scaffolds to encourage substrate channeling and reduce toxicity from pathway intermediates [*3, 11*]. With an appreciation that the reactions of the heterologous pathway are part of a much larger network of reactions occurring within the cell, other recent advances have relied on systems level tools to better incorporate the heterologous pathway into the organism's metabolic program [*3*]. These advances include large scale metabolic models, which attempt to use experimental data to make *in silico* predictions of pathway performance [*2, 12*], machine

learning algorithms coupled to high-throughput mechanized strain design and construction platforms, which inform future designs based on past performance [*13*], and evolution-based methods, which allow the power of selection to guide the incorporation of the heterologous pathway into the native metabolism [*14*]. Using these tools an immense array of chemicals products have been produced in heterotrophic model organisms, including alcohols, fatty acids, alkanes and isoprenoids, which have uses as fuels, pharmaceuticals, flavors, fragrances and starting materials for traditional chemical synthesis [*1*].

Most of these engineered pathways have been optimized using simple sugars as the feedstock for growth. However, considering that most sugar-rich plants have agricultural requirements quite similar to food crops and that there is limited arable land available for farming, the impending conflict between the cultivation of food crops and energy crops becomes apparent [*4*]. One vision for avoiding this conflict is to use waste plant biomass, the portions of the plant remaining after food crops have been harvested, or biomass from grasses able to survive on low quality agricultural lands, which are unsuitable for the cultivation of food crops, as feedstocks for engineered strains [*6, 15*] (*Figure 1.1*). However, it has proven to be a formidable challenge to liberate simple sugars from the complex polysaccharides of lignocellulose, which form much of this biomass [*16*]. Current methods rely on a high temperature acid or base pretreatment of the biomass followed by enzymatic degradation using purified enzymes [*5*]. The purified enzymes add considerable cost to the process and would ideally be replaced by engineered strains that both digest the plant biomass as well as produce the final product [*17*]. This is an area of active research with many different chassis organisms being engineered for the production of a variety of different chemical products [*18*]. Areas of focus include development of strains with increased tolerance to the chemicals used for biomass pretreatment as well as those released during biomass degradation, development of strains for the simultaneous consumption of C5 and C6 sugars as well as disaccharides for faster fermentation and increased carbon utilization, and development of crop plants more amenable to degradation due to altered lignocellulose structure [*16, 18*].

1.3. Engineering cyanobacteria and algae

A more direct coupling of the synthetic power of photosynthesis to production pathways can be achieved by engineering photosynthetic organisms. This method circumvents the technically challenging process of extracting simple sugars from plant biomass for the cultivation of engineered heterotrophs. While in theory it is possible to engineer both land plants as well as photosynthetic microorganisms, such as cyanobacteria and microalgae, for the production of small molecule targets, microbial engineering is a more attractive target for a number of reasons: Product extraction is simplified in microbial systems [*19*], and the genetics of microbes are much less complex than those found in land plants [*20, 21*]. In microbial systems all generated biomass can contribute to product generation, unlike in plant systems where excess structural biomass is needed, for example roots and stems, that may not contribute to synthesis of the desired target molecule [*21*]. The photosynthetic efficiency of cyanobacteria is much greater than land plants [*22*], allowing improved yields from a given energy input, and photosynthetic microorganisms can be cultivated on land unsuitable for agriculture, since their only requirements are sunlight and aqueous culture media [*20*].

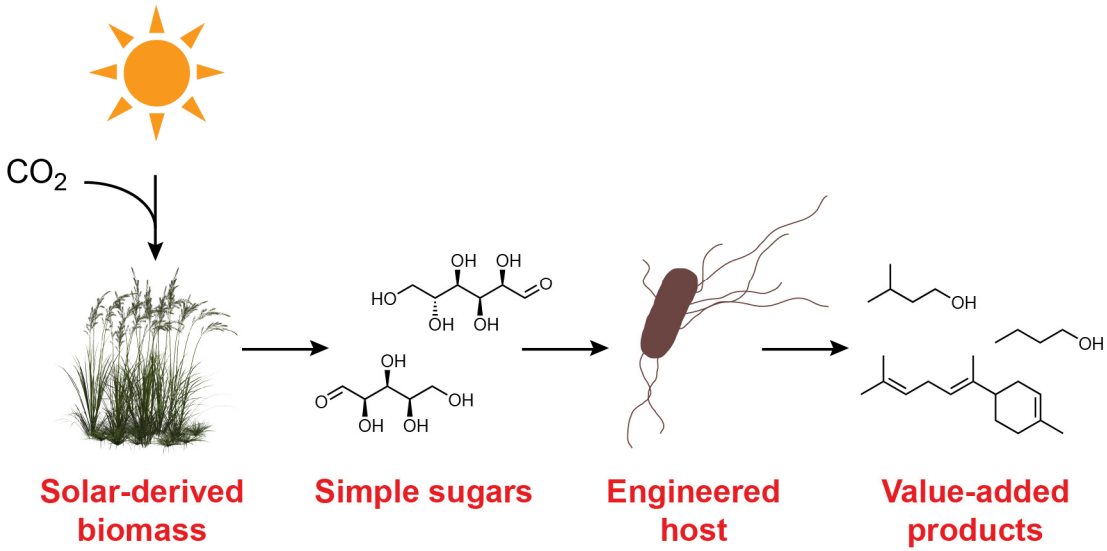

Figure 1.1. Sustainable chemical synthesis using engineered heterotrophic chassis. Plant biomass is generated from carbon dioxide and solar energy by the process of photosynthesis. For commonly employed synthetic biology hosts to be able to access the carbon and energy stored in the biomass, it must first be depolymerized into simple sugars. The released sugars are then feed to engineered heterotrophic strains for the production of value-added chemical products.

To date the most widely engineered photosynthetic microorganisms are microalgae and cyanobacteria [*7*]. Due to the complex genetic systems of eukaryotic organisms, advances in microalgae engineering have lagged efforts in cyanobacteria [*23*]. Most efforts in microalgae have focused on increasing production and extraction of oils for biofuel applications [*24*]. To improve the economic feasibility of the system, recent efforts have also started to explore advanced "refining" techniques to fractionate the resulting biomass into a number of products of different commercial values, for example separating high value compounds such as vitamins and polyunsaturated fatty acids for use as human food supplements from low value components such as oils, proteins and carbohydrates, which can be used for biofuel production, animal feed or fertilizer, and fermentative feedstocks, respectively [*25*].

Metabolic engineering efforts in cyanobacteria have been much more focused on the generation of heterologous products than those in microalgae [*23, 26*]. A sizable genetic toolbox exists for cyanobacteria, including methods for gene knock in and knock out via homologous recombination, replicating plasmid systems and constitutive and inducible promoters [*27, 28*]. Metabolic models have been constructed and are constantly being refined [*28*]. Many strategies similar to those pursued in heterotrophs have been applied to engineering efforts in cyanobacteria, including optimizing levels of protein expression and diverting carbon flux to desired heterologous pathways by overexpressing upstream enzymes, knocking out biosynthetic pathways that compete for common metabolic intermediates and incorporating irreversible reactions to trap carbon in the pathway [*26, 29*]. However, owing to their unique metabolic program some very specialized engineering strategies have been applied. These include increasing carbon fixation efficiency by overexpression of ribulose-1,5-bisphosphate carboxylase/oxygenase (RuBisCo), the carbon fixing enzyme of the Calvin-Benson Cycle [*30-32*], exploiting the large native NADPH pool by replacing NADH-dependent enzymes with NADPH-dependent variants [*33*] or overexpressing a transhydrogenase to interconvert the pools [*34*], and tuning the light capture apparatus to limit excessive light absorption beyond the photosynthetic capacity of the cells for increased overall photosynthetic productivity of dense cultures [*35, 36*] or incorporating heterologous photosynthetic pigments to broaden the spectrum of light able to be captured [*29*]. Using these tools an impressive array of products have been produced in cyanobacteria, including alcohols, diols, fatty acids, hydroxyl acids, carbohydrates and isoprenoids, with some compounds slated for testing in pilot-scale production facilities [*22, 23, 37*] (*Figure 1.2*). Though, there is much promise in the field of cyanobacteria metabolic engineering, there are also important caveats to consider: Better methods are needed for pest control in open-air production facilities, which are easily contaminated [*24*], greatly affecting production. The diurnal metabolism of cyanobacteria, which aligns with daily light/dark cycles, brings with it complex transcriptional and translational regulatory mechanism which are not fully understood and can result in unexpected expression outcomes during production experiments [*28*]. Additionally, there are preliminary reports of genetic instability via unknown mechanisms for certain transgenic strains [*38*], which could be detrimental to production efforts. Further investigation is needed of these unique aspects of cyanobacterial physiology.

1.4. Hybrid biological-inorganic devices

Building on the idea of a more direct interface between photosynthesis and production of value-added compounds, some have envisioned systems where inorganic components replace the

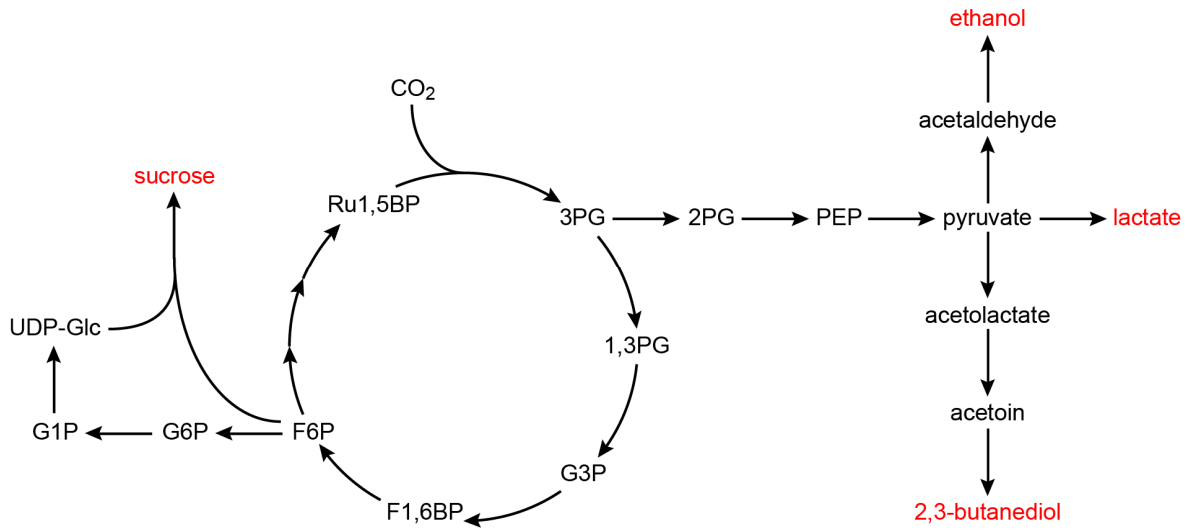

Figure 1.2. Cyanobacterial production of value-added chemicals. Cyanobacteria fix carbon dioxide using the Calvin-Benson Cycle, powered by solar energy captured during the light reactions of photosynthesis. As fixed carbon exits the Calvin-Benson Cycle it can be diverted to a number of value-added chemical products. Representative production pathways, which have achieved high yields at laboratory scale, are shown. Target molecules are shown in red. UDP-Glc, UDP-glucose; G1P, glucose-1-phosphate; G6P, glucose-6-phosphate; F6P, fructose-6-phospate; Ru1,5BP, ribulose-1,5-bisphosphate; F1,6BP, fructose-1,6-bisphosphate, G3P, glyceraldehyde-3-phosphate; 1,3PG, 1,3-phosphoglycerate; 3PG, 3-phosphoglycerate; 2PG, 2-phosphoglycerate; PEP, phosphoenolpyruvate.

biological photosynthetic apparatus and are directly interfaced with specific classes of microorganisms able to fuel their metabolism either directly with electrons or by harvesting reducing equivalents from soluble redox carriers generated by inorganic electrocatalysts [*8*]. These designs fall broadly into two categories: electrochemical systems and photochemical systems. Electrochemical systems rely on an external source of current to fuel microbial metabolism. These systems have the benefit of diversifying the potential energy inputs able to be used for biosynthesis. Any sustainable energy source could be used to power these systems, and in the case where solar power is used, the processes of light capture and biosynthesis are spatially separated, greatly simplifying reactor design. Photochemical systems rely on solar-active inorganic materials directly interfaced with microbial cultures. These have the advantage of being stand-alone devices, able to operate in a wide variety of settings regardless of other available infrastructure. However, owing to the complexity of these systems, they require quite advanced reactor designs. Advantages of both types of systems are their geographic flexibility, which eliminates competition with food crops, and their potential to exceed the efficiency of natural photosynthesis using advanced solar capture technology [*39*].

Within each of these types of systems another variable that must be considered is the nature of the interface between the inorganic components and the microbial production host (*Figure 1.3*). Some systems rely on a direct electrical connection between the microorganisms and the inorganic circuit [*40*]. Here the biological catalyst is seeded directly onto a conductive electrode surface, and the flow of electrons from the electrode into the cell is used to charge intracellular redox cofactors, which are then used to drive metabolism. These systems have the advantage of reduced overpotentials compared to catalyst-based systems [*8*], which will be discussed next. (The overpotential of an electrochemical system is the additional potential that must be applied beyond the calculated thermodynamic potential to accomplish a given reaction. Essentially it is a measurement of the amount of energy wasted or used non-productively in an electrochemical system. Though the details of direct electron transfer to microorganism are not well understood, a plausible explanation for the low overpotentials observed in these systems is that electrons most likely enter cellular metabolism via an enzymatic reaction. As catalysts, enzymes greatly decrease the activation energy of reactions and therefore operate near zero overpotential [*41*], unlike most inorganic electrocatalysts.) Drawbacks of direct electron transfer systems are that they require very high surface area electrodes for efficient electron delivery, which can be technically challenging to manufacture and seed, and because a very small pool of organisms have shown the ability to directly accept electrons from an electrode, the choice of chassis organism is quite restricted. Another model for integration of inorganic components with microbial systems is via a soluble redox carrier, which is generated at the electrode surface, diffuses into the aqueous culture media and delivers reducing equivalents to the microbial culture [*40*]. While some laboratory scale systems have relied on complex redox carriers, for example methyl viologen [*42*], these would likely be cost prohibitive in industrial settings and would complicate disposal of spent electrolysis media. The most feasible redox carriers for industrial scale operations are those generated *in situ* by efficient electrocatalysts, for example hydrogen gas, formate or carbon monoxide [*43*]. Advantages of systems with a soluble redox carrier are the wide range of organisms able to grow using these substrates, as well as the simplicity of reactor design. Caveats include the larger overpotentials observed with inorganic catalysts and the limited aqueous solubility of some redox carriers, for example hydrogen gas.

Using these diverse designs, a number of products have been generated from both native and metabolically engineered strains. Most work has focused on a few distinct classes of

microorganisms, specifically acetogens, methanogens and *Ralstonia eutropha*. Acetogen and methanogens are both obligately anaerobic microorganisms that rely on the Wood-Ljungdahl Pathway for carbon fixation (*Figure 1.4*). Acetogens are a class of facultatively autotrophic bacteria that can fix carbon dioxide to acetyl-CoA using reducing equivalents harvested from hydrogen gas. They can also grow on glycolytic substates. The acetyl-CoA nod of their metabolism is a central decision point under autotrophic growth conditions. Here fixed carbon can either be diverted for biomass accumulation or acetyl-CoA can by hydrolyzed to generate energy in the form of ATP by substrate level phosphorylation [*44*]. Methanogenic archaea, share a similar but distinct metabolic program. Depending on the specific class of methanogen, they can grow on a wide variety of substrates, including carbon dioxide/hydrogen, methanol, methyl amines, methyl sulfides, carbon monoxide and acetate. Similar to acetogens, the autotrophic metabolic program of methanogens fixes carbon dioxide using reducing equivalents from hydrogen gas. However, methanogens employ a modified Wood-Ljungdahl pathway to fix carbon dioxide to methyl-tetrahydromethanopterin (methyl-H_4MPT), a molecule functionally equivalent to methyl-tetrahydrofolate. methyl-H_4MPT is the central decision node of methanogen metabolism. The methyl group can be diverted to the Eastern branch of the Wood-Ljungdahl pathway for synthesis of acetyl-CoA, which in these organisms is then committed to biomass accumulation. Alternatively, the methyl group can be reduced all the way to methane, a pathway methanogens use for energy generation by creating a membrane ion gradient that can be dissipated for the synthesis of ATP using ATP synthase [*45*]. *Ralstonia eutropha* metabolism is quite distinct from acetogens and methanogens. It is both a facultative aerobe and facultative heterotroph, able to grow on a limited range of glycolytic substrates as well as carbon dioxide/hydrogen [*46, 47*]. When growing autotrophically it uses the Calvin-Benson cycle for carbon fixation, powered by harvesting reducing equivalents from hydrogen gas using an unusual oxygen-tolerant hydrogenase. We will first review the progress made using methanogens and acetogens before discussing advances employing *R. eutropha*.

Initial efforts in the field focused on the generation of native products. The first reported example of microbial electrosynthesis generated methane from electric current using neutral red as a soluble redox carrier to shuttle reducing equivalents from an electrode to a mixed culture containing methanogens [*48*]. Subsequent work was aimed at establishing systems for direct electron transfer for the production of both acetate and methane [*49, 50*], as well as efforts to identify an expanded pool of acetogens able to be propagated using direct electron transfer [*51*]. In these studies 2-oxobutyrate was occasionally seen as a significant coproduct in addition to acetate [*51*]. Further advances have focused on methane generation via a hydrogen intermediate using both non-precious metal catalysts as well as fully photosynthetic systems [*52*]. Outside the realm of strict microbial electrosynthesis, much research has focused on cultivating microorganism using synthesis gas (syngas), a gas mixture of hydrogen, carbon monoxide and carbon dioxide [*53*]. This currently is not a renewable energy source, as the majority of syngas is generated from the combustion of fossil fuels; however, multiple companies are exploring syngas generation from renewable biomass sources, which may transform this to a renewable synthesis strategy [*53*]. Additionally it may be possible to employ syngas production strains for microbial electrosynthesis applications. A diverse array of acetogenic species have been tested for their native product profile, and production strains have been found for ethanol, acetate, butanol, butyrate and 2,3-butanediol [*54*].

Multiple strategies have been employed to expand the product profile of Wood-Ljungdahl Pathway-utilizing microorganisms beyond their native products. One of these strategies has been

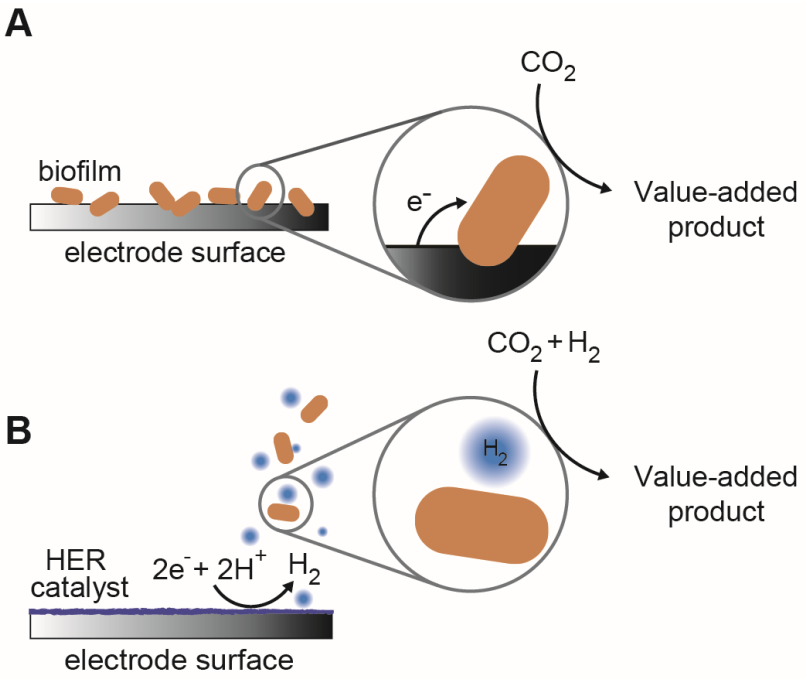

Figure 1.3. Methods of interfacing inorganic and biological components in hybrid devices. (A) Direct electron transfer. Some organisms are able to grow on electrode surfaces and directly accept electrons as a source of energy to fuel their cellular metabolism. Designs incorporating this method of biological-inorganic interface must use high surface area electrodes to accommodate high culture densities and are restricted to the small group of electroactive microorganisms. (B) Soluble redox carriers. An alternative strategy for interfacing components within a hybrid device is to use a soluble redox carrier to ferry reducing equivalents from the electrode surface to a dispersed culture of microorganisms. Some designs have relied on chemically complex redox shuttles, such as redox dyes; however, these would likely be cost prohibitive to use in industrial settings. Promising candidates for redox shuttles include hydrogen, formate and carbon monoxide, all of which can be generated *in situ* from water and carbon dioxide using high efficiency electrocatalysts.

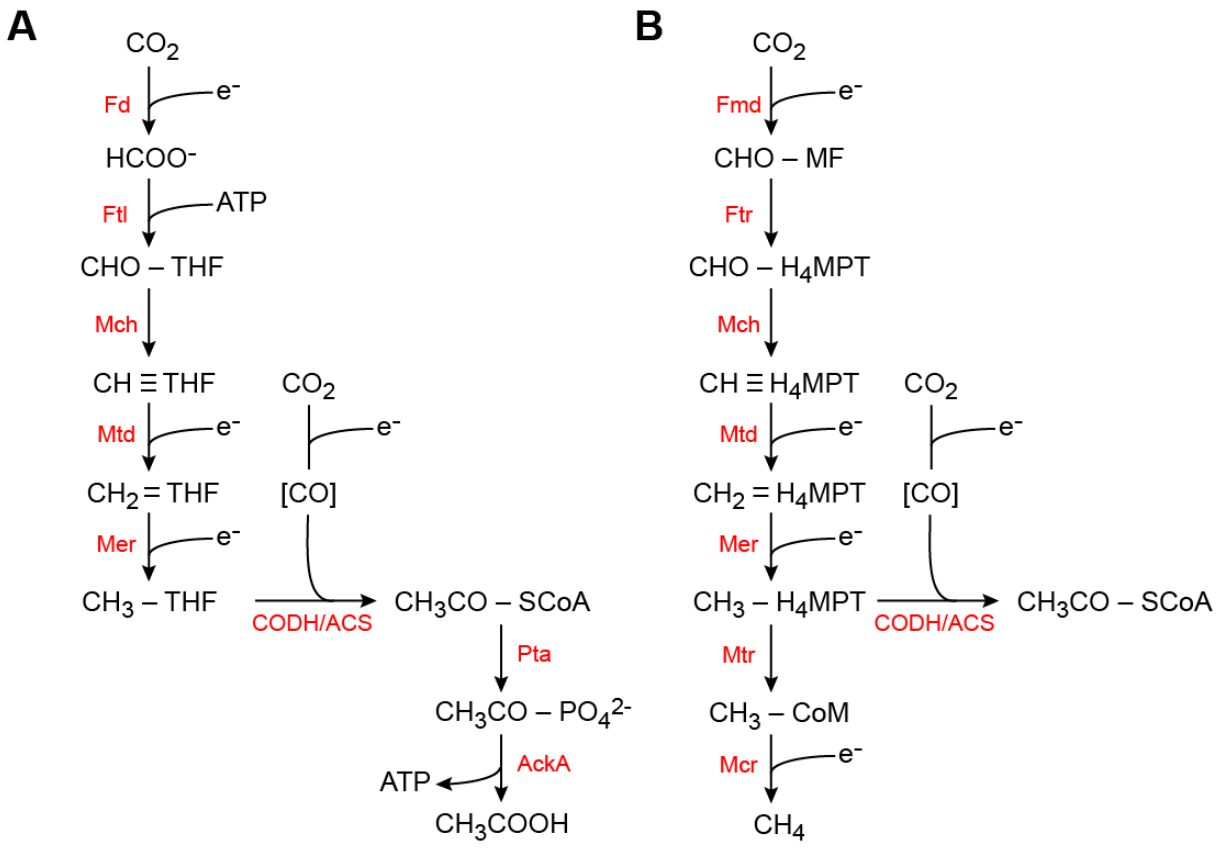

Figure 1.4. Acetogen and methanogen metabolism. (A) Autotrophic acetogen metabolism. When growing autotrophically, acetogens reduce two molecules of carbon dioxide to form the acetyl group of acetyl-CoA. Acetyl-CoA serves as an important decision point in acetogen metabolism. It can be either directly diverted to the generation of biomass or can be hydrolyzed to acetate and free coenzyme A for the generation of energy in the form of ATP, formed by substrate level phosphorylation. Most acetogen engineering efforts aim to divert acetyl-CoA to product molecules using heterologous pathways. (B) Methanogen metabolism. Two distinct modes exist for methanogen metabolism, one is used for energy generation, and the other is used for the accumulation of biomass. For energy generation, methanogens reduce carbon dioxide to methane, which establishes a membrane ion gradient through the activity of pathway enzymes. The ion gradient can be used for ATP generation by ATP synthase. For biomass generation methanogens divert reduced carbon in the form of methyl-tetrahydromethanopterin to the Wood-Ljungdahl pathway for the generation of acetyl-CoA. The only published methanogen metabolic engineering effort to date has diverted carbon from acetyl-CoA to the production of the isoprenoid geraniol. Enzyme names are shown in red. CHO-THF, 10-formyltetrahydrofolate; CH≡THF, 5,10-methenyltetrahydrofolate; CH_2=THF, 5,10-methylenetetrahydrofolate; CH_3-THF, 5-methyltetrahydrofolate; CH_3CO-SCoA, acetyl-CoA; CH_3CO-PO_4^{2-}, acetylphosphate; CHO-MF, formylmethanofuran; CHO-H_4MPT, 5-formyltetrahydromethanopterin; CH≡H_4MPT, 5,10-methenyltetrahydromethanopterin; CH_2=H_4MPT, 5,10-methylenetetrahydromethanopterin; CH_3-H_4MPT, 5-methyltetrahydromethanopterin; CH_3-CoM, methyl-coenzyme M; Fd, formate dehydrogenase; Ftl, formate tetrahydrofoate ligase; Mch, methenyltetrahydrofolate cylcohydrolase/ methylenetetrahydromethanopterin cylcohydrolase; Mtd, methylenetetrahydrofolate dehydrogenase/ methylenetetrahydromethanopterin dehydrogenase; Mer, methylenetetrahydrofolate reductase/ methylenetetrahydromethanopterin reductase; CODH/ACS, carbon monoxide dehydrogenase/ acetyl-CoA synthase; Pta, phosphotransacetylase; AckA, acetate kinase A; Fmd, formylmethanofuran dehydrogenase; Ftr, formylmethanofuran: tetrahydromethanopterin formyltransferase.

to feed electrochemically-produced, acetogen-derived acetate to engineered heterotrophic microorganisms, which can active it to acetyl-CoA for the synthesis of more complex products [*55*]. This strategy has been successfully employed for the generation of fuels, isoprenoids and bioplastics from solar-derived acetate [*56*]. Direct engineering of acetogens and methanogens has also been pursued as a strategy to expand the accessible product scope of these organisms. A limited genetic toolbox exists for both acetogens and methanogens, including replicating plasmids, selectable markers, a limited number of validated promoters and methods for transformation and homologous recombination [*57-59*]. Using these tools heterologous production of ethanol, butanol, acetone and butyrate have been achieved in acetogens [*60-65*]. Also, geraniol, an isoprenoid fragrance compound, was produced using an engineered methanogen strain [*66*].

Development of electrosynthesis in *R. eutropha* has very much followed the same trajectory as seen for acetogens and methanogens. Very early experiments in the 1960s determined that the strain could be cultivated by applying an electric current to the culture media to produce hydrogen gas [*67*]; however, these early experiments were only concerned with biomass generation and did not attempt to make any value-added products. *R. eutropha* naturally accumulates large amounts of polyhydroxyalkanoates (PHA), a class of bioplastics, when grown under nitrogen limiting conditions, which can amount to more than 70% of dry cell weight [*68*]. Initial engineering efforts focused on increasing this accumulation even further as well as tuning polymer properties by generating copolymers with different ratios of varying hydroxyacid subunits [*69, 70*]. These efforts, as well as later efforts to generate small molecule targets from heterologous pathways relied on the well-developed genetic toolbox available for *R. eutropha* [*71, 72*]. Targets for metabolic engineering using heterologous pathways have included methylketones as well as branched alcohols, such as isobutanol, isopropanol and 3-methyl-1-butanol [*73-75*]. Optimization of these pathways frequently relied on diverting carbon flux from the native PHA pathway, resulting in mixed success [*71*]. Because some of this work has been performed under heterotrophic conditions, it is not certain that all of these previous engineering efforts will translate to functional production strains under autotrophic conditions in hybrid biological-inorganic devices; however, many recent studies have built off of this previous work to generate electrochemical and photochemical production systems for heterologous products in *R. eutropha*. These include the generation of isobutanol and 3-methyl-1-butanol using an electrochemical system with a formate intermediate [*76*], the generation of isopropanol using an electrochemical system with a hydrogen intermediate [*77*], and the generation of all three alcohols, isopropanol, isobutanol and 3-methyl-1-butanol, from an electrochemical system with a hydrogen intermediate [*78*]. While these successes are promising, caveats of *R. eutropha* hybrid systems include reduced efficiencies seen with the operation of most reductive electrocatalysts in high percentage oxygen environments, as well as the potential to generate explosive gas mixtures when generating hydrogen gas in oxygen rich atmospheres.

1.5. Thesis organization

The following work aims to build from these previous accomplishments in the field of sustainable microbial biosynthesis. Specifically, it is focused on the generation of novel hybrid biological-inorganic devices for the production of a wide variety of value-added chemicals from sustainable energy sources and carbon dioxide. Chapter 2 details the development of a platform for sustainable methane synthesis using either an electrochemical system with a novel, inexpensive biocompatible hydrogen-generating catalyst or a photochemical system employing a completely

solar-powered semiconductor electrode assembly for light-driven methane production. Chapter 3 details another completely solar-powered production system for a variety of advanced chemical products using a similar photoactive electrode assembly. This system is able to produce high titers of acetate by directly interfacing acetogenic microorganisms with high surface area nanowire semiconductor electrodes. The acetate is then upgraded to a variety of more complex chemical products using engineered *E. coli* strains. Finally to generate a simplified single-organism production platform with a broad product scope, methods are developed for metabolic engineering in the model methanogen, *Methanococcus maripaludis*. These efforts focus on robust expression of heterologous pathways as well as investigating and harnessing the unique pool of redox cofactors found in this organism.

1.6. References

1. Rabinovitch-Deere, C. A., Oliver, J. W. K., Rodriguez, G. M., Atsumi, S., Synthetic biology and metabolic engineering approaches to produce biofuels. *Chem. Rev.* **2013**, 113(7) 4611-4632.

2. Peralta-Yahya, P. P., Zhang, F., Del Cardayre, S. B., Keasling, J. D., Microbial engineering for the production of advanced biofuels. *Nature* **2012**, 488(7411) 320-328.

3. Purnick, P. E. M., Weiss, R., The second wave of synthetic biology: From modules to systems. *Nat. Rev. Mol. Cell Biol.* **2009**, 10(6) 410-422.

4. Nonhebel, S., Renewable energy and food supply: Will there be enough land? *Renew. Sustainable Energy Rev.* **2005**, 9(2) 191-201.

5. Himmel, M. E., Ding, S.-Y., Johnson, D. K., Adney, W. S., Nimlos, M. R., Brady, J. W., Foust, T. D., Biomass recalcitrance: Engineering plants and enzymes for biofuels production. *Science* **2007**, 315(5813) 804-807.

6. Tilman, D., Hill, J., Lehman, C., Carbon-negative biofuels from low-input high-diversity grassland biomass. *Science* **2006**, 314(5805) 1598-1600.

7. Gomaa, M. A., Al-Haj, L., Abed, R. M. M., Metabolic engineering of cyanobacteria and microalgae for enhanced production of biofuels and high-value products. *J. Appl. Microbiol.* **2016**, 121(4) 919-931.

8. Rabaey, K., Rozendal, R. A., Microbial electrosynthesis — revisiting the electrical route for microbial production. *Nat. Rev. Micro.* **2010**, 8(10) 706-716.

9. Bailey, J. E., Toward a science of metabolic engineering. *Science* **1991**, 252(5013) 1668-1675.

10. Stephanopoulos, G., Synthetic biology and metabolic engineering. *ACS Synth. Biol.* **2012**, 1(11) 514-525.

11. Khalil, A. S., Collins, J. J., Synthetic biology: Applications come of age. *Nat. Rev. Genet.* **2010**, 11(5) 367-379.

12. Jouhten, P., Metabolic modelling in the development of cell factories by synthetic biology. *Comput. Struct. Biotechnol. J.* **2012**, 3(4) e201210009.

13. Kell, D. B., Metabolomics, modelling and machine learning in systems biology – towards an understanding of the languages of cells. *FEBS J.* **2006**, 273(5) 873-894.

14. Cobb, R. E., Sun, N., Zhao, H., Directed evolution as a powerful synthetic biology tool. *Methods* **2013**, 60(1) 81-90.

15. Elkins, J. G., Raman, B., Keller, M., Engineered microbial systems for enhanced conversion of lignocellulosic biomass. *Curr. Opin. Biotechnol.* **2010**, 21(5) 657-662.

16. Mccann, M. C., Carpita, N. C., Biomass recalcitrance: A multi-scale, multi-factor, and conversion-specific property. *J. Exp. Bot.* **2015**, 66(14) 4109-4118.

17. Bokinsky, G., Peralta-Yahya, P. P., George, A., Holmes, B. M., Steen, E. J., Dietrich, J., Soon Lee, T., Tullman-Ercek, D., Voigt, C. A., Simmons, B. A., Keasling, J. D., Synthesis of three advanced biofuels from ionic liquid-pretreated switchgrass using engineered escherichia coli. *Proc. Natl. Acad. Sci. U.S.A.* **2011**, 108(50) 19949-19954.

18. Chen, R., Dou, J., Biofuels and bio-based chemicals from lignocellulose: Metabolic engineering strategies in strain development. *Biotechnol. Lett.* **2016**, 38(2) 213-221.

19. Tatsis, E. C., O'connor, S. E., New developments in engineering plant metabolic pathways. *Curr. Opin. Biotechnol.* **2016**, 42 126-132.

20. Wang, B., Wang, J., Zhang, W., Meldrum, D., Application of synthetic biology in cyanobacteria and algae. *Front. Microbiol.* **2012**, 3(344).

21. Cook, C., Martin, L., Bastow, R., Opportunities in plant synthetic biology. *J. Exp. Bot.* **2014**, 65(8) 1921-1926.

22. Oliver, N. J., Rabinovitch-Deere, C. A., Carroll, A. L., Nozzi, N. E., Case, A. E., Atsumi, S., Cyanobacterial metabolic engineering for biofuel and chemical production. *Curr. Opin. Chem. Biol.* **2016**, 35 43-50.

23. Savakis, P., Hellingwerf, K. J., Engineering cyanobacteria for direct biofuel production from CO_2. *Curr. Opin. Biotechnol.* **2015**, 33 8-14.

24. Hannon, M., Gimpel, J., Tran, M., Rasala, B., Mayfield, S., Biofuels from algae: Challenges and potential. *Biofuels* **2010**, 1(5) 763-784.

25. Chew, K. W., Yap, J. Y., Show, P. L., Suan, N. H., Juan, J. C., Ling, T. C., Lee, D.-J., Chang, J.-S., Microalgae biorefinery: High value products perspectives. *Bioresour. Technol.* **2017**, 229 53-62.

26. Angermayr, S. A., Gorchs Rovira, A., Hellingwerf, K. J., Metabolic engineering of cyanobacteria for the synthesis of commodity products. *Trends Biotechnol.* **2015**, 33(6) 352-361.

27. Al-Haj, L., Lui, Y., Abed, R., Gomaa, M., Purton, S., Cyanobacteria as chassis for industrial biotechnology: Progress and prospects. *Life* **2016**, 6(4) 42.

28. Berla, B., Saha, R., Immethun, C., Maranas, C., Moon, T. S., Pakrasi, H., Synthetic biology of cyanobacteria: Unique challenges and opportunities. *Front. Microbiol.* **2013**, 4(246).

29. Gao, X., Sun, T., Pei, G., Chen, L., Zhang, W., Cyanobacterial chassis engineering for enhancing production of biofuels and chemicals. *Appl. Microbiol. Biotechnol.* **2016**, 100(8) 3401-3413.

30. Iwaki, T., Haranoh, K., Inoue, N., Kojima, K., Satoh, R., Nishino, T., Wada, S., Ihara, H., Tsuyama, S., Kobayashi, H., Wadano, A., Expression of foreign type I ribulose-1,5-bisphosphate carboxylase/ oxygenase (EC 4.1.1.39) stimulates photosynthesis in cyanobacterium *Synechococcus* PCC7942 cells. *Photosynthesis Res.* **2006**, 88(3) 287.

31. Atsumi, S., Higashide, W., Liao, J. C., Direct photosynthetic recycling of carbon dioxide to isobutyraldehyde. *Nat. Biotechnol.* **2009**, 27(12) 1177-1180.

32. Ruffing, A. M., Improved free fatty acid production in cyanobacteria with *Synechococcus sp*. PCC 7002 as host. *Front. Bioeng. Biotechnol.* **2014**, 2 17.

33. Li, C., Tao, F., Ni, J., Wang, Y., Yao, F., Xu, P., Enhancing the light-driven production of D-lactate by engineering cyanobacterium using a combinational strategy. *Sci. Rep.* **2015**, 5 9777.

34. Angermayr, S. A., Paszota, M., Hellingwerf, K. J., Engineering a cyanobacterial cell factory for production of lactic acid. *Appl. Environ. Microbiol.* **2012**, 78(19) 7098-7106.

35. Kirst, H., Formighieri, C., Melis, A., Maximizing photosynthetic efficiency and culture productivity in cyanobacteria upon minimizing the phycobilisome light-harvesting antenna size. *Biochim. Biophys. Acta* **2014**, 1837(10) 1653-1664.

36. Melis, A., Solar energy conversion efficiencies in photosynthesis: Minimizing the chlorophyll antennae to maximize efficiency. *Plant Sci.* **2009**, 177(4) 272-280.

37. Case, A. E., Atsumi, S., Cyanobacterial chemical production. *J. Biotechnol.* **2016**, 231 106-114.

38. Jones, P. R., Genetic instability in cyanobacteria – an elephant in the room? *Front. Bioeng. Biotechnol.* **2014**, 2(12).

39. Blankenship, R. E., Tiede, D. M., Barber, J., Brudvig, G. W., Fleming, G., Ghirardi, M., Gunner, M. R., Junge, W., Kramer, D. M., Melis, A., Moore, T. A., Moser, C. C., Nocera, D. G., Nozik, A. J., Ort, D. R., Parson, W. W., Prince, R. C., Sayre, R. T., Comparing photosynthetic and photovoltaic efficiencies and recognizing the potential for improvement. *Science* **2011**, 332(6031) 805-809.

40. Thrash, J. C., Coates, J. D., Review: Direct and indirect electrical stimulation of microbial metabolism. *Environ. Sci. Technol.* **2008**, 42(11) 3921-3931.

41. Barton Cole, E., Bocarsly, A. B., Photochemical, electrochemical, and photoelectrochemical reduction of carbon dioxide. *Carbon dioxide as chemical feedstock*, ed Arresta, M., (Wiley-VCH Verlag GmbH & Co. KGaA, Weinheim) **2010**, pp 291-316.

42. Kim, T. S., Kim, B. H., Electron flow shift in *Clostridium acetobutylicum* fermentation by electrochemically introduced reducing equivalent. *Biotechnol. Lett.* **1988**, 10(2) 123-128.

43. Yishai, O., Lindner, S. N., Gonzalez De La Cruz, J., Tenenboim, H., Bar-Even, A., The formate bio-economy. *Curr. Opin. Chem. Biol.* **2016**, 35 1-9.

44. Ragsdale, S. W., Pierce, E., Acetogenesis and the Wood–Ljungdahl pathway of CO_2 fixation. *Biochim. Biophys. Acta* **2008**, 1784(12) 1873-1898.

45. Thauer, R. K., Kaster, A.-K., Seedorf, H., Buckel, W., Hedderich, R., Methanogenic archaea: Ecologically relevant differences in energy conservation. *Nat. Rev. Micro.* **2008**, 6(8) 579-591.

46. Pohlmann, A., Fricke, W. F., Reinecke, F., Kusian, B., Liesegang, H., Cramm, R., Eitinger, T., Ewering, C., Potter, M., Schwartz, E., Strittmatter, A., Vosz, I., Gottschalk, G., Steinbuchel, A., Friedrich, B., Bowien, B., Genome sequence of the bioplastic-producing "Knallgas" bacterium *Ralstonia eutropha* H16. *Nat. Biotech.* **2006**, 24(10) 1257-1262.

47. Sichwart, S., Hetzler, S., Broker, D., Steinbuchel, A., Extension of the substrate utilization range of *Ralstonia eutropha* strain H16 by metabolic engineering to include mannose and glucose. *Appl. Environ. Microbiol.* **2011**, 77(4) 1325-1334.

48. Park, D. H., Laivenieks, M., Guettler, M. V., Jain, M. K., Zeikus, J. G., Microbial utilization of electrically reduced neutral red as the sole electron donor for growth and metabolite production. *Appl. Environ. Microbiol.* **1999**, 65(7) 2912-2917.

49. Cheng, S., Xing, D., Call, D. F., Logan, B. E., Direct biological conversion of electrical current into methane by electromethanogenesis. *Environ. Sci. Technol.* **2009**, 43(10) 3953-3958.

50. Nevin, K. P., Woodard, T. L., Franks, A. E., Summers, Z. M., Lovley, D. R., Microbial electrosynthesis: Feeding microbes electricity to convert carbon dioxide and water to multicarbon extracellular organic compounds. *MBio* **2010**, 1(2).

51. Nevin, K. P., Hensley, S. A., Franks, A. E., Summers, Z. M., Ou, J., Woodard, T. L., Snoeyenbos-West, O. L., Lovley, D. R., Electrosynthesis of organic compounds from carbon dioxide is catalyzed by a diversity of acetogenic microorganisms. *Appl. Environ. Microbiol.* **2011**, 77(9) 2882-2886.

52. Nichols, E. M., Gallagher, J. J., Liu, C., Su, Y., Resasco, J., Yu, Y., Sun, Y., Yang, P., Chang, M. C. Y., Chang, C. J., Hybrid bioinorganic approach to solar-to-chemical conversion. *Proc. Natl. Acad. Sci. U.S.A.* **2015**, 112(37) 11461-11466.

53. Bengelsdorf, F. R., Straub, M., Dürre, P., Bacterial synthesis gas (syngas) fermentation. *Environ. Technol.* **2013**, 34(13-14) 1639-1651.

54. Daniell, J., Köpke, M., Simpson, S., Commercial biomass syngas fermentation. *Energies* **2012**, 5(12) 5372.

55. Hu, P., Chakraborty, S., Kumar, A., Woolston, B., Liu, H., Emerson, D., Stephanopoulos, G., Integrated bioprocess for conversion of gaseous substrates to liquids. *Proc. Natl. Acad. Sci. U.S.A.* **2016**, 113(14) 3773-3778.

56. Liu, C., Gallagher, J. J., Sakimoto, K. K., Nichols, E. M., Chang, C. J., Chang, M. C. Y., Yang, P., Nanowire–bacteria hybrids for unassisted solar carbon dioxide fixation to value-added chemicals. *Nano Lett.* **2015**, 15(5) 3634-3639.

57. Buan, N., Kulkarni, G., Metcalf, W. Genetic methods for *Methanosarcina* species. *Methods enzymol.* **2011**, pp 23-42.

58. Sarmiento, F., Leigh, J. A., Whitman, W. B., Genetic systems for hydrogenotrophic methanogens. *Methods Enzymol.* **2011**, 494 43-73.

59. Leang, C., Ueki, T., Nevin, K. P., Lovley, D. R., A genetic system for *Clostridium ljungdahlii*: A chassis for autotrophic production of biocommodities and a model homoacetogen. *Appl. Environ. Microbiol.* **2013**, 79(4) 1102-1109.

60. Köpke, M., Held, C., Hujer, S., Liesegang, H., Wiezer, A., Wollherr, A., Ehrenreich, A., Liebl, W., Gottschalk, G., Dürre, P., *Clostridium ljungdahlii* represents a microbial production platform based on syngas. *Proc. Natl. Acad. Sci. U.S.A.* **2010**, 107(29) 13087-13092.

61. Banerjee, A., Leang, C., Ueki, T., Nevin, K. P., Lovley, D. R., Lactose-inducible system for metabolic engineering of *Clostridium ljungdahlii*. *Appl. Environ. Microbiol.* **2014**, 80(8) 2410-2416.

62. Ueki, T., Nevin, K. P., Woodard, T. L., Lovley, D. R., Converting carbon dioxide to butyrate with an engineered strain of *Clostridium ljungdahlii*. *MBio* **2014**, 5(5) e01636-01614.

63. Hoffmeister, S., Gerdom, M., Bengelsdorf, F. R., Linder, S., Fluchter, S., Ozturk, H., Blumke, W., May, A., Fischer, R. J., Bahl, H., Durre, P., Acetone production with metabolically engineered strains of *Acetobacterium woodii*. *Metab. Eng.* **2016**, 36 37-47.

64. Liew, F., Henstra, A. M., Kpke, M., Winzer, K., Simpson, S. D., Minton, N. P., Metabolic engineering of *Clostridium autoethanogenum* for selective alcohol production. *Metab. Eng.* **2017**, 40 104-114.

65. Mock, J., Zheng, Y., Mueller, A. P., Ly, S., Tran, L., Segovia, S., Nagaraju, S., Kopke, M., Durre, P., Thauer, R. K., Energy conservation associated with ethanol formation from H_2 and CO_2 in *Clostridium autoethanogenum* involving electron bifurcation. *J. Bacteriol.* **2015**, 197(18) 2965-2980.

66. Lyu, Z., Jain, R., Smith, P., Fetchko, T., Yan, Y., Whitman, W. B., Engineering the autotroph *Methanococcus maripaludis* for geraniol production. *ACS Synth. Biol.* **2016**, 5(7) 577-581.

67. Schlegel, H. G., Lafferty, R., Growth of 'Knallgas' bacteria (*Hydrogenomonas*) using direct electrolysis of the culture medium. *Nature* **1965**, 205(4968) 308-309.

68. Volova, T. G., Kalacheva, G. S., Altukhova, O. V., Autotrophic synthesis of polyhydroxyalkanoates by the bacteria *Ralstonia eutropha* in the presence of carbon monoxide. *Appl. Microbiol. Biotechnol.* **2002**, 58(5) 675-678.

69. Kichise, T., Fukui, T., Yoshida, Y., Doi, Y., Biosynthesis of polyhydroxyalkanoates (PHA) by recombinant *Ralstonia eutropha* and effects of PHA synthase activity on *in vivo* PHA biosynthesis. *Int. J. Biol. Macromol.* **1999**, 25(1-3) 69-77.

70. Jeon, J. M., Brigham, C. J., Kim, Y. H., Kim, H. J., Yi, D. H., Kim, H., Rha, C., Sinskey, A. J., Yang, Y. H., Biosynthesis of poly(3-hydroxybutyrate-co-3-hydroxyhexanoate) (P(HB-co-HHx)) from butyrate using engineered *Ralstonia eutropha*. *Appl. Microbiol. Biotechnol.* **2014**, 98(12) 5461-5469.

71. Nybo, S. E., Khan, N. E., Woolston, B. M., Curtis, W. R., Metabolic engineering in chemolithoautotrophic hosts for the production of fuels and chemicals. *Metab. Eng.* **2015**, 30 105-120.

72. Bi, C., Su, P., Muller, J., Yeh, Y. C., Chhabra, S. R., Beller, H. R., Singer, S. W., Hillson, N. J., Development of a broad-host synthetic biology toolbox for *Ralstonia eutropha* and its application to engineering hydrocarbon biofuel production. *Microb. Cell Fact.* **2013**, 12 107.

73. Muller, J., Maceachran, D., Burd, H., Sathitsuksanoh, N., Bi, C., Yeh, Y. C., Lee, T. S., Hillson, N. J., Chhabra, S. R., Singer, S. W., Beller, H. R., Engineering of *Ralstonia eutropha* H16 for autotrophic and heterotrophic production of methyl ketones. *Appl. Environ. Microbiol.* **2013**, 79(14) 4433-4439.

74. Lu, J., Brigham, C. J., Gai, C. S., Sinskey, A. J., Studies on the production of branched-chain alcohols in engineered *Ralstonia eutropha*. *Appl. Microbiol. Biotechnol.* **2012**, 96(1) 283-297.

75. Grousseau, E., Lu, J., Gorret, N., Guillouet, S. E., Sinskey, A. J., Isopropanol production with engineered *Cupriavidus necator* as bioproduction platform. *Appl. Microbiol. Biotechnol.* **2014**, 98(9) 4277-4290.

76. Li, H., Opgenorth, P. H., Wernick, D. G., Rogers, S., Wu, T. Y., Higashide, W., Malati, P., Huo, Y. X., Cho, K. M., Liao, J. C., Integrated electromicrobial conversion of CO_2 to higher alcohols. *Science* **2012**, 335(6076) 1596.

77. Torella, J. P., Gagliardi, C. J., Chen, J. S., Bediako, D. K., Colon, B., Way, J. C., Silver, P. A., Nocera, D. G., Efficient solar-to-fuels production from a hybrid microbial-water-splitting catalyst system. *Proc. Natl. Acad. Sci. U.S.A.* **2015**, 112(8) 2337-2342.

78. Liu, C., Colón, B. C., Ziesack, M., Silver, P. A., Nocera, D. G., Water splitting–biosynthetic system with CO_2 reduction efficiencies exceeding photosynthesis. *Science* **2016**, 352(6290) 1210-1213.

Chapter 2: *A hybrid bioinorganic approach to solar-to-chemical conversion*

This work was published in the following scientific journal:

Nichols, E. M.,* Gallagher, J. J.,* Liu, C., Su, Y., Resasco, J., Yu, Y., Sun, Y., Yang, P., Chang, M. C. Y., Chang, C. J., Hybrid bioinorganic approach to solar-to-chemical conversion. *Proc. Natl. Acad. Sci. U.S.A.* **2015**, 112 11461-11466. (*These authors contributed equally to this work.)

This work was performed in collaboration with the following persons:

All studies were performed in close collaboration with Eva Nichols. Chong Liu prepared the photoelectrodes and assisted in the design of the photochemical cells and photochemical experiments.

2.1 Introduction

Methods for the sustainable conversion of carbon dioxide to value-added chemical products are of technological and societal importance [*1-3*]. Elegant advances in traditional approaches to CO_2 reduction driven by electrical and/or solar input using homogeneous [*4-16*], heterogeneous *[17-26*], and biological [*7, 27-31*] catalysts point out key challenges in this area, namely (i) the chemoselective conversion of CO_2 to a single product while minimizing the competitive reduction of protons to hydrogen, (ii) long-term stability under environmentally friendly aqueous conditions, and (iii) unassisted light-driven CO_2 reduction that does not require external electrical bias and/or sacrificial chemical quenchers. Indeed, synthetic homogeneous and heterogeneous CO_2 catalysts are often limited by product selectivity and/or aqueous compatibility, whereas enzymes show exquisite specificity but are generally less robust outside of their protective cellular environment. In addition, the conversion of electrosynthetic systems to photosynthetic ones is non-trivial owing to the complexities of effectively integrating components of light capture with bond-making and bond-breaking chemistry.

Inspired by the process of natural photosynthesis in which light-harvesting, charge-transfer, and catalytic functions are integrated to achieve solar-driven CO_2 fixation [*32-35*], we have initiated a program in solar-to-chemical conversion to harness the strengths inherent to both inorganic materials chemistry and biology [*36*]. As shown in (*Figure 2.1*), our strategy to drive synthesis with sustainable electrical and/or solar energy input [*37*] interfaces a biocompatible photo(electro)chemical hydrogen evolution reaction (HER) catalyst with a microorganism that uses this sustainably generated hydrogen as an electron donor for CO_2 reduction. Important previous reports have shown the feasibility of electrosynthesis [*38-42*] but have not yet established solar-driven processes. We selected methane as an initial target for this approach owing to the ease of product separation, the potential for integration into existing infrastructures for the delivery and use of natural gas (of which CH_4 is the principle component), and the fact that direct conversion of CO_2 to CH_4 with synthetic catalysts remains a formidable challenge due to large overpotentials and poor CH_4/H_2 selectivity. Two of the most active and selective direct electrocatalysts for CO_2 to CH_4 conversion reported to date produce methane with 61% [*43*] and 76% [*44*] Faradaic efficiencies, but require overpotentials of η = 1.28 V and η = 1.52 V, respectively. Promising advances in photothermal reduction of CO_2 to CH_4 also have been recently reported [*45*]. In comparison to fully inorganic catalysts, a distinct conceptual advantage of this hybrid materials biology approach, where the materials component performs water splitting to generate hydrogen and the biological component utilizes these reducing equivalents for CO_2 fixation, is that one can leverage the fact that biological catalysts operate at near thermodynamic potential [*46*]. As such, the only overpotential involved is associated with hydrogen evolution from water, a more facile reaction to catalyze via sustainable electrochemical and photochemical means compared to CO_2 reduction. Coupled with the diversity of potential chemical products available via synthetic biology, the marriage between artificial and natural platforms can create opportunities to develop catalyst systems with enhanced function over the individual parts in isolation.

In developing hybrid bioinorganic platforms for solar-to-chemical conversion of CO_2, we drew inspiration from both tandem organometallic-microbial systems [*47, 48*], in which products of microbial metabolism are further transformed by organometallic catalysts, as well as biological electrosynthesis, in which organisms accept reducing equivalents from an electrode either in the

form of soluble electron carriers (for example, H_2 or formate) [*41, 49, 50*] or via direct electron transfer [*36, 51-53*]. Engineered strains of *Ralstonia eutropha* have been used for the aerobic production of isobutanol and 3-methyl-1-butanol [*41*], and isopropanol [*42*]. However, owing to the oxygen requirements of this organism and the relative inefficiency of its carbon fixation pathways [*54*], product titers and production efficiencies are relatively modest, and generation of reactive oxygen species is a serious concern. In addition, no photosynthetic systems of this type have been reported. As such, we turned our attention to the use of a pure culture of *Methanosarcina barkeri*, an obligately anaerobic archaeon that fuels its metabolism via the 8-proton, 8-electron reduction of CO_2 to CH_4 [*55*]. Prior studies have reported methanogenic electrosynthesis [*51, 53, 56*]; however, a fully light-driven system remains to be realized. Additionally, mixed cultures and multiple possible sources of reducing equivalents have complicated Faradaic efficiency measurements in previous studies [*51, 53, 56*]. Through the design of our hybrid system, we sought to surmount some of these aforementioned challenges.

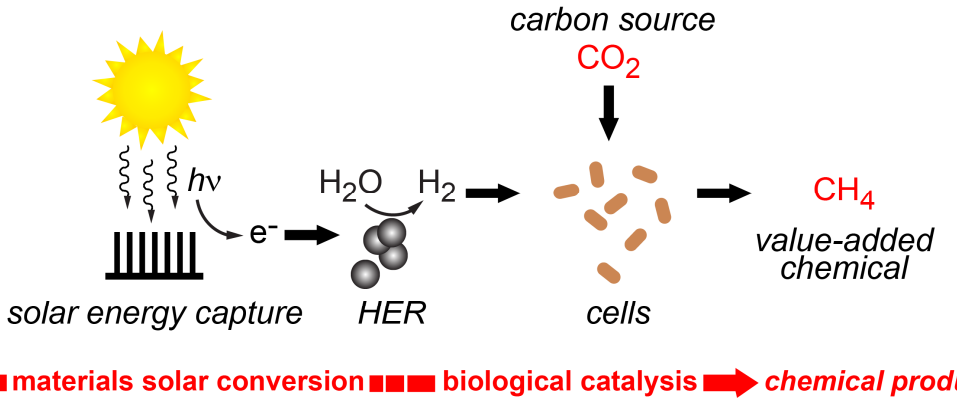

Figure 2.1. General scheme depicting a hybrid bioinorganic approach to solar-to-chemical conversion. Sustainable energy inputs in the form of electrical potential or light can be used to generate hydrogen from water using inorganic hydrogen evolution reaction (HER) catalysts; biological hydrogen-driven CO_2 fixation can subsequently generate value-added products such as methane. This materials biology interface can be generalized to other chemical intermediates and end products by mixing and matching different compatible inorganic and biological components.

Here we report an integrated bioinorganic catalyst platform for solar-to-chemical CO_2 conversion using sustainable inorganic hydrogen generators in conjunction with CO_2-fixing archaea. Under electrosynthetic conditions with a platinum cathode, a culture of *M. barkeri* shows chemoselective conversion of CO_2 to CH_4 with high Faradaic efficiencies (up to 86%) and low overpotential (η = 360 mV). The system is also capable of high yield production, cumulatively generating 110 mL (4.3 mmol) of methane over 7 d. Isotope labeling with $^{13}CO_2$ establishes that CH_4 is uniquely derived from CO_2 for cultures in both rich media and minimal, carbon-free media. Replacement of Pt with a newly synthesized earth-abundant α-NiS electrocatalyst allows for CH_4 generation at similar titers. Moreover, employing a photoactive silicon cathode reduces the overpotential to 175 mV upon irradiation with 740 nm light. Unassisted light-driven methane generation was achieved using tandem solar absorption by a photoactive *n*-TiO_2 anode and *p*-InP cathode assembly. Taken together, the results demonstrate the feasibility of combining compatible inorganic and biological systems to achieve solar-to-chemical conversion from light, H_2O, and CO_2, affording a starting point for the realization of sustainable fixation of CO_2 to value-added molecules.

2.2 Materials and methods

Materials. Reagents were purchased from commercial sources as noted below in *Commercial materials* and used without further purification. Ultra high purity gases purchased from Praxair (Danbury, CT) were used for all anaerobic manipulations. ^{13}C-labeled CO_2 was purchased from Cambridge Isotopes (Tewksbury, MA). Distilled water (dH_2O) was deionized to a resistivity of 18.2 MΩ·cm using a Millipore Milli-Q UF Plus system (ddH_2O).

Commercial materials. Sodium chloride, magnesium sulfate heptahydrate, ammonium chloride, potassium phosphate monobasic, potassium phosphate dibasic, sodium phosphate monobasic, sodium phosphate dibasic, manganese(II) chloride tetrahydrate, methanol, and pressure release aluminum crimp seals (20 mm) were purchased from Fisher Scientific (Pittsburgh, PA). Calcium chloride dihydrate, iron(II) sulfate heptahydrate, nickel(II) chloride hexahydrate, boric acid, cobalt(II) chloride hexahydrate, copper(II) chloride dihydrate, sodium molybdate dihydrate, sodium sulfide, L-cysteine, biotin, folic acid, pyridoxine hydrochloride, thiamine hydrochloride, riboflavin, nicotinic acid, calcium D-(+)-pantothenate, vitamin B_{12}, *p*-aminobenzoic acid, and thioctic acid were purchased from Sigma Aldrich (St. Louis, MO). Yeast extract was purchased from EMD Biosciences (Darmstadt, Germany). Casitone (pancreatic digest of casein) was purchased from BD (Franklin Lakes, NJ). Zinc sulfate heptahydrate was purchased from Mallinckrodt Chemicals (St. Louis, MO). Thioacetamide was purchased from Alfa Aesar (Ward Hill, MA). Resazurin was purchased from Eastman Kodak Company (Rochester, NY). Balch tubes (18 x 150 mm), anaerobic media bottles (250 mL and 2 L) and butyl rubber stoppers (20 mm) were purchased from Chemglass (Vineland, NJ).

Strain details and culture conditions. *Methanosarcina barkeri* (ATCC 43241) was purchased from the American Type Culture Collection (Manassas, VA). All culture manipulations were performed inside a Vacuum Atmospheres Nexus One glovebox with an atmosphere of 90% nitrogen and 10% hydrogen. Oxygen levels and humidity levels within the box were controlled using a STAK-PAK palladium catalyst and desiccant system in a Coy Laboratory Products unheated fan box. *M. barkeri* primary cultures were propagated in 18 × 150 mm Balch tubes with butyl rubber stoppers and aluminum crimp seals using ATCC medium 1043 with deoxygenated methanol (1% v/v) as the growth substrate. Secondary cultures were started by diluting late exponential phase primary cultures 1:100 into 1 L of ATCC medium 1043 in a 2 L anaerobic media bottle with deoxygenated methanol (1% v/v) as the growth substrate. All cultures were grown at 37 °C with shaking (200 rpm). The primary culture was propagated by diluting 1:100 into fresh ATCC 1043 medium every 4 d for approximately 3-4 months, or until changes in growth patterns were observed. Glycerol stocks were used for long-term culture storage.

Medium preparation. ATCC 1043 medium was used as the standard medium for the cultivation of *Methanosarcina barkeri* ATCC 42431. To prepare the medium, all components (listed below) except iron sulfate, sodium bicarbonate, and reducing agent were dissolved in the appropriate volume of ddH_2O. The solution was brought to a vigorous boil while sparging with an 80% N_2/20% CO_2 gas mixture. Once boiling, iron sulfate and sodium bicarbonate were added and boiling was continued until the solution became a bright pink color. The solution was moved to an ice bath and cooled to room temperature under constant sparging with the above gas mixture. The medium was subsequently transferred to a N_2-degassed serum bottle using a modified Drummond Original

Pipet-Aid Pipet Controller with the gas inlet line dispensing an 80% N_2/20% CO_2 gas mixture. The serum bottle was sealed with a butyl rubber stopper and aluminum crimp, and 10 mL reducing agent (see preparation below) were injected per liter of medium using a N_2-flushed syringe. The sealed medium was autoclaved, resulting in a light yellow solution.

A stock of reducing agent was prepared by adding a 0.01% (w/v) resazurin solution (200 µL) to ddH_2O (200 mL) and sparging the solution with N_2 for 20 min. Under continuous N_2 flow, L-cysteine (6 g) was added, followed by sodium sulfide nonahydrate (6 g). The N_2 sparge was continued until the sodium sulfide had dissolved and the solution was completely colorless. After preparation, the reducing agent was stored under N_2 atmosphere in a 250 mL serum bottle sealed with a butyl rubber stopper and aluminum crimp.

Per L, the medium contains:

K_2HPO_4	348 mg
KH_2PO_4	227 mg
NH_4Cl	500 mg
$MgSO_4 \cdot 7H_2O$	500 mg
$CaCl_2 \cdot 2H_2O$	250 mg
NaCl	2.25 g
Yeast extract	2 g
Casitone	2 g
SL-6 trace elements solution	3 mL
Wolfe's vitamin solution	10 mL
Resazurin solution (0.01% (w/v))	1 mL
$FeSO_4 \cdot 7H_2O$	2 mg
$NaHCO_3$	850 mg
Reducing agent	10 mL

Per liter, the SL-6 trace elements solution contains:

$ZnSO_4 \cdot 7H_2O$	100 mg
$MnCl_2 \cdot 4H_2O$	30 mg
H_3BO_3	300 mg
$CoCl_2 \cdot 6H_2O$	200 mg
$CuCl_2 \cdot 2H_2O$	10 mg
$NiCl_2 \cdot 6H_2O$	20 mg
$Na_2MoO_4 \cdot 2H_2O$	30 mg

To prepare a minimal (carbon-free) version of ATCC 1043 medium, yeast extract, casitone, and sodium bicarbonate were omitted from the standard recipe above. The sodium bicarbonate was replaced with a phosphate buffering system composed of $Na_2HPO_4 \cdot 7H_2O$ (4.84 g/L of media) and $NaH_2PO_4 \cdot H_2O$ (1.88 g/L of media). This medium was used for initial electrolysis experiments with Pt. Additionally, a N_2-sparged version of this medium was used for isotopic labeling studies.

Slight modifications were made to the minimal medium used for unassisted photochemical experiments. To prepare the catholyte, yeast extract, casitone, and resazurin were omitted from the standard medium recipe, though trace resazurin was still present from the reducing agent. In addition to sodium bicarbonate, the phosphate buffering system described above was added in order to increase ionic strength. The same medium was used to prepare the anolyte, except the reducing agent was omitted.

Design of photo/electrochemical cells. Gas evolution experiments were conducted in custom-made two-compartment glass electrochemical cells (Adams and Chittenden Scientific Glass; Berkeley, CA) (*Figure 2.2*). The anode chamber (80 mL) (*Figure 2.2* a) was closed at the top with a GL45 media bottle cap with silicone septum. The cathodic chamber (150 mL) (b) was sealed with a gas-tight lid possessing five distinct ports: 1) electrical connection to cathode (c), 2) electrical connection to reference electrode (d), 3) CO_2 line for solution sparging (e), 4) connection to GC for headspace sampling (f), and 5) re-sealable septum for manual gas injection/sampling (g).

Ports d, e, and f on the lid (size Ace #7) were sealed with front-sealing PTFE bushing closures (5846-44) and port c (size Ace #15) was sealed with a rear-sealing PTFE bushing closure (5846-48) (Ace Glass; San Francisco, CA). Port g (size Ace #7) was sealed with a front-sealing nylon bushing closure (5846-04, Ace Glass). Bushings for ports c-f were modified in the following manner: a $^1/_{16}$ in hole was drilled all the way through the center of the bushing, and ¼ in - 28 screw threads were drilled in the center, 8 mm deep from the outer side of the bushing. A 4 in long stainless steel rod ($^1/_{16}$ in OD) was inserted through the bushings for ports c and d and further sealed using a $^1/_{16}$ in TEFZEL ferrule and flangeless male nut (P-200 and XP-235X, respectively; Upchurch Scientific; Oak Harbour, WA) that could be screwed directly into the newly made opening on the bushing. Ports e and f were constructed in a similar manner, but replacing the stainless steel rods with $^1/_{16}$ in OD PEEK tubing (1531, Upchurch Scientific). The PEEK tubing was connected to Swagelok ball valves (40 series $^1/_8$ in tube fitting; Swagelok; Solon, OH) using PEEK unions (P-703, Upchurch Scientific), $^1/_8$ in OD stainless steel tubing, and $^1/_{16}$ in and $^1/_8$ in TEFZEL ferrules and flangeless male nuts (P-300X and P-335X, respectively; Upchurch Scientific). A piece of $^1/_8$ in OD stainless steel tubing was used to connect the ball valve of port f to the stem of a Quick-Connect (SS-QM2-S-200, Swagelok), which could be attached directly to the GC inlet that had been modified with a Quick-Connect body (SS-QM2-B-200, Swagelok). The bushing for port g was modified as follows: a $^1/_{16}$ in hole was drilled all the way through the center of the bushing, and a #8-32 screw thread was drilled in the center, ½ in deep from the outer side of the bushing. An 8 mm diameter teflon-coated silicone septum (Ace Glass) was placed behind the modified bushing of the manual gas injection port, and a ½ in, #8-32 sealing socket head cap screw (95198A535, McMaster-Carr; Santa Fe Springs, CA) was used to block access to the port when not in use. All electrodes used in the cathodic chamber were entirely contained within the chamber for the duration of the experiment to minimize leaks and were connected to a potentiostat *via* the stainless steel feed-through rods.

The headspace volume of the cathodic chamber was 100 mL. For electrochemical and photoelectrochemical experiments, the anode and cathode chambers were separated by a cation exchange membrane (Nafion 117, Sigma Aldrich); for experiments with no externally applied potential, an anion exchange membrane was used (AMV membrane; AGC Engineering Co., LTD, Chiba, Japan) to minimize pH changes.

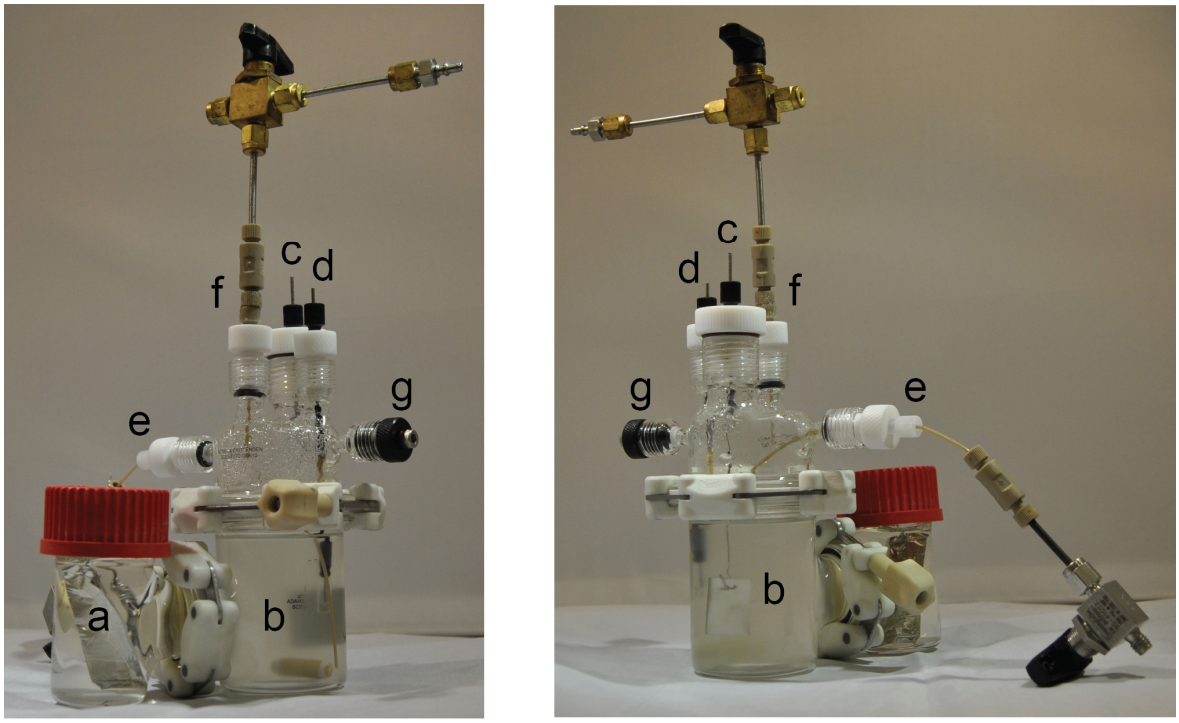

Figure 2.2. Electrolysis cell photographs. The electrolysis cell as described above (see Design of photo/electrochemical cells) viewed from different angles. Important design features are highlighted: (a) anode chamber with platinum anode visible, (b) cathode chamber with platinum cathode and silver/silver chloride reference electrode visible, (c) electrical connection to cathode (d) electrical connection to reference electrode, (e) CO_2 line for solution sparging, (f) GC connection for headspace sampling, and (g) re-sealable septum for manual gas injection/sampling.

General experimental setup. A *M. barkeri* secondary culture was harvested after 4 d of growth by centrifugation at 6,000 × *g* for 7 min at 4 °C using o-ring-sealed centrifuge bottles. After centrifugation, the pellets were combined and washed twice with methanol-free media (200 mL). The final washed pellet was resuspended in fresh methanol-free media (20 mL). At this point, the OD_{600nm} of the culture was determined by diluting the cell suspension 1:100 into 10 mM Tris buffer (pH 8.5).

The electrolysis cells were assembled inside an anaerobic glovebox. The appropriate media was added to the cathodic (130 mL) and anodic (70 mL) compartments as specified in *Media preparation*. Additionally, a magnetic stirbar was added to the cathodic compartment. The resuspended cell pellet was used to inoculate the cathodic side of the electrolysis cell to a final OD_{600nm} of 0.35. Appropriate electrodes were added to the cathodic and anodic compartments, and the tightly sealed electrolysis cells were removed from the anaerobic chamber. Once outside, the cathodic compartment was sparged with CO_2 for 5 min using the internal sparge line. Helium (1 mL) was injected into the cathodic headspace as a gaseous internal standard. The electrolysis cells were submerged to the horizontal flanges in water baths set to 37 °C. The cultures were stirred at 300 rpm for the duration of the experiment. In experiments with 24 h (12 h) timepoints, the experimental interval consisted of 23 h (11.5 h) of electrolysis followed by a 1 h (0.5 h) period for headspace analysis and sparging. GC-MS analysis was performed at each timepoint by direct introduction of the headspace into a GC sampling loop as described in *Headspace analysis by gas chromatography*. Immediately after sampling, the headspace of the cathodic chamber was

exchanged by sparging with fresh CO_2 for 5 min *via* the internal sparge line, followed by injection of a helium (1 mL) internal standard.

Electrochemical details. All electrochemical experiments were performed using a BASi Epsilon potentiostat (West Lafayette, IN). Pt gauze (electrochemical grade, purchased from Alfa Aesar or Sigma Aldrich) was used as the anode in all experiments except the unassisted full-splitting, where a *n*-TiO_2-coated FTO anode was used instead. The reference electrode was an aqueous Ag/AgCl electrode (3.5 M KCl) purchased from BASi. All reference electrodes were externally calibrated to potassium ferricyanide in pH 7 phosphate buffer ($Fe^{3+/2+}$ couple is 0.436 V vs SHE) before and after each experiment. No iR compensation was applied.

Calculation of overpotentials for biological galvanostatic experiments. Potentials during galvanostatic experiments were measured with respect to a Ag/AgCl reference electrode that had been externally calibrated to $K_3[Fe(CN)_6]$ in pH 7 phosphate buffer ($E_{1/2}$ = 0.437 V vs SHE). Overpotentials were determined from the potentials measured at t = 5 min; we surmise that the decay in applied potential over time does not indicate instability of the catalyst but rather is caused by drift of the Ag/AgCl reference due to sulfide poisoning. Taking into consideration that CO_2-sparged 1043 medium has a pH of 6.5, overpotentials for CO_2 reduction to CH_4 (E = -0.21 V vs SHE at pH 6.5, 25 °C, 1 atm) were calculated as follows:

$$\eta_{CH4} = -0.21 - (\text{V vs SHE})_{\text{t=5 min}}$$

Headspace analysis by gas chromatography. Headspace samples were analyzed with a multiple gas analyzer 8610C GC system equipped with a Haysep D column ($^1/_8$ in × 6 ft) and a 13X Mol Sieve column ($^1/_8$ in × 6 ft) (SRI Instruments; Torrance, CA). All gases were detected with a thermal conductivity detector (TCD) with Ar as the carrier gas at a setpoint flow rate of 23 mL/min. The oven program was as follows: Hold at 35 °C for 7.4 min, ramp to 60 °C (40 °C/min) followed by a hold for 4 min, and ramp to 220 °C (40 °C/min) followed by a hold for 2 min. Events were set as follows: Valves 1 and 2 inject at 0.5 min; stop-flow solenoid is on at 3.2 min and off at 8.4 min, valve 1 returns to load at 8.4 min, and valve 2 returns to load at 15.5 min.

Helium (1 mL) was injected into the headspace of each experiment as an inert internal standard; He and H_2 peaks are adequately baseline-separated using the aforementioned method. Representative elution times for gases of interest are as follows: He standard (1.93 min), H_2 (2.16 min), CH_4 (5.98 min), CO_2 (9.31 min).

Headspace samples were introduced onto the GC by first using an evacuated 350 mL Strauss flask to evacuate the GC sample loop (1 mL), and then opening the sample loop to the headspace using the Swagelok ball valve located on the cap of the electrochemical cell. This procedure allowed for direct sampling of the headspace with little oxygen contamination.

Hydrogen and methane were quantified according to calibration curves prepared by injecting known volumes of H_2 and CH_4 into an electrochemical cell prepared identically to those used in gas measurement experiments (*Figure 2.3*). At the start of each set of experiments, one sample of known H_2 and CH_4 concentration was run to ensure that the GC remained properly calibrated.

Calculation of Faradaic efficiency for methane. All CH_4 Faradaic efficiency calculations are based on cumulative measured CH_4 (V_T) over the duration of the experiment (3 d or 7 d). For each

biological methane production experiment, a corresponding non-electrolyzed/non-illuminated control with identical electrodes was performed to account for differences in residual methanol (a potential growth substrate) after washing of the culture. The cumulative amount of CH_4 measured in each control experiment is denoted as V_C. Faradaic efficiency for methane was calculated as follows:

$$\mathrm{FE}_{\mathrm{CH_4}} = \frac{\mathrm{V}\mathcal{F}}{125Q\mathrm{RT}}$$

where $V = V_T - V_C$ in mL (assumed at 1 atm); $\mathcal{F}$ is Faraday's constant; Q is the charge passed in C; R is the universal gas constant (0.082 L atm K^{-1} mol^{-1}); T is the temperature (310 K). Error represents standard deviations.

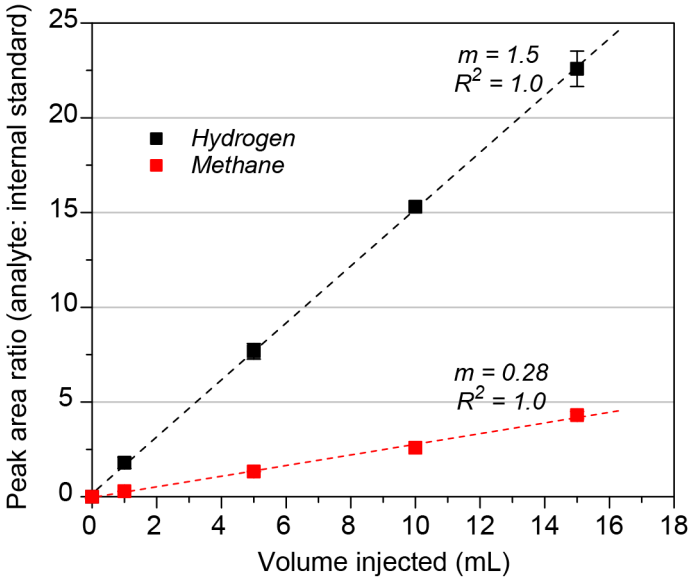

Figure 2.3. GC calibration curve for H_2 and CH_4 quantification. Hydrogen and methane calibration curves were generated by injecting known amounts of H_2 and CH_4 into an electrochemical cell prepared identically to those used in gas measurement experiments. Headspace samples were introduced onto a gas chromatograph by first evacuating the sample loop (1 mL) and subsequently opening it to the electrochemical cell. Peak areas determined by gas chromatography are reported as a ratio compared to He. Data are mean ± SD (n = 3).

Isotopic quantification by high-resolution mass spectrometry. The high resolution GC-MS data was collected using an Agilent 7890A chromatograph (Santa Clara, CA) and an AutoSpec Premier mass spectrometer (Waters; Manchester, UK) equipped with an electron impact ion source and Masslynx software. For gas chromatography, an HP-5 column (0.0250 mm × 30 m, 0.25 µm film thickness; Agilent) was used. The carrier gas was helium and the oven temperature was maintained at 50 °C. Samples were introduced directly to the column *via* a splitless manual injection using a 1 mL gas-tight Hamilton syringe (Hamilton Company; Reno, NV) that had been flushed with N_2. For methane detection, 500 µL of electrolysis cell headspace was injected onto the instrument. The source temperature of the mass spectrometer was maintained at 150 °C and electron energy was set at 70 eV. For methane detection, the instrument was tuned to 10,000 resolution using the N_2 parent ion (28 *m/z*) and fragment (14 *m/z*). Methane was detected using

voltage scanning from 8 to 33 *m/z* with water (18 *m/z*), an O_2 fragment (16 *m/z*) or a N_2 fragment (14 *m/z*) used as reference peaks as appropriate.

Limit of detection calculations for isotopically labeled electrolysis experiments. To determine the limit of detection of the high resolution gas chromatograph-mass spectrometer, successively diluted samples of methane gas were injected onto the instrument until a methane signal could no longer be detected. The last concentration at which a methane peak was detectable was 0.5% (v/v). For each isotopically labeled electrolysis experiment, the sample was also analyzed using the SRI Instruments gas chromatograph (as described above in *Headspace analysis by gas chromatography*) after analyzing the headspace using the high resolution GC-MS instrument. Using this method, the total volume of methane generated during the 3 d experiment could be quantified. To determine the percent of unlabeled methane potentially present in the system but undetectable by the high resolution GC-MS, the volume equivalent to 0.5% of the 100 mL electrolysis cell headspace (500 μL) was divided by the total amount of detected methane.

Synthesis of α-NiS catalyst. Freshly prepared solutions of $NiCl_2 \cdot 6H_2O$ (0.2 M), thioacetamide (0.4 M), and 5 % (v/v) ammonium hydroxide were prepared using ddH_2O. Nickel chloride solution (2 mL) and thioacetamide solution (2 mL) were combined in a 10 mL microwave reaction vial and sparged with N_2 for 10 min. Upon addition of ammonium hydroxide solution (40 μL), a small amount of yellow precipitate was observed. The reaction tube was then capped under N_2 and microwaved for 30 min at 150 °C with a 5 min temperature ramp using a CEM microwave reactor (Matthews, NC). Following the reaction, the supernatant was decanted and the black particles were washed three times with ddH_2O and once with isopropanol by centrifuging the sample, decanting the supernatant, and resuspending the particles. Drying under vacuum overnight yielded a fine black powder (22 mg, 61% yield). The product was characterized by rotating disk electrochemistry (RDE) and galvanostatic experiments, powder X-ray diffraction (pXRD), energy-dispersive X-ray spectroscopy (EDX), transmission electron microscopy (TEM), high-resolution TEM, inductively coupled plasma-optical emission spectroscopy (ICP-OES), and thermogravimetric analysis (TGA) as described in *General characterization methods for α-NiS* . The catalyst was stored in air for 3-4 months, after which time it was found to be no longer active for HER.

General characterization methods for α-NiS. Powder X-ray diffraction (pXRD) was performed on a Bruker GADDS Hi-Star D8 diffractometer (Billerica, MA) using Co Kα radiation (1.790 Å). Transmission electron microscopy (TEM) and energy dispersive X-ray (EDX) spectroscopy was performed with a Hitachi TEM (Tokyo, Japan) using copper grids (Ted Pella, Redding, CA). High resolution TEM was performed with a 200kV FEI monochromated F20 UT Tecnai instrument (Hillsboro, OR). Thermal gravimetric analysis (TGA) was performed with a TA Instruments Q5000 TGA (Newcastle, DE).

Determination of Ni:S ratio by inductively coupled plasma-optical emission spectrometry (ICP-OES). ICP-OES measurements were performed on a Perkin Elmer Optima 5300 DV instrument (Waltham, MA) with an internal standard containing 50 μg Sc^{3+}/mL. A calibration curve was made using [Ni] ($NiCl_2 \cdot 6H_2O$) and [S] (H_2SO_4) concentrations of 1 μM, 10 μM, 100 μM, and 1 mM. α-NiS samples were dissolved in concentrated HNO_3 and then diluted to 7% (v/v) HNO_3 using ddH_2O. This solution was filtered before analysis using a 0.45 μm PVDF syringe filter (Whatman; Maidstone, UK). The nickel to sulfur ratio was found to be 0.80, with respective concentrations of 0.144 and 0.180 mM.

Rotating disk electrochemistry setup. For rotating disk electrochemistry (RDE) experiments, a 1 M sodium phosphate buffer, pH 7 (10 mL) was degassed by sparging with N_2 for 15 min. A glassy carbon electrode (A = 0.071 cm^2) was polished before use, then coated with a 3 μL drop of NiS ink (see *Preparation of Pt and α-NiS/C electrodes*) and allowed to dry for 20 min in air. The rotation speed was set to 1,500 rpm. The reference electrode was an aqueous Ag/AgCl electrode (3.5 M KCl) purchased from BASi, which was referenced to $K_3[Fe(CN)_6]$ after the experiment. The counter electrode was a Pt wire, which was polished before use.

Preparation of Pt and α-NiS/C electrodes. Platinum cathodes were fabricated from Pt foil (2.5 cm × 1.7 cm × 0.125-0.135 mm) (Sigma Aldrich) and connected to stainless steel feed-through rods with Pt wire (Sigma Aldrich). Prior to each experiment, Pt cathodes were cleaned by electrooxidation at 0.6 V vs SHE for 2 min in 1 M HCl, followed by repeated rinsing with ddH_2O.

α-NiS/C cathodes were prepared by deposition of an ink of α-NiS on carbon cloth. α-NiS powder (5 mg) was weighed into a 4 mL sample vial using a microbalance. Ethanol (600 μL), ddH_2O (200 μL), and a solution of 5% (w/v) nafion in aliphatic alcohols (Sigma Aldrich) (40 μL) were added and the vial was sonicated for 20-30 min. Meanwhile, Pt wire (0.5 mm diameter, Sigma Aldrich) was threaded through the top of a 1.5 cm × 4.5 cm strip of carbon cloth (Fuel Cell Earth; Wakefield, MA). This Pt wire was used only as an inert conductive material and was never submersed in electrolyte. α-NiS ink (240 μL) was applied to the bottom 3 cm of carbon cloth and allowed to dry for 2-4 h before use. Because both sides of the Pt and α-NiS/C electrodes are catalytically active, their geometric surface areas are 8.5 cm^2 and 9.0 cm^2, respectively.

Preparation of silicon photocathodes. 4 in planar <100> *p*-silicon wafers (10-30 Ωcm) were cleaned in piranha solution and a 1:10 buffered HF etch, followed by rinsing with dH_2O and centrifuge drying at room temperature. Arsenic doping was performed using a rapid temperature annealing (RTA) process. In preparation for this procedure, 6 in silicon handle wafers were spin coated with arsenic dopant solution at 3000 rpm for 1 min, followed by baking on a hotplate at 150 °C in air for 30 min. Immediately after cooling, a 6 in handle wafer and freshly cleaned 4 in wafer were placed together such that the arsenic-coated side was in contact with the wafer to be doped. After one or two dummy runs to ensure reliable heating and cooling profiles, the wafers were placed in the RTA chamber (Allwin21 Rapid Thermal Processing System) and purged with Ar for 5 min. Optimal doping conditions were found to vary from batch to batch, so normally 3-4 wafers were prepared using slightly different conditions and their photoactivity was evaluated at a later point. Standard RTA conditions were 900 °C for 3-4 min or 1000 °C for 60-90 s. Following As doping, atomic layer deposition (ALD) of crystalline TiO_2 was performed in order to protect the photocathode from corrosion during illumination in neural aqueous media. Immediately preceding ALD, the doped silicon wafer was pre-treated with 1:10 buffered HF to remove native oxide. ALD was performed using a home-built setup with $TiCl_4$ and H_2O as precursors; a typical recipe is 600 cycles at 300 °C.

A thin layer (10-20 nm) of nickel/molybdenum alloy was sputtered on top of the TiO_2 layer to act as a HER catalyst. For this step, it is imperative that the Ni/Mo layer not be too thick, as light transmission to the semiconductor may be impeded. Dummy runs were performed in advance in order to establish a suitable recipe. Rectangles of TiO_2-coated silicon (2.5 × 3 cm^2) were cleaned

for 2 min with oxygen plasma to remove organics then taped to a handle wafer around the edges using Kapton tape (to prevent side-deposition, which may shunt the electrode). Sputtering was performed at 50 W DC (nickel target) and 150 W RF (Mo target) for 8 min with the nickel shutter open and the Mo shutter closed.

Electrical contact with the finished piece of silicon was made by first gently scratching a 2 × 2 cm^2 region on the backing of the silicon with a diamond scribe and then applying a thin layer of gallium-indium eutectic (Sigma Aldrich). A roughly 1 × 1 cm^2 piece of conductive double-sided carbon tape was placed on the short edge of a 2.5 × 6 cm^2 piece of titanium foil (Sigma Aldrich). Subsequently, a thin layer of silver paste (SPI Supplies; West Chester, PA) was applied on top of the GaIn eutectic, and the silicon chip was gently pressed onto the carbon sticker and Ti foil. Once dry, epoxy resin (Loctite® Hysol 1C; Düsseldorf, Germany) was applied to the front and back of the silicon/titanium assembly, taking care to leave no gaps where water could enter the device. The electrode was allowed to dry at ambient temperature in air for at least 24 h before use. The photoactive geometric surface area of the finished cathodes was 7.0 cm^2. Before use in a biological experiment, the fabricated electrode was soaked in 1043 media for 24 h to remove any soluble fabrication materials that may be toxic to the cells.

Preparation of indium phosphide photocathodes. A 5 nm layer of Zn and a 50 nm layer of Au were sequentially thermally evaporated onto the back side of an InP wafer, which was then subjected to a RTA process (450 °C for 30 min) to fabricate an ohmic contact. The annealing process transforms the Zn/Au layer into a Zn-Au alloy and a fraction of the Zn diffuses into the underlying InP layer, forming a p^+-InP layer. The presence of the Zn-Au alloy layer prevents oxidation of metallic Zn. During this step, the color of the film changes from golden yellow to silver. Next, the wafer was sonicated sequentially in acetone and isopropanol and blown dry with N_2. The wafer was etched in a 1:1 mixture of conc. HCl:conc. H_3PO_4 for 5-10 sec, then rinsed with dH_2O water three times and blown dry. Immediately after this step, the sample was placed into the chamber of a home-built ALD and coated with 7-10 nm of amorphous TiO_2 at 150 °C ($TiCl_4$ and H_2O were used as precursors). The TiO_2-passivated wafer was sputtered with a 5 nm layer of Pt to act as a HER catalyst.

An approximately 1.5 x 2 cm^2 piece of *p*-InP/Pt wafer was used to fabricate each electrode. A 1 × 1 cm^2 piece of conductive double-sided carbon tape was placed on the short edge of a 2 × 6 cm^2 piece of titanium foil (Sigma Aldrich). Subsequently, a thin layer of silver paste (SPI Supplies) was applied to the back side of the indium phosphide and gently pressed onto the carbon sticker and Ti foil. Once dry, epoxy resin (Loctite® Hysol 1C) was applied to the front and back of the InP/titanium assembly, taking care to leave no gaps where water could enter the device. The electrode was allowed to dry at ambient temperature in air for at least 24 h before use. The photoactive geometric surface area of the finished cathodes was 3.0 cm^2. Before use in a biological experiment, the fabricated electrode was soaked in 1043 media for 24 h to remove any soluble fabrication materials that may be toxic to the cells.

Preparation of titanium dioxide photoanodes. Titanium dioxide nanowires were synthesized via hydrothermal methods according to published procedures [*37, 57*]. A 3 x 4 cm^2 piece of fluorine-doped tin oxide- (FTO) coated glass was cleaned by sonicating first in acetone and then three times in isopropanol, then blown dry. The freshly cleaned FTO plates were placed in a

Teflon-lined autoclave container, conductive side facing down. It was critical to mechanically remove any residual TiO_2 from the walls of the Teflon container by sonicating in dH_2O for at least 2 h, followed by sonication in 6M HCl for 30 min and multiple rinses with dH_2O. In a typical synthesis, 0.5 mL titanium tetraisopropoxide (Sigma Aldrich) was injected into 30 mL of 6M HCl and shaken well before pouring into the Teflon container such that 75% of the FTO substrate was immersed. The assembled autoclave was placed into a pre-heated oven at 200 °C for 2-2.5 h. To terminate growth, the autoclave was removed from the oven and cooled to room temperature for 3 h before opening.

The coated FTO plates were removed and rinsed with copious dH_2O, then blown dry before being annealed in air (30 min ramp to 450 °C, 30 min anneal, followed by natural cooling). They were subsequently introduced into the chamber of a home-built ALD and coated with 10 nm of amorphous TiO_2 (precursors were $TiCl_4$ and H_2O).

To assemble the electrode, a 0.5 × 2 cm^2 piece of conductive double-sided carbon tape was placed in the region at the top of the anode that was not coated with *n*-TiO_2 nanowires (and hence remained conductive: average resistance should be < 100 Ω). Subsequently, a thin layer of silver paste (SPI Supplies) was applied to the conductive carbon and gently pressed onto a 2 x 4 cm^2 piece of Ti foil. Once dry, epoxy resin (Loctite® Hysol 1C) was applied around the junction with the Ti foil, taking care to leave no gaps where water could enter the device. The electrode was allowed to dry at ambient temperature in air for at least 24 h before use. The photoactive geometric surface area of the finished cathodes was 9.0 cm^2.

Details of photoelectrochemical setup. Titanium wire (GalliumSource, LLC; Santa Cruz, CA) and silver paste (SPI Supplies) were used to make an electrical connection between the titanium foil support of the photocathode and the stainless steel feed-through rod of the electrochemical cell. The entire photoactive region of the photocathode was submersed in media and illuminated with a 740 nm LED (Mightex Systems; Toronto, Canada) with an intensity of 20 mW/cm^2. The electrolysis cell was heated to 37 °C in a water bath and stirred at 300 rpm for the duration of the experiment.

Details of photochemical setup. The standard electrochemical cell design described above was slightly modified for unassisted photochemical experiments. A 1 in diameter quartz window was added to the anodic chamber, 180° from the membrane, to prevent initial filtering of the full spectrum light by glass. The *n*-TiO_2 photoanode was placed in the center of the anodic compartment, and immediately behind it was added a 1 in diameter 455 nm filter (Edmund Optics; Barrington, NJ), which was necessary to prevent blue light from reaching the culture [*58, 59*]. Instead of Nafion-117, an AMV anion exchange membrane was used (AGC Engineering Co., LTD; Chiba, Japan). Titanium wire (GalliumSource, LLC) and silver paste (SPI Supplies) were used to make an electrical connection between the titanium foil support of the photocathode and the stainless steel feed-through rod of the electrochemical cell. A full-spectrum 300 W Xenon arc lamp (Newport Corp.; Santa Clara, CA) was used as a light source, with an intensity of 2.2 W/cm^2. The light beam passed first through the *n*-TiO_2 anode, then through the 455 nm filter and the membrane before finally impinging on the cathode. The photoanode was illuminated with a 1 in diameter light spot. The entire photoactive region of the photocathode was submersed in media and illuminated.

Photocurrent under illumination was measured with a BASi potentiostat using a standard two-electrode cell setup (reference and counter leads were shorted on the *n*-TiO_2 anode, and working lead was attached to the *p*-InP cathode).

2.3 Results and discussion

Selection of biological catalyst. Careful organism selection is critical to the successful realization of an integrated bioinorganic system. The autotrophic obligate anaerobe *Methanosarcina barkeri* [*55*] is amenable to integration with inorganic catalysts for a variety of reasons. *M. barkeri* can use H_2 as a source of reducing equivalents for the reduction of CO_2 to CH_4; the cathode of a water-splitting device could serve as a potential source of this H_2. Owing to the anaerobic metabolism of the organism, oxygen is not required at the cathode, thereby improving Faradaic efficiency for the product of interest, simplifying gas delivery to the culture, and preventing generation of potentially harmful reactive oxygen species. Furthermore, CH_4 is generated with high efficiency as a byproduct of normal metabolism. Finally, *M. barkeri* requires no added sources of reduced carbon and can produce CH_4 in minimal media containing only supplemental vitamins and minerals.

Electrochemical reduction of carbon dioxide to methane with a hybrid platinum/archaea catalyst platform. Initial experiments were performed using a platinum cathode to electrochemically generate H_2, which was subsequently used *in situ* by *M. barkeri* to reduce CO_2 to CH_4. (*Figure 2.4 A*) shows a general schematic of the gastight, two-compartment electrochemical cell that was specially fabricated for batch-mode electrolysis and subsequent headspace analysis by gas chromatography (GC). Separation of the cathodic and anodic chambers with an ion-permeable membrane prevented any noticeable diffusion of O_2 into the culture. After inoculation of the cathodic chamber with *M. barkeri* (130 mL final volume, OD_{600nm} = 0.35) and saturation of the carbon-free catholyte with pure CO_2, galvanostatic electrolysis was performed at a current of 2.5 mA (j = 0.29 mA/cm^2, η = 360 mV) for 12 h (See *Calculation of overpotentials for biological galvanostatic experiments* for the method used for the calculation of overpotentials.). The headspace was analyzed by GC and replaced by sparging with fresh CO_2 before restarting the electrolysis. Methane production was linear under these conditions and cumulatively resulted in 16.8 ± 0.6 mL CH_4 (0.660 ± 0.024 mmol) over 3 d (All volumes reported in this work assume 1 atm pressure and a temperature of 310 K.) with an average Faradaic efficiency of 81 ± 3% (n = 3) (All errors represent standard deviation unless otherwise noted.) (*Figure 2.4 B*). Electrolysis was subsequently conducted in rich media containing yeast extract and casitone; variation of the applied current from 1 mA (j = 0.12 mA/cm^2) to 7.5 mA (j = 0.88 mA/cm^2) shows that CH_4 generation is proportional to applied current, suggesting that the system is operating in a hydrogen-limited regime (*Figure 2.4 C*). The highest Faradaic efficiency, 86 ± 3%, was observed with an applied current of 2.5 mA (j = 0.29 mA/cm^2). A slight decrease in Faradaic efficiency was observed at higher current densities. We speculate that increased rates of HER cause H_2 to be less effectively delivered to the culture solution with loss to the headspace.

To test the limits of CH_4 production of the system, the organisms were electrolyzed at 7.5 mA for 7 d (*Figure 2.4 D*). The headspace of the cathodic chamber was sampled at 24 h intervals and subsequently exchanged with fresh CO_2. During each 24 h period, 15.6 ± 0.7 mL CH_4 (0.613 ± 0.028 mmol) were produced; this value corresponds to cumulative methane production of 109 ± 5 mL (4.28 ± 0.20 mmol) over 7 d at an average Faradaic efficiency of 75 ± 4% (n = 3). Moreover, the hybrid bioinorganic system showed no loss in efficiency over the course of the experiments, which were terminated due to time constraints rather than a decrease in performance. Taken together, these data establish that there are no viability concerns on the timescale tested and presage the possibility of extended operation with a single inoculation of biomass.

A series of isotopic labeling experiments were conducted to show that the observed methane was derived from carbon dioxide as the source feedstock. Electrolysis cells containing nitrogen-sparged rich media were inoculated with *M. barkeri*. The headspace of one cell was filled with $^{12}CO_2$ and another with $^{13}CO_2$, and both were subjected to a galvanostatic electrolysis at a current of 2.5 mA. High resolution gas chromatography-mass spectrometry was used to show that only $^{13}CH_4$ was observed when electrolyzed under an atmosphere of $^{13}CO_2$ (*Figure 2.4 F*), whereas only $^{12}CH_4$ was observed in the $^{12}CO_2$ control experiment (*Figure 2.4 E*). Based on the limit of detection and amount of methane generated, < 4% of the observed methane could potentially come from sources other than CO_2. Similarly, only ^{13}C-labeled methane was observed when the electrolysis was performed in minimal media (*Figure 2.5*). Based on the limit of detection and amount of methane generated, < 7.5% of the observed methane could potentially come from sources other than CO_2 under these conditions.

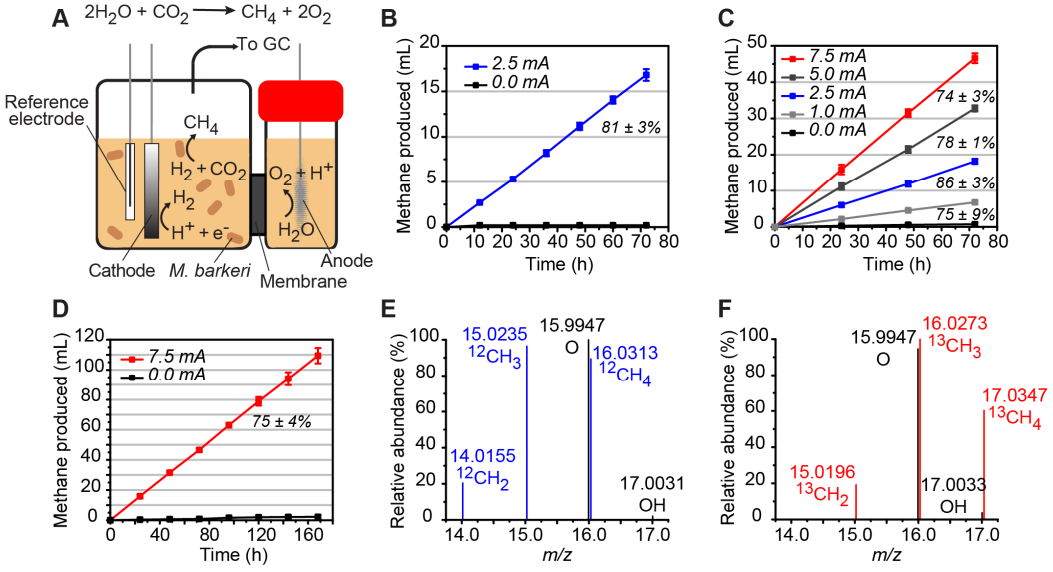

Figure 2.4. Electrocatalytic reduction of carbon dioxide to methane with a hybrid platinum/M. barkeri platform. (A) Schematic of generalized electrolytic setup showing *in situ* generation of hydrogen at the cathode followed by hydrogen-driven reduction of carbon dioxide to methane by the *M. barkeri* biocatalyst. (B) Cumulative methane generation and associated average Faradaic efficiency in minimal media. (C) Cumulative methane generation and associated average Faradaic efficiencies at various currents in rich media. (D) Cumulative long-term methane generation and associated average Faradaic efficiency in rich media. (E, F) High-resolution mass spectrometry of headspace gases after electrolysis under an atmosphere of $^{12}CO_2$ (E) and $^{13}CO_2$ (F) in rich media. Error bars represent standard deviation with n = 3 independent experiments in all cases.

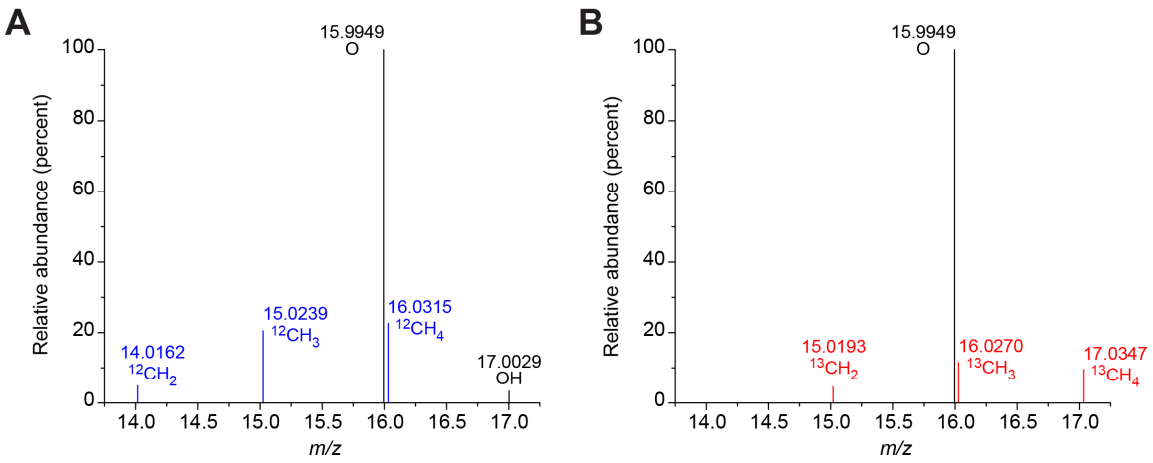

C

$^{12}CO_2$

m/z	Abundance	Formula
14.0162	4.91	$^{12}CH_2$
15.0239	20.55	$^{12}CH_3$
16.0315	22.70	$^{12}CH_4$

$^{13}CO_2$

m/z	Abundance	Formula
15.0193	4.62	$^{13}CH_2$
16.0270	11.55	$^{13}CH_3$
17.0347	9.57	$^{13}CH_4$

D

$^{12}CO_2$

m/z	Abundance	Formula
14.0155	20.53	$^{12}CH_2$
15.0235	96.51	$^{12}CH_3$
16.0313	89.52	$^{12}CH_4$

$^{13}CO_2$

m/z	Abundance	Formula
15.0196	19.25	$^{13}CH_2$
16.0273	100.00	$^{13}CH_3$
17.0347	60.38	$^{13}CH_4$

Figure 2.5. High-resolution mass spectra of headspace gases after electrolysis under $^{12}CO_2$ or $^{13}CO_2$ atmospheres. Experimental setup is as described. After set-up under N_2 in the specified media, the headspace of the electrolysis cell was replaced with $^{12}CO_2$ or $^{13}CO_2$. He (1 mL) was added as an internal standard for final methane quantification. Each experiment was electrolyzed at 2.5 mA for 72 h using a platinum cathode and anode. The headspace was analyzed using high-resolution mass spectrometry, with representative mass spectra presented. (A) $^{12}CO_2$ headspace, carbon-free media, (B) $^{13}CO_2$ headspace, carbon-free media, (C) Abundances of parent ions and fragments in carbon-free media and (D) Abundances of parent ions and fragments in rich media (see *Figure 2.4 E-F* for corresponding spectra).

Synthesis and characterization of α-NiS HER catalyst and its use in carbon dioxide to methane conversion. After demonstrating CO_2-to-CH_4 conversion by *M. barkeri* during *in situ* electrolysis using a platinum HER cathode, we sought to replace the precious metal catalyst with an earth-abundant alternative. Several HER catalysts containing only first-row transition metals have been recently reported [*60-63*]; among these examples, metal chalcogenides have featured prominently [*64-70*]. In addition to low overpotential and long-term stability, another requirement for a bio-materials hybrid system is that the catalyst must operate in aqueous media within a biologically relevant pH range (pH 5-8) and be non-toxic to the organism. Relatively few published examples meet all of these criteria. As such, we developed nanoparticulate α-NiS as a biocompatible HER catalyst for integration with *M. barkeri* cultures.

Nanoparticulate nickel sulfide was prepared by microwave irradiation (250 °C, 30 min) of an aqueous solution of nickel chloride, thioacetamide, and ammonium hydroxide (*Figure 2.6 A*). The

resulting black powder was rinsed with water and isopropanol and dried under vacuum overnight. The newly synthesized catalyst was stored in a capped vial in air and retained activity for several months. Characterization by powder X-ray diffraction confirmed that the product is crystalline and identified the primary phase as α-NiS (JCPDS number 77-1624) (*Figure 2.6 B*). TEM images show polydisperse hexagonal particles of 20-100 nm in diameter (*Figure 2.7*). The nickel-to-sulfur ratio was verified to be 1:1 by EDX spectroscopy based on the nickel L and sulfur K peaks (*Figure 2.6 C*), a result which was further corroborated by ICP-OES measurements. High resolution TEM images taken along the [010] axis confirm the assignment of single crystalline α-NiS based on the (100) and (001) lattice planes (*Figure 2.6 D*). Thermogravimetric analysis shows negligible loss of mass until 600 °C, suggesting the absence of surface-bound organics (*Figure 2.8*).

Electrocatalytic properties of the α-NiS particles were evaluated using rotating disk electrochemistry and chronopotentiometry. As shown in the polarization curve (*Figure 2.6 E*), crystalline α-NiS is an active HER catalyst in pH 7 potassium phosphate buffer and achieves current densities of 1 and 5 mA/cm^2 at overpotentials of η = 275 and 350 mV, respectively. The observed Tafel slope of 111 mV/dec is similar to the predicted 118 mV/dec for a process in which the Volmer step (formation of an adsorbed H intermediate) is rate-determining [*71*]. The exchange current density, j_0, is 3.5×10^{-2} mA/cm^2 based on extrapolation of the Tafel plot (*Figure 2.6 F*). These parameters compare favorably to other heterogeneous, first-row transition metal HER catalysts, especially given the ease of synthesis (*Table 2.1*).

A suspension of NiS powder in 3:1 ethanol:water with nafion binder was deposited on conductive carbon cloth to fabricate larger-scale electrodes for hydrogen generation and long-term stability measurements. Galvanostatic experiments at a current of 2.5 mA were run for 24 h; the Faradaic efficiency for hydrogen generation was found to be 95 ± 4% (n = 3) (*Figure 2.9*). As shown in *Figure 2.10*, the potential applied during these experiments does not significantly decay over the course of several days, indicating that the catalyst is stable under such conditions.

Having established the efficacy and stability of α-NiS as a catalyst for HER at biologically relevant pH, we sought to interface it with a *M. barkeri* culture for electrochemical methane production. A piece of conductive carbon cloth with 1.4 mg deposited α-NiS catalyst was used as an earth-abundant replacement for platinum. In a galvanostatic experiment at 2.5 mA (j_{avg} = 0.28 mA/cm^2, η = 695 mV), 5.1 ± 0.2 mL CH_4 (0.20 ± 0.01 mmol) were generated in 24 h, cumulatively generating 15.4 ± 0.8 mL CH_4 (0.605 ± 0.031 mmol) over 3 d with an average Faradaic efficiency of 73 ± 5% (n = 3) (*Figure 2.11*). These values are comparable to those obtained for the corresponding platinum experiments. When the current was increased to 7.5 mA (j_{avg} = 0.83 mA/cm^2), experiments using α-NiS/C were virtually indistinguishable from Pt in terms of daily and cumulative methane, producing 108 ± 4 mL CH_4 (4.24 ± 0.16 mmol) over 7 d with an average Faradaic efficiency of 74 ± 2% (n = 3) (*Figure 2.6 G*).

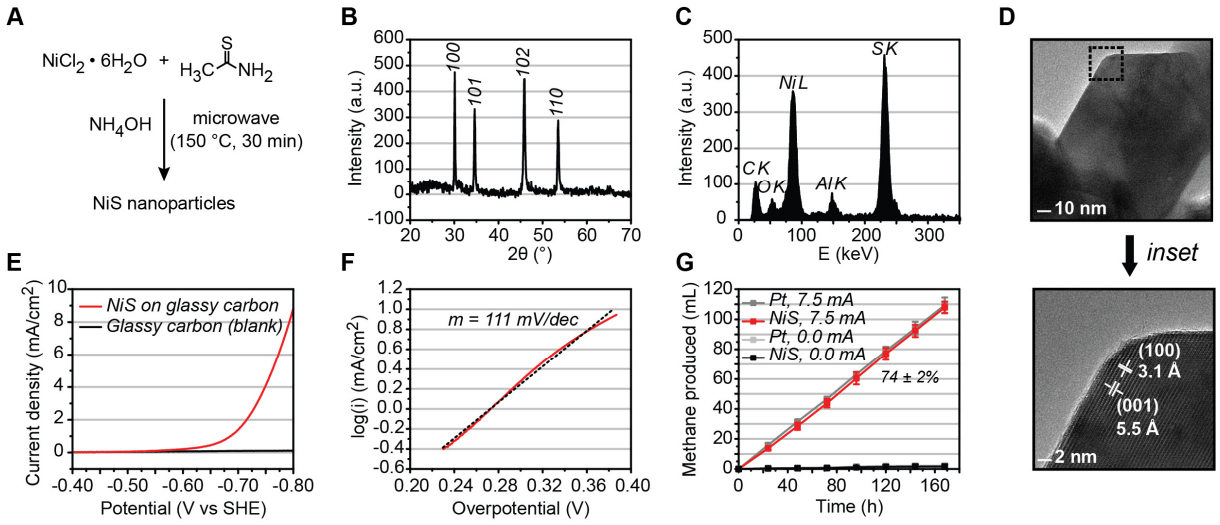

Figure 2.6. Synthesis and characterization of a biocompatible, earth-abundant HER catalyst for use in hybrid bioinorganic systems for solar-to-chemical conversion. (A) Synthesis of α-NiS nanoparticles. (B) pXRD pattern of α-NiS. (C) EDX spectrum of α-NiS. (D) HRTEM images of α-NiS. (E) Polarization curve (RDE) of α-NiS on glassy carbon compared to glassy carbon background, 1 M KP_i (pH 7), scan rate 5 mV/sec, rotation speed 1500 rpm. (F) Corresponding Tafel plot. (G) Cumulative long-term methane generation and associated average Faradaic efficiency using an α-NiS/carbon cloth cathode is comparable to results obtained with platinum cathodes. Error bars represent standard deviation with n = 3 independent experiments.

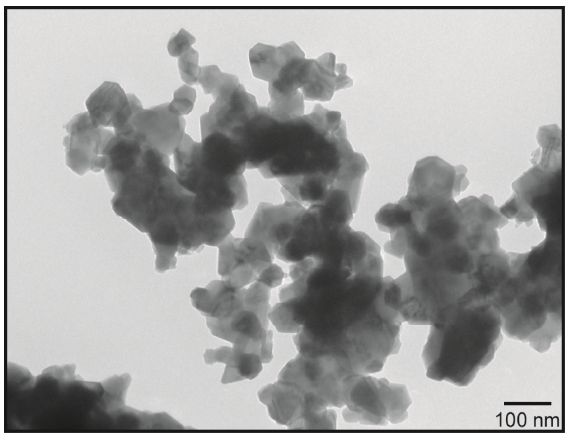

Figure 2.7. TEM characterization of α-NiS nanoparticles. TEM image of α-NiS nanoparticles showing polydisperse hexagonal particles 20-100 nm in diameter.

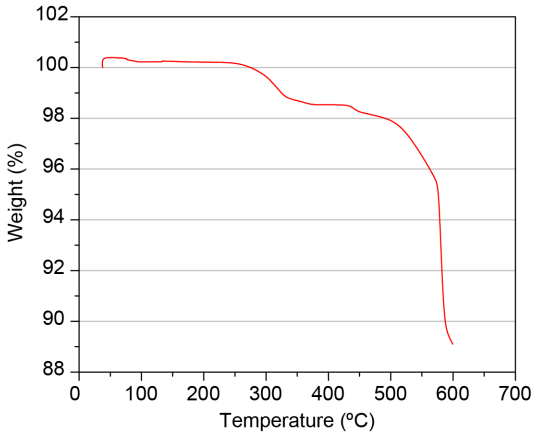

Figure 2.8. Thermogravimetric analysis of α-NiS catalyst. The absence of a significant loss in mass until ca. 450°C indicates a lack of surface-bound ligands on the α-NiS nanoparticles. Experiment was performed under an atmosphere of N_2 to prevent sample oxidation.

Catalyst	Onset (mV)	η (mV) at 2 mA/cm^2	Tafel slope (mV/dec)	j_o (mA/cm^2)	Ref.
α-NiS	140	300	111	3.5×10^{-2}	This work
FeS	325	700	150	6.6×10^{-4}	*66*
Co_9S_8@C	100	190	–	–	*68*
FeP[a]	30	60	–	–	*61*
Ni_3S_2/Ni	180	~180	118	–	*69*
NiS_2	175	310	69	–	*70*
Co/P/O film	50	385	140	3.0×10^{-2}	*60*
Co-S film	43	83	93	0.256	*65*
Ni-S film	170	260	77	–	*67*

Table 2.1. Comparison of various first row transition metal HER catalysts at neutral pH. Faradaic efficiencies for H_2 are quantitative in all cases. All values are reported at pH 7 unless otherwise noted. [a] Values are reported at pH 6.5.

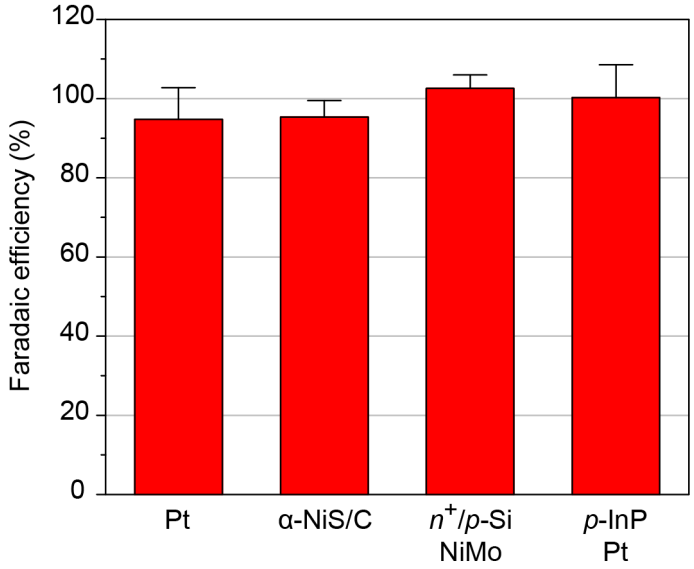

Figure 2.9. Faradaic efficiencies for H_2 generation for electrolysis, photoassisted electrolysis, and unassisted water splitting with Pt, α-NiS/C, n^+/p-Si/NiMo, and p-InP/Pt cathodes. Experimental setup is as described, except that no *M. barkeri* was inoculated into the electrolysis cell. A galvanostatic experiment was conducted using Pt, α-NiS/C, or illuminated n^+/*p*-Si/NiMo by passing a current of 2.5 mA for 24 h (*n* = 3 independent experiments). The *p*-InP/Pt cathodes were illuminated at 2.2 W/cm^2 for 1-6 h (*n* = 4 independent experiments). H_2 in the headspace was quantified by gas chromatography using He as an internal standard. Faradaic efficiencies (FE) for H_2 were calculated according to the following equation:

$$\mathbf{FE}_{\mathbf{H_2}} = \frac{\mathbf{V}\mathcal{F}}{\mathbf{500}Q\mathbf{RT}}$$

where V is the volume of H_2 measured in mL (assumed at 1 atm); $\mathcal{F}$ is Faraday's constant; *Q* is charge passed in C; R is the universal gas constant (0.082 L atm K^{-1} mol^{-1}); T is the temperature (310 K). Error bars represent standard deviations.

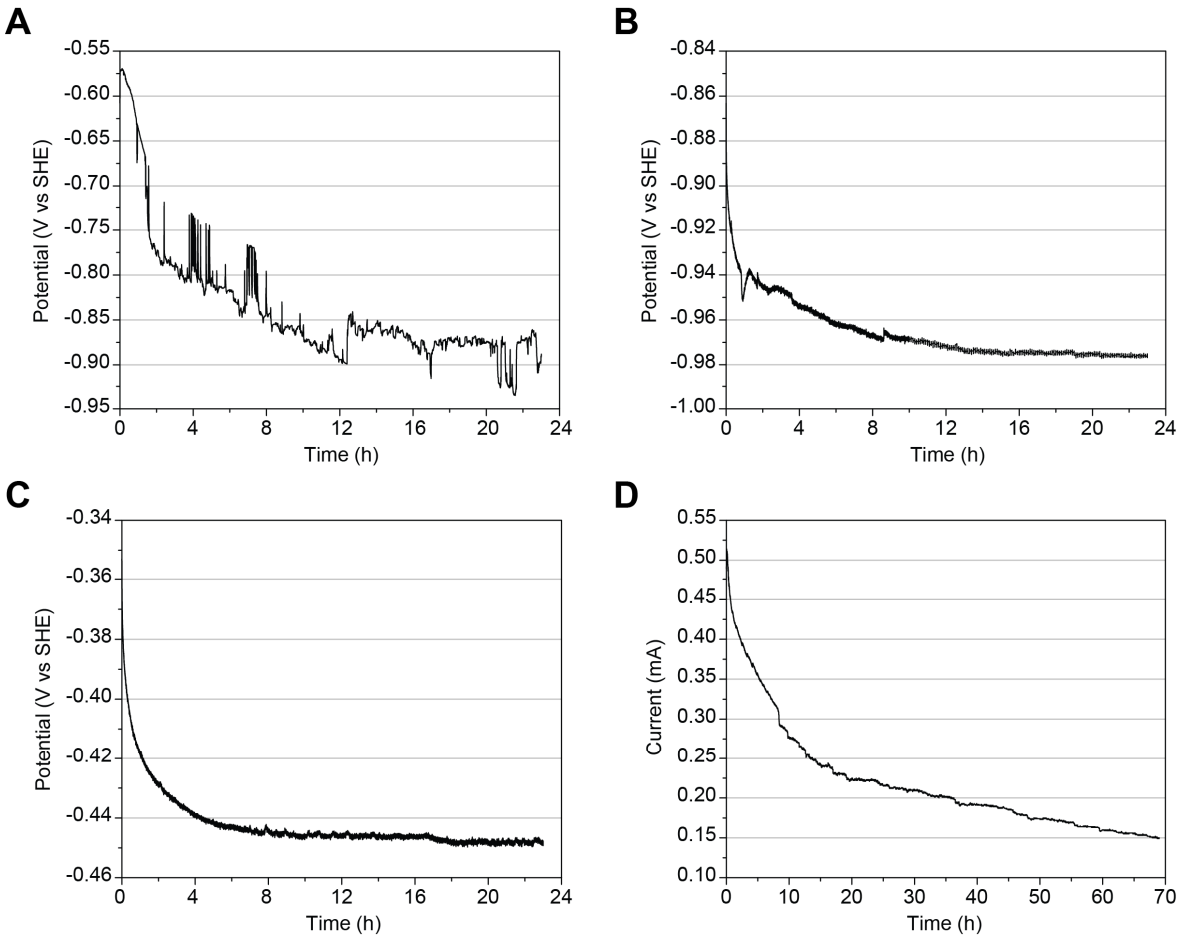

Figure 2.10. Representative galvanostatic and potentiostatic traces for (photo)electrochemical and photochemical experiments with a M. barkeri culture. For each of the galvanostatic experiments shown (A-C), a current of 2.5 mA was passed for 24 h. A standard three-electrode cell setup was used, where the anode is Pt mesh, and the cathode is as listed below. For the potentiostatic experiment (D), a two-electrode cell setup was used in which the counter and reference leads were shorted on the illuminated *n*-TiO_2 anode, and the working lead was attached to the illuminated *p*-InP/Pt cathode. The full cell potential was maintained at 0 V for 72 h. (A) Pt cathode, (B) α-NiS/C cathode, (C) n^+/*p*-Si/NiMo cathode illuminated at λ = 740 nm, and (D) *n*-TiO_2 and *p*-InP/Pt linked assembly illuminated with full spectrum and λ > 455 nm, respectively.

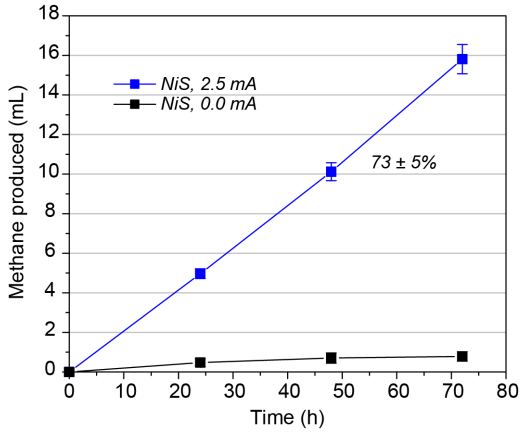

Figure 2.11. Galvanostatic experiment (2.5 mA) with α-NiS/C cathode. Experimental setup and electrode preparation is as described. Cumulative methane generation and associated average Faradaic efficiency in rich media are shown compared to a non-electrolyzed control. Error bars represent standard deviation with n = 3 independent experiments.

Photoelectrochemical generation of methane from carbon dioxide. Having performed electrochemical conversion of CO_2 to CH_4, we next sought to develop a photoelectrochemical system in which a portion of the potential required for water splitting is contributed by light. Indeed, transforming electrochemical systems to photochemical ones remains challenging. To achieve this goal, we sought to employ semiconductor photocathodes coated with a thin film HER catalyst. The overall performance of such an assembly is determined by a tradeoff between efficient catalysis and light absorption: thicker films confer superior electrocatalytic activity and stability, whereas thinner and more transparent films allow for greater photon capture. Though α-NiS proved effective as an earth-abundant HER electrocatalyst, previously published work from our laboratories on the electrodeposition of a related cobalt sulfide film on planar n^+/p-Si showed that the current density under illumination drastically diminished as the thickness of the film increased [*65*]. For this reason, we chose to employ a nickel/molybdenum alloy, a previously characterized earth-abundant HER catalyst, which has shown favorable performance under photocatalytic conditions despite having a slightly larger overpotential than platinum [*72*]. Photoactive cathodes were prepared by sputtering a thin layer of Ni/Mo alloy atop TiO_2-passivated n^+/p-Si (*Figure 2.12 A*). To confirm hydrogen evolution, abiotic galvanostatic experiments at a current of 2.5 mA (j_{avg} = 0.36 mA/cm^2) were run for 24 h while illuminating the cathode with 740 nm light (20 mW/cm^2); Faradaic efficiencies for H_2 were 103 ± 3% (*Figure 2.9*). A light toxicity control experiment with *M. barkeri* showed that methane generation is not affected by illumination at this wavelength (*Figure 2.13 A*). Biological galvanostatic electrolysis at 2.5 mA with the photocathode (740 nm illumination) generated 17.6 ± 2.1 mL CH_4 (0.692 ± 0.083 mmol) with a Faradaic efficiency of 82 ± 10% (n = 3) with only 175 mV overpotential (*Figure 2.12 B*).

Unassisted light-driven synthesis of methane from carbon dioxide. Finally, we sought to construct a fully light-driven hybrid bioinorganic system for CO_2-to-CH_4 conversion through the use of a tandem semiconductor assembly. In this setup, full-spectrum light first impinges on a large band gap anode (nanowire n-TiO_2 on fluorine-doped tin oxide (FTO)), where water oxidation generates oxygen [*37*]. The filtered, lower energy light subsequently illuminates a smaller band gap cathode (p-InP coated with Pt), where water reduction generates hydrogen (*Figure 2.12 C*). The electrochemical cell design described above required slight modifications for unassisted photochemical experiments: a 1 in diameter quartz window was added to the anodic chamber to

prevent initial filtering of the full spectrum light by glass, and the anode and cathode compartments were separated by an anion exchange membrane to minimize pH changes. This linked two-electrode assembly generates non-zero photocurrent under illumination (i_{avg} = 0.17 mA, j_{avg} = 0.057 mA/cm^2 during the first hour) (*Figure 2.10 D*). The Faradaic efficiency for hydrogen generation in abiotic experiments is 100 ± 8% (*Figure 2.9*) (n = 4). Prior to introduction of *M. barkeri* into such a system, galvanostatic control electrolyses of a *M. barkeri* culture were performed using Pt electrodes under illuminated and non-illuminated conditions. When only the *n*-TiO_2/FTO anode was used as a light filter, lower than expected Faradaic efficiencies for methane were observed in the illuminated experiment (*Figure 2.13 B*); this is in agreement with literature concerning the photosensitivity of methanogenic archaea to blue light [*58, 59*]. Installation of a 455 nm filter directly after the photoanode restored the Faradaic efficiency for methane to expected levels (*Figure 2.13 B*). Experiments to produce methane using this hybrid bioinorganic system were conducted similarly to those described earlier except headspace analysis was performed only once per experiment after 72 h. On average, 1.75 mL CH_4 (68.8 nmol) (n = 2) were produced in illuminated experiments, while only 0.58 mL CH_4 (22.8 nmol) (n = 3) were produced in identical non-illuminated controls (*Figure 2.12 D*). We note that higher background levels of methane production were observed in these unassisted photochemical experiments compared with the electrochemical and photoelectrochemical experiments and speculate that this may be due to biological corrosion of the multi-component photocathode, a phenomenon previously documented in other systems [*53, 73*]. Subtraction of the background methane results in an average Faradaic efficiency of 74%. This result clearly demonstrates the successful conversion of CO_2 to CH_4 using light as the sole energy input.

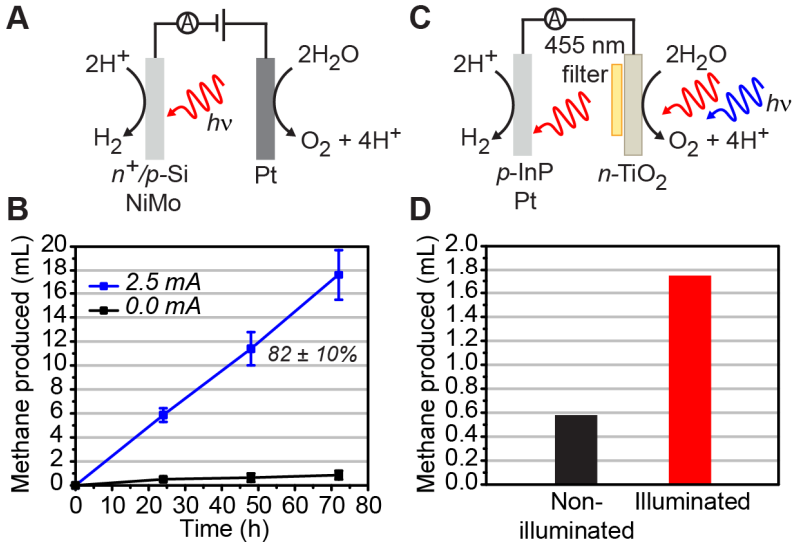

Figure 2.12. Photoelectrochemical and unassisted solar-driven conversion of carbon dioxide to methane with hybrid bioinorganic catalysts. (A) Schematic of electrode setup for photoelectrochemical water splitting. (B) Cumulative photoelectrochemically-derived methane and associated average Faradaic efficiency with a n^+/*p*-Si/NiMo photocathode illuminated with 740 nm light in rich media. Error bars represent standard deviation with n = 3 independent experiments. (C) Schematic of electrode setup for unassisted solar water splitting. (D) Average methane produced after 72 h under illuminated (n = 2) and non-illuminated (n = 3) conditions using a *n*-TiO_2 photoanode and a *p*-InP/Pt photocathode with no applied potential.

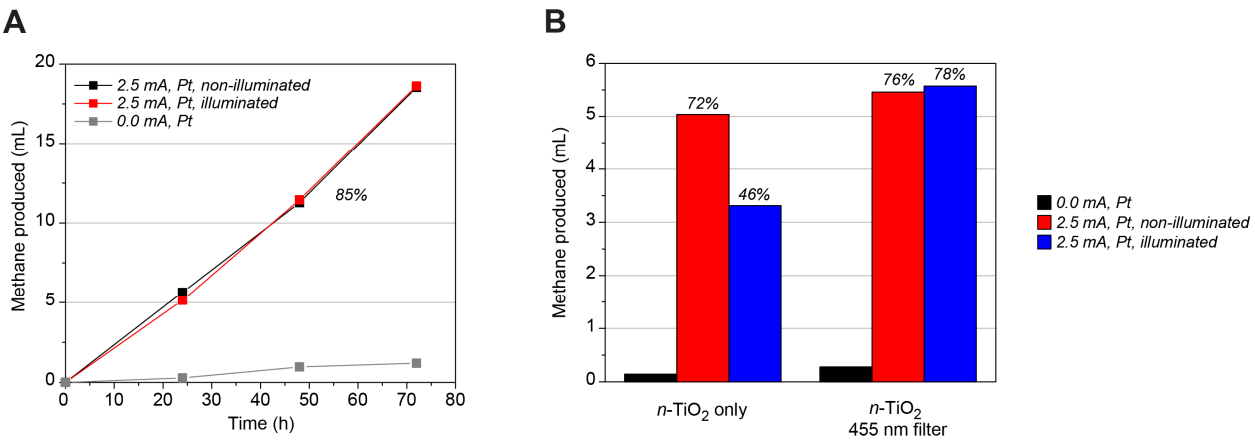

Figure 2.13. Evaluation of microbial light toxicity. Experimental setup is as described. (A) Illuminated (λ = 740 nm) and non-illuminated galvanostatic electrolyses (2.5 mA, Pt cathode) show comparable methane production, indicating that illumination with this wavelength does not affect methane production over the course of 72 h (n = 1). (B) Illuminated (full spectrum light) and non-illuminated galvanostatic electrolyses (2.5 mA, Pt cathode) were performed. When n-TiO_2/FTO was used as the only light filter, a lower than expected Faradaic efficiency for methane was observed in the illuminated experiment, indicating that blue light is toxic to the culture. Upon addition of a 455 nm filter after the n-TiO_2/FTO, Faradaic efficiencies for methane were similar between illuminated and non-illuminated experiments (n = 1).

2.4 Conclusions

In summary, we have established a hybrid bioinorganic approach to solar-to-chemical conversion by transforming carbon dioxide and water to the value-added chemical product methane. The present integrated system couples inorganic hydrogen generation catalysts powered by sustainable electrical and/or solar energy inputs with a biological catalyst that can harvest reducing equivalents from H_2 to convert carbon dioxide to methane with up to 86% Faradaic efficiency. The data show that the low aqueous solubility and mass transfer rate of hydrogen do not preclude it from being an effective molecular redox carrier and offer a starting platform for potential integration with sustainable sources of electricity (e.g. solar, wind, hydrothermal, nuclear, etc.). Indeed, a solar-to-chemical efficiency of 10% and an electrical-to-chemical efficiency of 52%, which compare favorably to previously reported systems [*74*], are possible given caveats of materials and biological integration, assuming efficiency values of 20% for solar-to-electrical conversion using a commercially available photovoltaic and 70% for electrical-to-hydrogen conversion in an optimized system [*75*], as well as 86% energetic efficiency for H_2 to CH_4 based on thermodynamic values. Furthermore, we have developed an earth-abundant nanoparticulate nickel sulfide HER catalyst that operates effectively under biologically compatible conditions. At an applied current of 7.5 mA, use of the α-NiS catalyst results in 110 mL (4.3 mmol) of methane over 7 d with a Faradaic efficiency of 74%, comparable to Pt. Moreover, we have demonstrated that use of a photoactive silicon cathode results in an overpotential of only 175 mV, allowing for greater methane generation from a defined quantity of electrical energy. Finally, combining a n-TiO_2 photoanode with a p-InP photocathode allows for fully unassisted light-driven conversion of CO_2 to CH_4. By realizing an effective artificial photosynthesis platform for the production of a value-added chemical product from light, CO_2, and water, these results provide a starting point for achieving sustainable chemistry with materials biology.

2.5 References

1. Lewis, N. S., Nocera, D. G., Powering the planet: Chemical challenges in solar energy utilization. *Proc. Natl. Acad. Sci. U.S.A.* **2006**, 103(43) 15729-15735.

2. Gray, H. B., Powering the planet with solar fuel. *Nat. Chem.* **2009**, 1(1) 7.

3. Meyer, T. J., Chemical approaches to artificial photosynthesis. *Acc. Chem. Res.* **1989**, 22(5) 163-170.

4. Benson, E. E., Kubiak, C. P., Sathrum, A. J., Smieja, J. M., Electrocatalytic and homogeneous approaches to conversion of CO_2 to liquid fuels. *Chem. Soc. Rev.* **2009**, 38(1) 89-99.

5. Morris, A. J., Meyer, G. J., Fujita, E., Molecular approaches to the photocatalytic reduction of carbon dioxide for solar fuels. *Acc. Chem. Res.* **2009**, 42(12) 1983-1994.

6. Finn, C., Schnittger, S., Yellowlees, L. J., Love, J. B., Molecular approaches to the electrochemical reduction of carbon dioxide. *Chem. Commun.* **2012**, 48(10) 1392-1399.

7. Appel, A. M., Bercaw, J. E., Bocarsly, A. B., Dobbek, H., DuBois, D. L., Dupuis, M., Ferry, J. G., Fujita, E., Hille, R., Kenis, P. J., Kerfeld, C. A., Morris, R. H., Peden, C. H., Portis, A. R., Ragsdale, S. W., Rauchfuss, T. B., Reek, J. N., Seefeldt, L. C., Thauer, R. K.,Waldrop, G. L., Frontiers, opportunities, and challenges in biochemical and chemical catalysis of CO_2 fixation. *Chem. Rev.* **2013**, 113(8) 6621-6658.

8. Costentin, C., Robert, M., Saveant, J. M., Catalysis of the electrochemical reduction of carbon dioxide. *Chem. Soc. Rev.* **2013**, 42(6) 2423-2436.

9. Fisher, B. J., Eisenberg, R., Electrocatalytic reduction of carbon dioxide by using macrocycles of nickel and cobalt. *J. Am. Chem. Soc.* **1980**, 102(24) 7361-7363.

10. Hawecker, J., Lehn, J., Ziessel, R., Electrocatalytic reduction of carbon dioxide mediated by $Re(bipy)(CO)_3Cl$ (bipy = 2,2'-bipyridine). *J. Chem. Soc., Chem. Commun.* **1984**, 6(6) 328-330.

11. Beley, M., Collin, J. P., Ruppert, R., Sauvage, J. P., Electrocatalytic reduction of carbon dioxide by nickel $cyclam^{2+}$ in water: Study of the factors affecting the efficiency and the selectivity of the process. *J. Am. Chem. Soc.* **1986**, 108(24) 7461-7467.

12. Bourrez, M., Molton, F., Chardon-Noblat, S., Deronzier, A., $[Mn(bipyridyl)(CO)_3Br]$: An abundant metal carbonyl complex as efficient electrocatalyst for CO_2 reduction. *Angew. Chem. Int. Ed. Engl.* **2011**, 50(42) 9903-9906.

13. Schneider, J., Jia, H., Kobiro, K., Cabelli, D. E., Muckerman, J. T., Fujita, E., Nickel(II) macrocycles: Highly efficient electrocatalysts for the selective reduction of CO_2 to CO. *Energy Environ. Sci.* **2012**, 5(11) 9502-9510.

14. Kang, P., Meyer, T. J., Brookhart, M., Selective electrocatalytic reduction of carbon dioxide to formate by a water-soluble iridium pincer catalyst. *Chem. Sci.* **2013**, 4(9) 3497-3502.

15. Thoi, V. S., Kornienko, N., Margarit, C. G., Yang, P., Chang, C. J., Visible-light photoredox catalysis: Selective reduction of carbon dioxide to carbon monoxide by a nickel N-heterocyclic carbene-isoquinoline complex. *J. Am. Chem. Soc.* **2013**, 135(38) 14413-14424.

16. Agarwal, J., Shaw, T. W., Stanton, C. J., Majetich, G. F., Bocarsly, A. B., Schaefer, H. F., NHC-containing manganese(I) electrocatalysts for the two-electron reduction of CO_2. *Angew. Chem. Int. Ed. Engl.* **2014**, 53(20) 5152-5155.

17. Hori, Y., Electrochemical CO_2 reduction on metal electrodes. *Modern aspects of electrochemistry, No. 42,* eds Vayenas, C. G., White, R. E., Gamboa-Aldeco, M. E., (Springer, New York) **2008**, pp 89-189.

18. Kumar, B., Llorente, M., Froehlich, J., Dang, T., Sathrum, A., Kubiak, C. P., Photochemical and photoelectrochemical reduction of CO_2. *Annu. Rev. Phys. Chem.* **2012**, 63541-569.

19. Barton, E. E., Rampulla, D. M., Bocarsly, A. B., Selective solar-driven reduction of CO_2 to methanol using a catalyzed p-GaP based photoelectrochemical cell. *J. Am. Chem. Soc.* **2008**, 130(20) 6342-6344.

20. Rosen, B. A., Salehi-Khojin, A., Thorson, M. R., Zhu, W., Whipple, D. T., Kenis, P. J., Masel, R. I., Ionic liquid-mediated selective conversion of CO_2 to CO at low overpotentials. *Science* **2011**, 334(6056) 643-644.

21. Zhu, W., Michalsky, R., Metin, O., Lv, H., Guo, S., Wright, C. J., Sun, X., Peterson, A. A., Sun, S., Monodisperse Au nanoparticles for selective electrocatalytic reduction of CO_2 to CO. *J. Am. Chem. Soc.* **2013**, 135(45) 16833-16836.

22. Kim, D., Resasco, J., Yu, Y., Asiri, A. M., Yang, P., Synergistic geometric and electronic effects for electrochemical reduction of carbon dioxide using gold-copper bimetallic nanoparticles. *Nat. Commun.* **2014**, 5:4948 doi: 10.1038/ncomms5948.

23. Lu, Q., Rosen, J., Zhou, Y., Hutchings, G. S., Kimmel, Y. C., Chen, J. G., Jiao, F., A selective and efficient electrocatalyst for carbon dioxide reduction. *Nat. Commun.* **2014**, 5:3242 doi: 10.1038/ncomms4242.

24. Zhang, S., Kang, P., Ubnoske, S., Brennaman, M. K., Song, N., House, R. L., Glass, J. T., Meyer, T. J., Polyethylenimine-enhanced electrocatalytic reduction of CO_2 to formate at nitrogen-doped carbon nanomaterials. *J. Am. Chem. Soc.* **2014**, 136(22) 7845-7848.

25. Medina-Ramos, J., Pupillo, R. C., Keane, T. P., DiMeglio, J. L., Rosenthal, J., Efficient conversion of CO_2 to CO using tin and other inexpensive and easily prepared post-transition metal catalysts. *J. Am. Chem. Soc.* **2015**, 137(15) 5021-5027.

26. Min, X., Kanan, M. W., Pd-catalyzed electrohydrogenation of carbon dioxide to formate: High mass activity at low overpotential and identification of the deactivation pathway. *J. Am. Chem. Soc.* **2015**, 137(14) 4701-4708.

27. Parkinson, B. A., Weaver, P. F., Photoelectrochemical pumping of enzymatic CO_2 reduction. *Nature* **1984**, 309(5964) 148-149.

28. Shin, W., Lee, S. H., Shin, J. W., Lee, S. P., Kim, Y., Highly selective electrocatalytic conversion of CO_2 to CO at -0.57 V (NHE) by carbon monoxide dehydrogenase from *Moorella thermoacetica*. *J. Am. Chem. Soc.* **2003**, 125(48) 14688-14689.

29. Parkin, A., Seravalli, J., Vincent, K. A., Ragsdale, S. W., Armstrong, F. A., Rapid and efficient electrocatalytic CO_2/CO interconversions by *Carboxydothermus hydrogenoformans* CO dehydrogenase I on an electrode. *J. Am. Chem. Soc.* **2007**, 129(34) 10328-10329.

30. Reda, T., Plugge, C. M., Abram, N. J., Hirst, J., Reversible interconversion of carbon dioxide and formate by an electroactive enzyme. *Proc. Natl. Acad. Sci. U.S.A.* **2008**, 105(31) 10654-10658.

31. Woolerton, T. W., Sheard, S., Reisner, E., Pierce, E., Ragsdale, S. W., Armstrong, F. A., Efficient and clean photoreduction of CO_2 to CO by enzyme-modified TiO_2 nanoparticles using visible light. *J. Am. Chem. Soc.* **2010**, 132(7) 2132-2133.

32. Gust, D., Moore, T. A., Moore, A. L., Mimicking photosynthetic solar energy transduction. *Acc. Chem. Res.* **2001**, 34(1) 40-48.

33. Magnuson, A., Anderlund, M., Johansson, O., Lindblad, P., Lomoth, R., Polivka, T., Ott, S., Stensjo, K., Styring, S., Sundstrom, V., Hammarstrom, L., Biomimetic and microbial approaches to solar fuel generation. *Acc. Chem. Res.* **2009**, 42(12) 1899-1909.

34. Armstrong, F. A., Hirst, J., Reversibility and efficiency in electrocatalytic energy conversion and lessons from enzymes. *Proc. Natl. Acad. Sci. U.S.A.* **2011**, 108(34) 14049-14054.

35. Braun, A., Boudoire, F., Bora, D. K., Faccio, G., Hu, Y., Kroll, A., Mun, B. S., Wilson, S. T., Biological components and bioelectronic interfaces of water splitting photoelectrodes for solar hydrogen production. *Chem. Eur. J.* **2015**, 21(11) 4188-4199.

36. Liu, C., Gallagher, J. J., Sakimoto, K. K., Nichols, E. M., Chang, C. J., Chang, M. C., Yang, P., Nanowire-bacteria hybrids for unassisted solar carbon dioxide fixation to value-added chemicals. *Nano Lett.* **2015**, doi: 10.1021/acs.nanolett.5b01254.

37. Liu, C., Tang, J., Chen, H. M., Liu, B., Yang, P., A fully integrated nanosystem of semiconductor nanowires for direct solar water splitting. *Nano Lett.* **2013**, 13(6) 2989-2992.

38. Nevin, K. P., Woodard, T. L., Franks, A. E., Summers, Z. M., Lovley, D. R., Microbial electrosynthesis: Feeding microbes electricity to convert carbon dioxide and water to multicarbon extracellular organic compounds. *MBio* **2010**, 1(2) e00103-10. doi:10.1128/mBio.00103-10.

39. Rabaey, K., Rozendal, R. A., Microbial electrosynthesis - revisiting the electrical route for microbial production. *Nat. Rev. Microbiol.* **2010**, 8(10) 706-716.

40. Lovley, D. R., Nevin, K. P., Electrobiocommodities: Powering microbial production of fuels and commodity chemicals from carbon dioxide with electricity. *Curr. Opin. Biotechnol.* **2013**, 24(3) 385-390.

41. Li, H., Opgenorth, P. H., Wernick, D. G., Rogers, S., Wu, T. Y., Higashide, W., Malati, P., Huo, Y. X., Cho, K. M., Liao, J. C., Integrated electromicrobial conversion of CO_2 to higher alcohols. *Science* **2012**, 335(6076) 1596.

42. Torella, J. P., Gagliardi, C. J., Chen, J. S., Bediako, D. K., Colon, B., Way, J. C., Silver, P. A., Nocera, D. G., Efficient solar-to-fuels production from a hybrid microbial-water-splitting catalyst system. *Proc. Natl. Acad. Sci. U.S.A.* **2015**, 112(8) 2337-2342.

43. Hori, Y., Takahashi, I., Koga, O., Hoshi, N., Selective formation of C2 compounds from electrochemical reduction of CO_2 at a series of copper single crystal electrodes. *J. Phys. Chem. B* **2002**, 106(1) 15-17.

44. Manthiram, K., Beberwyck, B. J., Alivisatos, A. P., Enhanced electrochemical methanation of carbon dioxide with a dispersible nanoscale copper catalyst. *J. Am. Chem. Soc.* **2014**, 136(38) 13319-13325.

45. Meng, X., Wang, T., Liu, L., Ouyang, S., Li, P., Hu, H., Kako, T., Iwai, H., Tanaka, A., Ye, J., Photothermal conversion of CO_2 into CH_4 with H_2 over group VIII nanocatalysts: An alternative approach for solar fuel production. *Angew. Chem. Int. Ed. Engl.* **2014**, 53(43) 11478-11482.

46. Thauer, R. K., Biochemistry of methanogenesis: A tribute to Marjory Stephenson. 1998 Marjory Stephenson Prize Lecture. *Microbiology* **1998**, 144 (Pt 9) 2377-2406.

47. Anbarasan, P., Baer, Z. C., Sreekumar, S., Gross, E., Binder, J. B., Blanch, H. W., Clark, D. S., Toste, F. D., Integration of chemical catalysis with extractive fermentation to produce fuels. *Nature* **2012**, 491(7423) 235-239.

48. Sirasani, G., Tong, L., Balskus, E. P., A biocompatible alkene hydrogenation merges organic synthesis with microbial metabolism. *Angew. Chem. Int. Ed. Engl.* **2014**, 53(30) 7785-7788.

49. Schlegel, H. G., Lafferty, R., Growth of 'Knallgas' bacteria (*Hydrogenomonas*) using direct electrolysis of the culture medium. *Nature* **1965**, 205(4968) 308-309.

50. Song, J., Kim, Y., Lim, M., Lee, H., Lee, J. I., Shin, W., Microbes as electrochemical CO_2 conversion catalysts. *ChemSusChem* **2011**, 4(5) 587-590.

51. Cheng, S., Xing, D., Call, D. F., Logan, B. E., Direct biological conversion of electrical current into methane by electromethanogenesis. *Environ. Sci. Technol.* **2009**, 43(10) 3953-3958.

52. Van Eerten-Jansen, M. C., Veldhoen, A. B., Plugge, C. M., Stams, A. J., Buisman, C. J., Ter Heijne, A., Microbial community analysis of a methane-producing biocathode in a bioelectrochemical system. *Archaea* **2013**, 2013481784.

53. Siegert, M., Yates, M. D., Call, D. F., Zhu, X., Spormann, A., Logan, B. E., Comparison of nonprecious metal cathode materials for methane production by electromethanogenesis. *A.C.S. Sustain. Chem. Eng.* **2014**, 2(4) 910-917.

54. Fast, A. G., Papoutsakis, E. T., Stoichiometric and energetic analyses of non-photosynthetic CO_2-fixation pathways to support synthetic biology strategies for production of fuels and chemicals. *Curr. Opin. Chem. Eng.* **2012**, 1(4) 380-395.

55. Mah, R. A., Smith, M. R., Baresi, L., Studies on an acetate-fermenting strain of *Methanosarcina*. *Appl. Environ. Microbiol.* **1978**, 35(6) 1174-1184.

56. Villano, M., Aulenta, F., Ciucci, C., Ferri, T., Giuliano, A., Majone, M., Bioelectrochemical reduction of CO_2 to CH_4 via direct and indirect extracellular electron transfer by a hydrogenophilic methanogenic culture. *Bioresour. Technol.* **2010**, 101(9) 3085-3090.

57. Liu, B., Aydil, E. S., Growth of oriented single-crystalline rutile TiO_2 nanorods on transparent conducting substrates for dye-sensitized solar cells. *J. Am. Chem. Soc.* **2009**, 131(11) 3985-3990.

58. Olson, K. D., McMahon, C. W., Wolfe, R. S., Light sensitivity of methanogenic archaebacteria. *Appl. Environ. Microbiol.* **1991**, 57(9) 2683-2686.

59. Lyon, E. J., Shima, S., Buurman, G., Chowdhuri, S., Batschauer, A., Steinbach, K., Thauer, R. K., UV-A/blue-light inactivation of the 'metal-free' hydrogenase (Hmd) from methanogenic archaea. *Eur. J. Biochem.* **2004**, 271(1) 195-204.

60. Cobo, S., Heidkamp, J., Jacques, P. A., Fize, J., Fourmond, V., Guetaz, L., Jousselme, B., Ivanova, V., Dau, H., Palacin, S., Fontecave, M., Artero, V., A janus cobalt-based catalytic material for electro-splitting of water. *Nat. Mater.* **2012**, 11(9) 802-807.

61. Callejas, J. F., McEnaney, J. M., Read, C. G., Crompton, J. C., Biacchi, A. J., Popczun, E. J., Gordon, T. R., Lewis, N. S., Schaak, R. E., Electrocatalytic and photocatalytic hydrogen production from acidic and neutral-pH aqueous solutions using iron phosphide nanoparticles. *A.C.S. Nano* **2014**, 8(11) 11101-11107.

62. Gong, M., Zhou, W., Tsai, M. C., Zhou, J., Guan, M., Lin, M. C., Zhang, B., Hu, Y., Wang, D. Y., Yang, J., Pennycook, S. J., Hwang, B. J., Dai, H., Nanoscale nickel oxide/nickel heterostructures for active hydrogen evolution electrocatalysis. *Nat. Commun.* **2014**, 54695 doi: 10.1038/ncomms5695.

63. Jiang, N., You, B., Sheng, M., Sun, Y., Electrodeposited cobalt-phosphorous-derived films as competent bifunctional catalysts for overall water splitting. *Angew. Chem. Int. Ed. Engl.* **2015**, 127doi: 10.1002/anie.201501616.

64. Kong, D., Cha, J. J., Wang, H., Lee, H. R., Cui, Y., First-row transition metal dichalcogenide catalysts for hydrogen evolution reaction. *Energy Environ. Sci.* **2013**, 6(12) 3553-3558.

65. Sun, Y., Liu, C., Grauer, D. C., Yano, J., Long, J. R., Yang, P., Chang, C. J., Electrodeposited cobalt-sulfide catalyst for electrochemical and photoelectrochemical hydrogen generation from water. *J. Am. Chem. Soc.* **2013**, 135(47) 17699-17702.

66. Di Giovanni, C., Wang, W., Nowak, S., Grenèche, J., Lecoq, H., Mouton, L., Giraud, M., Tard, C., Bioinspired iron sulfide nanoparticles for cheap and long-lived electrocatalytic molecular hydrogen evolution in neutral water. *A.C.S. Catalysis* **2014**, 4(2) 681-687.

67. Jiang, N., Bogoev, L., Popova, M., Gul, S., Yano, J., Sun, Y., Electrodeposited nickel-sulfide films as competent hydrogen evolution catalysts in neutral water. *J. Mater. Chem. A* **2014**, 2(45) 19407-19414.

68. Feng, L., Li, G., Liu, Y., Wu, Y., Chen, H., Wang, Y., Zou, Y., Wang, D., Zou, X., Carbon-armored Co_9S_8 nanoparticles as all-pH efficient and durable H_2-evolving electrocatalysts. *A.C.S. Appl. Mater. Interfaces* **2015**, 7(1) 980-988.

69. Tang, C., Pu, Z., Liu, Q., Asiri, A. M., Luo, Y., Sun, X., Ni_3S_2 nanosheets array supported on Ni foam: A novel efficient three-dimensional hydrogen-evolving electrocatalyst in both neutral and basic solutions. *Int. J. Hydrogen Energy* **2015**, 40(14) 4727-4732.

70. Tang, C., Pu, Z., Liu, Q., Asiri, A. M., Sun, X., NiS_2 nanosheets array grown on carbon cloth as an efficient 3D hydrogen evolution cathode. *Electrochim. Acta* **2015**, 153508-514.

71. Conway, B. E., Tilak, B. V., Interfacial processes involving electrocatalytic evolution and oxidation of H_2, and the role of chemisorbed H. *Electrochim. Acta* **2002**, 47(22-23) 3571-3594.

72. McKone, J. R., Marinescu, S. C., Brunschwig, B. S., Winkler, J. R., Gray, H. B., Earth-abundant hydrogen evolution electrocatalysts. *Chem. Sci.* **2014**, 5(3) 865-878.

73. Daniels, L., Belay, N., Rajagopal, B. S., Weimer, P. J., Bacterial methanogenesis and growth from CO_2 with elemental iron as the sole source of electrons. *Science* **1987**, 237(4814) 509-511.

74. Jhong, H., Ma, S., Kenis, P. J., Electrochemical conversion of CO_2 to useful chemicals: Current status, remaining challenges, and future opportunities. *Curr. Opin. Chem. Eng.* **2013**, 2(2) 191-199.

75. Zeng, K., Zhang, D., Recent progress in alkaline water electrolysis for hydrogen production and applications. *Prog. Energy Combust. Sci.* **2010**, 36(3) 307-326.

Chapter 3: *Nanowire-bacteria hybrids for unassisted solar carbon dioxide fixation to value-added chemicals*

This work was published in the following scientific journal:

Liu, C.,* Gallagher, J. J.,* Sakimoto, K. K., Nichols, E. M., Chang, C. J., Chang, M. C. Y., Yang, P., Nanowire–bacteria hybrids for unassisted solar carbon dioxide fixation to value-added chemicals. *Nano Lett.* **2015**, 15(5) 3634-3639. (*These authors contributed equally to this work.)

This work was performed in collaboration with the following person:

All studies were performed in close collaboration with Chong Liu, who designed, built and optimized the solar-powered nanowire device for acetate production.

3.1 Introduction

Natural photosynthesis, which harvests 130 terawatts of solar energy annually to generate up to 115 billion metric tons of biomass from the reduction of CO_2, provides motivation for the development of artificial systems that can capture the energy of the sun to convert CO_2 and H_2O into value-added chemicals of societal benefit [*1-9*]. However, such an approach has not been fully realized owing to a host of unmet basic scientific challenges [*10*]. For example, enzymes isolated from microorganisms and plants can selectively catalyze CO_2 reduction with low energy barriers [*11-13*]; however, they do not self-repair outside their native cellular context and are often intolerant to oxygen. Consequently, bio-derived CO_2-reducing catalytic systems are not directly applicable to oxygen-containing CO_2 sources such as flue gas. Another challenge for artificial photosynthesis is the selective synthesis of complex organic molecules [*13-16*]. Nature transforms CO_2 into a variety of complex molecules using a limited number of biosynthetic intermediates as building blocks [*17*]. However, in the case of artificial photosynthesis, the selection of such an intermediate is difficult [*3, 13, 17*]: ideally, mass transport requires it to be water-soluble and it should also be easily incorporated into many biosynthetic pathways [*18*].

Guided by these constraints, we sought to develop a strategy for artificial photosynthesis, where biocatalysts in their native cellular environments are interfaced directly with semiconductor light-absorbers for unassisted solar CO_2 reduction. Specifically, we envisioned a two-step strategy that mimics natural photosynthesis, where light capture by a biocompatible nanowire array can interface and directly provide reducing equivalents to living organisms for the targeted synthesis of value-added chemical products from CO_2 (*Figure 3.1*). Such an integration of materials science and biology separates the demanding dual requirements for light-capture efficiency and catalytic activity and provides a route to link efficient solar conversion in robust solid-state devices with the broad synthetic capabilities of living cells [*10*].

Here, employing these design principles, we demonstrate a stand-alone, solar-powered device[*6, 19-23*] comprised of silicon (Si) and titanium dioxide (TiO_2) nanowire arrays as the light-capturing units [*21*], which mimic the "Z-scheme" [*2, 24, 25*] of photosynthesis, and *Sporomusa ovata* as the cellular catalyst [*26, 27*], which can effectively reduce CO_2 to acetate under mild conditions (*e.g.* neutral pH and temperatures under 30 °C). Additionally, by employing the nanowire array we were able to stably cultivate strict anaerobes under an aerobic gas headspace (21% O_2) by creating a local anaerobic environment within the array. The nanowire morphology affords high reaction rates of *S. ovata* (up to *ca.* 2 $mol \cdot m^{-3} \cdot sec^{-1}$) that are comparable to conventional high-temperature gas phase catalysis (*e.g.* Fischer-Tropsch, water-gas shift, and cracking reactions) [*28*]. Also, the acetate intermediate represents a biosynthetic precursor to a wide variety of potential fine and commodity chemicals *via* acetyl coenzyme A (acetyl-CoA), including functionalized aliphatics and aromatics, lipids, alkanes, as well as complex natural products. By simply selecting specific genetically engineered *Escherichia coli* strains [*18, 29-31*], this hybrid nanowire-bacteria system can be programmed to produce a variety of products with minimal modification, providing a versatile and amenable platform for solar-driven CO_2 reduction to value-added fuels, chemicals, and materials.

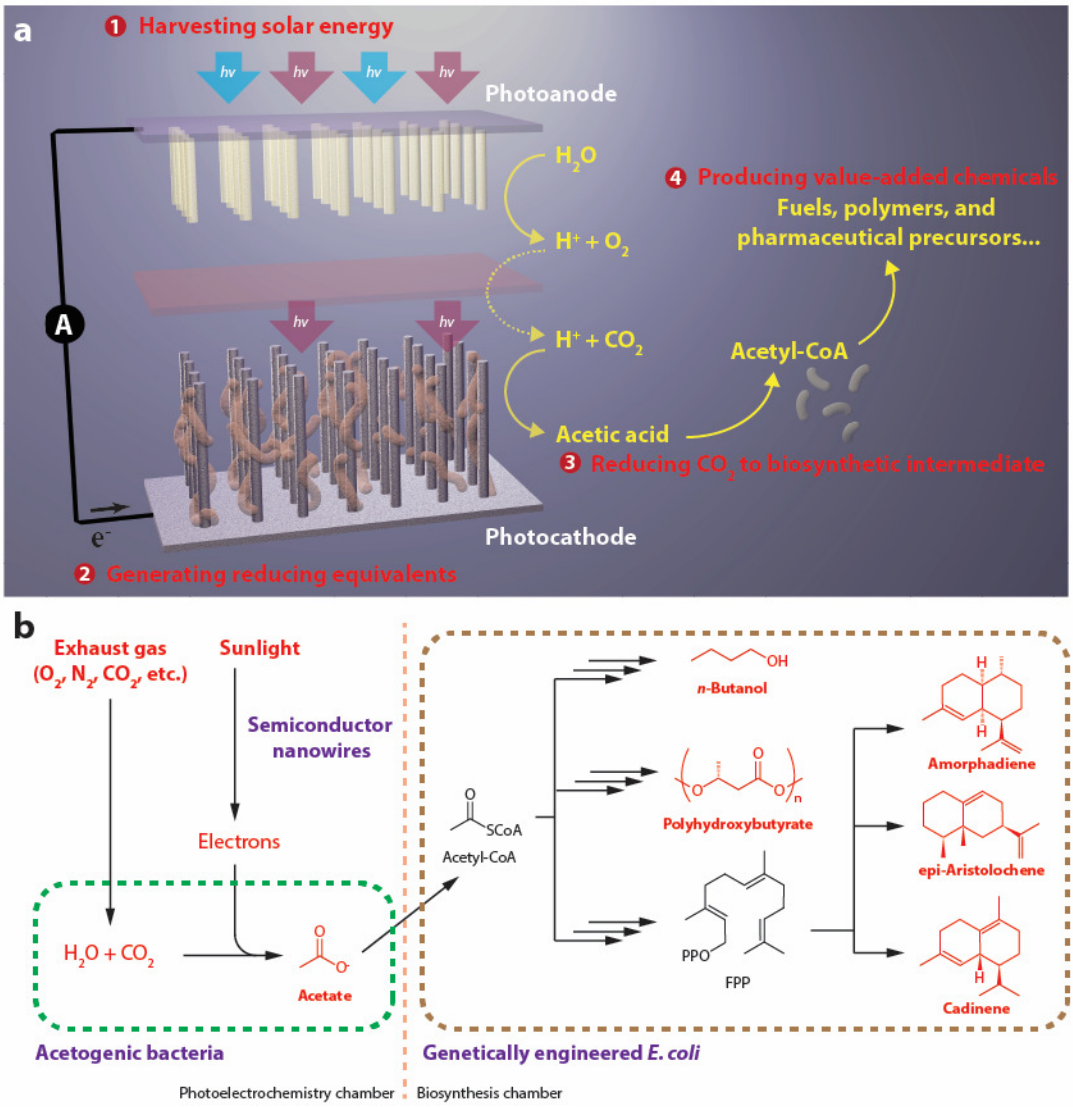

Figure 3.1. Schematic of a general artificial photosynthesis approach. (a) The proposed approach for solar-powered CO_2 fixation includes four steps: 1) harvesting solar energy; 2) generating reducing equivalents; 3) reducing CO_2 to biosynthetic intermediates; 4) producing value-added chemicals. An integration of materials science and biology, the nanowire-bacteria hybrids combine the advantages of solid-state devices with living organisms. (b) As a proof of concept, we demonstrate that under mild conditions sunlight can provide the energy to directly treat exhaust gas and generate acetate as the biosynthetic intermediate, which is upgraded into liquid fuels, biopolymers, and pharmaceutical precursors. FPP, farnesyl pyrophosphate.

3.2 Materials and methods

Preparation of Si and TiO_2 nanowire arrays. Silicon (Si) nanowire arrays were fabricated using reactive-ion etching of patterned single-crystalline Si wafers, based on a previous report [*21*]. To obtain Si nanowire photocathodes with enhanced performance, a thin, highly doped n^+ layer was formed on the surface of the lightly doped *p*-Si nanowires for better photovoltage output, similar to a previously reported approach [*21, 32*]. In addition, a 30 nm conformal-coated TiO_2 layer was deposited at 300 °C in a home-built atomic layer deposition (ALD) setup in order to maintain stable performance in a pH neutral electrolyte for prolonged periods of time[*33*]. Moreover, about 10 nm Ni was quasi-conformal sputtered onto the electrode, to enhance the charge transfer from the electrode to the bacteria. Similar co-deposition of Pt and Ni was realized for the oxygen-tolerant nanowire-bacteria composite electrode. On the other hand, titanium oxide (TiO_2) nanowire photoanodes were synthesized *via* hydrothermal methods reported in the literature [*21, 34*]. After growth, the nanowire electrode was annealed in air for 30 min at 450 °C and coated with 10 nm TiO_2 *via* ALD to enhance photoresponse [*35*].

Electrochemical and photoelectrochemical (PEC) characterization. All experiments were performed within a set of custom-built PEC cells, whose basic structure is shown in (*Figure 3.2 a*). The setup is a two-chamber PEC cell with the working electrode and reference electrode (Ag/AgCl, 1M KCl, CH Instruments, Inc.) in one chamber and the Pt wire counter electrode in the other chamber. A Nafion 117 membrane (Sigma-Aldrich) separates the two chambers. Each chamber has a gas inlet/outlet. The purging gas for each chamber can be independently defined. A peristaltic pump (IDEX Health & Science LLC) is used for media exchange via a solution inlet port in each chamber. Each chamber contains a quartz window for PEC experiments. During experiments the setup was left at ambient temperature, which fluctuated between 20-26 °C. For unassisted solar-driven CO_2 reduction a third photoanode chamber was connected to the working electrode chamber to accommodate a photoanode of the same surface area as the photocathode. A second Nafion 117 membrane separated the two chambers (*Figure 3.2 b*).

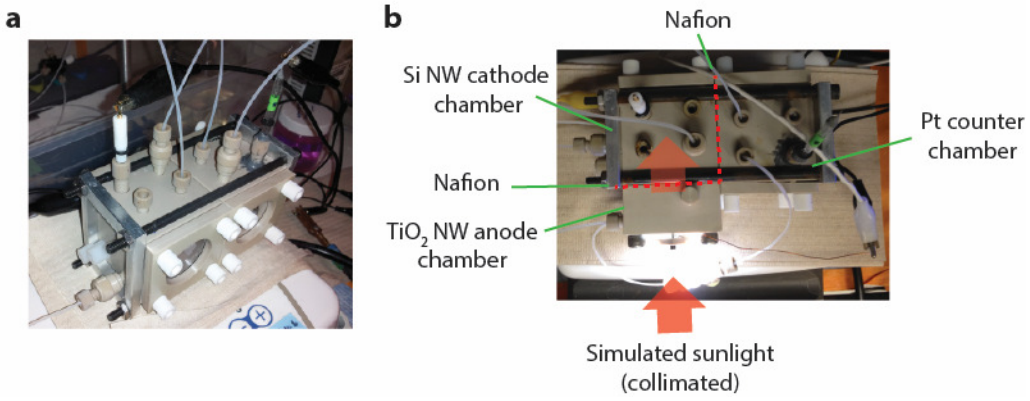

Figure 3.2. Electrochemical and photoelectrochemical (PEC) setup. (a) Image of the two-chamber electrochemical setup for CO_2 reduction with a nanowire-bacteria hybrid photocathode. (b) Three-chamber PEC setup for unassisted solar CO_2 reduction using the integrated system. Here, one collimated light beam illuminates first a TiO_2 nanowire photoanode (through its back side), second the Nafion membrane that separates the photocathode and photoanode chambers, and finally the Si nanowire-bacteria photocathode. The Pt counter electrode chamber was used during the incubation period of integrating *S. ovata* into the Si electrode.

Electrochemical and PEC measurements were performed using Gamry Interface 1000 potentiostats. The uncertainty of voltage reported here is about 30 mV. The pH of the brackish water solution is typically between 6.3-6.7 during the measurement. Since the reported voltage is *versus* reversible hydrogen electrode (RHE), the following calculation was used:

$$\mathrm{V}\ vs.\ \mathrm{RHE\ (volt)} = \mathrm{V\ vs.\ Ag/AgCl\ (volt)} + 0.209\ \mathrm{(volt)} + 0.059 \times \mathrm{pH}$$

The overpotential η for CO_2 reduction into acetic acid is defined as the voltage difference between the applied electrochemical bias and the standard electrochemical potential for CO_2 reduction into acetic acid:

$$\eta\ \mathrm{(volt)} = \mathrm{V}\ vs.\ \mathrm{RHE\ (volt)} + 0.143\ \mathrm{(volt)}$$

Collimated light from a 300W Xenon lamp with AM 1.5G filter (Newport, Corp.) was used for unassisted solar-powered CO_2 fixation experiments, while a 740 nm uniform illumination LED (Mightex Systems, 21 mW/cm^2) was used for experiments with the Si nanowire-bacteria photocathode alone. The energy conversion efficiency of the unassisted solar-powered CO_2 reduction was calculated according to the following equation:

$$\text{energy conversion efficiency}\ (100\%) = \frac{1.09\ \mathrm{V} \times \mathrm{i(A \cdot cm^{-2})}}{0.1\ \mathrm{W \cdot cm^{-2}}}$$

Here $\mathrm{i(A \cdot cm^{-2})}$ is the current density of the electrode, $0.1\ \mathrm{W \cdot cm^{-2}}$ the light intensity of the simulated sunlight and 1.09 V the thermodynamic potential needed to reduce CO_2 to acetate [*36*]:

$$2\ CO_2 + 2\ H_2O \rightarrow CH_3COOH + 2\ O_2 \qquad \Delta E^{o}_{overall} = 1.09\ \mathrm{V}$$

Integration of electrodes with bacterium *S. ovata*. An inoculum of *S. ovata* was grown under strict anaerobic conditions in a Balch tube at 30 °C. For autotrophic growth of *S. ovata* hydrogen was used as the electron donor (80% H_2/20% CO_2). A brackish water medium modified from the DSMZ-recommended growth medium (DSMZ 311) was used for growth (see *Media for S. ovata culturing*). Such a "phosphate-enhanced" medium helps the mass transport of protons during electrochemical CO_2 reduction [*37*], thus preventing a local pH change near the electrode that may hinder the colonization by *S. ovata*. To achieve higher acetic acid concentrations, a slightly modified M9-MOPS minimal medium was used (see *Media for S. ovata culturing*). *S. ovata* was gradually adapted to growth in M9-MOPS medium. The medium was functional for solar-driven CO_2 reduction, achieving an acetic acid concentration of ~6 g/L (~100 mM).

The bacteria were seeded into the electrode within the electrochemical cells using organic-free minimal media, similar to previously reported methods [*27*]. Unless specifically mentioned, the sparging gas is 20% CO_2/80% N_2, and the media contains no organic carbon source except a trace vitamin supplement. In general, 10% inoculation was conducted in the cathode chamber of an assembled electrochemical cell, where the cathode/photocathode was constantly biased at -0.1 V *vs*. RHE. The dispersion was cultured for 12 hours under an 80% H_2/20% CO_2 environment, and then 2/3 of the electrolyte was replaced with fresh media. The culture was incubated for 24 hours

under 20% CO_2/80% N_2, and again 2/3 of the electrolyte was replaced with fresh media. At this stage the electrochemical bias was maintained, and the nanowire cathode acted as the sole electron donor for bacterial metabolism. After two more cycles of this media exchange procedure, the nanowire-bacteria hybrid electrode is obtained in the cathode chamber with minimal planktonic cells suspended in the bulk solution. At which point, the nano-bio hybrids are ready for use.

After the experiment, the Si nanowire-bacteria hybrid electrode was examined by SEM. Specifically, critical point drying was used for the nanowire electrode samples to minimize the effect of capillary force. The cell loading density was determined by counting the number of cells within a given area of the SEM images. Four replicates were performed for each condition (n = 4), and more than 5000 cells were counted in each replicate. In the case of the planar electrode, the electrode area was directly measured from a top-down view in SEM. In the case of the nanowire-bacteria composite electrode, cross-section SEM images were taken, and it was assumed that the visible cells in the SEM images are only within one unit cell of the nanowire array lattice (2 μm). Based on this assumption, the cell loading density over the projected electrode was determined.

Oxygen tolerance measurements were performed under similar conditions as described above. *S. ovata* was introduced into the working electrode chamber, and the nanowire-bacteria hybrids were formed under a constant electrochemical bias (-0.2 V *vs*. RHE). Then the purging gas was switched to 21% O_2/10% CO_2/69 % N_2, and the electrochemical cell was electrolyzed for five more days, during which time the composition of the solution was analyzed twice.

Media for *S. ovata* culturing. The composition of the modified medium ("phosphate-enhanced medium") is as follows per 1000 mL:

K_2HPO_4	0.348 g
KH_2PO_4	0.227 g
$Na_2HPO_4 \cdot 7H_2O$	2.145 g
$NaH_2PO_4 \cdot H_2O$	0.938 g
NH_4Cl	0.500 g
$MgSO_4 \cdot 7H_2O$	0.500 g
$CaCl_2 \cdot 2H_2O$	0.250 g
NaCl	0.918 g
$FeSO_4 \cdot 7H_2O$	0.002 g
$NaHSeO_3$	10^{-7} mol/L
$NaHCO_3$	4.000 g
Cysteine-HCl	0.300 g
$Na_2S \cdot 9H_2O$	0.300 g
SL-10 trace element solution	1 mL
Vitamin solution	10 mL
Yeast extract	2.000 g

Compared to the DSMZ-recommended growth medium [*26*], the concentration of phosphate buffer is increased by 5 times from 3.7 mM to 18.5 mM without changing the overall K^+ and Na^+ concentration. Initial growth of *S. ovata* was performed in the full recipe. For electrochemical and

photoelectrochemical experiments, Na_2S, cysteine-HCl, and yeast extract was omitted to ensure an organic-free medium containing only the trace vitamin supplement. To further enhance the buffer strength with higher acetate titer, a modified M9-MOPS medium was used. Compared to standard M9-MOPS medium 10 mL vitamin solution was added.

Quantitative analysis of acetate production. Aliquots of the electrolyte were periodically sampled during the experiment. During the sampling process the potentiostat stopped recording data, which results in the gaps in the curves shown. The production of acetate was analyzed by quantitative proton nuclear magnetic resonance (^{1}H-qNMR) spectroscopy, with sodium 3-(trimethylsilyl)-2,2',3,3'-tetradeuteropropionate (TMSP-d4, Cambridge Isotope Laboratories, Inc.) as the internal standard. Trace amounts of formic acid (~0.1 mM) were occasionally observed, and there was not a measurable concentration of 2-oxobutyrate as previously reported [*27*] which may relate to the modified media composition used in the current study. For the isotope labeling experiment, ^{13}C-labeled bicarbonate was used, and the same procedure was applied. Both ^{1}H-qNMR and ^{13}C-NMR techniques were applied to analyze the end product. Because the purging CO_2/N_2 mixture is not ^{13}C labeled, not all of the produced acetate molecules are ^{13}C-labeled.

The concentration of the major product, acetic acid, was measured before and after the experiment. The Faradaic efficiency of acetate production, $X_{acetate}$, is calculated based on the following equation:

$$X_{\text{acetate}} = \frac{\Delta C_{\text{acetic acid}}(\text{mol}\cdot\text{L}^{-1}) \times V_{\text{solution}}(\text{L}) \times 8 \times F(\text{C}\cdot\text{mol}^{-1})}{\int i\ (\text{A}\cdot\text{cm}^{-2}) \times A(\text{cm}^2)\ dt}$$

Here $\Delta C_{\text{acetic acid}}(\text{mol}\cdot\text{L}^{-1})$ is the acetic acid concentration difference between two sampling points, $V_{\text{solution}}(\text{L})$ is the volume of working electrode chamber, $F(\text{C}\cdot\text{mol}^{-1})$ is the Faraday constant, and $\int i\ (\text{A}\cdot\text{cm}^{-2}) \times A(\text{cm}^2)\ dt$ is the amount of charge that has been passed through the working electrode. No gas bubbles were visible on the electrode when *S. ovata* was introduced.

Numerical simulation. Numerical simulation of the O_2 mass transport within the nanowire array was performed using the COMSOL Multiphysics finite-element-analysis software package. In the simulation only the mass transport of O_2 is accounted for. As shown in the Tafel plots of *Figure 3.4 d*, the Tafel slopes of the nanowire and planar electrodes loaded with bacteria are the same, which indicates that proton and bicarbonate mass transport are not rate limiting in the experiment. A constant diffusion layer thickness (L_{diff}) was assumed to be 500 μm. Attempts to change L_{diff} (from 50 to 5000 μm) did not yield significant differences in simulation results. The O_2 concentration at the nanowire surface ($C_{surface}$) was calculated from the Nernst equation based on the potential applied to the electrode (-0.2 V *vs*. RHE). The diffusion coefficient of O_2 gas (D_{Oxygen}) is 1.99×10^{-5} cm^2/sec (at 298 K), and the saturated concentration of O_2 (C_{max}) is 0.259 mmol/L (at 298 K, equilibrated with air). The simulated nanowire has a 1 μm diameter, 30 μm length, and 2 μm periodicity (square lattice, periodic boundary condition). Because of the large difference in length scale between the diffusion layer and the length of nanowire, two separate domains were applied.

Mathematical model for O_2 concentration profile in the nanowire array. Below is a model of O_2 depletion within the nanowire array. In general, the 3-dimensional problem of mass transport is simplified into a one-dimensional model assuming the nanowire array behaves as a porous electrode. The constructed model is based on a previous report for redox mass transport in dye-sensitized solar cells [*38*].

The reaction of interest is oxygen reduction in an aqueous electrolyte:

$$4H^+ + O_2 + 4e^- \rightarrow 2H_2O$$

Assumptions for the model:

1. The nanowire array and the liquid surrounding it are treated as a homogenous porous medium with an averaged redox concentration that is only dependent on the direction along the nanowire. The amount of liquid that is occupied is represented by the dimensionless porosity ε_p, which is the volume percentage of the liquid phase.

$$\varepsilon_p = \frac{a^2 - \pi r^2}{a^2}$$

   Here a is the periodicity of the square lattice of the nanowire array, and r is the radius of the nanowire.

   By treating the nanowire array as a homogenous porous medium, only the concentration profile along the nanowire length must be considered. This direction is defined as the x-axis, and the concentration of O_2 is represented as $C(x)$.

   The boundary of the nanowire array is defined as:

   $x > 0$ nanowire array (porous media)

   $x < 0$ bulk solution

2. Since an oxygen molecule is charge-neutral and convection of the liquid is minimal within the diffusion layer, the mass transport of oxygen is completely diffusional.
3. The current passing through the nanowire surface could be considered as a homogeneous reaction within the porous media, represented as an "injection rate" P_{inj}. The relationship between the current density on the surface of the nanowire and P_{inj} could be written as:

$$P_{inj} = \frac{i \cdot 2\pi r}{Fa^2}$$

   Here i is current density in the unit of [A/m^2], P_{inj} is in the unit of [mol/m^3], and F is the Faraday constant.

4. The oxygen reduction reaction (ORR) is considered to be first-order dependent on the oxygen concentration at the electrode surface, and the Tafel assumption is applied owing to the large overpotential η applied on the cathode.

Governing equation:

The differential equation for the mass transport of O_2 in the nanowire array could be represented as:

$$D\frac{d^2C}{dx^2}-\frac{1}{4}\frac{P_{inj}}{\varepsilon_p}=0$$

As assumed above, the overpotential η versus oxygen reduction is quite large and the current density *i* could be represented as the Tafel equation associated with the local O_2 concentration.

$$i=\frac{C(x)}{C_{sat}}\cdot i_{sat}=\frac{C(x)}{C_{sat}}\cdot i_0 e^{\frac{\alpha nF}{RT}\eta}$$

$$C_{sat}=0.036g/L=1.125\times10^{-3}mol/L=1.125mol/m^3$$

Here C_{sat} is the saturated oxygen concentration equilibrated with 1 atm O_2 gas. In practice, the partial pressure of O_2 is maintained at 21% in the headspace. i_{sat} is the current density observed when the mass transport of O_2 is not a limiting factor.

Combining all equations together, the differential equation in the porous media is:

$$D\frac{d^2C(x)}{dx^2}-\frac{1}{4\varepsilon_p}\frac{2\pi r}{Fa^2}i_{sat}\frac{C(x)}{C_{sat}}=0$$

If k^2 is defined as follows:

$$k^2=\frac{1}{4D\varepsilon_p}\frac{2\pi r}{Fa^2}i_{sat}\frac{1}{C_{sat}}$$

Then the equation could be written quite simply:

$$\frac{d^2C(x)}{dx^2}-k^2C(x)=0$$

Considering the fact that C(x) is decreasing at x>0, the solution should be:

$$C(x)\propto e^{-kx}$$

i.e. the concentration within the porous media decays exponentially.

Based on the above discussion, it is found that the oxygen concentration profiles in the proximity of planar and nanowire electrodes are different. In the case of a planar electrode, the concentration of oxygen drops almost linearly, consistent with the diffusion layer model (*Figure 3.3 a*). In contrast, the concentration of oxygen decreases logarithmically in the nanowire array, analogous

to a porous electrode (*Figure 3.3 b*). The fundamental differences in the oxygen concentration profiles of planar and nanowire electrodes allow us to design an integrated bacteria/nanowire electrode for aerobic CO_2 reduction with strictly anaerobic bacteria (*Figure 3.8*).

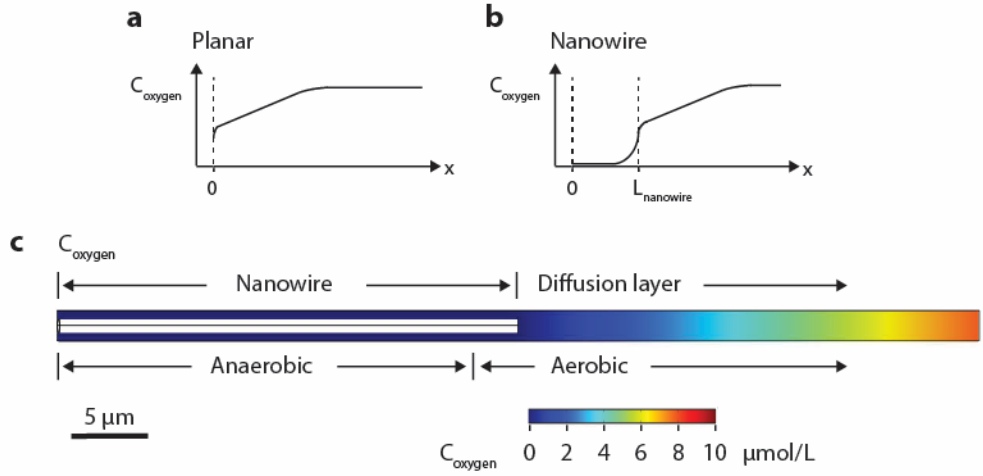

Figure 3.3. Oxygen depletion capacity of nanowire and planar electrodes. Scheme of the O_2 concentration profile near the planar (a) and nanowire array (b) electrodes. (c) An additional simulation result of the O_2 concentration profile near a nanowire array electrode. Notably here a wider region of the diffusion layer is plotted using a linear scale for C_{oxygen}, highlighting the linear decrease of O_2 concentration within the diffusion layer.

***E. coli* culturing and biosynthesis of value-added chemicals.** Electrocompetent *E. coli* BW25113 were transformed with appropriate plasmids, as shown in (*Table 3.1 a* and *Table 3.2*). The cells were plated on LB plates containing appropriate antibiotics. After overnight incubation at 37 °C, colonies were picked into selective LB broth media. After 8-12 hours of growth, the cells were inoculated 1:100 into selective M9-MOPS media containing 1% (w/v) glucose. The culture was then sequentially grown in M9-MOPS-glucose again, M9-MOPS with 50 mM sodium acetate (twice), and finally transferred to culture flasks that contained M9-MOPS media containing solar-derived acetate (90-100 mM) for production experiments. The solar-derived acetate media was generated in the electrochemical cell under aerobic conditions (21% O_2/10% CO_2/69% N_2) using simulated sunlight. All production experiments were carried out in triplicate.

n-Butanol production experiments were performed as previously reported under microaerobic conditions [*29*]. The cells were inoculated to an OD_{600nm} of 0.05 in 250 mL baffled screw-top anaerobic culture flasks containing 50 mL media supplemented with 50 µg/ml carbenicillin and 25 µg/ml chloramphenicol and kanamycin. The cells were grown aerobically (shaking at 200 rpm with the screw-caps loose) at 37 °C to an OD_{600nm} of 0.3-0.4, at which point the cultures were induced by adding 1mM IPTG and 0.2% L-arabinose. At induction the caps were closed tightly to prevent butanol evaporation. The cultures were then maintained at 30 °C with shaking (200 rpm) for 5 days. Every 24 hours, 2 mL culture samples were removed for butanol and acetate analysis. The samples were cleared of cells by centrifuging at 14000 rpm for 10 min in a table-top microcentrifuge, transferred to new tubes and frozen at -80 °C for later analysis.

Isoprenoid production experiments were conducted similarly, but under aerobic conditions [*39*]. Here, cells were inoculated to an OD_{600nm} of 0.05 in 250 mL baffled culture flasks containing 40 mL media supplemented with 50 µg/ml carbenicillin and 25 µg/ml chloramphenicol. The cultures were induced at an OD_{600nm} of 0.2-0.3 by adding 1mM IPTG. At induction an organic overlay of

10 mL dodecane was added to each flask. Every 24 hours, a 1 mL sample of the organic overlay and a 1 mL sample of the culture were harvested.

A similar protocol, using aerobic conditions, was used for PHB production [*31*]. Cells were inoculated to an OD_{600nm} of 0.05 in 250 mL baffled culture flasks containing 50 mL media supplemented with 25 μg/ml chloramphenicol and kanamycin. The cultures were induced at an OD_{600nm} of 0.3-0.4 by adding 1mM IPTG and 0.2% L-arabinose. At the end of the 5-day experiment, 40 mL of culture were harvested by centrifuging at 9800 x g for 5 min. 1 mL of cleared culture media was retained for acetate analysis. The cell pellets were resuspended in 5 mL of deionized water, transferred to pre-weighed 20 mL glass scintillation vials and lyophilized.

Construction of plasmids. Standard molecular biology techniques were used for plasmid construction. *E. coli* DH10B-T1^R served as the cloning host. All PCR amplifications were carried out with Phusion polymerase (New England Biolabs). Plasmids were assembled using the Gibson method [*40*], and sequences were verified using Sanger sequencing (Quintara Biosciences, Berkeley, CA). Detailed descriptions of the plasmids and primers are contained in *Table 3.1*.

*pBBR1-MCS2-pTrc-ACS**. The Trc promoter was amplified from pTrc99a [*41*] using primers pTrcF3 and pTrcR3. The L641P ACS mutant was amplified using primers ACS.Ec.F4 and ACS.Ec.R7. The two PCR products were joined using splicing by overlap extension (SOE) PCR with primers pTrcF3 and ACS.Ec.F7. The resulting PCR fragment was inserted into the EcoRI/SacII sites of pBBR1-MCS2 [*29*].

pBT33-phaA.phaB.phaC. The phaA.phaB operon was amplified from pBT33-Bu2 [*29*] using primers PhaB R6 and PhaA F2. The PCR product was inserted into the NdeI/XhoI sites of pBT33-MSC2-crt [*29*] to generate pBT33-phaA.phaB-crt. A synthetic version of the phaC gene was amplified using primers PhaC F5 and PhaC R2 and inserted into the SpeI/XhoI sites of pBT33-phaA.phaB-crt to generate pBT33-phaA.phaB.phaC-crt. The Trc-crt region of pBT33-phaA.phaB.phaC-crt was removed by digestion with XhoI and XbaI. The plasmid was closed by inserting the overlapping oligonucleotides PhaABC_F and PhaABC_R.

Quantification of production experiments. Detailed analysis methods for the organic compounds have been reported previously [*29, 39, 42*]. *n*-Butanol was measured using a Trace GC Ultra (Thermo Scientific) with an HP-5MS column (0.25 mm × 30 m, 0.25 μM film thickness, J & W Scientific), after extraction with an equal-volume of toluene (500 μL) containing the isobutanol internal standard (100 mg/L). For isoprenoid quantification, 250 μL of the dodecane layer was mixed with 250 μL ethyl acetate containing 5 mg/L trans-caryophyllene as an internal standard. The samples were analyzed using the same instrument described above. Compounds were identified by comparison of the full mass spectrum to authentic standards (butanol) or library compounds (isoprenoids). For quantification, the peak area of the compounds of interest was compared to the peak areas of an authentic standard calibration curve (butanol) or the peak area of the internal standard (isoprenoids). To measure PHB content, dry lyophilized cell samples of known weight were treated with conc. H_2SO_4 at 90 °C for 60 min to convert PHB into its monomer, crotonic acid. Samples were analyzed by liquid chromatography (1200 Series, Agilent Technologies) using an Aminex HPX-87H column (BioRad) with 7 mM H_2SO_4 as the mobile phase and acrylic acid as the internal standard. The eluent was monitored by UV at 214 nm. Acetate

a

Plasmid	Description	Source
pBT33-Bu2	*phaA.hbd (Ara), crt (Trc), araC, Cm^r, p15a*	*29*
pCWori-ter.adhE2	*ter.adhE2 (double Tac), lacIq, Cb^r, ColE1*	*29*
pBBR1-MCS2-pTrc-ACS*	*ACS* (Trc), lacIq, Km^r, pBBR*	this study
pAM45	*AtoB.HMGS.HMGR (lacUV5), MK.PMK.PMD.IDI.ispA (lacUV5), Cm^r, p15a*	*39*
pADS	*ADS (Trc), lacIq, Cb^r, ColE1*	*43*
pCAS	*CAS (Trc), lacIq, Cb^r, ColE1*	*44*
pEAS	*EAS (Trc), lacIq, Cb^r, ColE1*	*44*
pBT33-phaA.phaB.phaC	*phaA.phaB.phaC (Ara), araC, Cm^r, p15a*	this study

b

Primer	Sequence
pTrcF3	CACTAGGAATTCCGACTGCACGGTGCACCAATGCTTCT
pTrcR3	ACTAGTGGATCCTGTGCTGGTGCCTAGGCTGTTTCCTGTGTGAAATTGTTATCC
ACS.Ec.F4	AGGCACCAGCACAGGATCCACTAGTTTTAAGAAGCAATATCATATGAGCCAAATTC ACAAACACACC
ACS.Ec.R7	GCTCCACCGCGGTGGCGGCCGCTCTAGA TTACGATGGCATCGCGATAGCCTGC
PhaA F2	AAGGAGATATACATATGACTGATGTTGTGATTGTAAGCGCTGCACGTACTGCTGTT GGTAAGTTCGGTGGCTCCCTGGC
PhaB R6	CTCGAGCTCGAGCGGAGGTAGACTAGTTTAGCCCATGTGCAGGCCACCGTTCAG GG
PhaC F5	GGCTAAACTAGTCCGGAGGTATAATTAATGGCGACCGGCAAAGGCGCGG
PhaC R2	ATGCTACTCGAGTCATGCCTTGGCTTTGACGTA
PhaABC_F	CTCGAGACGCTGGTGATCTAGAGTCGACCTGCAGGCATGCAAGCTTGGCTGTTT TGGCGG
PhaABC_R	TCTAGATCACCAGCGTCTCGAGTCATGCCTTGGCTTTGACGTATCGCCCAGGCG CGGGTTCG

Table 3.1. Plasmids (a) and primers (b) used in this study.

was quantified using an Agilent 1200 Series HPLC equipped with a Phenomenex Rezex RFQ Fast Fruit H+ column (100 x 7.80mm), by mixing culture media samples (450 µL) with a 4% (v/v) valeric acid internal standard (50 µL). Acetate and valeric acid were detected using a diode array detector by monitoring absorbance at 210 nm. To quantify the production yield $X_{product}$ of the target compounds, a theoretical production scenario is assumed (see *Calculation of the theoretical number of acetate molecules needed to synthesize one molecule of product, $N_{acetate,theoretical}$*), and $X_{product}$ was calculated based on the consumption of acetate.

Calculation of the theoretical number of acetate molecules needed to synthesize one molecule of product, $N_{acetate,theoretical}$. To derive $N_{acetate,theoretical}$ the following ideal scenarios are considered for specific products.

n-butanol:

$$3\ CH_3COOH \rightarrow\ C_4H_9OH + 2\ CO_2 +\ H_2$$

isoprenoids:

$$21\ CH_3COOH\ \rightarrow\ 2\ C_{15}H_{24} + 12\ CO_2 + 18\ H_2O$$

PHB:

$$\frac{9}{4}n\ CH_3COOH\ \rightarrow\ (C_4H_6O_2)_n + \frac{3}{2}n\ H_2O +\ \frac{1}{2}n\ CO_2$$

The above equations are considered as the biocatalytic reactions of maximum efficiency, based on the following reasoning:

1. The reactant of biocatalyst should be acetic acid, and the end products should be the target molecule, CO_2, and H_2O. CO_2 and H_2O are considered because they cannot be further metabolized by *E. coli*.

2. In the above equation no O_2 molecules are considered. Any metabolism involving O_2 molecules can be considered as a linear combination between the above equations and the "combustion" reaction between acetic acid and O_2:

$$CH_3COOH + 2\ O_2\ \rightarrow\ 2\ CO_2 + 2\ H_2O$$

Therefore the theoretical maximum conversion efficiency is based on an O_2-free reaction that involves only acetic acid, target molecules, CO_2, and H_2O. Based on these equations, $N_{acetate,theoretical}$ is 3, 10.5, and 2.25 for *n*-butanol, isoprenoid compounds, and PHB biopolymer.

3.3 Results and discussion

Construction of a nanowire-bacteria hybrid device. Assembly of the hybrid system begins with interfacing light-absorbing Si nanowire arrays with an acetogenic organism, *S. ovata*. Si nanowire arrays capture light for efficient solar energy conversion and provide high surface areas to interface with catalysts [*21, 25*]. The strictly anaerobic homoacetogen *S. ovata [26]* metabolizes CO_2 *via* the energy-efficient Wood-Ljungdahl pathway and has been reported to accept electrons

from graphite electrodes to reduce CO_2 to acetate [*27*]. The integration was realized by directly culturing *S. ovata* within a Si nanowire array passivated by a 30 nm TiO_2 protection layer, using bicarbonate-buffered brackish water media with trace vitamins as the only organic component. After an initial incubation period, a steady-state nanowire-bacteria hybrid structure was formed. In such a structure, the bacteria formed an interconnected network among the nanowires. Careful characterization with scanning electron microscopy (SEM) indicates that bacteria populate the array quite uniformly without apparent mass transport issues (*Figure 3.4 a-c*). The cell loading of *S. ovata* within the nanowire array is 4.4 ± 1.0 times of that observed on a planar Si electrode (1.4 ± 0.1 *vs.* 0.32 ± 0.07 cells per geometric μm^2, n = 4) (*Figure 3.5 d*), revealing increased contact interfaces between bacteria and electrodes in this high surface-area platform.

The proposed half-reaction of CO_2 reduction is:

$$2\,CO_2 + 7\,H^+ + 8\,e^- \rightarrow CH_3COO^- + 2\,H_2O \quad E^0 = +0.143\ V\ vs.\ RHE$$

Performing a classical electrochemical analysis without solar illumination (*Figure 3.4 d*), the nanowire-bacteria hybrids were capable of reducing CO_2 to acetate under continuous sparging with 20% CO_2/80% N_2 with an overpotential η less than 200 mV at 0 V vs reversible hydrogen electrode (RHE), similar to reported literature values [*27*]. Additionally, the Tafel slope of bacterial catalyzed CO_2 reduction is distinctly different from that of abiotic proton reduction, implying different reaction mechanisms (n = 2). On average, each cell could produce $(1.1 \pm 0.3) \times 10^6$ molecules of acetate every second or *ca.* 10^{12} molecules of acetate over the course of about five days at -0.2 V *vs.* RHE (*Figure 3.5 d*). The microorganism, which operates at ambient temperature, possesses a volumetric reaction rate of *ca.* 2 $mol \cdot m^{-3} \cdot sec^{-1}$, comparable to what is observed for conventional gas phase catalysts (0.1-10 $mol \cdot m^{-3} \cdot sec^{-1}$) that require much higher temperatures (higher than 100 °C) [*28*]. This reaction rate corresponds to an electron flux of *ca.* 8 electrons per second per nm^2 (-0.2 V *vs.* RHE), suitable to couple with efficient solar devices at 10 mA/cm^2 when integrated into a high surface-area electrode [*1, 6, 23, 25*].

Solar-powered acetate production using the hybrid nanowire-bacteria device. Encouraged by the high reaction rate observed from the nanowire-bacteria hybrid device under electrochemical conditions we next sought to construct a completely solar-powered CO_2-reduction device. Analogous to the two photosystems found in nature [*2, 24, 25*], Si and TiO_2 nanowires were used as two robust semiconductor light-absorbers to provide the thermodynamic driving force for CO_2 reduction [*21*]. Specifically, an ion-conductive membrane was placed in between the two electrodes to separate reaction products, and the water-oxidizing TiO_2 nanowire electrode was placed in front of the nanowire-bacteria composite to prevent possible bacterial photodamage (*Figure 3.2 b*). Without any additional energy input, non-zero photocurrent was observed (light chopping experiment *Figure 3.4 e*). The overall system produced about 0.3 mA/cm^2 photocurrent under simulated sunlight (AM 1.5G, 100 mW/cm^2) and was stable for more than 120 hours (*Figure 3.4 e*, *Figure 3.6* (photocathode characterization)). Starting from an electrolyte free of organic compounds, acetic acid was steadily produced with a Faradaic efficiency of 86 ± 9% (n = 6). The peak photocurrent reached 0.35 mA/cm^2, which corresponds to an energy conversion efficiency of 0.38% for acetic acid production (requires 1.08 V thermodynamically). The acetic acid titers were *ca.* 1.2 g/L (20 mM) within 5 days and could reach over 6 g/L (*ca.* 100 mM) in M9-MOPS minimal

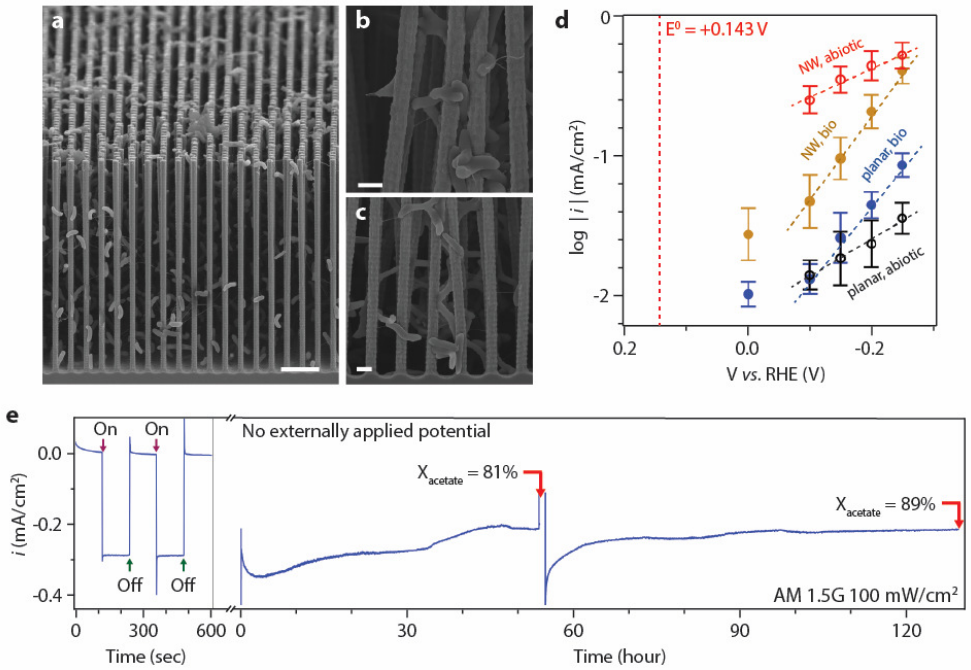

Figure 3.4. Unassisted solar-powered acetate production from the nanowire-bacteria hybrid device. (a) Cross-sectional SEM image of the three-dimensional network in the nanowire-bacteria hybrid. (b,c) Magnified images at different depths of the nanowire array. (d) Tafel plots, the logarithmic current density *versus* applied electrochemical voltage, are plotted for different electrode configurations (n = 2). Detailed data is summarized in *Figure 3.5 d*. Filled blue circle ("planar, bio"), planar electrode loaded with bacteria; filled yellow circle ("NW, bio"), nanowire electrode loaded with bacteria; open black circle ("planar, abiotic"), bare planar electrode; open red circle ("NW, abiotic"), bare nanowire electrode. (e) Measurement of unassisted solar-powered CO_2 reduction for more than five days, n = 6. During the experiment the system was purged with 20% CO_2/80% N_2. In the plot $X_{acetate}$ is the product selectivity (Faradaic efficiency) of acetic acid generation. The scale bars are 5 μm (a) and 1 μm (b,c).

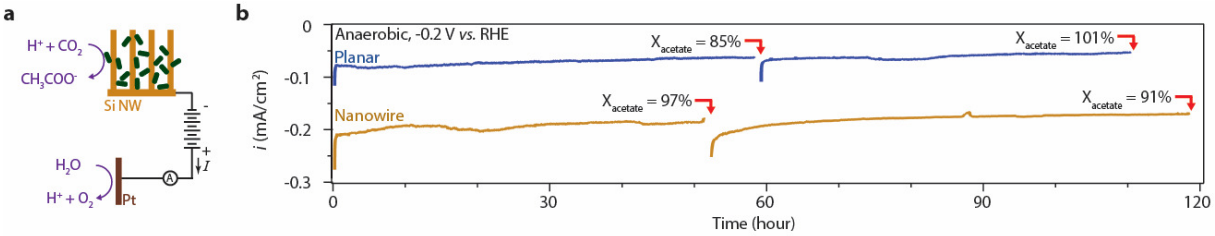

c

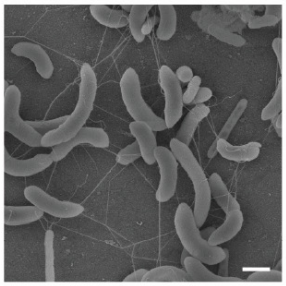

d

Calculated single-cell activity from Tafel plots

	i_0 (μA/cm²) [a]	$dV/d\log(i)$ (mV/dec) [b]	cell density (μm⁻²) [c]	$i_{-0.2\ V\ vs.\ RHE}$ (mA/cm²) [d]	$TOF_{-0.2\ V\ vs.\ RHE}$ (cell⁻¹·sec⁻¹) [e]
planar, bio	0.64±0.05 [f]	187±14	0.32±0.07	0.042±0.011	1.1±0.3×10⁶
NW, bio	1.4±0.2 [f]	160±21	1.4±0.1	0.19±0.05	1.0±0.3×10⁶
planar, abiotic	7.1±0.9 [g]	381±47	N. A.	0.022±0.008	N. A.
NW, abiotic	150±21 [g]	474±63 [h]	N. A.	0.41±0.10	N. A.

Figure 3.5. Electrochemical CO_2 reduction using the nanowire-bacteria hybrid electrode. (a) Schematic of bacteria-catalyzed CO_2 reduction with a Si nanowire cathode. (b) The Si nanowire-bacteria hybrid electrode possesses a high reaction rate of electrochemical CO_2 fixation and acetate production. Production is compared to a planar electrode. Degenerately doped Si was applied to minimize the serious resistance. The product selectivity to acetate ($X_{acetate}$) during each time interval is displayed. (c) Representative SEM images of *S. ovata*. Geometrical information for *S. ovata* was derived to calculate the single-cell activity. (d) Electrochemical data summarized from *Figure 3.4 d* (n = 2). The selectivity of acetate production $X_{acetate}$ is larger than 70% for all reported biotic data. As shown in the table, the Tafel slope $dV/d\log(i)$ is distinctly different in the presence of bacteria, indicating a difference of reaction mechanism between abiotic proton reduction and bio-catalyzed CO_2 reduction. [a] Exchange current density i_0 per geometric electrode area. [b] Tafel slope, which is a measure of the apparent kinetic barrier. [c] *S. ovata* cell loading density per geometric electrode area. [d] Current density measured at -0.2 V *vs*. RHE. [e] Single-cell turnover frequency (TOF) measured at -0.2 V *vs*. RHE. [f] Measured based on the electrochemical potential of acetic acid formation (+0.143 V *vs*. RHE). [g] Measured based on the electrochemical potential of proton reduction (0 V *vs*. RHE). [h] The Tafel slope may be convoluted with mass transport when the current density is high. The scale bar in (c) is 1 μm.

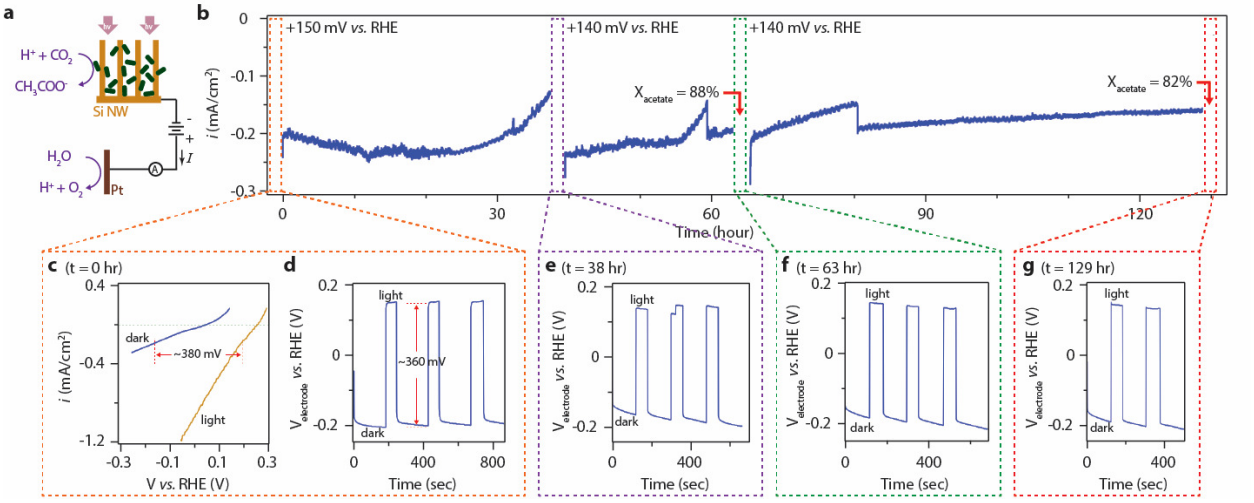

Figure 3.6. Stable performance of the nanowire-bacteria hybrid photocathode for solar CO_2 reduction. (a) Setup schematic for solar-assisted CO_2 reduction with the Si nanowire-bacteria hybrid as the photocathode. (b) Representative data for long term testing of solar-assisted CO_2 reduction under constant bias (0-38 hours: +150 mV *vs.* RHE, 38-129 hours: +140 mV *vs.* RHE), n = 3. (c) Linear scan voltammetry curves (10 mV/sec) of the integrated photocathode in dark and light. The stability of the hybrid electrode was tested by measurement of photovoltage output at different intervals during the experiment: (d) t = 0 hour; (e) t = 38 hours; (f) t = 63 hours; (g) t = 129 hours. The photovoltage was measured chronopotentiometrically at 0.2 mA/cm^2 with chopped illumination (740 nm LED light source). The photovoltages measured over the period of 5 days were stable and consistent with the value extracted from (c).

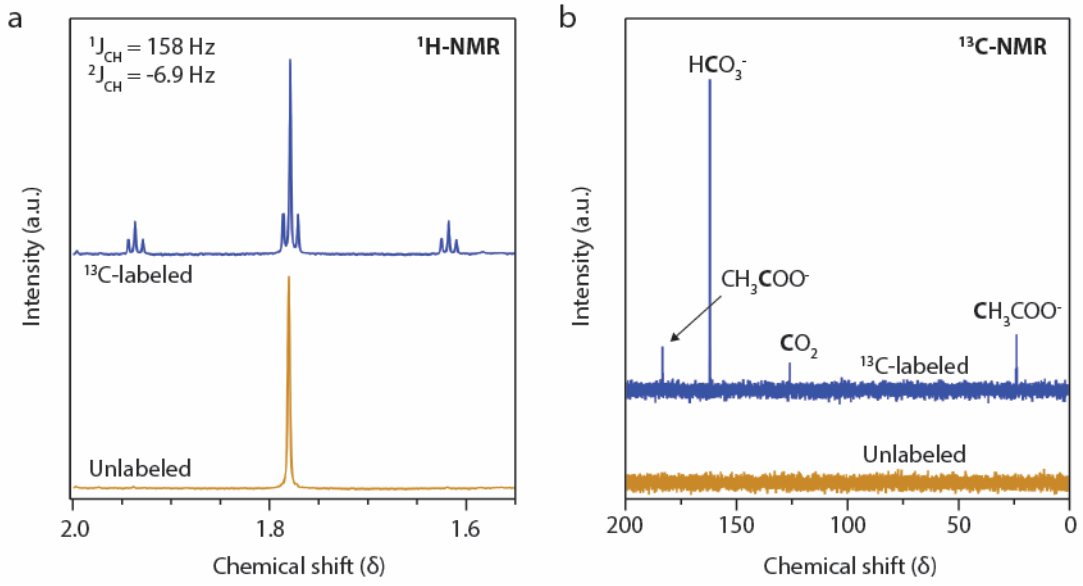

Figure 3.7. Isotope labeling experiment for CO_2-fixation with nanowire-bacteria hybrids. (a) ^{1}H-NMR spectra of acetate produced from unlabeled and ^{13}C-labeled electrolyte. For ^{13}C-labled samples, the high abundance of ^{13}C in the acetate magnifies $^1J_{CH}$ and $^2J_{CH}$ coupling, resulting in the satellite peaks in the spectrum. (b) ^{13}C-NMR spectra of acetate produced from unlabeled and ^{13}C-labeled electrolyte. With the addition of $NaH^{13}CO_3$, the ^{13}C-signal is strongly enhanced in bicarbonate, dissolved CO_2, and acetate.

media, which has a higher pH buffering capacity. In separate control experiments no acetic acid was detected without incorporation of *S. ovata*, and an isotope-labeling experiment demonstrates that the acetate is produced from CO_2 (*Figure 3.7*). These results highlight our ability to upgrade CO_2 to chemicals beyond one-carbon targets. In next-generation designs we are targeting even higher efficiencies through further improvement of peripheral limitations such as CO_2 mass transport in the electrolyte and the large band gap of the photoanode [*25*]. Nevertheless, it represents a unique materials-biological hybrid for artificial photosynthesis, which demonstrates unassisted light-driven CO_2 fixation to acetic acid.

Aerobic cultivation of obligate anaerobes using the nanowire device. An interesting benefit of the nanowire array arises from its selective control of mass transport within the wire assembly [*25, 45*]. Specifically, the design of the nanowire–bacteria hybrids allows for the continuation of CO_2 reduction, a reaction catalyzed by the strict anaerobe, *S. ovata*, under a headspace containing 21% oxygen when an oxygen reduction reaction electrocatalyst (in this case, Pt) is loaded onto the nanowires. The similar Tafel slopes of CO_2 reduction for planar and nanowire electrodes (*Figure 3.4 d*) inform us that mass transport of protons and CO_2 is not a limiting factor within the nanowire array. However, with its limited solubility in water, oxygen can be depleted within the nanowire array logarithmically, compared to only a linear depletion observed with a planar electrode (*Figure 3.3*). This arrangement effectively creates a local anaerobic environment at the bottom of the nanowire arrays, as modeled by a numerical simulation (*Figure 3.8 a*). Experimentally, after *S. ovata* had colonized the electrode anaerobically, we switched to an aerobic gas environment with 21% oxygen partial pressure (21% O_2/10% CO_2/69% N_2). Only the nanowire array loaded with Pt maintained its ability to reduce CO_2 and consistently produce acetic acid with a Faradaic efficiency of about 70% (t = 85 h) (*Figure 3.8 b*). Compared to the data obtained under anaerobic conditions (20% CO_2/80% N_2), the loss of Faradaic efficiency observed under aerobic conditions (∼15%) is related to the oxygen reduction reaction, which can be greatly minimized with improved design of the nanowire–bacteria hybrids. In general, our observation implies that (1) in our system most, if not all, of the acetate is produced from bacteria interfacing directly with nanowires and (2) combining nanowire arrays with CO_2-reducing microorganisms can allow anaerobes to be used in a wider range of applications, such as CO_2 scrubbing from exhaust gas or even open air operation.

Solar-driven production of advanced chemical products using synthetic biology. Taking advantage of the power of synthetic biology [*18*], a wide spectrum of complex organic molecules can be synthesized directly from solar-derived acetate. Under aerobic or microaerobic conditions, *E. coli* can activate acetate into the common biochemical intermediate acetyl-CoA, which then can be used for the biosynthesis of a variety of complex molecules by employing heterologously expressed synthetic pathways. The first steps in constructing this two organism biosynthetic platform were (1) identifying an *E. coli* strain which grows well in minimal (carbon-free) media with acetate as its sole carbon and (2) determining optimal media conditions under which both *S. ovata* and *E. coli* could thrive. To address these questions a panel of *E. coli* strains were screened for growth on acetate in the *S. ovata* media, M9-MOPS (a well-established *E. coli* minimal media) or mixtures of the two (*Figure 3.9*). This experiment revealed that *E.coli* growth on acetate was severely impaired in the *S. ovata* media. This growth defect persisted in dilutions up to 50% *S. ovata* media/ 50% M9-MOPS. Only at dilutions above 75% M9-MOPS was normal growth observed. A similar experiment was performed with *S. ovata*. Normal growth was observed in 100% M9-MOPS media with a vitamin supplement added; therefore, this was selected as the media

condition for the two organism production experiment. Additionally, in the *E. coli* screening experiment fairly large differences in growth were observed between the different strains. Based on this result, strain BW25113 was chosen as the production host.

The way in which *E. coli* metabolizes acetate is by activating it to acetyl-CoA using either of two ATP-dependent enzyme systems, acetyl-CoA synthase (acs), which is important for scavenging acetate at low concentrations, or the two enzyme acetate kinase A (ackA) – phosphotransacetylase (pta) system, which can assimilate acetate at high concentrations [*46*]. Once activated, acetyl-CoA can then be used for energy generation and biosynthesis *via* the tricarboxylic acid cycle and glyoxylate bypass. Importantly, because energy generation from acetate relies on oxidative phosphorylation for ATP synthesis, growth on acetate is only possible in the presence of oxygen. Because the metabolic program for acetate assimilation is substantially different from that observed during glycolytic growth [*46*], the conditions under which most production pathways are optimized, additional optimization was required to achieve robust production from the solar-derived acetate. The butanol biosynthetic pathway was used as a model pathway to determine optimal production conditions [*29*]. To increase flux to the acetyl-CoA node, a plasmid containing a constitutively active version of the acs was co-transformed along with the plasmids carrying the butanol pathway. (Wild type acs activity is normally regulated by acetylation [*47*].) Additionally, it rapidly became apparent that it would be necessary to balance the competing priorities of culture aeration, to provide sufficient oxygen for acetate metabolism, with product evaporation, which occurs more readily in well aerated cultures. To optimize production with these conflicting priorities, experiments were performed under a number of different aeration conditions, including aerobic growth, microaerobic growth with plastic film used to seal the cultures, and microaerobic growth in tightly sealed screw top flasks, opened daily to allow aeration (*Figure 3.10*). The microaerobic conditions in the screw top flasks resulted in the highest titers, so these conditions were selected for future production experiments. Another interesting observation that was made during these experiments was that slower growing strains resulted in higher product titers. To further optimize production, slow growing strains were selected after transformation and acclimatization to minimal media with acetate as the sole carbon source. Using these strains higher average titers were achieved (*Figure 3.10 d*). Selected strains were used for the final production experiment with solar derived acetate. Other optimization strategies included using an organic overlay to limit butanol evaporation and seeding larger inoculums of biomass directly into inducing media; however, both of these strategies actually resulted in significant decreases in product titer, so they were not used for the final production experiments [*46*].

Based on this optimization, *E. coli* transformed with heterologous synthetic pathways was integrated with the solar-powered nanowire-acetogen device to produce *n*-butanol [*29*], PHB biopolymer [*31*], and three isoprenoid compounds [*30*], with H_2O and CO_2 as the starting materials and sunlight as the energy source (*Figure 3.11* and *Table 3.2*). During the *E. coli* production experiments, the accumulation of the target molecules is correlated with the consumption of acetate (*Figure 3.12 a*), implying the conversion of acetate into the desired products. Interestingly, production experiments employing media from the solar-powered nanowire-acetogen device outperformed production experiments using M9-MOPS with acetate added, both in terms of product yield and acetate consumption (*Figure 3.13*). This seems to indicate that the acetogens are secreting additional small molecules into the media which aid in *E. coli* growth. By the nature of

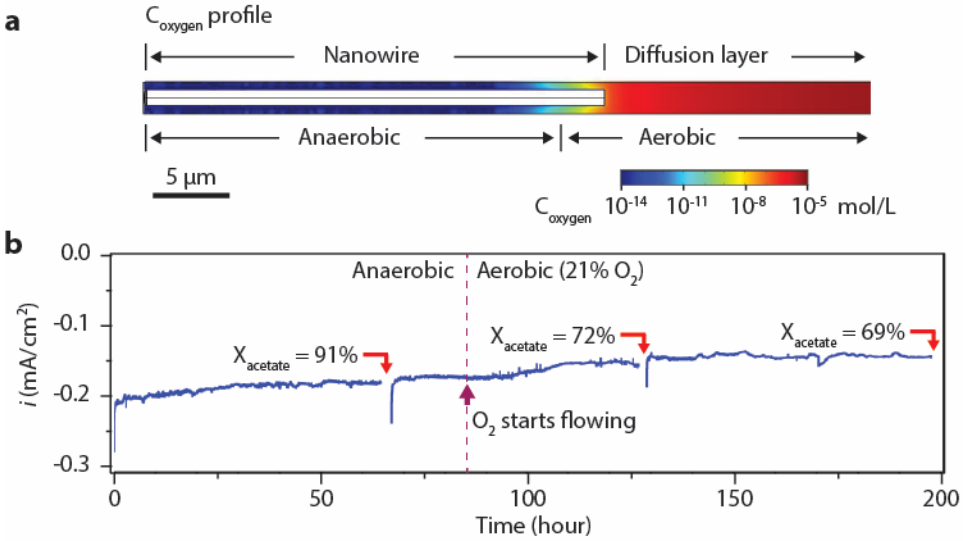

Figure 3.8. Enhanced oxygen tolerance for nanowire-bacteria hybrids. (a) A numerical simulation illustrates that integrating bacteria into a nanowire array allows for the survival of strict anaerobes in an aerobic environment. The oxygen concentration in the electrolyte decreases logarithmically from the nanowire array's entrance, creating a local anaerobic environment. This is in contrast to the linear decrease of oxygen concentration for a planar electrode (*Figure 3.3*). (b) Experimental demonstration of aerobic CO_2 reduction by *S. ovata* when Pt was loaded onto the nanowire electrode, n = 3. Constant electrochemical bias (-0.2 V *vs*. RHE) was applied to the Si nanowire electrode, and the current was plotted against time. As highlighted in the plot, the sparging gas was switched from anaerobic (20% CO_2/80% N_2) to aerobic (21% O_2/10% CO_2/69% N_2) at t = 85 hours.

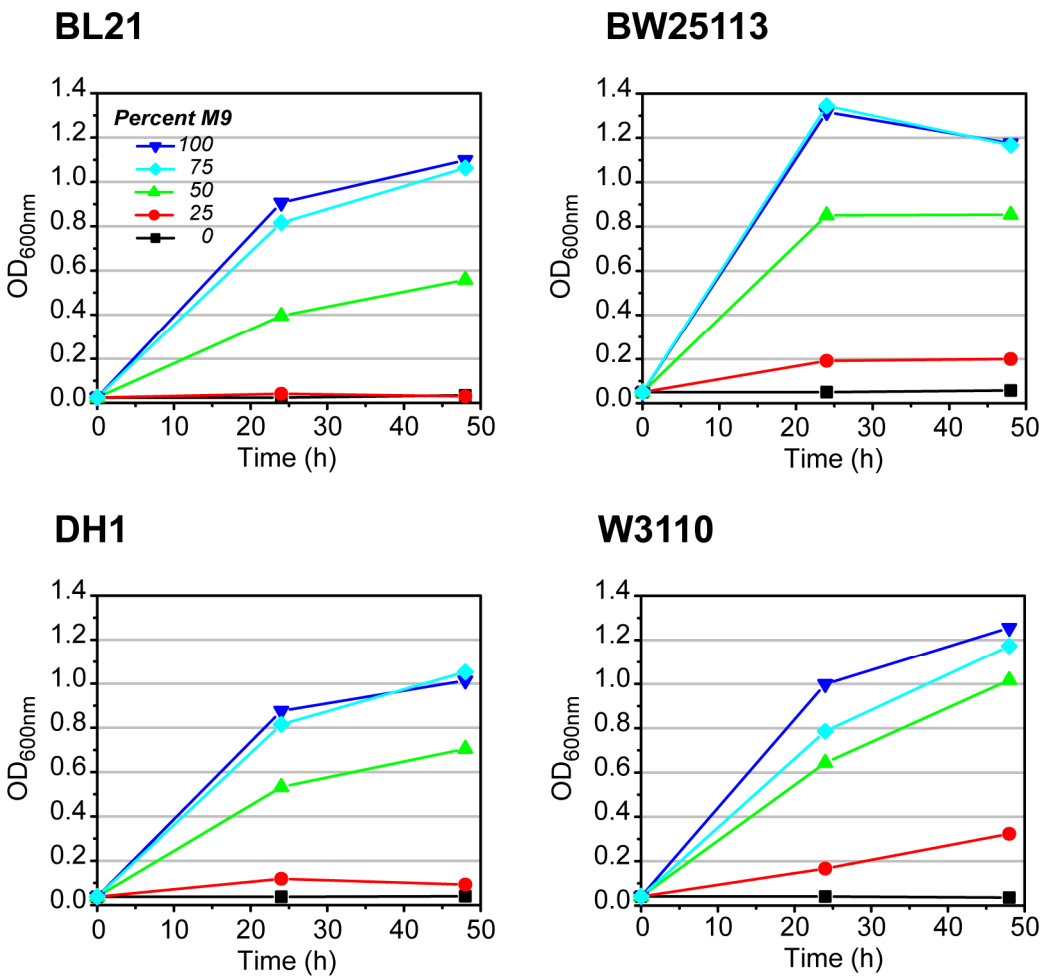

Figure 3.9. E. coli growth in minimal media with acetate as the sole carbon source. Different strains of *E. coli* were screened for their ability to grow in *S. ovata* media, M9-MOPS or mixtures of the two with acetate (35 mM) as the sole carbon source. M9-MOPS-acetate acclimatized cells were diluted 1:100 into fresh media at the start of the experiment. Growth was measure by monitoring the OD_{600mn} of the cultures over 2 d.

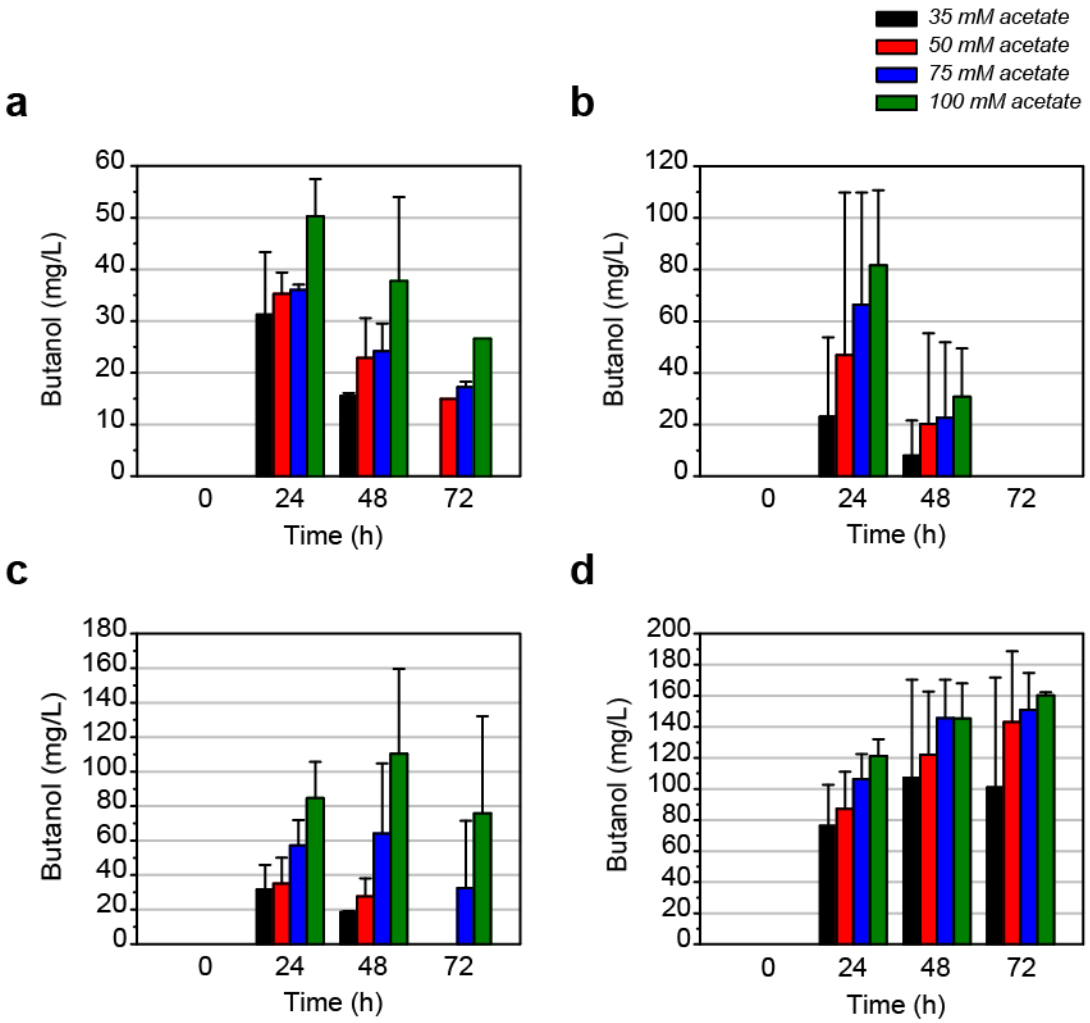

Figure 3.10. Butanol production from acetate under different aeration conditions. *E. coli* BW25113 expressing the butanol biosynthetic pathways was grown under aerobic conditions (a), under microaerobic conditions, with the flasks sealed with plastic film (b), or under microaerobic conditions in tightly sealed screw top flasks, opened daily to allow aeration (c). During the experiments shown in (b and c), it was observed that slow growing strains produced higher butanol titers. Slow growing strains were selected and used for the production experiment shown in (d). All production experiments were performed in 80% M9-MOPS/ 20% *S. ovata* medium. Cultures were sampled daily, and butanol was measured using GC-MS. The concentration of acetate used as the growth substrate is denoted by color. The experiment shown in (a) used a strain of BW25113 transformed with just the two plasmids of the butanol biosynthetic pathway. All other experiments shown used a strain transformed with the two plasmids of the butanol pathways as well as a plasmid carrying a constitutively active version of acetyl-CoA synthase. Each production experiment was performed in triplicate. Error bars denote standard deviation.

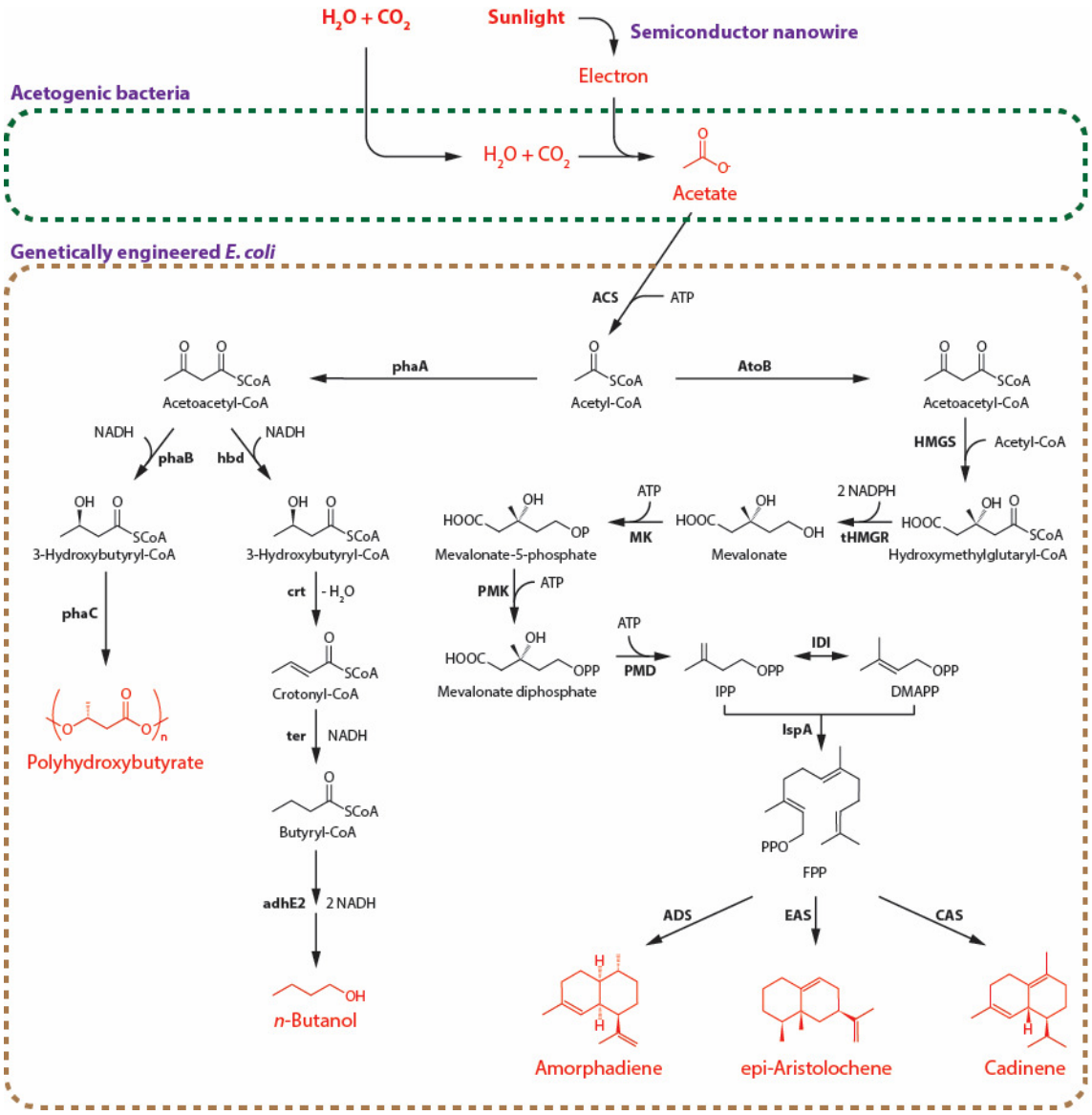

Figure 3.11. Synthetic enzymatic pathways for the biosynthesis of target organic compounds. Each product was produced in a different genetically engineered *E. coli* strain. All pathways begin with acetyl-CoA, which was generated by the activation of solar-derived acetate. IPP, isopentenyl pyrophosphate; DMAPP, dimethylallyl pyrophosphate. ACS, acetyl-CoA synthase; phaA, acetoacetyl-CoA thiolase/synthase; hbd, phaB, 3-hydroxybutyryl-CoA dehydrogenase; crt, crotonase; ter, *trans*-enoyl-CoA reductase; adhE2, bifunctional butyraldehyde and butanol dehydrogenase; phaC, PHA synthase; AtoB, acetyl-CoA acetyltransferase; HMGS, hydroxymethylglutaryl-CoA synthase; tHMGR, truncated hydroxymethylglutary-CoA reductase; MK, mevalonate kinase; PMK, phosphomevalonate kinase; PMD, phosphomevalonate decarboxylase; IDI, isopentenyl diphosphate-isomerase; IspA, farnesyl diphosphoate synthase; ADS, amorphadiene synthase; EAS, epi-aristolochene cyclase; CAS, cadinene synthase.

Biocatalytic production using genetically engineered *E. coli*

Product	Plasmids	$X_{product}$ (100%)	Titer (mg/L)
n-Butanol	pBT33-Bu2, pCWori-ter.adhE2, pBBR1-MCS2-pTrc-ACS*	25.6±2.1	198±22
Amorphadiene	pAM45, pADS	25.1±2.8	124±10
epi-Aristolochene	pAM45, pEAS	10.6±2.3	39±8
Cadinene	pAM45, pCAS	4.7±1.6	22±7
Polyhydroxybutyrate	pBT33-phaA.phaB.phaC, pBBR1-MCS2-pTrc-ACS*	51.8±8.6	490±177

Table 3.2. Biocatalytic production of diverse organic compounds using genetically engineered E. coli. Solar-derived acetic acid from nanowire-bacteria hybrids was used as the feedstock to yield a variety of chemicals in M9-MOPS media (t = 5 d). No organic substrates were provided except the solar-derived acetic acid, which was generated under aerobic conditions using simulated sunlight. $X_{product}$ is acetate-to-product conversion efficiency. n = 3 for all reported values.

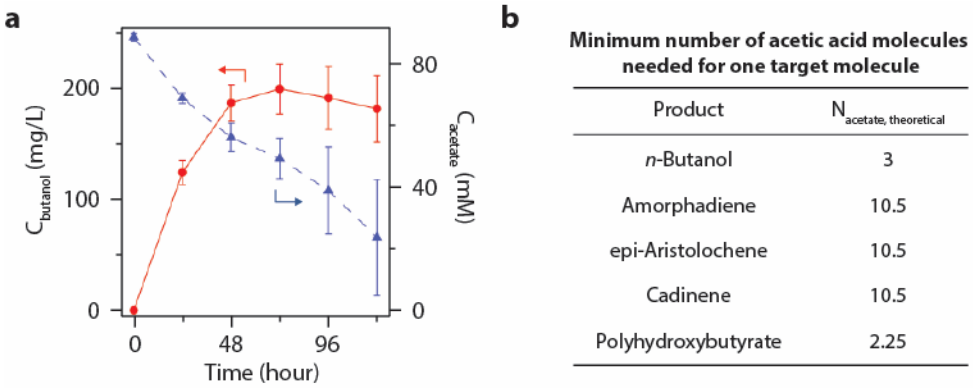

Minimum number of acetic acid molecules needed for one target molecule

Product	$N_{acetate, theoretical}$
n-Butanol	3
Amorphadiene	10.5
epi-Aristolochene	10.5
Cadinene	10.5
Polyhydroxybutyrate	2.25

Figure 3.12. Production of target organic molecules with genetically engineered E. coli strains. (a) Time course of *n*-butanol production using solar-derived acetate from the nanowire-bacteria hybrid system. As a representative example, the accumulation of *n*-butanol is accompanied by the consumption of acetate. Due to *n*-butanol evaporation, a slight decrease is observed in butanol concentrations in later days of the experiment. (b) Display of the theoretical number of acetate molecules needed to synthesize one product molecule, $N_{acetate,theoretical}$. These values were used in the calculation of the acetate-to-product conversion efficiency, $X_{product}$, in *Table 3.2*.

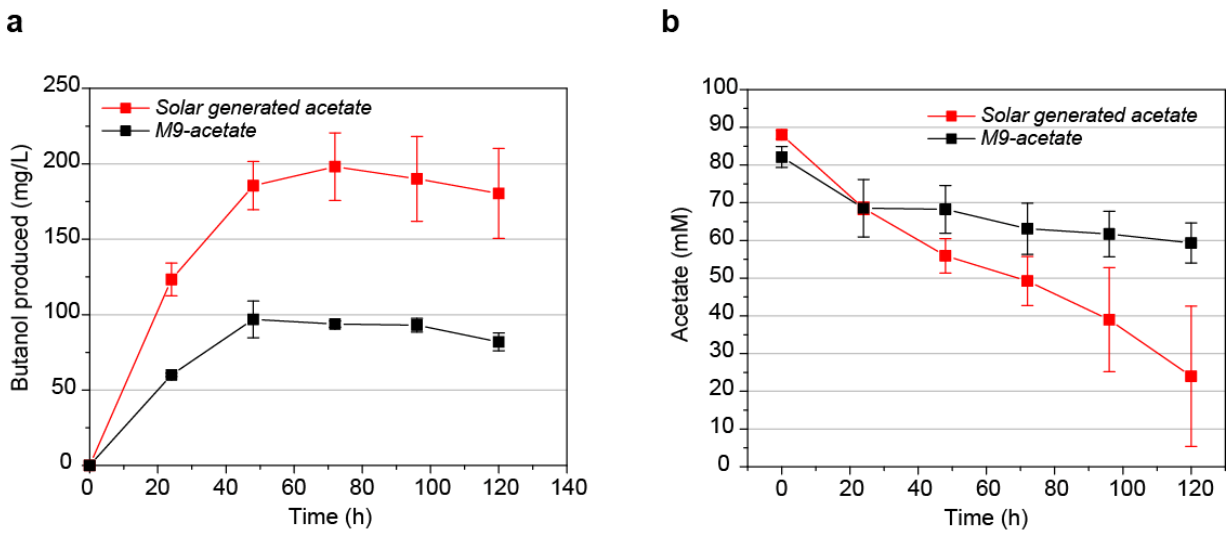

Figure 3.13. Butanol production and acetate consumption under different media conditions. (a) Butanol production and (b) acetate consumption using media from the solar-powered nanowire-acetogen device or M9-MOPS with acetate (100 mM) added. Increased butanol production and acetate consumption is observed in the media from the nanowire-acetogen hybrids. Production experiments were performed in triplicate. Error bars denote standard deviation.

the solar-powered system, these molecules must be derived from carbon dioxide, water and sunlight, which hints at an interesting methodology to enrich minimal media for enhanced microbial growth using sustainable and readily available inputs.

Using the two organism biosynthetic platform, the yield of target molecules was as high as 26% for *n*-butanol, 25% for one of the isoprenoid compounds (amorphadiene), and up to 52% for PHB biopolymer (*Table 3.2*), which is comparable with literature values [*29-31*]. Taking into account the 0.38% efficiency for CO_2 conversion to acetic acid, a solar energy-conversion efficiency of 0.20% is achieved from CO_2 to PHB biopolymer, a renewable and biodegradable plastic. Overall, the production of different organic products with vastly different synthetic pathways proves the versatility of the integrated approach which starts from one common biochemical building block, analogous to natural photosynthesis.

3.4 Conclusions

The results reported here outline a solar-energy conversion process that combines the strengths of semiconductor nanodevices and bacteria-based biocatalysts. Key advantages of the nanowire-based device are the enhanced oxygen tolerance that allows exhaust gas to be directly fed into the system, thereby enabling use of strict anaerobes with aerobes, as well as the high measured CO_2 fixation activity of the nanowire–bacteria hybrid. Moreover, this modular platform simplifies the overall system design by allowing for the production of a variety of molecular targets, without any setup change in the components for light capture and CO_2 reduction into acetate, by varying only the downstream microorganisms.

3.5 References

1. Lewis, N. S., Nocera, D. G., Powering the planet: Chemical challenges in solar energy utilization. *Proc. Natl. Acad. Sci. U.S.A.* **2006**, 103(43) 15729-15735.

2. Barber, J., Photosynthetic energy conversion: Natural and artificial. *Chem. Soc. Rev.* **2009**, 38(1) 185-196.

3. Concepcion, J. J., House, R. L., Papanikolas, J. M., Meyer, T. J., Chemical approaches to artificial photosynthesis. *Proc. Natl. Acad. Sci. U.S.A.* **2012**, 109(39) 15560-15564.

4. Magnuson, A., Anderlund, M., Johansson, O., Lindblad, P., Lomoth, R., Polivka, T., Ott, S., Stensjo, K., Styring, S., Sundstrom, V., Hammarstrom, L., Biomimetic and microbial approaches to solar fuel generation. *Acc. Chem. Res.* **2009**, 42(12) 1899-1909.

5. Gust, D., Moore, T. A., Moore, A. L., Solar fuels via artificial photosynthesis. *Acc. Chem. Res.* **2009**, 42(12) 1890-1898.

6. Luo, J., Im, J. H., Mayer, M. T., Schreier, M., Nazeeruddin, M. K., Park, N. G., Tilley, S. D., Fan, H. J., Gratzel, M., Water photolysis at 12.3% efficiency via perovskite photovoltaics and earth-abundant catalysts. *Science* **2014**, 345(6204) 1593-1596.

7. Zhao, Y., Swierk, J. R., Megiatto, J. D., Jr., Sherman, B., Youngblood, W. J., Qin, D., Lentz, D. M., Moore, A. L., Moore, T. A., Gust, D., Mallouk, T. E., Improving the efficiency of water splitting in dye-sensitized solar cells by using a biomimetic electron transfer mediator. *Proc. Natl. Acad. Sci. U.S.A.* **2012**, 109(39) 15612-15616.

8. Tachibana, Y., Vayssieres, L., Durrant, J. R., Artificial photosynthesis for solar water-splitting. *Nat. Photon.* **2012**, 6(8) 511-518.

9. Gray, H. B., Powering the planet with solar fuel. *Nat. Chem.* **2009**, 1(1) 7.

10. Blankenship, R. E., Tiede, D. M., Barber, J., Brudvig, G. W., Fleming, G., Ghirardi, M., Gunner, M. R., Junge, W., Kramer, D. M., Melis, A., Moore, T. A., Moser, C. C., Nocera, D. G., Nozik, A. J., Ort, D. R., Parson, W. W., Prince, R. C., Sayre, R. T., Comparing photosynthetic and photovoltaic efficiencies and recognizing the potential for improvement. *Science* **2011**, 332(6031) 805-809.

11. Reda, T., Plugge, C. M., Abram, N. J., Hirst, J., Reversible interconversion of carbon dioxide and formate by an electroactive enzyme. *Proc. Natl. Acad. Sci. U.S.A.* **2008**, 105(31) 10654-10658.

12. Bachmeier, A., Hall, S., Ragsdale, S. W., Armstrong, F. A., Selective visible-light-driven CO_2 reduction on a p-type dye-sensitized NiO photocathode. *J. Am. Chem. Soc.* **2014**, 136(39) 13518-13521.

13. Appel, A. M., Bercaw, J. E., Bocarsly, A. B., Dobbek, H., Dubois, D. L., Dupuis, M., Ferry, J. G., Fujita, E., Hille, R., Kenis, P. J., Kerfeld, C. A., Morris, R. H., Peden, C. H., Portis, A. R., Ragsdale, S. W., Rauchfuss, T. B., Reek, J. N., Seefeldt, L. C., Thauer, R. K., Waldrop, G. L., Frontiers, opportunities, and challenges in biochemical and chemical catalysis of CO_2 fixation. *Chem. Rev.* **2013**, 113(8) 6621-6658.

14. Kumar, B., Llorente, M., Froehlich, J., Dang, T., Sathrum, A., Kubiak, C. P., Photochemical and photoelectrochemical reduction of CO_2. *Annu. Rev. Phys. Chem.* **2012**, 63 541-569.

15. Barton, E. E., Rampulla, D. M., Bocarsly, A. B., Selective solar-driven reduction of CO_2 to methanol using a catalyzed p-gap based photoelectrochemical cell. *J. Am. Chem. Soc.* **2008**, 130(20) 6342-6344.

16. Li, C. W., Ciston, J., Kanan, M. W., Electroreduction of carbon monoxide to liquid fuel on oxide-derived nanocrystalline copper. *Nature* **2014**, 508(7497) 504-507.

17. Li, H., Liao, J. C., Biological conversion of carbon dioxide to photosynthetic fuels and electrofuels. *Energy Environ. Sci.* **2013**, 6(10) 2892-2899.

18. Keasling, J. D., Manufacturing molecules through metabolic engineering. *Science* **2010**, 330(6009) 1355-1358.

19. Khaselev, O., Turner, J. A., A monolithic photovoltaic-photoelectrochemical device for hydrogen production via water splitting. *Science* **1998**, 280(5362) 425-427.

20. Brillet, J., Yum, J.-H., Cornuz, M., Hisatomi, T., Solarska, R., Augustynski, J., Graetzel, M., Sivula, K., Highly efficient water splitting by a dual-absorber tandem cell. *Nat. Photon.* **2012**, 6(12) 824-828.

21. Liu, C., Tang, J., Chen, H. M., Liu, B., Yang, P., A fully integrated nanosystem of semiconductor nanowires for direct solar water splitting. *Nano Lett.* **2013**, 13(6) 2989-2992.

22. Reece, S. Y., Hamel, J. A., Sung, K., Jarvi, T. D., Esswein, A. J., Pijpers, J. J., Nocera, D. G., Wireless solar water splitting using silicon-based semiconductors and earth-abundant catalysts. *Science* **2011**, 334(6056) 645-648.

23. Cox, C. R., Lee, J. Z., Nocera, D. G., Buonassisi, T., Ten-percent solar-to-fuel conversion with nonprecious materials. *Proc. Natl. Acad. Sci. U.S.A.* **2014**, 111(39) 14057-14061.

24. Nozik, A. J., p-n photoelectrolysis cells. *Appl. Phys. Lett.* **1976**, 29(3) 150-153.

25. Liu, C., Dasgupta, N. P., Yang, P., Semiconductor nanowires for artificial photosynthesis. *Chem. Mater.* **2014**, 26(1) 415-422.

26. Möller, B., Oßmer, R., Howard, B. H., Gottschalk, G., Hippe, H., *Sporomusa*, a new genus of gram-negative anaerobic bacteria including *Sporomusa sphaeroides* spec. nov. And *Sporomusa ovata* spec. nov. *Arch. Microbiol.* **1984**, 139(4) 388-396.

27. Nevin, K. P., Woodard, T. L., Franks, A. E., Summers, Z. M., Lovley, D. R., Microbial electrosynthesis: Feeding microbes electricity to convert carbon dioxide and water to multicarbon extracellular organic compounds. *MBio* **2010**, 1(2).

28. Levenspiel, O., *Chemical Reaction Engineering*, 3rd ed., (John Wiley & Sons, New York) **1999**, p 5.

29. Bond-Watts, B. B., Bellerose, R. J., Chang, M. C., Enzyme mechanism as a kinetic control element for designing synthetic biofuel pathways. *Nat. Chem. Biol.* **2011**, 7(4) 222-227.

30. Chang, M. C., Eachus, R. A., Trieu, W., Ro, D. K., Keasling, J. D., Engineering *Escherichia coli* for production of functionalized terpenoids using plant p450s. *Nat. Chem. Biol.* **2007**, 3(5) 274-277.

31. Sim, S. J., Snell, K. D., Hogan, S. A., Stubbe, J., Rha, C., Sinskey, A. J., PHA synthase activity controls the molecular weight and polydispersity of polyhydroxybutyrate in vivo. *Nat. Biotechnol.* **1997**, 15(1) 63-67.

32. Boettcher, S. W., Warren, E. L., Putnam, M. C., Santori, E. A., Turner-Evans, D., Kelzenberg, M. D., Walter, M. G., Mckone, J. R., Brunschwig, B. S., Atwater, H. A., Lewis, N. S., Photoelectrochemical hydrogen evolution using Si microwire arrays. *J. Am. Chem. Soc.* **2011**, 133(5) 1216-1219.

33. Seger, B., Pedersen, T., Laursen, A. B., Vesborg, P. C., Hansen, O., Chorkendorff, I., Using TiO_2 as a conductive protective layer for photocathodic H_2 evolution. *J. Am. Chem. Soc.* **2013**, 135(3) 1057-1064.

34. Liu, B., Aydil, E. S., Growth of oriented single-crystalline rutile TiO_2 nanorods on transparent conducting substrates for dye-sensitized solar cells. *J. Am. Chem. Soc.* **2009**, 131(11) 3985-3990.

35. Hwang, Y. J., Hahn, C., Liu, B., Yang, P., Photoelectrochemical properties of TiO_2 nanowire arrays: A study of the dependence on length and atomic layer deposition coating. *ACS Nano* **2012**, 6(6) 5060-5069.

36. *Acetogenesis*, ed Drake, H. L., (Chapman & Hall, New York) **1994**.

37. Jeremiasse, A. W., Hamelers, H. V. M., Kleijn, J. M., Buisman, C. J. N., Use of biocompatible buffers to reduce the concentration overpotential for hydrogen evolution. *Environ. Sci. Technol.* **2009**, 43(17) 6882-6887.

38. Papageorgiou, N., Grätzel, M., Infelta, P. P., On the relevance of mass transport in thin layer nanocrystalline photoelectrochemical solar cells. *Sol. Energy Mater. Sol. Cells* **1996**, 44(4) 405-438.

39. Anthony, J. R., Anthony, L. C., Nowroozi, F., Kwon, G., Newman, J. D., Keasling, J. D., Optimization of the mevalonate-based isoprenoid biosynthetic pathway in *Escherichia coli* for production of the anti-malarial drug precursor amorpha-4,11-diene. *Metab. Eng.* **2009**, 11(1) 13-19.

40. Gibson, D. G., Young, L., Chuang, R. Y., Venter, J. C., Hutchison, C. A., 3rd, Smith, H. O., Enzymatic assembly of DNA molecules up to several hundred kilobases. *Nat. Methods* **2009**, 6(5) 343-345.

41. Amann, E., Ochs, B., Abel, K. J., Tightly regulated *tac* promoter vectors useful for the expression of unfused and fused proteins in *Escherichia coli*. *Gene* **1988**, 69(2) 301-315.

42. Karr, D. B., Waters, J. K., Emerich, D. W., Analysis of poly-beta-hydroxybutyrate in *Rhizobium japonicum* bacteroids by ion-exclusion high-pressure liquid chromatography and UV detection. *Appl. Environ. Microbiol.* **1983**, 46(6) 1339-1344.

43. Martin, V. J., Pitera, D. J., Withers, S. T., Newman, J. D., Keasling, J. D., Engineering a mevalonate pathway in *Escherichia coli* for production of terpenoids. *Nat. Biotechnol.* **2003**, 21(7) 796-802.

44. Martin, V. J., Yoshikuni, Y., Keasling, J. D., The in vivo synthesis of plant sesquiterpenes by *Escherichia coli*. *Biotechnol. Bioeng.* **2001**, 75(5) 497-503.

45. Xiang, C., Meng, A. C., Lewis, N. S., Evaluation and optimization of mass transport of redox species in silicon microwire-array photoelectrodes. *Proc. Natl. Acad. Sci. U.S.A.* **2012**, 109(39) 15622-15627.

46. Wolfe, A. J., The acetate switch. *Microbiol. Mol. Biol. Rev.* **2005**, 69(1) 12-50.

47. Starai, V. J., Gardner, J. G., Escalante-Semerena, J. C., Residue leu-641 of acetyl-CoA synthetase is critical for the acetylation of residue lys-609 by the protein acetyltransferase enzyme of S*almonella enterica*. *J. Biol. Chem.* **2005**, 280(28) 26200-26205.

Chapter 4: *Engineering Methanococcus maripaludis for the production of multi-carbon products from carbon dioxide*

4.1 Introduction

A long-standing goal in synthetic chemistry has been the synthesis of complex, multi-carbon products from carbon dioxide using only sustainable energy sources, an achievement that would mimic photosynthesis, a process with an immense global biosynthetic capacity [*1-3*]. The abundance and low cost of carbon dioxide as a starting material make this an attractive vision for the future of synthetic chemistry. Additionally, such as system could have profound environmental impacts due to the contributions of carbon dioxide emissions to global warming. Much progress has been made toward this goal using completely inorganic catalyst systems as well as hybrid biological-inorganic systems [*4-8*]. However, many challenges still remain. While completely inorganic systems can display quite high efficiency and product selectivity for one carbon products, both of these metrics suffer when multi-carbon products are attempted [*9*]. Additionally, many of the best catalysts rely on toxic or expensive metals for their catalytic activity. Hybrid biological-inorganic devices have a much expanded product scope, owing to the biosynthetic capacity of microorganisms; however, they often suffer from low yields, poor product selectivity and greater engineering complexity [*10*]. The problems of yield and selectivity within these systems often become more apparent when the biological components are engineered to produce non-native products, as has been consistently observed in efforts to engineer acetogens [*11-13*], which require continued flux through the acetogenesis pathway and therefore the production of acetate in order to maintain ATP pools with the cell. In industrial settings, acetate can be a difficult co-product as it shares many molecular features with water miscible, polar targets, which makes downstream separation from these products a challenge. Some of the most promising hybrid systems to date rely on interfacing engineered *Ralstonia eutropha* strains with electrocatalysts [*14, 15*]. While these systems show good efficiency and product yields, they too have their caveats. The main liability of these platforms is their oxygen requirement, imposed by the metabolism of *R. eutropha*. Aerobic operation of most hydrogen-generating electrocatalysts results in the generation of reactive oxygen species, which are quite toxic to most organisms [*14, 15*]. To overcome this toxicity more complicated reactor or catalyst designs are needed or expensive additives are required in the electrolysis media. Additionally, aerobic hydrogen production can result in explosive gas mixtures, which could prove to be a substantial safety concern at large scales. Also, the low solubility of oxygen presents a formidable challenge for uniform gas delivery in industrial scale fermenters [*16*]. Another drawback of these systems is the high ATP demands of the native *R. eutropha* carbon fixation pathway [*17*].

Building on the successes of previous hybrid biological-inorganic systems and informed by their limitations [*14, 15, 18-20*], we have sought to develop *Methanococcus maripaludis* as a biological catalyst for incorporation into improved hybrid systems for the sustainable synthesis of multi-carbon products from carbon dioxide. *M. maripaludis* is an obligately anaerobic methanogenic archaea, which natively fixes carbon dioxide into methane and biomass at mesophilic temperatures using the energy efficient Wood-Ljungdahl pathway [*21*]. It is also capable of diazotrophic growth, fixing gaseous nitrogen into ammonia for incorporation into organic molecules [*22*]. There is a burgeoning genetic toolbox for this organism [*23*], as well as an ever growing number of studies exploring its physiology and metabolism [*24*]. Additionally, our laboratory has found that many of the tools and methods developed for *Methanosarcina* species, another model methanogenic archaea with a substantial genetic toolbox [*25*], are transferable to *M. maripaludis*, greatly expanding the resources available for genetic manipulation. In addition to its genetic tractability,

its fast growth rate (~2 h doubling time) makes it an attractive organism for engineering, in comparison to other slower-growing acetogens and methanogens.

Additional benefits of using *M. maripaludis* as a chassis for electrosynthesis become apparent when considering the practicalities of interfacing a biological catalyst with inorganic systems. Its obligately anaerobic metabolism eliminates the problems associated with aerobic electrocatalysis, such as generation of reactive oxygen species, the potential for explosive gas mixtures and the challenges associated with oxygen delivery to large volumes. Its versatile metabolism, supported by either formate or mixtures of carbon dioxide and hydrogen gas, is also amenable to integration with inorganic catalysts. Efficient electrocatalysts exist for the conversion of carbon dioxide and water to formate [*26, 27*], a highly soluble product easily delivered in aqueous solutions. Similarly, many efficient bio-compatible electrocatalysis exist for the generation of hydrogen in microbial culture media [*19*], and carbon dioxide is highly soluble in aqueous solutions making delivery facile. In terms of product selectivity, engineered methanogens, similar to engineered acetogens, will likely still need to produce methane using the methanogenesis pathway in order to maintain ATP pools within the cell. However, from a practical prospective a methane co-product is much more desirable than an acetate co-product. Methane, as a gas, will be phase separated from any aqueously soluble target molecules. Additionally, it is the principal component of natural gas and is already used for power generation, lending itself to on-site consumption in an industrial setting to satisfy the energy requirements of manufacturing.

With these benefits in mind, this work shows the advances that have been made toward developing *M. maripaludis* as an efficient biological catalyst for integration into hybrid bioinorganic carbon fixation systems. Specifically, progress has been made in the robust expression of a multi-enzyme pathway, the 3-hydroxybutyrate (3HB) biosynthetic pathway [*28*], which produces a monomer that can be polymerized into polyhydroxybutyrate (PHB), a commercially available bioplastic [*29*]. Investigations into the expression of this pathway led to the discovery that the pool of redox cofactors found in this species may be distinct from most commonly used heterotrophic model organisms, containing NAD^+/NADH concentrations approximately 3% of those found in *Escherichia coli*. Efforts are ongoing to fully understand the pool of redox cofactors present in this organism and harness them for pathway construction. Additionally, preliminary studies have attempted to dysregulate the nitrogen fixation machinery of this organism for constitutive nitrogen fixation, with the ultimate goal being incorporation of fixed nitrogen into value-added products.

4.2 Materials and methods

Materials. Reagents were purchased from commercial sources as noted below in *Commercial materials* and used without further purification. Ultra high purity gases purchased from Praxair (Danbury, CT) were used for all anaerobic manipulations. Distilled water (dH_2O) was deionized to a resistivity of 18.2 MΩ·cm using a Millipore Milli-Q UF Plus system (ddH_2O).

Commercial materials. Sodium chloride, magnesium sulfate heptahydrate, ammonium chloride, potassium phosphate monobasic, potassium phosphate dibasic, sodium phosphate monobasic, sodium phosphate dibasic, manganese(II) chloride tetrahydrate, methanol, and pressure release aluminum crimp seals (20 mm) were purchased from Fisher Scientific (Pittsburgh,

PA). Calcium chloride dihydrate, iron(II) sulfate heptahydrate, nickel(II) chloride hexahydrate, boric acid, cobalt(II) chloride hexahydrate, copper(II) chloride dihydrate, sodium molybdate dihydrate, sodium sulfide, L-cysteine, biotin, folic acid, pyridoxine hydrochloride, thiamine hydrochloride, riboflavin, nicotinic acid, calcium D-(+)-pantothenate, vitamin B_{12}, *p*-aminobenzoic acid, and thioctic acid were purchased from Sigma Aldrich (St. Louis, MO). Yeast extract was purchased from EMD Biosciences (Darmstadt, Germany). Casitone (pancreatic digest of casein) was purchased from BD (Franklin Lakes, NJ). Zinc sulfate heptahydrate was purchased from Mallinckrodt Chemicals (St. Louis, MO). Resazurin was purchased from Eastman Kodak Company (Rochester, NY). Balch tubes (18 x 150 mm), anaerobic media bottles (250 mL and 2 L) and butyl rubber stoppers (20 mm) were purchased from Chemglass (Vineland, NJ).

Strain details and culture conditions. *Methanococcus maripaludis* LL (ATCC BAA-2049) was purchased from the American Type Culture Collection (Manassas, VA). All culture manipulations were performed inside a Vacuum Atmospheres Nexus One glovebox with an atmosphere of 90% nitrogen and 10% hydrogen. Oxygen levels and humidity levels within the box were controlled using a STAK-PAK palladium catalyst and desiccant system in a Coy Laboratory Products unheated fan box. *M. maripaludis* cultures were propagated in 18 × 150 mm Balch tubes with butyl rubber stoppers and aluminum crimp seals using modified McCas medium with formate (0.2 M) as the growth substrate. All cultures were grown at 37 °C without shaking. Stock cultures were stored at room temperature in the dark after growth and were propagated by diluting 1:100 into fresh McCas media at least every 2 weeks. The stock cultures were used until changes in growth patterns were observed. Glycerol stocks were used for long-term culture storage.

Medium preparation. Modified McCas medium [*30*] was used as the standard medium for the cultivation of *M. maripaludis*. To prepare the medium, all components (listed below) except the reducing agent were dissolved in the appropriate volume of ddH_2O. The solution was brought to a vigorous boil while sparging with an 80% N_2/20% CO_2 gas mixture. The solution was boiled until it became a bright pink color, at which point it was moved to an ice bath and cooled to room temperature under constant sparging with the above gas mixture. The medium was subsequently transferred to 80% N_2/20% CO_2-degassed Balch tubes using a modified Drummond Original Pipet-Aid Pipet Controller with the gas inlet line dispensing an 80% N_2/20% CO_2 gas mixture. The tubes were sealed with butyl rubber stoppers and aluminum crimps, and 100 µL reducing agent (see preparation below) was injected per 10 mL of medium using a N_2-flushed syringe. The sealed medium was autoclaved, resulting in a tan colored solution with gray to black precipitate visible.

A similar procedure was followed for the preparation of bottle plates, except after boiling and cooling 50 mL of the modified McCas medium was dispensed into 80% N_2/20% CO_2-degassed 250 mL serum bottles to which 750 mg of agar had been added before degassing. The bottles were sealed with butyl rubber stoppers and aluminum crimps, and 500 µL reducing agent was injected using a N_2-flushed syringe. The sealed medium was autoclaved, resulting in a tan colored solution. After autoclaving the medium was moved into the anaerobic glovebox where puromycin was added to a final concentration of 2.5 µg/mL and the medium was allowed to solidify at room temperature.

A stock of reducing agent was prepared by adding a 0.01% (w/v) resazurin solution (200 µL) to ddH_2O (200 mL) and sparging the solution with N_2 for 20 min. Under continuous N_2 flow, L-cysteine (6 g) was added, followed by sodium sulfide nonahydrate (6 g). The N_2 sparge was

continued until the sodium sulfide had dissolved and the solution was completely colorless. After preparation, the reducing agent was stored under an N_2 atmosphere in a 250 mL serum bottle sealed with a butyl rubber stopper and aluminum crimp.

Per liter, the modified McCas medium contains:

ddH_2O	500 mL
N-free general salts solution	500 mL
$NaHCO_3$	5 g
NaCl	10.5 g
K_2HPO_4	140 mg
$FeSO_4 \cdot 7H_2O$	10 mg
N-free trace minerals solution (100X)	10 mL
Wolfe's vitamin solution	10 mL
Resazurin solution (0.01% (w/v))	1 mL
Sodium acetate	850 mg
MOPS (2 M, pH 7)	100 mL
Magnesium formate dihydrate	15 g
NH_4Cl	500 mg
Casamino acids	2 g

Per liter, the N-free general salts solution contains:

KCl	670 mg
$MgCl_2 \cdot 6H_2O$	5.5 g
$MgSO_4 \cdot 7H_2O$	6.9 g
$CaCl_2 \cdot 2H_2O$	280 mg
ddH_2O	1 L

To prepare the N-free trace minerals solution trisodium citrate was dissolved in water, and the pH was adjusted to 6.5. Then the remaining salts (see below) were added.

Per liter, the N-free trace minerals solution contains:

Trisodium citrate dihydrate	2.1 g
$MnSO_4 \cdot H_2O$	500 mg
$CoCl_2 \cdot 6H_2O$	100 mg
$ZnSO_4 \cdot 7H_2O$	100 mg
$CuCl_2 \cdot 2H_2O$	6.8 mg
$AlK(SO_4)_2 \cdot 12H_2O$	10 mg
H_3BO_3	10 mg
$Na_2MoO_4 \cdot 2H_2O$	100 mg
$NiCl_2 \cdot 6H_2O$	25 mg
Na_2SeO_3	200 mg
VCl_3	10 mg
$Na_2WO_4 \cdot 2H_2O$	3.3 mg

Construction of plasmids. Standard molecular biology techniques were used for plasmid construction. *E. coli* DH10B-T1^R served as the cloning host. All PCR amplifications were carried out with Phusion or Q5 polymerases (New England Biolabs). Plasmids were assembled using the Gibson method [*31*], and sequences were verified using Sanger sequencing (Quintara Biosciences, Berkeley, CA). The sequences of gBlocks and primers used for plasmid construction can be found in Appendix 1.

pTrc33-CRF-Δhpt::adhE-pac. pTrc33 [*32*] was digested with BamHI/XbaI. Inserts were generated by PCR using primers MMP0146-pTrc33 Gibson R and Pac-MMP0146 Gibson F to amplify the downstream homology arm from *M. maripaludis* genomic DNA, primers Pac-MMP0146 Gibson R and F-Pac-adhE-Pac Gibson to amplify the puromycin resistance cassette from pWM321 [*33*], primers R-Promoter-adhE-Pac Gibson and F-Promoter-adhE-Pac Gibson to amplify the *M. barkeri pmcrB* promoter from gblock MBpmcrB, primers Ec-adhE-F1 and hpcE-adhE Gibson F to amplify *adhE* from *E. coli* genomic DNA, and primers hpcE-adhE Gibson R and pTrc33-MMP0143 Gibson F to amplify the upstream homology arm from *M. maripaludis* genomic DNA. The *pmcrB* promoter and *adhE* were joined by splicing by overlap extension (SOE) PCR with primers hpcE-adhE Gibson F and R-Promoter-adhE-Pac Gibson. The inserts and vector were joined using the Gibson method.

pTrc33-CRF-Δhpt::adhE-Strep-pac. pTrc33-CRF-Δhpt::adhE-pac was digested with BamHI/XhoI. Inserts were generated by PCR using primers PmcrB R and Strep-adhE Gibson F to amplify *adhE* from pTrc33-CRF-Δhpt::adhE-pac, and primers adhE-Strep Gibson and pTrc33-MMP0143 Gibson F to amplify the upstream homology arm from pTrc33-CRF-Δhpt::adhE-pac. The inserts and vector were joined using the Gibson method.

pTrc33-CRF-Δhpt::MMCOadhE-Strep-pac. pTrc33-CRF-Δhpt::adhE-pac was digested with BamHI/XhoI. The upstream homology arm insert was generated by PCR using primers hpcE-MMCOECadhE-GibsonR and pTrc33-MMP0143 Gibson F amplifying from pTrc33-CRF-Δhpt::adhE-pac. gblocks MMCOECadhE 1, MMCOECadhE 2, and MMCOECadhE 3 were also used as inserts. The inserts and vector were joined using the Gibson method.

pTrc33-CRF-Δhpt::phaA-phaB-tesB-pac. pTrc33-CRF-Δhpt::adhE-pac was digested with BamHI/XhoI. The upstream homology arm insert was generated by PCR using primers hpcE-MMCOECadhE-GibsonR and pTrc33-MMP0143 Gibson F amplifying from pTrc33-CRF-Δhpt::adhE-pac. gblocks phaA, phaB, and tesB were also used as inserts. The inserts and vector were joined using the Gibson method.

pTrc33-CRF-Δhpt::phaA-hbd-tesB-pac. pTrc33-CRF-Δhpt::adhE-pac was digested with BamHI/XhoI. The upstream homology arm insert was generated by PCR using primers hpcE-MMCOECadhE-GibsonR and pTrc33-MMP0143 Gibson F amplifying from pTrc33-CRF-Δhpt::adhE-pac. gblocks phaA, hbd, and tesB were also used as inserts. The inserts and vector were joined using the Gibson method.

pTrc33-CRF-Δhpt::phaA-Strep-phaB-Strep-tesB-Strep-pac. pTrc33-CRF-Δhpt::adhE-pac was digested with BamHI/XhoI. Inserts were generated by PCR using primers MMCOphaA R and

PhaB-Strep-PhaA GR to amplify *phaA* from pTrc33-CRF-Δhpt::phaA-phaB-tesB-pac, primers PhaB-Strep-PhaA GF and tesB-Strep-phaB GR to amplify *phaB* from pTrc33-CRF-Δhpt::phaA-phaB-tesB-pac, primers tesB-Strep-phaB GF and hpcE-Strep-tesB GR to amplify *tesB* from pTrc33-CRF-Δhpt::phaA-phaB-tesB-pac, and primers hpcE-Strep-tesB GF and pTrc33-MMP0143 Gibson F to amplify the upstream homology arm from pTrc33-CRF-Δhpt::phaA-phaB-tesB-pac. The *phaA*, *phaB* and *tesB* inserts were joined by SOE PCR using primers MMCOphaA R and hpcE-Strep-tesB GR. The inserts and vector were then joined using the Gibson method.

pTrc33-CRF-Δhpt::phaA-Strep-hbd-Strep-tesB-Strep-pac. pTrc33-CRF-Δhpt::adhE-pac was digested with BamHI/XhoI. Inserts were generated by PCR using primers MMCOphaA R and PhaB-Strep-PhaA GR to amplify *phaA* from pTrc33-CRF-Δhpt::phaA-phaB-tesB-pac, primers hbd-Strep-PhaA GF and tesB-Strep-hbd GR to amplify *hbd* from pTrc33-CRF-Δhpt::phaA-hbd-tesB-pac, primers tesB-Strep-hbd GF and hpcE-Strep-tesB GR to amplify *tesB* from pTrc33-CRF-Δhpt::phaA-phaB-tesB-pac, and primers hpcE-Strep-tesB GF and pTrc33-MMP0143 Gibson F to amplify the upstream homology arm from pTrc33-CRF-Δhpt::phaA-phaB-tesB-pac. The *phaA*, *hbd*, and *tesB* inserts were joined by SOE PCR using primers MMCOphaA R and hpcE-Strep-tesB GR. The inserts and vector were then joined using the Gibson method.

pTrc33-CRF-Δhpt::phaA-Strep-phaB-Strep-tesB-Strep-(syntheticRBS)-pac. pTrc33-CRF-Δhpt::adhE-pac was digested with BamHI/XhoI. Inserts were generated by PCR using primers MMCOphaA R and phaB-sRBS-phaA GR to amplify *phaA* from pTrc33-CRF-Δhpt::phaA-Strep-phaB-Strep-tesB-Strep-pac, primers phaB-sRBS-phaA GF and tesB-sRBS-phaB GR were used to amplify *phaB* from pTrc33-CRF-Δhpt::phaA-Strep-phaB-Strep-tesB-Strep-pac, and primers tesB-sRBS-phaB GF and pTrc33-MMP0143 Gibson F were used to amplify *tesB* and the upstream homology arm from pTrc33-CRF-Δhpt::phaA-Strep-phaB-Strep-tesB-Strep-pac, The inserts and vector were then joined using the Gibson method.

pTrc33-CRF-Δhpt::phaA-Strep-phaB-Strep-tesB-Strep-terminator-(canonicalRBS)-pac. pTrc33-CRF-Δhpt::adhE-pac was digested with BamHI/XhoI. Inserts were generated by PCR using primers MMCOphaA R and phaB-cRBS-phaA GR to amplify *phaA* from pTrc33-CRF-Δhpt::phaA-Strep-phaB-Strep-tesB-Strep-pac, primers phaB-cRBS-phaA GF and tesB-cRBS-phaB GR were used to amplify *phaB* from pTrc33-CRF-Δhpt::phaA-Strep-phaB-Strep-tesB-Strep-pac, primers tesB-cRBS-phaB GF and T73 tesB GF were used to amplify *tesB* from pTrc33-CRF-Δhpt::phaA-Strep-phaB-Strep-tesB-Strep-pac, and primers pflaB1-T73 GR3, plaB1-T73 GR2, hpcE T73 GR and pTrc33-MMP0143 Gibson F were used to amplify the upstream homology arm from pTrc33-CRF-Δhpt::phaA-Strep-phaB-Strep-tesB-Strep-pac and install a terminator. The inserts and vector were then joined using the Gibson method.

pTrc33-CRF-Δhpt::pmcrB-phaA-pflaB1-phaB-phdrC1-tesB-pac. pTrc33-CRF-Δhpt::adhE-pac was digested with BamHI/XhoI. Inserts were generated by PCR using primers MMCOphaA R and pflaB1-phaA GR to amplify *phaA* from pTrc33-CRF-Δhpt::phaA-phaB-tesB-pac, primers pflaB1-phaA GF and phaB-pflaB1 GR were used to amplify the *pflaB1* promoter from *M. maripaludis* genomic DNA, primers phaB-pflaB1 GF and phdrC1-phaB GR were used to amplify *phaB* from pTrc33-CRF-Δhpt::phaA-phaB-tesB-pac, primers phdrC1-phaB GF and tesB-phdrC1 GR were used to amplify the *phdrC1* promoter from *M. maripaludis* genomic DNA, and primers tesB-phdrC1 GF and pTrc33-MMP0143 Gibson F were used to amplify *tesB* and the upstream homology arm from pTrc33-CRF-Δhpt::phaA-phaB-tesB-pac. All inserts were joined using SOE

PCR with primers MMCOphaA R and pTrc33-MMP0143 Gibson F. The inserts and vector were joined using the Gibson method.

pTrc33-CRF-Δhpt::pmcrB-phaA-pflaB1-hbd-phdrC1-tesB-pac. pTrc33-CRF-Δhpt::adhE-pac was digested with BamHI/XhoI. Inserts were generated by PCR using primers MMCOphaA R and pflaB1-phaA GR to amplify *phaA* from pTrc33-CRF-Δhpt::phaA-phaB-tesB-pac, primers pflaB1-phaA GF and hbd-pflaB1 GR were used to amplify the *pflaB1* promoter from *M. maripaludis* genomic DNA, primers hbd-pflaB1 GF and phdrC1-hbd GR were used to amplify *hbd* from pTrc33-CRF-Δhpt::phaA-hbd-tesB-pac, primers phdrC1-hbd GF and tesB-phdrC1 GR were used to amplify the *phdrC1* promoter from *M. maripaludis* genomic DNA, and primers tesB-phdrC1 GF and pTrc33-MMP0143 Gibson F were used to amplify *tesB* and the upstream homology arm from pTrc33-CRF-Δhpt::phaA-phaB-tesB-pac. All inserts were joined using SOE PCR with primers MMCOphaA R and pTrc33-MMP0143 Gibson F. The inserts and vector were joined using the Gibson method.

pTrc33-CRF-Δhpt::pmcrB-phaA-Strep-pflaB1-phaB-Strep-phdrC1-tesB-Strep-pac. pTrc33-CRF-Δhpt::adhE-pac was digested with BamHI/XhoI. Inserts were generated by PCR using primers MMCOphaA R and pflaB1-phaAS GR to amplify *phaA* from pTrc33-CRF-Δhpt::phaA-Strep-phaB-Strep-tesB-Strep-pac, primers pflaB1-phaAS GF and phaB-pflaB1 GR were used to amplify the *pflaB1* promoter from *M. maripaludis* genomic DNA, primers phaB-pflaB1 GF and phdrC1-phaBS GR were used to amplify *phaB* from pTrc33-CRF-Δhpt::phaA-Strep-phaB-Strep-tesB-Strep-pac, primers phdrC1-phaBS GF and tesB-phdrC1 GR were used to amplify the *phdrC1* promoter from *M. maripaludis* genomic DNA, and primers tesB-phdrC1 GF and pTrc33-MMP0143 Gibson F were used to amplify *tesB* and the upstream homology arm from pTrc33-CRF-Δhpt::phaA-Strep-phaB-Strep-tesB-Strep-pac. All inserts were joined using SOE PCR with primers MMCOphaA R and pTrc33-MMP0143 Gibson F. The inserts and vector were joined using the Gibson method.

pTrc33-CRF-Δhpt::pmcrB-phaA-Strep-pflaB1-hbd-Strep-phdrC1-tesB-Strep-pac. pTrc33-CRF-Δhpt::adhE-pac was digested with BamHI/XhoI. Inserts were generated by PCR using primers MMCOphaA R and pflaB1-phaAS GR to amplify *phaA* from pTrc33-CRF-Δhpt::phaA-Strep-phaB-Strep-tesB-Strep-pac, primers pflaB1-phaAS GF and hbd-pflaB1 GR were used to amplify the *pflaB1* promoter from *M. maripaludis* genomic DNA, primers hbd-pflaB1 GF and phdrC1-hbdS GR were used to amplify *hbd* from pTrc33-CRF-Δhpt::phaA-Strep-hbd-Strep-tesB-Strep-pac, primers phdrC1-hbdS GF and tesB-phdrC1 GR were used to amplify the *phdrC1* promoter from *M. maripaludis* genomic DNA, and primers tesB-phdrC1 GF and pTrc33-MMP0143 Gibson F were used to amplify *tesB* and the upstream homology arm from pTrc33-CRF-Δhpt::phaA-Strep-phaB-Strep-tesB-Strep-pac. All inserts were joined using SOE PCR with primers MMCOphaA R and pTrc33-MMP0143 Gibson F. The inserts and vector were joined using the Gibson method.

pTrc33-CRF-Δhpt::pmcrB-phaA-Strep-terminator-pflaB1-hbd-Strep-terminator-pac. pTrc33-CRF-Δhpt::pmcrB-phaA-Strep-pflaB1-hbd-Strep-phdrC1-tesB-Strep-pac was digested with BamHI/NotI. Inserts were generated by PCR using primers pflaB1-T73 GF and pflaB1-T73 GR3 to amplify a terminator from pTrc33-CRF-Δhpt::phaA-Strep-phaB-Strep-tesB-Strep-terminator-(canonicalRBS)-pac, and primers pflaB1-T73 GR and Trc hbd GF to amplify *hbd* from pTrc33-CRF-Δhpt::pmcrB-phaA-Strep-pflaB1-hbd-Strep-phdrC1-tesB-Strep-pac. The inserts were joined

by SOE PCR using primers pflaB1-T73 GR3 and Trc hbd GF. The inserts and vector were joined using the Gibson method to form a cloning intermediate. This cloning intermediate was then digested with BamHI. Inserts were generated by PCR using primers hpcE T3050 GF and T3050 hbd GR to amplify a terminator from a primer mix of T3050 hbd GF, T3050 hbd GF2 and hpcE T3050 GR, and primers hpcE T3050 GR and pTrc33-MMP0143 Gibson F to amplify the upstream homology arm from pTrc33-CRF-Δhpt::pmcrB-phaA-Strep-pflaB1-hbd-Strep-phdrC1-tesB-Strep-pac. The inserts were joined by SOE PCR using primers T3050 hbd GR and pTrc33-MMP0143 GF. The inserts and vector were then joined using the Gibson method.

pTrc33-CRF-Δhpt::phdrC1-phaA-Strep-terminator-pflaB1-hbd-Strep-terminator-pac. pTrc33-CRF-Δhpt::adhE-pac was digested with BamHI/XhoI. Inserts were generated by PCR using primers phdrC1 pac GR and phaA phdrC1 GF to amplify the *phdrC1* promoter from pTrc33-CRF-Δhpt::pmcrB-phaA-Strep-pflaB1-hbd-Strep-phdrC1-tesB-Strep-pac, and primers phaA phdrC1 GR and pTrc33-MMP0143 Gibson F to amplify *phaA*, a terminator, the *pflaB1* promoter, *hbd*, another terminator and the upstream homology arm from pTrc33-CRF-Δhpt::pmcrB-phaA-Strep-terminator-pflaB1-hbd-Strep-terminator-pac. The inserts were joined by SOE PCR using primers phdrC1 pac GR and pTrc33-MMP0143 Gibson F. The inserts and vector were then joined using the Gibson method.

pTrc33-CRF-Δhpt::pmcrB-hbd-pac. pTrc33-CRF-Δhpt::adhE-pac was digested with BamHI/XhoI. Inserts were generated by PCR using primers hbd-pmcrB GR, hbd-pmcrB GR2 and hpcE-hbd GR2 to amplify *hbd* from pTrc33-CRF-Δhpt::pmcrB-phaA-pflaB1-hbd-phdrC1-tesB-pac, and primers hpcE-hbd GR and pTrc33-MMP0143 Gibson F to amplify the upstream homology arm from pTrc33-CRF-Δhpt::pmcrB-phaA-pflaB1-hbd-phdrC1-tesB-pac. The inserts and vector were joined using the Gibson method.

pTrc33-CRF-Δhpt::pmcrB-hbd-Strep-pac. pTrc33-CRF-Δhpt::adhE-pac was digested with BamHI/XhoI. Inserts were generated by PCR using primers hbd-pmcrB GR, hbd-pmcrB GR2 and hpcE-hbdS GF to amplify *hbd* from pTrc33-CRF-Δhpt::pmcrB-phaA-Strep-pflaB1-hbd-Strep-phdrC1-tesB-Strep-pac, and primers hpcE-Strep-tesB GF and pTrc33-MMP0143 Gibson F to amplify the upstream homology arm from pTrc33-CRF-Δhpt::pmcrB-phaA-pflaB1-hbd-phdrC1-tesB-pac. The inserts and vector were joined using the Gibson method.

pTrc33-CRF-Δhpt::pmcrB-tesB-pac. pTrc33-CRF-Δhpt::adhE-pac was digested with BamHI/XhoI. The insert was generated by PCR using primers tesB-pmcrB GR, hbd-pmcrB GR2 and pTrc33-MMP0143 Gibson F to amplify *tesB* and the upstream homology arm from pTrc33-CRF-Δhpt::pmcrB-phaA-pflaB1-hbd-phdrC1-tesB-pac. The insert and vector were joined using the Gibson method.

pTrc33-CRF-Δhpt::pmcrB-tesB-Strep-pac. pTrc33-CRF-Δhpt::adhE-pac was digested with BamHI/XhoI. The insert was generated by PCR using primers tesB-pmcrB GR, hbd-pmcrB GR2 and pTrc33-MMP0143 Gibson F to amplify *tesB* and the upstream homology arm from pTrc33-CRF-Δhpt::pmcrB-phaA-Strep-pflaB1-hbd-Strep-phdrC1-tesB-Strep-pac. The insert and vector were joined using the Gibson method.

pTrc33-CRF-Δhpt::pmcrB-phaA-Strep-pmcrB-hbd-Strep-pmcrB-tesB-Strep-pac. pTrc33-CRF-Δhpt::pmcrB-phaA-Strep-pflaB1-hbd-Strep-phdrC1-tesB-Strep-pac was digested with

BamHI/NotI. The insert was generated by PCR using primers pmcrB phaA GR and Trc hbd GF to amplify *hbd* from pTrc33-CRF-Δhpt::pmcrB-hbd-Strep-pac. The insert and vector were joined using the Gibson method to generate a cloning intermediate. This cloning intermediate was then digested with BamHI. The next insert was generated by PCR using primers pmcrB hbd GR and pTrc33-MMP0143 Gibson F to amplify *tesB* and the upstream homology arm from pTrc33-CRF-Δhpt::pmcrB-tesB-Strep-pac. The insert and vector were joined using the Gibson method.

pTrc33-CRF-Δhpt::patpD-MMP1349-phdrC1-MMP1578-pac. pTrc33-CRF-Δhpt::adhE-pac was digested with BamHI/XhoI. Inserts were generated by PCR using primers pTrc33-MMP0143 Gibson F and pTrcNADHGIbson to amplify the upstream homology arm from pTrc33-CRF-Δhpt::adhE-pac, primers MMP1349-F and MMP1349-mcis-clone-R to amplify *MMP1349* from *M. maripaludis* genomic DNA, primers hdrcI-mcis-clone-F and HdrcI-mcis-clone-R to amplify the *phdrC1* promoter from *M. maripaludis* genomic DNA, primers MMP1578-Mcis-clone-F and MMP1578R to amplify *MMP1578* from *M. maripaludis* genomic DNA. The inserts and vector were joined using the Gibson method.

pTrc33-CRF-nif-mut. pTrc33 [*32*] was digested with BamHI/XbaI. Inserts were generated by PCR using primers pTrc33-MMP0851 Gibson F and MMP0852-R to amplify the upstream homology arm from *M. maripaludis* genomic DNA, primers Pnif-mut-F and nifH-Pac-GibsonR to amplify the nitrogenase promoter region and *nifH* from a mixture of Pnif-mut gblock and *M. maripaludis* genomic DNA in a SOE PCR reaction, primers nifH-Pac-GibsonF and Pac-nifD-GibsonR to amplify the puromycin resistance gene from pWM321 [*33*], primers Pac-nifD-GibsonF and nifD-pTrc33-GibsonR to amplify the downstream homology arm from *M. maripaludis* genomic DNA. The inserts and vector were joined using the Gibson method.

Transformation of *M. maripaludis*. *M. maripaludis* was transformed using protocols previously described for the transformation of *Methanosarcina* species [*34*]. Cultures were grown to late log phase (10 mL per transformation). The cells were harvested by centrifugation (2000 × *g* for 10 min) inside the anaerobic chamber. The media was removed, and the cells were washed with 5 mL of transformation buffer (see below) per 10 mL initial culture volume. The cells were collected by centrifugation again. The supernatant was discarded, and the cell pellet was resuspended in 1 mL transformation buffer per 10 mL initial culture volume. For each transformation to be performed 300 µL transformation buffer was aliquoted into a 6 mL serum vial. These vials were closed with a butyl rubber stopper and removed from the anaerobic chamber. Using aseptic technique 2-4 µg of plasmid and 30 µL DOTAP liposomal transfection reagent (Roche) were added to each vial. The vials were closed again with butyl rubber stoppers and sealed with aluminum crimps. They were then degassed by purging with argon for 5 min and returned to the anaerobic chamber. At this point 1 mL of the cell suspension was added to each vial. The vials were incubated at 37 °C for 1 h. After the incubation the entire contents of the vial was transferred to 10 mL of fresh medium in a Balch tube. The cells were recovered at 37 °C for at least 4 h. After recovery, the cells were harvested by centrifugation and resuspended in 200 µL modified McCas medium. They were then spread on the surface of an anaerobic bottle plate. The plates were incubated at room temperature with the surface of the plate horizontal for at least 30 min to allow time for the cells to attach to the plate. After incubation the bottles were stood upright, with the surface of the plate now vertical. The headspace of the bottle plates was purged with an 80% H_2/20% CO_2 gas mixture for 5 min, and the bottles were ultimately pressurized to 200 kPa using this same gas mixture. The plates were incubated at 37 °C for 3-4 d, at which point colonies were

picked into selective liquid media inside of the anaerobic chamber. Once these culture reached saturation, presence of the desired knock in was confirmed using PCR. The cells could then be used for further experiments, always being propagated in selective media.

To prepare transformation buffer 200 mL of 50 mM HEPES (pH 7.5) with 200 µL of a 0.01% (w/v) resazurin solution added was degassed by boiling under an atmosphere of 20% CO_2/80% N_2 until the solution turned bright pink. The solution was then cooled to room temperature in an ice bath with constant sparging with the above gas mixture. The buffer was subsequently transferred to an 80% N_2/20% CO_2-degassed 250 mL serum bottle using a modified Drummond Original Pipet-Aid Pipet Controller with the gas inlet line dispensing an 80% N_2/20% CO_2 gas mixture. The bottle was closed using a butyl rubber stopper and aluminum crimp. Inside an anaerobic chamber the degassed HEPES buffer was combined with the remaining components of the transformation buffer (see below), and the solution was swirled until all solids had dissolved. The buffer was then filtered into a sterile 250 mL serum bottle using a 0.2 µm syringe filter. The bottle was closed with a sterile butyl rubber stopper and aluminum crimp. Within an hour of preparation, the buffer should become completely colorless. The buffer was stored at room temperature in the dark.

Per 100 mL, the transformation buffer contains:

HEPES (pH 7.5)	100 mL
Sucrose	12 g
NaCl	2.2 g
Cysteine	1 g
Dithiothreitol	771 mg

Purification of AdhE-Strep. 1 L of modified McCas media in a 2 L anaerobic bottle was inoculated 1:100 and grown overnight at 37 °C, shaking at 200 rpm. The cells were harvested by centrifuging for 10 min at 10,000 × *g* at 4 °C, and the pellet was frozen at -80 °C.

The pellet was thawed on ice and resuspened in lysis buffer (100 mM Tris, 150 mM NaCl, 2.5 mM DTT, 0.1 U DNase/mL, 1 mini-cOmplete EDTA-free protease inhibitor cocktail tablet (Roche) per 10 mL buffer, pH 8) (5 mL buffer/g cell pellet). The cells were lysed by sonication using a Misonix 3000 sonicator set at intensity 4 for a total duty time of 2 min in cycles of 2 s ON followed by 20 s OFF, with the tube containing the cells in an ice bath for the duration of the procedure. The soluble and insoluble fractions were separated by centrifuging at 10,000 x g for 20 min at 4 °C. DNA was precipitated by adding streptomycin sulfate to the lysate to a final concentration of 1% (w/v) slowly over 10 min with the lysate stirring at 4 °C. The precipitated DNA was then removed by centrifuging at 18,500 x g for 20 min at 4 °C. 3 nmol of avidin was added to the lysate, and it was then loaded onto a 2 mL Streptactin (Novagen) column that had been equilibrated with 6 mL wash buffer (100 mM Tris, 150 mM NaCl, 2.5 mM DTT, pH 8). After loading, the column was washed with 20 mL wash buffer. adhE-Strep was eluted from the column using 1 mL fractions of elution buffer (100 mM Tris, 150 mM NaCl, 2.5 mM desthiobiotin, 2.5 mM DTT, pH 8). Elution fractions were tested for protein content by measuring the absorbance at 280 nm. Fractions 1-4 contained the highest concentration of protein. These fractions were pooled

and concentrated using an Amicon Ultra 4 mL centrifugal filter (30,000 NMWL). Glycerol was added to 20% (v/v), and aliquots were flash frozen in liquid nitrogen and then stored at -80 °C. The final protein concentration of the aliquots was 1.38 mg/mL, which was determined using a calculated extinction coefficient (ε = 74,720 M^{-1} cm^{-1}).

Quantitative real time PCR. *M. maripaludis* cultures (10 mL) were inoculated 1:100 and grown for 5.5 h at 37 °C without shaking. 6 mL of the culture were harvested by centrifuging for 2 min at 13,000 x g at room temperature. After centrifuging, the pellets were kept on ice, and RNA was extracted using an RNeasy Mini Kit (Qiagen) according to the manufacturer's protocol. For cell lysis, 600 µL buffer RLT with β-mercaptoethanol added was used, and the samples were homogenized using QIAshredder columns. The RNA samples were eluted into 50 µL RNase-free water and quantified using a Nanodrop spectrophotometer. cDNA synthesis was performed using the iScript gDNA Clear cDNA Synthesis Kit (Bio-Rad) according to the manufacturer's protocol, with 500 ng of input RNA per sample. Appropriate no-RT controls were included. The final cDNA synthesis reaction was diluted to 100 µL using DNase-free water. Quantitative real-time PCR was performed using 2X iQ SYBR Green Supermix (Bio-Rad) according to the manufacturer's protocol, using a 2-step cycling method with a 55 °C annealing/extension temperature. Each well of the PCR plate was prepared by mixing a template mastermix (4 µL ddH_2O, 10 µL 2X iQ SYBR Green Supermix, 1 µL diluted cDNA synthesis reaction) with a primer mastermix (3.8 µL ddH_2O, 0.6 µL 10 µM forward primer, 0.6 µL 10 µM reverse primer). The PCR was performed using a Bio-Rad iQ5 Multicolor Real-Time PCR Detection System. The sequences of primers used for quantitative real-time PCR can be found in Appendix 1.

Western blotting experiments. A 10 mL saturated, overnight *M. maripaludis* culture was harvested by centrifuging for 10 min at 10,000 x g at 4 °C. The cell pellet was resuspended in 500 µL lysis buffer (50 mM KH_2PO_4, 1 mini-cOmplete EDTA-free protease inhibitor cocktail tablet (Roche) per 10 mL buffer, pH 7.4). The samples were mixed with 300 µL 0.1 mm glass disruption beads (Research Products International) in 2 mL O-ring sealed, screw cap tubes and were lysed using a BioSpec Products Mini-BeadBeater by beating for 1 min at 4 °C. Cell debris was pelleted by centrifuging for 10 min at 20, 000 x g at 4 °C. The supernatant was then removed to a fresh tube and total protein was quantified using Bradford reagent with a lysozyme standard curve. Gel samples were prepared by mixing the lysates with additional lysis buffer and Laemmli loading buffer. The samples were boiled for 10 min at 98 °C before being separated using SDS-PAGE gel electrophoresis. Once the gel run was complete, the contents of the gel were transferred to a PVDF membrane. After the transfer, the membrane was blocked with 5% non-fat milk in TBS-T overnight at 4 °C. The membrane was blotted using Mouse anti Strep-tag Classic:HRP antibody (Bio-Rad) (1:4000 dilution in 5% non-fat milk in TBS-T) for at least 2 h at room temperature or overnight at 4 °C. After staining, the membrane was washed for 10 min three times with fresh TBS-T. The blot was developed using Western Lightening Plus-ECL (PerkinElmer) and imaged using a Universal Hood II (Bio-Rad).

Cell lysate enzymatic assays. A 10 mL saturated, overnight *M. maripaludis* culture was harvested by centrifuging for 10 min at 10,000 x g at 4 °C. The cell pellet was resuspended in 500 µL lysis buffer (50 mM KH_2PO_4, 1 mini-cOmplete EDTA-free protease inhibitor cocktail tablet (Roche) per 10 mL buffer, pH 7.4). 1 mM DTT was included in the lysis buffer, except when assaying tesB activity. The samples were mixed with 300 µL 0.1 mm glass disruption beads in 2 mL O-ring sealed, screw cap tubes and were lysed using a BioSpec Products Mini-BeadBeater by

beating for 45 s at 4 °C. Cell debris was pelleted by centrifuging for 10 min at 20, 000 x g at 4 °C. The supernatant was then removed to a fresh tube and total protein was quantified using Bradford reagent with a lysozyme standard curve.

adhE: Aldehyde dehydrogenase activity was assayed by monitoring NAD^+ reduction at 340 nm (ε = 6,220 M^{-1} cm^{-1}) at 30 ºC. The assay mixture contained CoA (100 µM), NAD^+ (75 µM), and acetaldehyde (10 mM) in 50 mM CHES, 200 µM DTT, pH 9.5. The reaction was initiated by addition of acetaldehyde.

phaA: Thiolase activity was assayed in the forward direction by monitoring NADH oxidation at 340 nm (ε = 6,220 M^{-1} cm^{-1}) at 30 ºC in a coupled assay with His_{10}-hbd. The assay mixture contained acetyl-CoA (1 mM), NADH (100 µM), and His_{10}-hbd (7.5 U/mL) in 100 mM Tris-HCl, 10 mM $MgCl_2$, 1 mM DTT, pH 7.5. The reaction was initiated by addition of acetyl-CoA.

hbd: The reduction of acetoacetyl-CoA was assayed by monitoring the oxidation of NADH at 340 nm (ε = 6,220 M^{-1} cm^{-1}) at 30 ºC. The assay mixture contained acetoacetyl-CoA (100 µM) and NADH (100 µM) in 100 mM Tris-HCl, 10 mM $MgCl_2$, pH 7.5. The reaction was initiated by addition of acetoacetyl-CoA.

tesB: Thioesterase activity was assayed by monitoring the reaction of free CoA with 5,5'-dithio-bis-[2-nitrobenzoic acid] (DTNB) at 412 nm (ε = 41,150 M^{-1} cm^{-1}) at 30 ºC. The assay mixture contained propionyl-CoA (400 µM) and DTNB (300 µM) in PBS. The reaction was initiated by addition of cell lysate.

Ethanol detection using gas chromatography. Production cultures were sampled at 1, 3 and 5 d post-inoculation. 1 mL culture samples were cleared of biomass by centrifuging for 10 min at 20,000 x g at 4 °C. The cleared media was transferred to a fresh tube and stored at -80 °C until analyzed. The samples were thawed and 180 µL of cleared media was mixed with 20 µL of 10 g/L pentanol as an internal standard. These samples were analyzed on a Trace GC Ultra (Thermo Scientific) using an HP-5MS column (0.25 mm × 30 m, 0.25 µM film thickness, J & W Scientific) using a 1 µL sample injection. The oven program was as follows: 75 °C for 4 min, ramp to 300 °C at 45 °C/min, 300 °C for 2 min. Ethanol and pentanol were measured by flame ionization detection (FID) (flow: 350 ml/min air, 35 ml/min H_2 and 30 ml/min helium). Ethanol eluted at 2.7 min and pentanol eluted at 3.8 min. Ethanol was quantified against a standard curve of 31.25, 62.5, 125, 250, 500, and 1000 mg/L standards prepared in modified McCas media.

3HB detection using high performance liquid chromatography. Production cultures were sampled at 1, 3 and 5 d post-inoculation. 1 mL culture samples were stored at -80 °C until analysis. The culture samples were thawed and then centrifuged for 10 min at 20,000 x g at 4 °C to clear them of biomass. 10 µl of the cleared culture media was diluted into 190 µL of 50 µM adipic acid, which served as the internal standard. Samples were prepared in 96-well plates. Chromatography was performed on an Agilent 1290 HPLC equipped with an auto-sampler, using a Phenomenex Rezex-ROA Organic Acid H^+ column (150 × 4.6 mm), equipped with a Carbo-H^+ Security Guard cartridge. 0.5% (v/v) formic acid was used as the mobile phase with a flow rate of 0.3 ml/min and the column temperature set to 55 °C. 3HB was quantified using an attached mass spectrometer, an Agilent 6460 triple quadrupole MS with ESI source, operating in negative ion MRM transition

mode with the fragmentor voltage set at 70V. Between 5-8 min, the following transitions and collision energies were monitored: m/z 145.1→83.1, 10V (adipic acid, internal standard); m/z 103.1→59.2, 5V (3-hydroxybutyric acid). Samples were quantified relative to a standard curve of 7.8125, 15.625, 31.25, 62.5, 125, 250, 500, and 1000 mg/L 3HB prepared in modified McCas media.

Measurement of intracellular NAD^+/NADH pools. For quantification of the NAD^+ and NADH pools, overnight cultures of *M. maripaludis* or anaerobically grown *E. coli* were used. The assay was performed using an NAD/NADH-Glo Assay Kit (Promega) according to the manufacture's protocol for measuring the NAD^+ and NADH pools individually. Multiple dilutions were used for each cell type to obtain values within the linear range of the standard curve. For *E. coli* 500 µL, 250 µL and 125 µL of pelleted culture were used per sample. For *M. maripaludis* 1000 µL, 500 µL and 250 µL of pelleted culture were used per sample. Cell were harvested by centrifuging for 1 min at 13,000 x g at room temperature. For cell dry weight measurements, the biomass from 4 mL of culture was collected into a pre-massed 2 mL tube by two rounds of centrifugation for 1 min at 13,000 x g at room temperature. As much residual media as possible was removed and the samples were lyophilized overnight. The change in mass of the tubes was determined using a microbalance. Because the modified McCas medium always contains some precipitate after preparation, media used in this experiment was filtered using a 0.2 µm syringe filter before inoculation.

4.3 Results and discussion

Expression of a single enzyme pathway in *M. maripaludis*. Successful metabolic engineering strategies rely on understanding a number of important aspects of host physiology, including native mechanisms of protein expression, dominant carbon flux pathways and the flow of energy and reducing equivalents through the cell. Having an understanding of these facets of metabolism allow heterologous pathways to be expressed, carbon pools to be diverted to a desired target molecule and non-native pathways to be powered by the cell. While much progress has been made in understanding the physiology of *M. maripaludis*, many questions still remain. Also, very little work has been done to apply our current understanding of *M. maripaludis* metabolism to metabolic engineering questions, the only example being a recent report exploring geraniol production in *M. maripaludis* using a heterologously expressed synthase enzyme [*35*]. While modest product titers were achieved, many questions still remain to be answered about the system, such as expression levels of heterologous RNA and protein, as well as other bottlenecks in the pathway, including carbon flux through native enzymes preceding the heterologous enzyme and the effects of the heterologous enzyme on pools of redox cofactors. In order to further explore these important parameters in a simplified system, we chose to express a single enzyme pathway in *M. maripaldis*. Specifically, we chose adhE, an *E. coli* enzyme which catalyzes the conversion of acetyl-coenzyme A (acetyl-CoA) to ethanol [*36, 37*], as our optimization pathway (*Figure 4.1 B*). This pathway seemed a prudent choice for a number of reasons: (1) The product of the pathway is an industrially important chemical and is widely used as a biofuel. (2) The simplicity of the single enzyme pathway could greatly reduce engineering complexity and streamline the optimization process. (3) This enzyme pulls carbon directly from acetyl-CoA, a central node in *M. maripaludis* metabolism and a convenient starting point for the production of a variety of

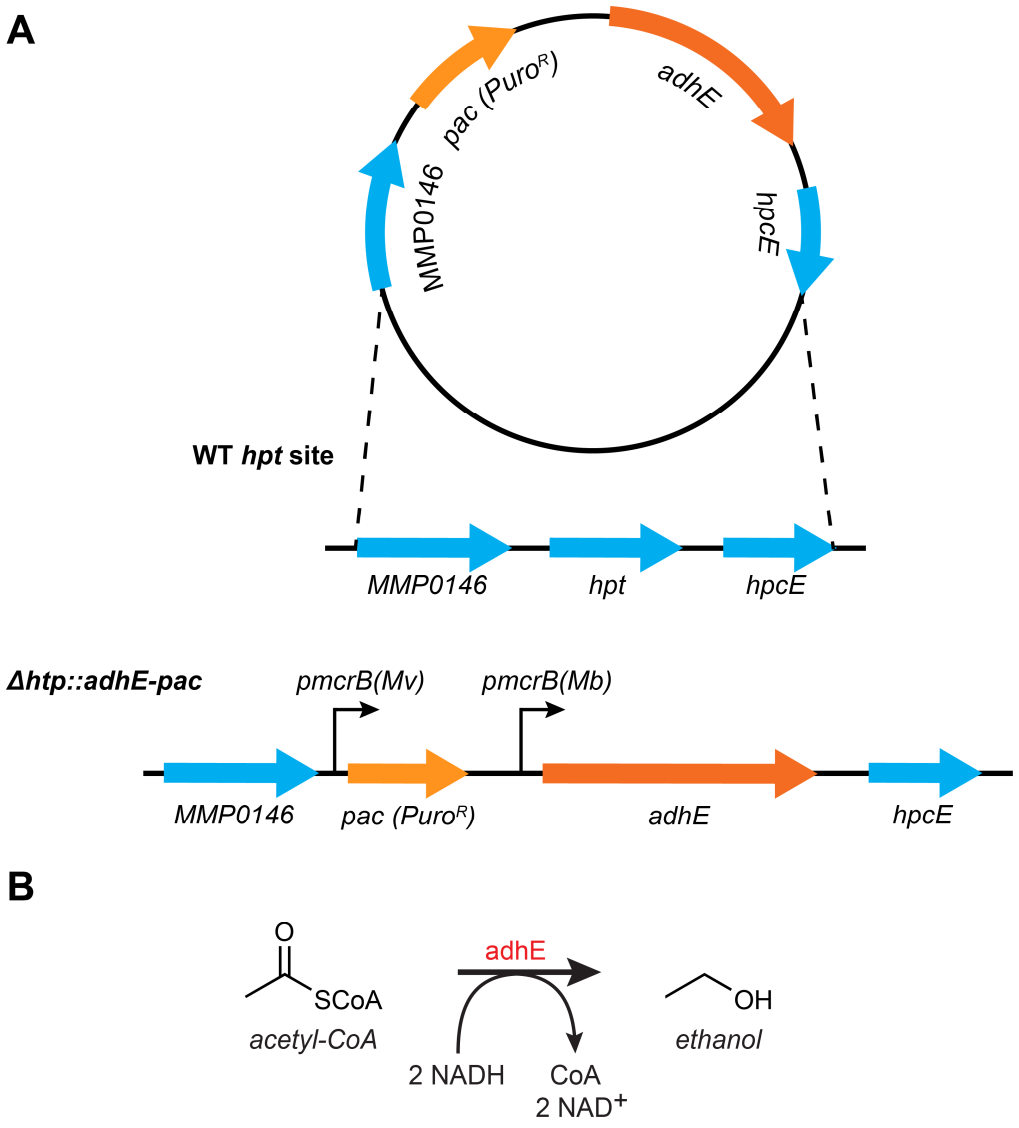

Figure 4.1. Genetic engineering strategies for M. maripaludis. (A) Transgenic *M. maripaludis* strains were generated via homologous recombination. A liposomal transfection reagent was used to deliver a plasmid containing the desired transgenic cassette flaked by 800 bp homology arms which targeted the construct to the *hpt* site. The transgenic cassette included a puromycin resistance gene (*pac*), which allowed selection of successful transformants. The *pac* gene was under the control of the methyl-coenzyme M (methyl-CoM) reductase promoter (*pmcrB*) from *Methanococous voltae* (*Mv*) and *adhE* was under the control of the methyl-CoM reductase promoter from *Methanosarcina barkeri* (*Mb*). (B) adhE catalyzes the transformation of acetyl-CoA to ethanol with reducing equivalents provided by NADH.

industrially relevant targets. Understanding carbon diversion from this central metabolic node could provide incredibly useful insight for the design of future pathways.

AdhE-expressing strains were generated by using liposomal transformation mediated homologous recombination [*34*] to knock the *adhE* gene into the hypoxanthine phosphoribosyltransferase (*hpt*) site with simultaneous knock out of the native *hpt* gene (*Figure 4.1 A*). It has been previously demonstrated that *hpt* knock outs lack any obvious phenotype under most growth conditions [*30*]. This knock in method was used to generate all other transgenic *M. maripaludis* strains reported in this study. The construct used for *ahdE* knock in included a puromycin resistance cassette (*pac*) [*38*], which allows selection of successful transformants. The *pac* gene was under the control of the methyl-coenzyme M (methyl-CoM) reductase promoter (*pmcrB*) from *Methanococous voltae* and *adhE* was under the control of the methyl-CoM reductase promoter from *Methanosarcina barkeri*.

The *adhE*-expressing strain was tested for ethanol production using gas chromatography; however, no product was observed. To begin troubleshooting the system quantitative real-time PCR experiments were performed to assess *adhE* transcript levels. The *adhE* transcript was found to be highly expressed in the transgenic strain (*Figure 4.2 A*). We next investigated levels of protein expression using Western blotting with two transgenic strains that carried Strep-tagged versions of the *adhE* gene, either encoded by the native *E. coli* codon sequence or by a *M. maripaludis* condon optimized version [*39, 40*]. We reasoned that codon optimization could be especially important in this case owing to the extremely low G+C content of *M. maripaludis* (~33%) [*41*]. In this experiment we observed robust protein expression from both strains; however, the codon optimized version of the gene did result in much higher protein levels (*Figure 4.2 B*). Based on this result all other heterologous genes expressed in this study were codon optimized. From the expression data it was clear that RNA and protein levels of the heterologous enzyme were not responsible for the lack of product formation. This implicated enzyme activity, resulting from an intrinsic lack of activity due to enzyme maturation or the cellular environment, a limited substrate pool or lack of redox cofactors to drive the reaction. To separate these potential causes, cell lysate activity assays for adhE were performed. No activity was observed. This would seem to indicate an instrisic activity problem with the enzyme; however, observing adhE activity in cell lysate can be very difficult due to background generated from competing reactions. To eliminate this point of confusion, adhE was purified from *M. maripaludis* (*Figure 4.3*) and tested for activity *in vitro*. No activity was observed. It seems that this enzyme is not active when expressed in this host. This could be due to the extreme redox sensitivity or complex quaternary structure of the protein [*36, 42*]. This result indicated that this single enzyme pathway would not be ideal for elucidating core metabolic engineering principles in this organism.

Expression of the 3HB pathway in *M. maripaludis*. The intrinsic activity problems of ahdE made it apparent that another model pathway would have to be selected to develop metabolic engineering strategies in *M. maripaludis*. The pathway for 3HB synthesis was selected [*28*] (*Figure 4.4*). This pathway had a number of features which made it an ideal choice: (1) 3HB is an industrially interesting product, because it can be polymerized into PHB, a commercially available bioplastic [*29*]. (2) It is composed of only three enzymes, which are structurally less complex than adhE and have been successfully heterologously expressed in a number of different hosts [*28, 43*]. (3) Once again this pathway pulls carbon directly from the acetyl-CoA node of metabolism.

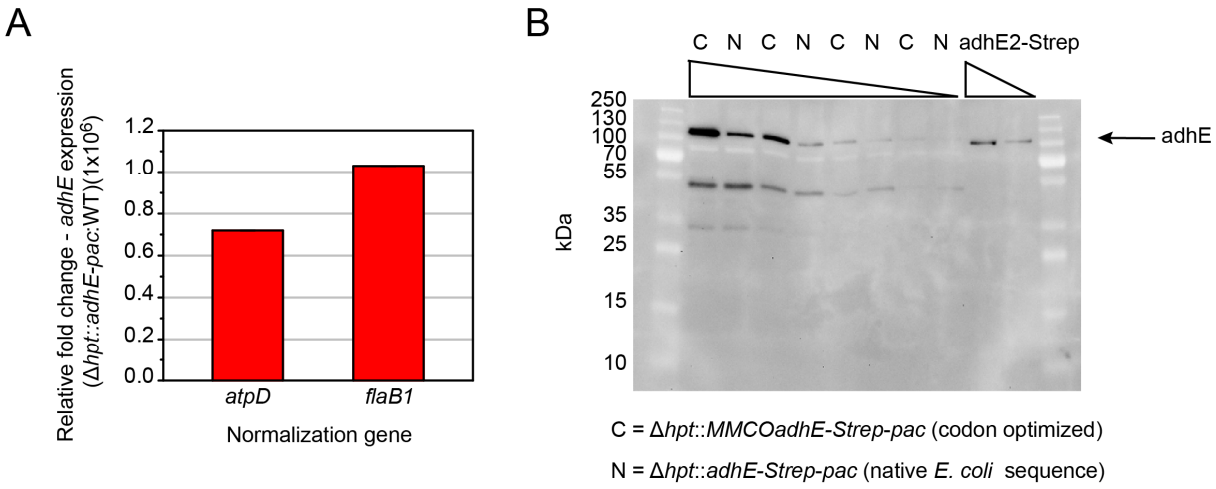

Figure 4.2. Characteriziation of the adhE-expressing M. maripaludis strains. (A) Comparison of *adhE* transcript abundance in the transgenic *M. maripaludis* strain expressing *adhE* (native *E. coli* sequence) to wild type *M. maripaludis*. Results are shown using two different normalization genes: *atpD*, an ATP synthase gene and *flaB1*, a flagellin gene. Each experiment was performed in triplicate. Error bars denote standard deviation. (B) Detection of adhE protein expression using Western blot. A strain expressing Strep-tagged *adhE* encoded by the native *E. coli* sequence is shown in comparison to a strain expressing a codon optimized version of the gene. The far right lanes contain a purified adhE2-Strep standard. Sample lanes contain 12.50-1.56 µg total protein. The adhE2 standard lanes contain 2.00-0.50 µg purified protein.

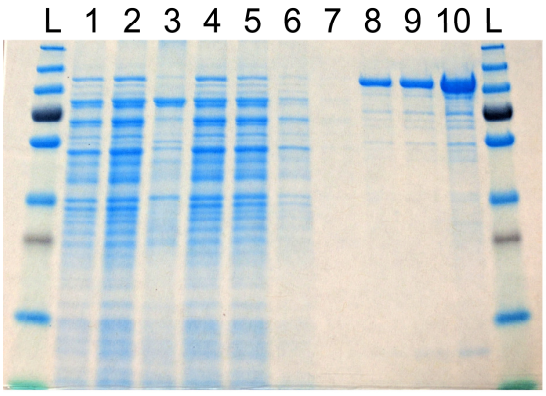

Lane 1: Crude cell lysate
Lane 2: Soluble fraction
Lane 3: Insoluble fraction
Lane 4: DNA precipitation supernatant
Lane 5: Column flow through
Lane 6: Wash 1
Lane 7: Wash 2
Lane 8: Fraction #2
Lane 9: Fraction #3
Lane 10: Concentrated fractions

Figure 4.3. Purification of adhE from M. maripaludis. adhE-Strep was purified from *M. maripaludis* using affinity purification with Streptactin resin. The pooled and concentrated fractions shown in lane 10 were tested for activity using an *in vitro* enzymatic assay. However, no activity was observed.

Having demonstrated robust overexpression of a single heterologous enzyme, this new pathway brought the added challenge of robustly expressing multiple enzymes. Many strategies were attempted for full pathway expression (*Figure 4.5*). Like bacterial systems, *M. maripaludis* is able to express genes from polycistronic operons. However, the translation initiation signals for the second and later genes on the transcript are not well understood. Because polycistronic constructs greatly simplify the cloning and expression of multiple genes, we first attempted to express the 3HB pathway using polycistronic designs. We tried a number of different intergenic regions to try to identify sequences containing the appropriate internal translation initiation signals. One design included intergenic regions from the *M. maripaludis* methyl-CoM reductase operon, a highly expressed operon, encoding a central methanogenesis enzyme. Another included synthetically designed ribosome binding sites (RBS), generated from the Salis RBS Calculator [*44, 45*]. A final design employed the *M. maripaludis* consensus RBS or close derivatives [*46*]. All polycistronic constructs were under the control of the *Methanosarcina barkeri pmcrB* (methyl-CoM reductase) promoter. However, all of these designs resulted in expression of only the first gene of the pathway. (See *Figure 4.6* for a representative Western blot.) Next we tried expression of the pathway using a monocistronic design, with the first gene of the pathway expressed from the *Methanosarcina barkeri pmcrB* (methyl-CoM reductase) promoter, and subsequent genes expressed from predicted high expression *M. maripaludis* promoters, specifically *pflaB1*, a flagellin promoter, and *phdrC1*, the heterodisulfide reductase promoter. These constructs also resulted in expression of only the first gene of the pathway. The same result was also observed when the *pmcrB* promoter in the monocistronic construct was replaced with the *M. maripaludis phdrC1* promoter, though, much reduced phaA expression was observed. Other designs incorporated transcriptional terminators into both the monocistronic and polycistronic constructs. The terminators were from highly expressed *Methanosarcina mazei* genes with well-defined 3′-ends, which were determined experimentally [*47*]. These too resulted in expression of only the first gene of the pathway.

To gain further insight into the lack of protein expression observed with these diverse constructs, quantitative real-time PCR was used to assess heterologous mRNA levels in some of these strains (*Figure 4.7*). It was observed that the *M. barkeri pmcrB* promoter gave incredibly high levels of mRNA expression, including from all of the genes of the pathway when polycistronic constructs were used. The putative high expression *M. maripaludis* promoters also gave high levels of overexpression, but much less than the *M. barkeri pmcrB* promoter. All of this data seemed to indicate that RNA abundance was not causing the observed protein expression problems, but that the heterologous transcripts were not being translated. Archaeal translation is not well understood, but the few studies available do indicate the presence of many messages with extremely short 5′-untranslated regions, seemingly lacking RBSs [*48-50*]. Some have postulated that this is due to the RBS being contained within the start of the coding region itself. With the limited information available about this novel mechanism of translation initiation, it seemed prudent to avoid construct designs that relied on this method of translation initiation.

From the previous data, the *M. barkeri pmcrB* promoter seemed to result in messages translated by a more canonical translation mechanism. Therefore we chose to build a construct with each gene expressed from a separate copy of this promoter. While we did have concerns about genetic stability, due to the repeated promoter sequence, others have had success with similar designs in yeast and *E. coli*. Using this construct design we were able to achieve robust expression of all enzymes of the pathway (*Figure 4.8*). However, when this strain was tested for 3HB production,

none was observed. To troubleshoot this production problem, we generated strains expressing each of the pathway enzymes alone and then tested for enzyme activity using cell lysate assays (*Figures 4.9 and 4.10*). These assays showed enzyme activity comparable to that observed from overexpression in *E. coli*. This result would then suggest that the production problem is not due to an intrinsic lack of enzyme activity, but likely caused by a lack of substrate or appropriate redox cofactors. As acetyl-CoA is a central metabolite in *M. maripaludis*, it seemed unlikely that this substrate would be limiting to the pathway. Therefore, we began to investigate the pool of redox cofactors found in *M. maripaludis*.

Characterization of the NAD^+/NADH pools in *M. maripaludis*. Methanogenesis is the central metabolic pathway found in *M. maripaludis*. It fixes carbon dioxide into methane and acetyl-CoA, which result in the generation of energy and biomass, respectively. The reducing power for this pathway is derived from hydrogen gas, with reducing equivalents delivered to the pathway enzymes using ferredoxin or coenzyme F_{420}, both of which are relatively rare redox carriers, not widely used outside of this specialized metabolic program [*51, 52*]. Since most metabolic engineering efforts to date have focused on organisms with glycolytic metabolisms, many well established heterologous biosynthetic pathways, including the 3HB pathway, require reducing equivalents in the form of NADH or NADPH.

Little is known about the pool of nicotinamide redox cofactors in *M. maripaludis*. The *M. maripaludis* genome does contains an NAD^+ biosynthetic pathway (*Figure 4.11*), and many genes within the genome are bioinformatically annotated as requiring NADH, though, none to our knowledge have been experimentally validated to use this cofactors. To bridge this knowledge gap, we began to investigate the size and redox state of the NAD pool in *M. maripaludis*. Using an enzyme-based luminescence assay we compared the intracellular concentrations of NAD^+ and NADH found in *M. maripaludis* to those found in anaerobically-grown *E. coli*, normalizing to dry cell weight (*Figure 4.12*). From this assay it was determined that while the ratio of oxidized to reduced cofactor is equivalent between the two species, the overall size of the NAD pool in *M. maripaludis* is approximately 3% of that found in *E. coli*. To further understand this result in the context of the overall pool of redox cofactors found within *M. maripaludis* we performed quantitative real-time PCR to measure expression of the NAD^+ biosynthetic pathway genes compared to those in the coenzyme F_{420} biosynthetic pathway and those that encode ferredoxins (*Figure 4.13*). This experiment revealed that expression of the NAD^+ biosynthetic pathway is downregulated relative to the genes involved in the synthesis of either of the redox cofactors used in methanogenesis. This result suggested that the small NAD pool observed in *M. maripaludis* was due to low levels of expression of the biosynthesis pathway genes. To try to increase the size of the NAD pool, we overexpressed the final two enzymes of the biosynthesis pathway. These enzymes were selected because this portion of the pathway is ATP consuming; it was hoped that increasing the rate of this irreversible step would drive synthesis of the final product. This engineered strain did have an increase NAD pool, almost double that found in wild type cells, with the ratio of oxidized to reduced cofactor maintained (*Figure 4.14 B*). Further characterization of this strain using quantitative real-time PCR revealed that the increase in the size of the pool was likely due to a 20 fold overexpression of a single biosynthetic enzyme (*Figure 14.4 C*). The other enzyme included in the construct did not show increased expression relative to wild type cells. This result foreshadows a potentially much larger increase in the size of the NAD pool with successful overexpression of the entire biosynthetic pathway.

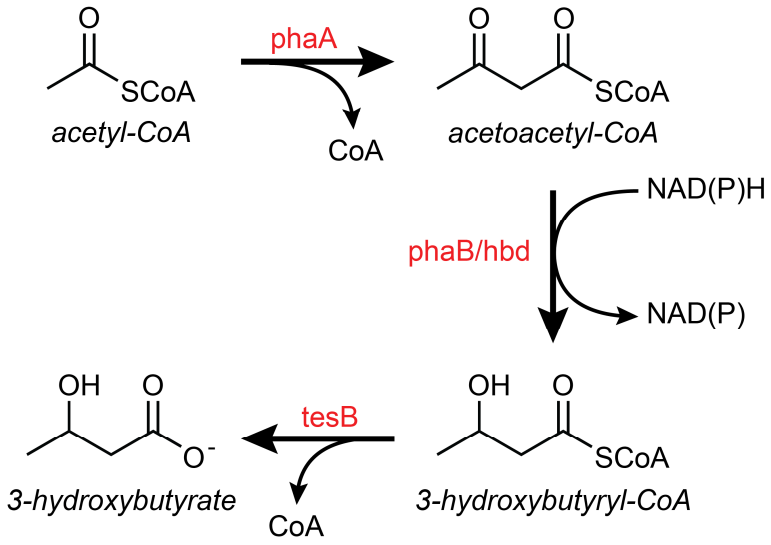

Figure 4.4. 3HB biosynthetic pathway. The 3HB biosynthetic pathway is composed of three enzymes that catalyzes the synthesis of 3HB from acetyl-CoA. The reduction of acetoacetyl-CoA to 3-hydroxybutyryl-CoA can be catalyzed by either of two different enzymes, phaB or hbd. phaB is NADPH dependent, and hbd is NADH dependent. They result in opposite stereochemistries of the final product. In preliminary expression studies in *M. maripaludis* both versions of the pathway were included. Later studies focused on the hdb version of the pathway for experimental simplicity. Enzyme names are shown in red. phaA, acetoacetyl-CoA thiolase/synthase; phaB, hbd, 3-hydroxybutyryl-CoA dehydrogenase; tesB, acyl-CoA thioesterase. phaA and phaB are from *Ralstonia eutropha*. hbd is from *Clostridium acetobutylicum*. tesB is from *E. coli*.

Polycistronic

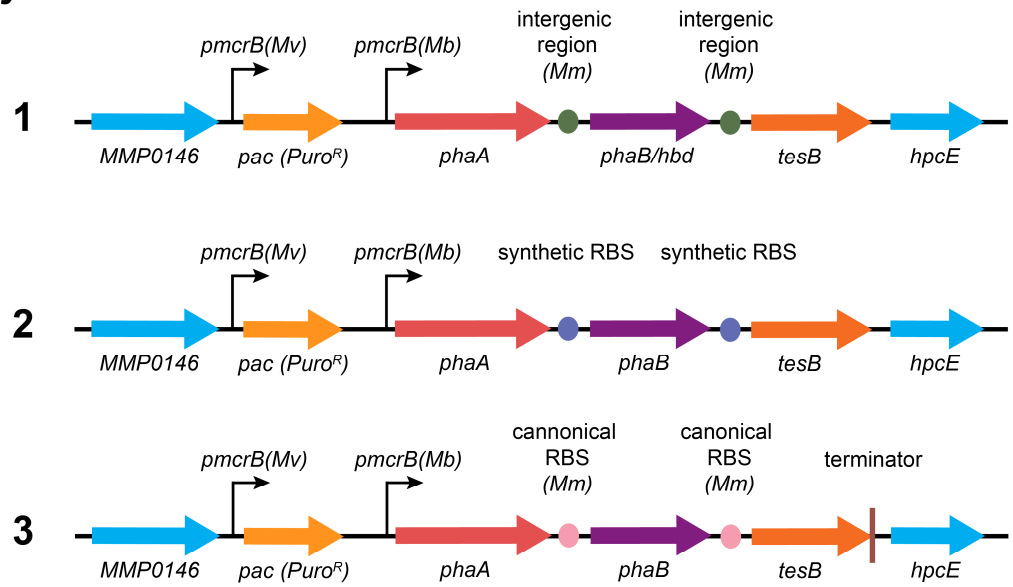

Monocistronic

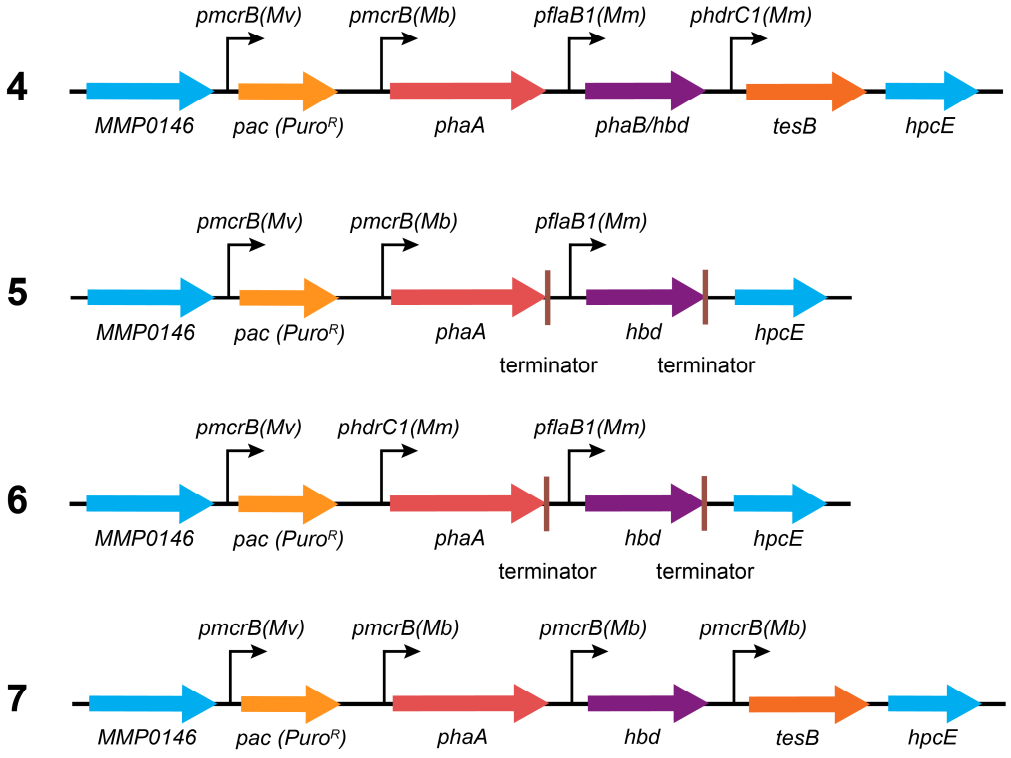

Figure 4.5. Summary of constructs used in this study. All constructs were targeted to the *hpt* site via homologous recombination. Promoters used: *pmcrB*, methyl-CoM reductase promoter from *M. voltae* (*Mv*) or *M. barkeri* (*Mb*). *pflaB1*, flagellin promoter, *phdrC1*, heterodisulfide reductase promoter, both from *M. maripaludis* (*Mm*). Intergenic regions were taken from the *M. maripaludis* methyl-CoM reductase operon. Synthetic RBS sequences were generated using an online calculator [*44, 45*]. Canonical RBS sequences were taken from previous studies [*46*]. Terminators were from highly expressed *Methanosarcina mazei* genes with well-defined 3´-ends, determined experimentally [*47*].

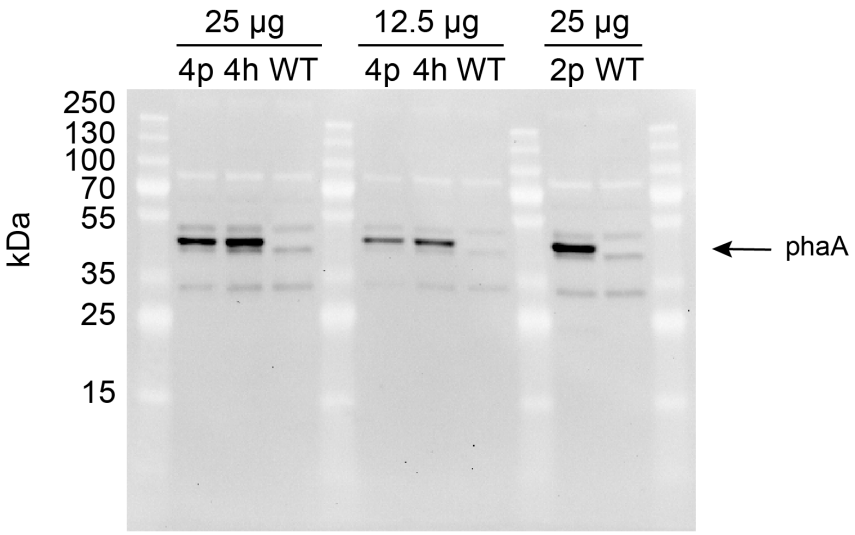

Figure 4.6. Representative Western blot of protein expression from preliminary construct designs. All pathway proteins were Strep-tagged and were detected using an anti-Strep-tag II antibody. The observed pattern of protein expression is representative of what was detected with constructs 1-5 in *Figure 4.5*. 4p, construct 4 with phaB as the middle pathway enzyme; 4h, construct 4 with hbd as the middle pathway enzyme; 2p, construct 2 with phaB as the middle pathway enzyme; WT, wild type. 25 µg or 12.5 µg of total cell protein were loaded per lane as indicated

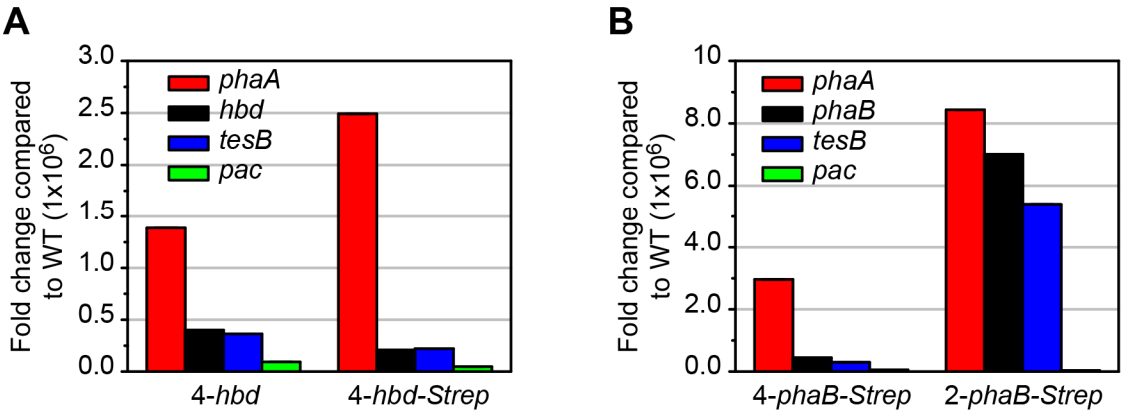

Figure 4.7. Quantitative real-time PCR analysis of 3HB pathway expression. Relative abundances of transcripts from the 3HB pathway genes and transcripts of the puromycin resistance gene were measured using quantitative real-time PCR with *atpD*, an ATP synthase gene, used for normalization. Each experiment was performed in triplicate. Error bars denote standard deviation. *4-hbd*, construct 4 with *hbd* as the middle pathway enzyme; *4-hbd-Strep*, construct 4 with *hbd* as the middle pathway enzyme with all pathway genes Strep-tagged; *4-phaB-Strep*, construct 4 with *phaB* as the middle pathway enzyme with all pathway genes Strep-tagged; *2-phaB-Strep*, construct 2 with *phaB* as the middle pathway enzyme with all pathway genes Strep-tagged; WT, wild type.

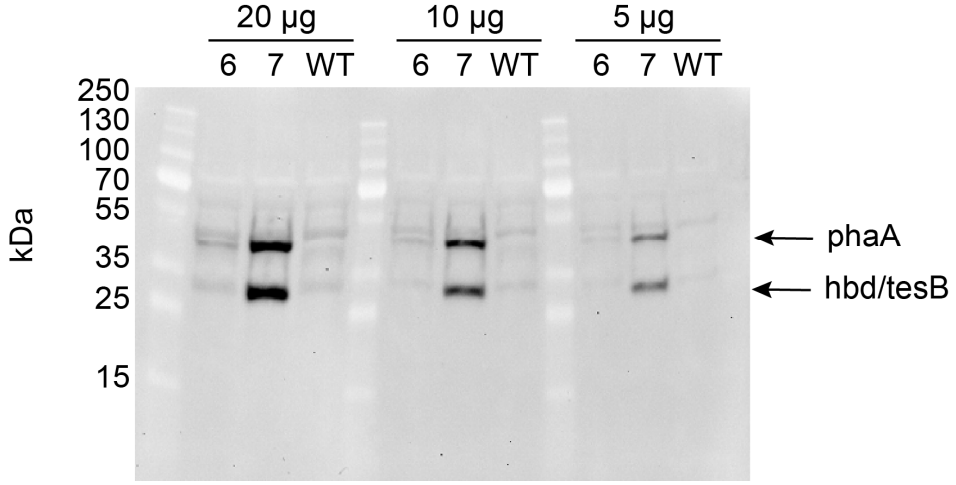

Figure 4.8. Expression of the full 3HB pathway in M. maripaludis. Western blot analysis of an *M. maripaludis* strain carrying construct 7, with each pathway gene under the control of a separate copy of the *pmcrB* promoter from *M. barkeri*. Expression of all pathway genes is observed. A strain carrying construct 6 is also included in this Western blot. Interestingly, a low level of phaA protein expression is observed from the *phdrC1* promoter. Heterologous expression from this promoter had not been observed when it was included in previous constructs. 20 µg, 10 µg or 5 µg of total cell protein were loaded per lane as indicated. WT, wild type. All pathway proteins were Strep-tagged and were detected using an anti-Strep-tag II antibody.

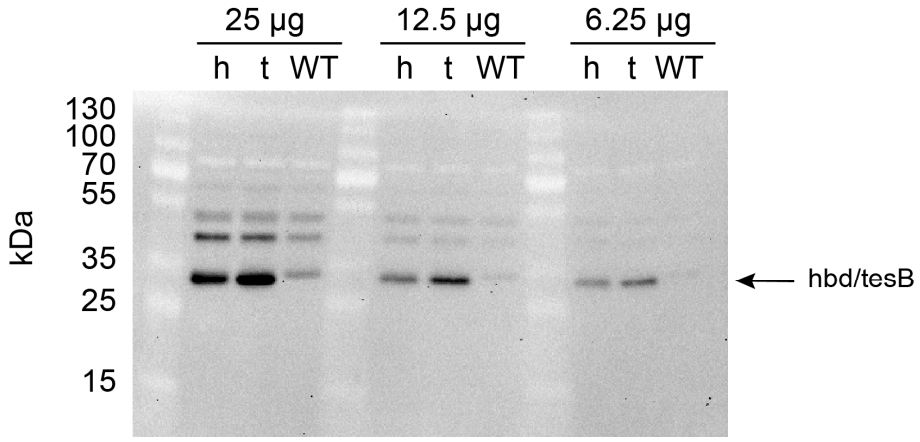

Figure 4.9. Expression of hbd and tesB in M. maripaludis. Western blot analysis of *M. maripaludis* strains expressing *hbd* or *tesB* individually. The genes were under the control of the *pmcrB* promoter from *M. barkeri*. 25 µg, 12.5 µg or 6.25 µg of total cell protein were loaded per lane as indicated. WT, wild type. Both proteins were Strep-tagged and were detected using an anti-Strep-tag II antibody.

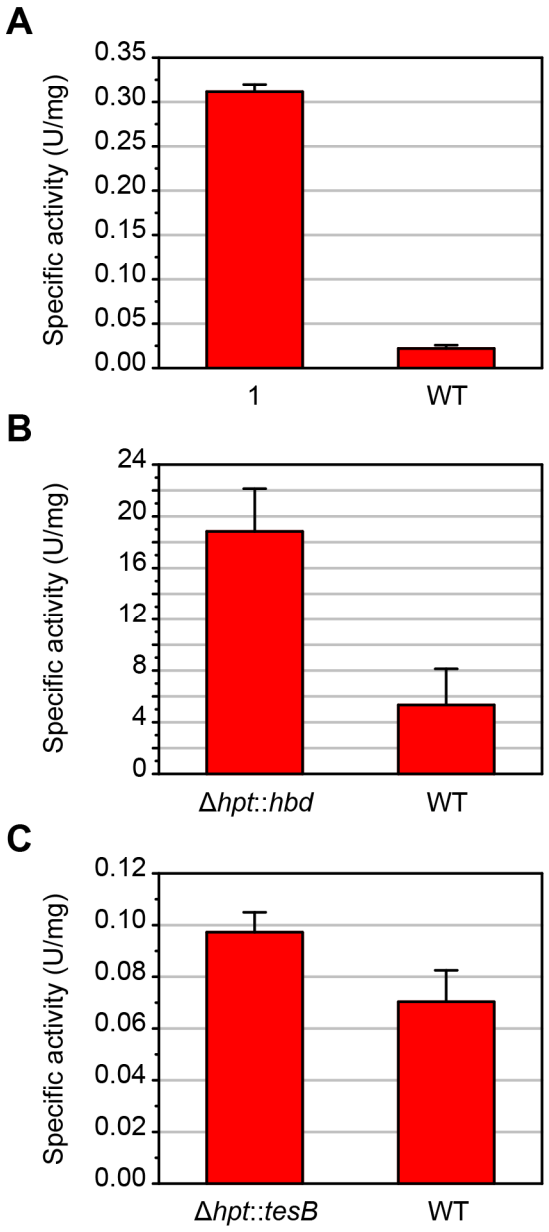

Figure 4.10. Cell lysate activity assays for 3HB pathway enzymes. Enzymatic activity of the 3HB pathway enzymes was determined in *M. maripaludis* whole cell lysates. (A) phaA activity, (B) hbd activity, (C) tesB activity. The observed activity was comparable to what has been previously measured in cell lysates of *E. coli* strains expressing these enzymes. To measure phaA activity a strain carrying construct 1 was used. None of the pathway enzymes in this construct were Strep-tagged. Based on protein expression data from a strain carrying a similar construct with all pathway proteins Strep-tagged, it was inferred that this strain only expresses phaA and none of the other pathway enzymes. To measure hbd and tesB activity, strains similar to those characterized in *Figure 4.9* were used; however, the strains used for cell lysate activity assays carried constructs with the enzymes untagged, unlike the Strep-tagged versions used for the Western blot. WT, wild type. Each experiment was performed in at least triplicate. Error bars denote standard deviation.

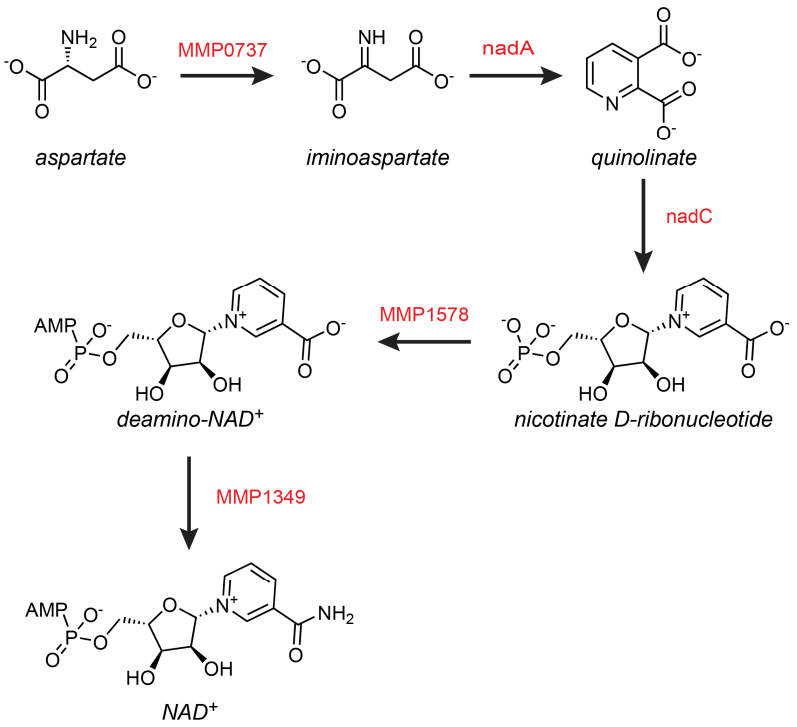

Figure 4.11. M. maripaludis NAD⁺ biosynthesis pathway. The *M. maripaludis* NAD⁺ biosynthesis pathway is composed of five enzymes and uses aspartate as the initial substrate for synthesis. Enzyme names are displayed in red. MMP0737, aspartate dehydrogenase; nadA, quinolinate synthase; nadC, quinolinate phosphoribosyl transferase:nicotinate-nucleotide pyrophosphorylase; MMP1578, nicotinamide-nucleotide adenylyltransferase; MMP1349, NAD⁺ synthase.

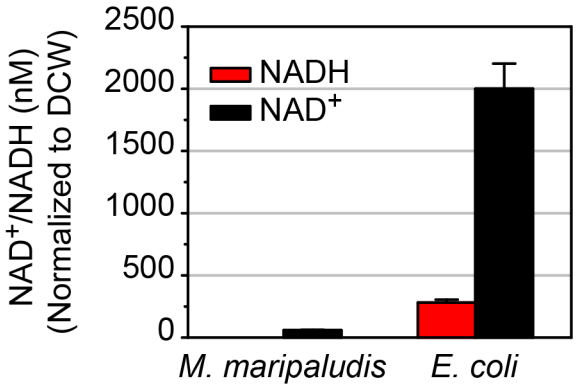

Figure 4.12. Quantification of NAD+ and NADH pools in M. maripaludis and E. coli. The concentration of NAD^+ and NADH in *M. maripaludis* and *E. coli* was determined using an enzyme based luminescence assay. *M. maripaludis* has approximately 3% of the NAD^+/NADH pool observed in *E. coli*. Values were normalized for comparison using dry cell weight (DCW). Each experiment was performed in triplicate. Error bars denote standard deviation.

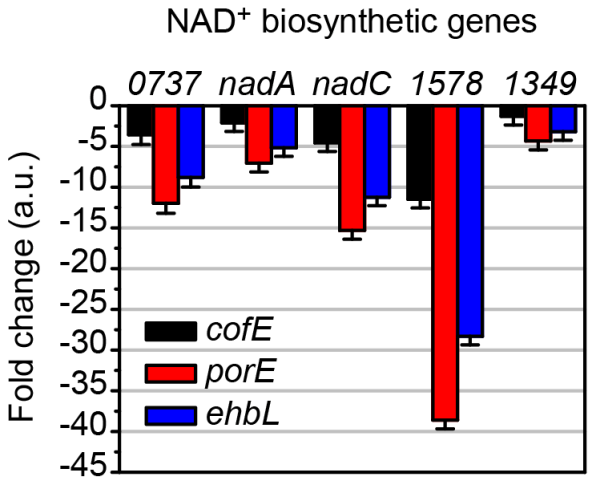

Figure 4.13. Analysis of the transcript abundance of the M. maripaludis NAD+ biosynthetic pathway enzymes. The relative transcript abundance of the NAD^+ biosynthetic pathway genes was compared to the abundance of a coenzyme F_{420} biosynthetic gene (*cofE*) and two ferredoxin genes (*porE*, *ehbL*) using quantitative real-time PCR. The level of expression of the NAD^+ biosynthetic pathway genes was downregulated relative to all three standards. *cofE*, coenzyme F_{420}:L-glutamate ligase; *porE*, ferredoxin, pyruvate oxidoreductase associated; *ehbL*, ferredoxin, energy conserving hydrogenase B associated. Each experiment was performed in triplicate. Error bars denote standard deviation.

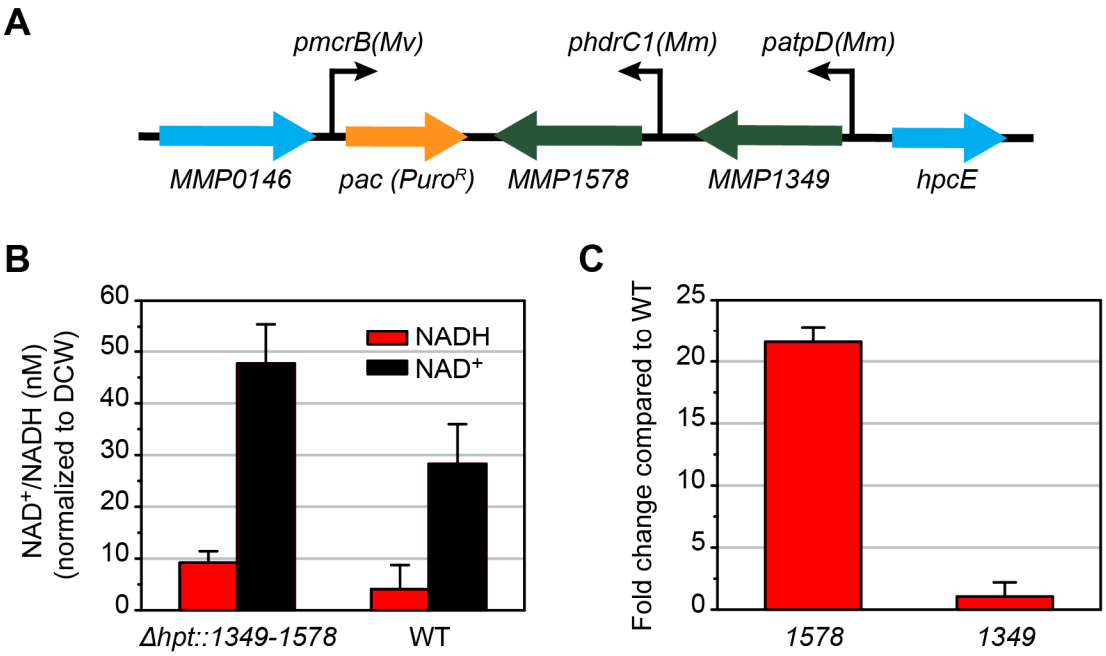

Figure 4.14. Characterization of a M. maripaludis strain overexpressing portions of the NAD⁺ biosynthetic pathway. (A) Diagram of the construct used in the generation of this strain. (B) Quantification of the NAD^+ and NADH pools in the engineered strain compared to the wild type strain. The pool size in the engineered strain is almost double that observed in the wild type strain. Each experiment was performed in triplicate. Error bars denote standard deviation. (C) Quantitative real-time PCR analysis of transcript abundance in the engineered strain compared to the wild type strain. It appears that only *MMP1578* is overexpressed (~20 fold) compared to wild type. *atpD*, an ATP synthase gene, was used for normalization. Each experiment was performed in triplicate. Error bars denote standard deviation.

Dysregulation of the nitrogenase gene cluster for enhanced nitrogen fixation capacity. In addition to being able to fix carbon dioxide into methane and acetyl-CoA, *M. maripaludis* can also fix nitrogen gas into ammonia for incorporation into organic molecules [*22*]. Its unique metabolic program allows it to grow in the absence of both fixed carbon and nitrogen sources. This is a very attractive attribute when considering industrial applications, as it would allow cultivation in extremely minimal, and therefore inexpensive growth media. Additionally, it would further expand the product scope of this organism to include nitrogen containing compounds, many of which could be used as agricultural fertilizers [*53*]. The current method for generating fixed nitrogen compounds from atmospheric nitrogen is the Haber process, which relies on extremely high temperatures and pressures, and is not a sustainable synthesis method since natural gas is used as a starting material for the process [*54*]. In contrast, a hybrid biological-inorganic production platform employing *M. maripaludis* could operate under ambient temperature and pressure and would be sustainable, requiring only carbon dioxide, nitrogen and a renewable electricity source.

The enzymatic machinery of nitrogen fixation and its regulation in *M. maripaludis* is well understood. The nitrogenase gene cluster contains eight genes (*Figure 4.15 A*). *nifD* and *nifK* encode the nitrogenase enzyme, a heterotetramer with two of each subunit. *nifH* encodes the nitrogenase reductase enzyme which delivers electrons for the reduction of nitrogen to the nitrogenase. *nifE* and *nifN* encode proteins responsible for the synthesis of the iron-molybdenum cofactor found at the nitrogenase active site. *nifX* shares homology to other proteins in the synthesis pathway for this cofactor; however, no phenotype is observed when it is knock out, and therefore may have a non-essential role in cofactor synthesis that can be rescued by other enzymes in the pathway [*22*]. *nifI$_1$* and *nifI$_2$* encode proteins that regulate nitrogenase activity in response to the availability of fixed nitrogen [*55*]. Because nitrogen fixation is a very energy intensive process, using at least 16 ATP per molecule of nitrogen fixed, it is tightly regulated at many levels to limit wasted energy when fixed nitrogen is available from the environment [*56*]. nifI$_1$ and nifI$_2$ regulate the process post-translationally by blocking the association between the nitrogenase and the nitrogenase reductase when fixed nitrogen sources are available [*55*]. High levels of 2-oxoglutarate, a readout of low fixed nitrogen availability, relieves this repression. The process is also regulated transcriptionally. Two repressor binding site sit immediately downstream of the transcription start site. Repressor binding is also regulated by 2-oxoglutarate levels [*57*].

In order to exploit the nitrogenase system for engineering purposes, we removed all know levels of regulation to make the system constitutively active. To do this we used homologous recombination to deliver a construct with the first transcriptional repressor binding site removed, which then also renders the second binding site inactive [*58*], and with the *nifI$_1$* and *nifI$_2$* genes replaced with the puromycin resistance cassette (*Figure 4.15 A*). This mutant strain showed no growth differences compared to wild type cells in rich media, media containing only amino acids, but no ammonium salts, or minimal media lacking both amino acids and ammonium salts. When quantitative real-time PCR was used to compare transcript levels of nitrogenase genes between the mutant and wild type strains grown in media containing only amino acids, large differences in transcript abundance were observed, indicating that at least transcriptionally the cluster was dysregulated (*Figure 4.15 B*). Future studies must investigate whether differences are also observed in levels of nitrogenase enzymatic activity. The transcriptional result is a promising initial step toward constitutive nitrogenase activity and diversion of fixed nitrogen to value-added products.

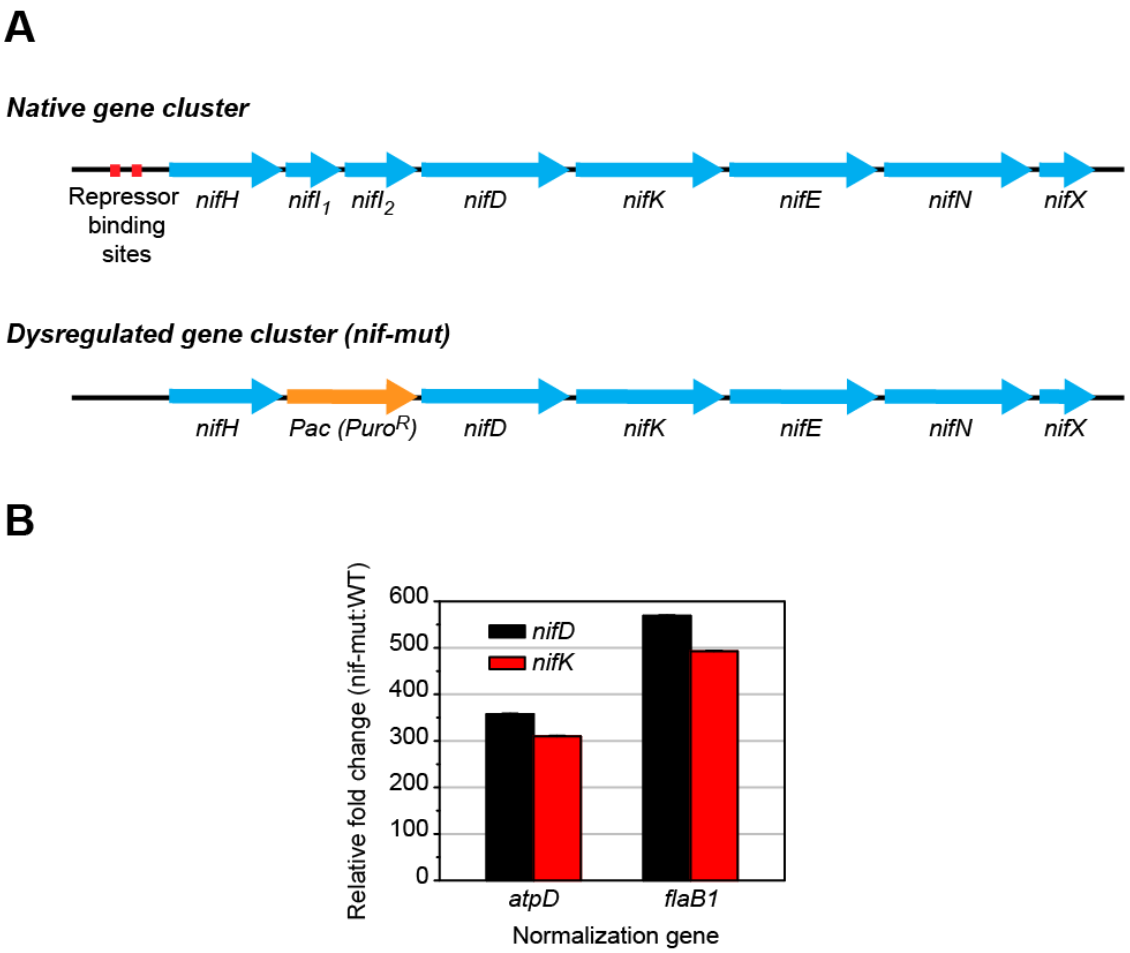

Figure 4.15. Dysregulation of the nitrogenase gene cluster. (A) Diagram of the wild type and dysregulated nitrogenase gene cluster. In the engineered gene cluster (nif-mut) the transcriptional repressor binding sites have been removed and the *nifI*$_1$ and *nifI*$_2$ genes, which encode regulatory proteins, have been replaced with the puromycin resistance cassette. (B). Comparison of transcript levels of nitrogenase gene cluster genes nifD and nifK, in the engineered strain compared to the wild type strain grown in media containing only amino acids as a nitrogen source. Much higher transcript levels are observed in the engineered strain compared to the wild type strain. Results are shown using two different normalization genes: *atpD*, an ATP synthase gene and *flaB1*, a flagellin gene. Each experiment was performed in triplicate. Error bars denote standard deviation.

4.4 Conclusions and future directions

In this study we have laid the groundwork for the successful engineering of *M. maripaludis* as a biological catalyst for incorporation into biological-inorganic devices for the production of multi-carbon value-added products from carbon dioxide and sustainable energy sources. Specifically, we have developed a robust expression system for the 3HB pathway and have shown that all the enzymes of the pathway are active in *M. maripaludis* cell lysates. We hypothesize that the lack of product synthesis that is observed from the *in vivo* pathway is due to a lack of appropriate redox cofactors, specifically NADH.

We have shown preliminary data that suggests that the size of the NAD pool can be increased by overexpression of portions of the biosynthetic pathway. Future efforts will focus on overexpression of the complete NAD^+ biosynthetic pathway, which will hopefully result in even larger increases in the size of the cofactor pool. It is tempting to speculate how this increased cofactor pool may integrate with the metabolism of the organism, and it is plausible to hypothesize that the increased pool may operate in many respects orthogonally to native metabolism. Since *M. maripaludis* maintains such a limited NAD pool, it is likely that its cellular requirements for this cofactor a quite low, which would allow reducing equivalents from an increased pool to be funneled exclusively to the target molecule, a feat difficult to envision in glycolytic organisms.

In the experiment overexpressing portions of the NAD^+ biosynthetic pathway, it was observed that when the size of the NAD pool almost doubled, the cells were able to maintain the native ratio of oxidized to reduced cofactor. However, it is unclear if a greatly increased NAD pool will be properly charged with reducing equivalents using the native cellular machinery. For this reason, we are also interested in exploring heterologous systems for charging an expanded NAD pool. A cytosolic hydrogenase from *Acetobacterium woodii* that uses hydrogen gas to simultaneously charge both ferredoxin and NAD^+ is a promising candidate. Hopefully, coupling these future advances to generate an expanded NADH pool with efforts to overexpress the 3HB pathway will result in a robust production strain. The insights learned from this engineering project can then be applied to generalize heterologous pathway expression in *M. maripaludis* to generate a diverse portfolio of target molecules from this promising biological catalyst.

Based on the promising initial results observed in efforts to dysregulate the nitrogenase gene cluster, this expanded product portfolio will also hopefully include nitrogen-containing targets.

4.5 References

1. Lewis, N. S., Nocera, D. G., Powering the planet: Chemical challenges in solar energy utilization. *Proc. Natl. Acad. Sci. U.S.A.* **2006**, 103(43) 15729-15735.

2. Gray, H. B., Powering the planet with solar fuel. *Nat. Chem.* **2009**, 1(1) 7.

3. Concepcion, J. J., House, R. L., Papanikolas, J. M., Meyer, T. J., Chemical approaches to artificial photosynthesis. *Proc. Natl. Acad. Sci. U.S.A.* **2012**, 109(39) 15560-15564.

4. Benson, E. E., Kubiak, C. P., Sathrum, A. J., Smieja, J. M., Electrocatalytic and homogeneous approaches to conversion of CO_2 to liquid fuels. *Chem. Soc. Rev.* **2009**, 38(1) 89-99.

5. Morris, A. J., Meyer, G. J., Fujita, E., Molecular approaches to the photocatalytic reduction of carbon dioxide for solar fuels. *Acc. Chem. Res.* **2009**, 42(12) 1983-1994.

6. Finn, C., Schnittger, S., Yellowlees, L. J., Love, J. B., Molecular approaches to the electrochemical reduction of carbon dioxide. *Chem. Commun.* **2012**, 48(10) 1392-1399.

7. Appel, A. M., Bercaw, J. E., Bocarsly, A. B., Dobbek, H., Dubois, D. L., Dupuis, M., Ferry, J. G., Fujita, E., Hille, R., Kenis, P. J., Kerfeld, C. A., Morris, R. H., Peden, C. H., Portis, A. R., Ragsdale, S. W., Rauchfuss, T. B., Reek, J. N., Seefeldt, L. C., Thauer, R. K., Waldrop, G. L., Frontiers, opportunities, and challenges in biochemical and chemical catalysis of CO_2 fixation. *Chem. Rev.* **2013**, 113(8) 6621-6658.

8. Costentin, C., Robert, M., Saveant, J.-M., Catalysis of the electrochemical reduction of carbon dioxide. *Chem. Soc. Rev.* **2013**, 42(6) 2423-2436.

9. Jhong, H.-R. M., Ma, S., Kenis, P. J. A., Electrochemical conversion of CO_2 to useful chemicals: Current status, remaining challenges, and future opportunities. *Curr. Opin. Chem. Eng.* **2013**, 2(2) 191-199.

10. Rabaey, K., Rozendal, R. A., Microbial electrosynthesis — revisiting the electrical route for microbial production. *Nat. Rev. Micro.* **2010**, 8(10) 706-716.

11. Köpke, M., Held, C., Hujer, S., Liesegang, H., Wiezer, A., Wollherr, A., Ehrenreich, A., Liebl, W., Gottschalk, G., Dürre, P., *Clostridium ljungdahlii* represents a microbial production platform based on syngas. *Proc. Natl. Acad. Sci. U.S.A.* **2010**, 107(29) 13087-13092.

12. Banerjee, A., Leang, C., Ueki, T., Nevin, K. P., Lovley, D. R., Lactose-inducible system for metabolic engineering of *Clostridium ljungdahlii*. *Appl. Environ. Microbiol.* **2014**, 80(8) 2410-2416.

13. Ueki, T., Nevin, K. P., Woodard, T. L., Lovley, D. R., Converting carbon dioxide to butyrate with an engineered strain of *Clostridium ljungdahlii*. *MBio* **2014**, 5(5) e01636-01614.

14. Torella, J. P., Gagliardi, C. J., Chen, J. S., Bediako, D. K., Colon, B., Way, J. C., Silver, P. A., Nocera, D. G., Efficient solar-to-fuels production from a hybrid microbial-water-splitting catalyst system. *Proc. Natl. Acad. Sci. U.S.A.* **2015**, 112(8) 2337-2342.

15. Liu, C., Colón, B. C., Ziesack, M., Silver, P. A., Nocera, D. G., Water splitting–biosynthetic system with CO_2 reduction efficiencies exceeding photosynthesis. *Science* **2016**, 352(6290) 1210-1213.

16. Cueto-Rojas, H. F., Van Maris, A. J., Wahl, S. A., Heijnen, J. J., Thermodynamics-based design of microbial cell factories for anaerobic product formation. *Trends Biotechnol.* **2015**, 33(9) 534-546.

17. Bar-Even, A., Noor, E., Milo, R., A survey of carbon fixation pathways through a quantitative lens. *J. Exp. Bot.* **2012**, 63(6) 2325-2342.

18. Liu, C., Gallagher, J. J., Sakimoto, K. K., Nichols, E. M., Chang, C. J., Chang, M. C. Y., Yang, P., Nanowire–bacteria hybrids for unassisted solar carbon dioxide fixation to value-added chemicals. *Nano Lett.* **2015**, 15(5) 3634-3639.

19. Nichols, E. M., Gallagher, J. J., Liu, C., Su, Y., Resasco, J., Yu, Y., Sun, Y., Yang, P., Chang, M. C. Y., Chang, C. J., Hybrid bioinorganic approach to solar-to-chemical conversion. *Proc. Natl. Acad. Sci. U.S.A.* **2015**, 112(37) 11461-11466.

20. Li, H., Opgenorth, P. H., Wernick, D. G., Rogers, S., Wu, T. Y., Higashide, W., Malati, P., Huo, Y. X., Cho, K. M., Liao, J. C., Integrated electromicrobial conversion of CO_2 to higher alcohols. *Science* **2012**, 335(6076) 1596.

21. Jones, W. J., Paynter, M. J. B., Gupta, R., Characterization of *Methanococcus maripaludis* sp. nov., a new methanogen isolated from salt marsh sediment. *Arch. Microbiol.* **1983**, 135(2) 91-97.

22. Leigh, J. A., Nitrogen fixation in methanogens: The archaeal perspective. *Curr. Issues Mol. Biol.* **2000**, 2(4) 125-131.

23. Sarmiento, F., Leigh, J. A., Whitman, W. B., Genetic systems for hydrogenotrophic methanogens. *Methods Enzymol.* **2011**, 494 43-73.

24. Goyal, N., Zhou, Z., Karimi, I. A., Metabolic processes of *Methanococcus maripaludis* and potential applications. *Microb. Cell Fact*. **2016**, 15(1) 107.

25. Kohler, P., Metcalf, W., Genetic manipulation of *Methanosarcina* spp. *Front. Microbiol.* **2012**, 3(259).

26. Yishai, O., Lindner, S. N., Gonzalez De La Cruz, J., Tenenboim, H., Bar-Even, A., The formate bio-economy. *Curr. Opin. Chem. Biol.* **2016**, 35 1-9.

27. Min, X., Kanan, M. W., Pd-catalyzed electrohydrogenation of carbon dioxide to formate: High mass activity at low overpotential and identification of the deactivation pathway. *J. Am. Chem. Soc.* **2015**, 137(14) 4701-4708.

28. Lee, S.-H., Park, S. J., Lee, S. Y., Hong, S. H., Biosynthesis of enantiopure (s)-3-hydroxybutyric acid in metabolically engineered *Escherichia coli*. *Appl. Microbiol. Biotechnol.* **2008**, 79(4) 633-641.

29. Steinbüchel, A., Biodegradable plastics. *Curr. Opin. Biotechnol.* **1992**, 3(3) 291-297.

30. Moore, B. C., Leigh, J. A., Markerless mutagenesis in *Methanococcus maripaludis* demonstrates roles for alanine dehydrogenase, alanine racemase, and alanine permease. *J. Bacteriol.* **2005**, 187(3) 972-979.

31. Gibson, D. G., Young, L., Chuang, R. Y., Venter, J. C., Hutchison, C. A., 3rd, Smith, H. O., Enzymatic assembly of DNA molecules up to several hundred kilobases. *Nat. Methods* **2009**, 6(5) 343-345.

32. Brown, M. E., Mukhopadhyay, A., Keasling, J. D., Engineering bacteria to catabolize the carbonaceous component of sarin: Teaching *E. coli* to eat isopropanol. *ACS Synth. Biol.* **2016**, 5(12) 1485-1496.

33. Metcalf, W. W., Zhang, J. K., Apolinario, E., Sowers, K. R., Wolfe, R. S., A genetic system for archaea of the genus *Methanosarcina*: Liposome-mediated transformation and construction of shuttle vectors. *Proc. Natl. Acad. Sci. U.S.A.* **1997**, 94(6) 2626-2631.

34. Buan, N., Kulkarni, G., Metcalf, W., Genetic methods for *Methanosarcina* species. *Methods Enzymol.* **2011**, 494 23-42.

35. Lyu, Z., Jain, R., Smith, P., Fetchko, T., Yan, Y., Whitman, W. B., Engineering the autotroph *Methanococcus maripaludis* for geraniol production. *ACS Synth. Biol.* **2016**, 5(7) 577-581.

36. Rudolph, F. B., Purich, D. L., Fromm, H. J., Coenzyme A-linked aldehyde dehydrogenase from *Escherichia coli*. I. Partial purification, properties, and kinetic studies of the enzyme. *J. Biol. Chem.* **1968**, 243(21) 5539-5545.

37. Goodlove, P. E., Cunningham, P. R., Parker, J., Clark, D. P., Cloning and sequence analysis of the fermentative alcohol-dehydrogenase-encoding gene of *Escherichia coli*. *Gene* **1989**, 85(1) 209-214.

38. Gernhardt, P., Possot, O., Foglino, M., Sibold, L., Klein, A., Construction of an integration vector for use in the archaebacterium *Methanococcus voltae* and expression of a eubacterial resistance gene. *Mol. Gen. Genet.* **1990**, 221(2) 273-279.

39. Puigbò, P., Guzmán, E., Romeu, A., Garcia-Vallvé, S., Optimizer: A web server for optimizing the codon usage of DNA sequences. *Nucleic Acids Res.* **2007**, 35(Web server issue) W126-W131.

40. Puigbo, P., Romeu, A., Garcia-Vallve, S., HEG-DB: A database of predicted highly expressed genes in prokaryotic complete genomes under translational selection. *Nucleic Acids Res.* **2008**, 36(Database issue) D524-D527.

41. Hendrickson, E. L., Kaul, R., Zhou, Y., Bovee, D., Chapman, P., Chung, J., Conway De Macario, E., Dodsworth, J. A., Gillett, W., Graham, D. E., Hackett, M., Haydock, A. K., Kang, A., Land, M. L., Levy, R., Lie, T. J., Major, T. A., Moore, B. C., Porat, I., Palmeiri, A., Rouse, G., Saenphimmachak, C., Soll, D., Van Dien, S., Wang, T., Whitman, W. B., Xia, Q., Zhang, Y., Larimer, F. W., Olson, M. V., Leigh, J. A., Complete genome sequence of the genetically tractable hydrogenotrophic methanogen *Methanococcus maripaludis*. *J. Bacteriol.* **2004**, 186(20) 6956-6969.

42. Kessler, D., Herth, W., Knappe, J., Ultrastructure and pyruvate formate-lyase radical quenching property of the multienzymic AdhE protein of *Escherichia coli*. *J. Biol. Chem.* **1992**, 267(25) 18073-18079.

43. Yun, E. J., Kwak, S., Kim, S. R., Park, Y.-C., Jin, Y.-S., Kim, K. H., Production of (S)-3-hydroxybutyrate by metabolically engineered Saccharomyces cerevisiae. *J. Biotechnol.* **2015**, 209 23-30.

44. Salis, H. M., Mirsky, E. A., Voigt, C. A., Automated design of synthetic ribosome binding sites to control protein expression. *Nat Biotech* **2009**, 27(10) 946-950.

45. Espah Borujeni, A., Channarasappa, A. S., Salis, H. M., Translation rate is controlled by coupled trade-offs between site accessibility, selective RNA unfolding and sliding at upstream standby sites. *Nucleic Acids Res.* **2014**, 42(4) 2646-2659.

46. Brown, J. W., Daniels, C. J., Reeve, J. N., Konisky, J., Gene structure, organization, and expression in archaebacteria. *Crit. Rev. Microbiol.* **1989**, 16(4) 287-337.

47. Dar, D., Prasse, D., Schmitz, R. A., Sorek, R., Widespread formation of alternative 3' UTR isoforms via transcription termination in archaea. *Nat. Microbiol.* **2016**, 1(10) 16143.

48. Wurtzel, O., Sapra, R., Chen, F., Zhu, Y., Simmons, B. A., Sorek, R., A single-base resolution map of an archaeal transcriptome. *Genome Res.* **2010**, 20(1) 133-141.

49. Jäger, D., Förstner, K. U., Sharma, C. M., Santangelo, T. J., Reeve, J. N., Primary transcriptome map of the hyperthermophilic archaeon *Thermococcus kodakarensis*. *BMC Genomics* **2014**, 15(1) 684.

50. Srivastava, A., Gogoi, P., Deka, B., Goswami, S., Kanaujia, S. P., In silico analysis of 5′-UTRs highlights the prevalence of Shine–Dalgarno and leaderless-dependent mechanisms of translation initiation in bacteria and archaea, respectively. *J. Theor. Biol.* **2016**, 402 54-61.

51. Taylor, M., Scott, C., Grogan, G., F_{420}-dependent enzymes – potential for applications in biotechnology. *Trends Biotechnol.* **2013**, 31(2) 63-64.

52. Knaff, D. B., Ferredoxin and ferredoxin-dependent enzymes. *Oxygenic photosynthesis: The light reactions*, eds Ort, D. R., Yocum, C. F., (Springer Netherlands, Dordrecht) **1996**, pp 333-361.

53. Jacquot, A., Li, Z., Gojon, A., Schulze, W., Lejay, L., Post-translational regulation of nitrogen transporters in plants and microorganisms. *J. Exp. Bot.* **2017**.

54. Leigh, G. J., Haber-Bosch and other industrial processes. *Catalysts for nitrogen fixation: Nitrogenases, relevant chemical models and commercial processes*, eds Smith, B. E., Richards, R. L., Newton, W. E., (Springer Netherlands, Dordrecht) **2004**, pp 33-54.

55. Dodsworth, J. A., Leigh, J. A., NifI inhibits nitrogenase by competing with Fe protein for binding to the MoFe protein. *Biochem. Biophys. Res. Commun.* **2007**, 364(2) 378-382.

56. Dodsworth, J. A., Cady, N. C., Leigh, J. A., 2-oxoglutarate and the PII homologues $NifI_1$ and $NifI_2$ regulate nitrogenase activity in cell extracts of *Methanococcus maripaludis*. *Mol. Microbiol.* **2005**, 56(6) 1527-1538.

57. Lie, T. J., Wood, G. E., Leigh, J. A., Regulation of *nif* expression in *Methanococcus maripaludis*: Roles of the euryarchaeal repressor NrpR, 2-oxoglutarate, and two operators. *J. Biol. Chem.* **2005**, 280(7) 5236-5241.

58. Lie, T. J., Leigh, J. A., Regulatory response of *Methanococcus maripaludis* to alanine, an intermediate nitrogen source. *J. Bacteriol.* **2002**, 184(19) 5301-5306.

Conclusions and future directions

The work presented in this thesis has shown the power of hybrid biological-inorganic synthesis platforms for the production of value-added chemicals from carbon dioxide and sustainable energy sources. Specifically, Chapter 2 focused on the development of systems for the production of methane, a potential biofuel and a natural byproduct of the metabolism of *M. barkeri*. These systems included electrochemical designs powered by electric current or photochemical designs which were stand-alone solar-powered devices. These designs achieved high Faradaic efficiencies (86%) and operated stably for long periods (at least 7 days). Building from this success, Chapter 3 explores the development of synthesis platforms for an expanded array of non-native target molecules. To achieve this goal, *S. ovata* was seeded into semiconductor nanowire arrays, which transform light energy into electric current, which can then be used to power acetogen metabolism. This assembly was able to generate quite high titers of acetate, up to 6 g/L. In order to upgrade this acetate to more advanced products, genetically engineered *E. coli* were incorporated into the system. Using established heterologous biosynthetic pathways, fuels, bioplastics and pharmaceutical precursors were generated from the solar-derived acetate. Seeking to combine the wide product scope of the two organisms system presented in Chapter 3 with the design simplicity of the single organism device developed in Chapter 2, Chapter 4 was focused on the development of metabolic engineering tools for *M. maripaludis*, a promising candidate for use as an engineered biocatalyst in these hybrid biological-inorganic devices. Tools were developed for robust expression of multi-gene pathways, and the unusual composition of the redox pool found in these organisms was explored. Efforts are ongoing to expand these initial discoveries to generate engineered strains of *M. maripaludis*, able to synthesize an array of complex, non-native products from carbon dioxide. One can envision the future industrial applications of these systems, where sustainable energy sources and waste carbon dioxide can be used for the synthesis of value-added chemicals, offering an alternative to conventional manufacturing practices, with substantially reduced environmental impacts.

Appendix 1: *Primers and gBlocks*

Table 1. Cloning primers (A), gBlocks (B), and quantitative real-time PCR primers (C) used in Chapter 4.

A

Name	Sequence
adhE-Strep Gibson	AGCTGAGAAAAAAGCGAAAAAATCCGCTAGCGCCTGGAGCCATCCGCAGTTCGAGAAGTAAATTATAAATTAAATTTAAATTGGTGAATTATTTTTCAGG
Ec-adhE-F1	CAAAATGATTTTAATAAATTAAGGAGGAAATTCATATGGCTGTTACTAATGTCGCTGAAC
F - Promoter - adhE-Pac Gibson	CGCTCTACGAGTGCGTTAAG
F-Pac - adhE-Pac Gibson	TCTTTTGTGTTCTCCGATAAATGAAGCATGCGAATTGCCCCCAGTGAATTAAAAATATAT
hbd-pflaB1 GF	CAAACCAAATACAGCACCATATGAAAAAAGTTTGTGTTATCGGAG
hbd-pflaB1 GR	TCCGATAACACAAACTTTTTTCATATGGTGCTGTATTTGGTTTGG
hbd-pmcrB GR	CAAAATGATTTTAATAAATTAAGGAGGAAATTCATATGAAAAAAGTTTGTGTTATCGGAG
hbd-pmcrB GR2	GATTTCATTGGGAATAGTGGACACTCGAGTAGGTGACCAGTCCCAAAATGATTTTAATAAATTAAGGAGGAAATTCA
hbd-Strep-phaA GF	AAGAAAATGGAGCCATCCGCAGTTCGAGAAGTAAGGTAATAAACGATGAAAAAAGTTTGT
hdrcI-mcis-clone-F	ACTTCCATTACCAATGCCTTAAGATTTTTCCCTTTTTCAAAAATAAATTAAATG
Hdrcl-mcis-clone-R	GCCGATTAGAAAAGCTCTCATTCGATTTCACCTCCCCG
hpcE T3050 GF	AATAATTCACCAATTTAAATTTAATTTATAATAG
hpcE T3050 GR	TCTTTTTCTCTTTTATCAAATCATTTCTATTATAAATTAAATTTAAATTGGTGAATTATT
hpcE T73 GR	TCTTTCCCGAGTCCCGCCTCGGGAGGGATTATAAATTAAATTTAAATTGGTGAATTATTT
hpcE-adhE Gibson F	CCTGAAAAATAATTCACCAATTTAAATTTAATTTATAATTTAAGCGGATTTTTTCGCTTTTTTC
hpcE-adhE Gibson R	AAAAAATCCGCTTAAATTATAAATTAAATTTAAATTGGTGAATTATTTTTCAGGTGAAATTTTGGATATAAAACCTTC
hpcE-hbd GR	TTTTACGACTACAGTAAATAAATTATAAATTAAATTTAAATTGGTGAATTATTTTTCAGG
hpcE-hbd GR2	AATAATTCACCAATTTAAATTTAATTTATAATTTATTTACTGTAGTCGTAAAATCCTTTG
hpcE-hbdS GF	ACCTGAAAAATAATTCACCAATTTAAATTTAATTTATAATTTACTTCTCGAACTGCGGAT
hpcE-MMCOECadhE-GibsonR	GTATGTGCTGGATTGAATTACAAAG
hpcE-Strep-tesB GF	CCATCCGCAGTTCGAGAAGTAAATTATAAATTAAATTTAAATTGGTGAATTATTTTTCAG
hpcE-Strep-tesB GR	TTAATTTATAATTTACTTCTCGAACTGCGGATGGCTCCAGTTGTGGTTTCTCATCACTCC
MMCOphaA R	ACCTTCTAAACGAATGAGATTTCATT
MMP0146-pTrc33 Gibson R	CAAGCTTGCATGCCTGCAGGTCGACTCTAGAGGATCGAAGATAAATCCTTTGAAATCAACTCTTGTAAA
MMP0852-R	GGTGAACTATGCTATAGATTATTTACTATATAAAG
MMP1349-F	GCGGCCGCTTCAGAAGCTGAATTATTCCCATTTTATTAAACTAGGGGGATAGCAATGATGAGAACAAACGAACAGTT
MMP1349-mcis-clone-R	CATTTAATTTATTTTTGAAAAAGGGAAAAATCTTAAGGCATTGGTAATGGAAGT

MMP1578-Mcis-clone-F	CGGGGAGGTGAAATCGAATGAGAGCTTTTCTAATCGGC
MMP1578R	ATATATTTTTAATTCACTGGGGGCAATTCCTCGAGTTATTCTTCATCGTAGTCTTTTTCG
nifD-pTrc33-GibsonR	CAAGCTTGCATGCCTGCAGGTCGACTCTAGAGGATCGCATCTTACAAGGCTTAATTTTGC
nifH-Pac-GibsonF	AGTAAATTACTTACCTTAAATTTTTAAGAGGGCAAAAAATGACCGAGTACAAGCCCACGG
nifH-Pac-GibsonR	GTGGCGAGGCGCACCGTGGGCTTGTACTCGGTCATTTTTTGCCCTCTTAAAAATTTAAGG
Pac-MMP0146 Gibson F	AATAACACAATAATTTGAATTTGAATACTCTTATTTTTTAGCTGTTTCTTTTTGTGTATCATAAA
Pac-MMP0146 Gibson R	AAATATTTATGATACACAAAAAGAAACAGCTAAAAAATAAGAGTATTCAAATTCAAATTATTGTG
Pac-nifD-GibsonF	GCGCACCTGGTGCATGACCCGCAAGCCCGGTGCCTGAGCAAATAAACCCCAAAATTACCC
Pac-nifD-GibsonR	AAAAATTTTTAAAGGGTAATTTTGGGGTTTATTTGCTCAGGCACCGGGCTTGCGGGTCAT
pflaB1-phaA GF	TGGGCGTTGCTCTCGCAGTTGAAAGAAAATAAGCGGCCGCCCAACAGAAAGAACATCCCG
pflaB1-phaA GR	CAGATTTTCGGGATGTTCTTTCTGTTGGGCGGCCGCTTATTTTCTTTCAACTGCGAGAGC
pflaB1-phaAS GF	GAAAATGGAGCCATCCGCAGTTCGAGAAGTAAGCGGCCGCCCAACAGAAAGAACATCCCG
pflaB1-phaAS GR	TTCTTTCTGTTGGGCGGCCGCTTACTTCTCGAACTGCGGATGGCTCCATTTTCTTTCAAC
pflaB1-T73 GF	TTTTCGGGATGTTCTTTCTGTTGGGCGGCCGCCCCTCCCGAGGCGGGACT
pflaB1-T73 GR	TTCTTTCTTTCCCGAGTCCCGCCTCGGGAGGGGCGGCCGCCCAACAGAAAGAACATCCCG
pflaB1-T73 GR2	TTAAACAACTTAAAACAGAGCAGGCCTTCGGGCCTGCTTTTTCTTTCTTTCCCGAGTCCC
pflaB1-T73 GR3	GGAGCCATCCGCAGTTCGAGAAGTAAACTCAATAAATTAAACAACTTAAAACAGAGCAGG
phaA phdrC1 GF	CTACTGCAGTTCTTGCAGCAGAAACGATAACAACGTCAGTCATTCGATTTCACCTCCCCG
phaA phdrC1 GR	AAAACAAAGATTAAATTATACCGGGGAGGTGAAATCGAATGACTGACGTTGTTATCGTTT
phaB-cRBS-phaA GF	GGAGCCATCCGCAGTTCGAGAAGTAACAGGTAGCGCTATGACACAAAGAATTGCTTACGT
phaB-cRBS-phaA GR	TCTTTGTGTCATAGCGCTACCTGTTACTTCTCGAACTGCGGATGGCTCCATTTTCTTTCA
phaB-pflaB1 GF	CATACCAAACCAAATACAGCACCATATGACACAAAGAATTGCTTACGTAA
phaB-pflaB1 GR	TACGTAAGCAATTCTTTGTGTCATATGGTGCTGTATTTGGTTTGG
phaB-sRBS-phaA GF	AAGGATATTAACGGAGATTTATTAGGAGAATTATAATGACACAAAGAATTGCTTACGTAA
phaB-sRBS-phaA GR	GTGTCATTATAATTCTCCTAATAAATCTCCGTTAATATCCTTACTTCTCGAACTGCGGAT
PhaB-Strep-PhaA GF	TTGAAAGAAAATGGAGCCATCCGCAGTTCGAGAAGTAAGGTAATAAACGATGACACAAAG
PhaB-Strep-PhaA GR	CGTTTATTACCTTACTTCTCGAACTGCGGATGGCTCCATTTTCTTTCAACTGCGAGAGC
phdrC1 pac GR	TTCCTTTTTTTATATATTTTTAATTCACTGGGGGCAATTCCGATTGCAATTTCTCCTTCG
phdrC1-hbd GF	TTTTACGACTACAGTAAATAACGATTGCAATTTCTCCTTCGT
phdrC1-hbd GR	ACGAAGGAGAAATTGCAATCGTTATTTACTGTAGTCGTAAAATCCTTTGC
phdrC1-hbdS GF	GACTACAGTAAATGGAGCCATCCGCAGTTCGAGAAGTAACGATTGCAATTTCTCCTTCGT
phdrC1-hbdS GR	GTACGAAGGAGAAATTGCAATCGTTACTTCTCGAACTGCGGATGGCTCCATTTACTGTAG
phdrC1-phaB GF	AATGGTGGATTGCACATGGGTTAACGATTGCAATTTCTCCTTCGT

phdrC1-phaB GR	ATGTACGAAGGAGAAATTGCAATCGTTAACCCATGTGCAATCCAC
phdrC1-phaBS GF	TTGCACATGGGTTGGAGCCATCCGCAGTTCGAGAAGTAACGATTGCAATTTCTCCTTCGT
phdrC1-phaBS GR	GTACGAAGGAGAAATTGCAATCGTTACTTCTCGAACTGCGGATGGCTCCAACCCATGTGC
pmcrB hbd GR	CTACAGTAAATGGAGCCATCCGCAGTTCGAGAAGTAAGCATGCTTCATTTATCGGAGAAC
pmcrB phaA GR	AATGGAGCCATCCGCAGTTCGAGAAGTAAGCGGCCGCGCATGCTTCATTTATCGGAGAAC
PmcrB R	CAAAAGATTTAAGTACCTTCTAAACGAATG
Pnif-mut-F	ATGGGACTATTATCGTTATTTTTTTGATAGGG
pTrc33-MMP0143 Gibson F	GCGGATAACAATTTCACACGAGCTCGGTACCCGGGATCCGATGGAACCAGCTTTTCTGAAATATC G
pTrc33-MMP0851 Gibson F	GCGGATAACAATTTCACACGAGCTCGGTACCCGGGATCCCAGGTTCGCCCAATTTACAG
pTrcNADHGIbson	TTCAGCTTCTGAAGCGGCCGCATTATAAATTAAATTTAAATTGGTGAATTATTTTTCAG
R-Promoter - adhE-Pac Gibson	CTTTTTTTATATATTTTTAATTCACTGGGGGCAATTCGCATGCTTCATTTATCGGAGAAC
Strep-adhE Gibson F	CTTCTCGAACTGCGGATGGCTCCAGGCGCTAGCGGATTTTTTCGCTTTTTTC
T3050 hbd GF	ATTCCATCTCAATCTCTGTTTTTTTACTTCTCGAACTGCGGATGGCTCCATTTACTGTAG
T3050 hbd GF2	TGATAAAAGAGAAAAAGAAAAGAATGGAATAAAAAGTTATTCCATCTCAATCTCTGTTTT
T3050 hbd GR	CTACAGTAAATGGAGCCATCCGCAG
T73 tesB GF	TTTACTTCTCGAACTGCGGATGGCTCCAGTTGTGGTTTCTCATCACTC
tesB-cRBS-phaB GF	AGCCATCCGCAGTTCGAGAAGTAACAAGTAGCGCTATGTCACAAGCATTAAAAAACCTCT
tesB-cRBS-phaB GR	TGCTTGTGACATAGCGCTACTTGTTACTTCTCGAACTGCGGATGGCTCCAACCCATGTGC
tesB-phdrC1 GF	ATACCGGGGAGGTGAAATCGAATGTCACAAGCATTAAAAAACCTCT
tesB-phdrC1 GR	TTAAGAGGTTTTTTAATGCTTGTGACATTCGATTTCACCTCCCCG
tesB-pmcrB GR	AAAATGATTTTAATAAATTAAGGAGGAAATTCATATGTCACAAGCATTAAAAAACCTC
tesB-sRBS-phaB GF	AGAAGTAACTCCCCTTAATCATATAGGAAGCACGCATGTCACAAGCATTAAAAAACCTCT
tesB-sRBS-phaB GR	ATGCTTGTGACATGCGTGCTTCCTATATGATTAAGGGGAGTTACTTCTCGAACTGCGGAT
tesB-Strep-hbd GF	CAGTAAATGGAGCCATCCGCAGTTCGAGAAGTAAGTGATTTTATGTCACAAGCATTAAAA
tesB-Strep-hbd GR	AAATCACTTACTTCTCGAACTGCGGATGGCTCCATTTACTGTAGTCGTAAAATCCTTTGC
tesB-Strep-phaB GF	GCACATGGGTTGGAGCCATCCGCAGTTCGAGAAGTAAGTGATTTTATGTCACAAGCATT
tesB-Strep-phaB GR	GTGACATAAAATCACTTACTTCTCGAACTGCGGATGGCTCCAACCCATGTGCAATCCACC
Trc-hbd GF	GTGAGCGGATAACAATTTCACACGAGCTCGGTACCCGGGATCCTTACTTCTCGAACTGCGGATG GCTCCATTTACTGTAG

B

Name	Sequence
hbd	ACTTTGCATCGGAGGAGGAATGGGCGTTGCTCTCGCAGTTGAAAGAAAATAAGGTAATAAA CGATGAAAAAAGTTTGTGTTATCGGAGCTGGTACCATGGGTTCAGGAATAGCTCAAGCATTC GCAGCTAAAGGATTTGAAGTTGTCTTAAGAGATATCAAAGACGAATTCGTAGACAGAGGTTT AGATTTTATCAACAAAAACCTCTCAAAATTAGTTAAAAAAGGTAAAATCGAAGAAGCTACAAA AGTAGAGATTTTAACAAGAATCTCAGGTACAGTAGACTTAAACATGGCAGCTGACTGTGACT TAGTAATCGAAGCAGCTGTAGAAAGAATGGACATCAAAAAGCAAATTTTTGCAGACTTAGAT AACATCTGTAAACCTGAAACAATATTAGCATCCAACACTTCAAGCTTATCAATCACTGAAGTA GCATCTGCAACTAAAAGACCTGATAAAGTTATTGGCATGCACTTCTTTAACCCTGCACCTGTT ATGAAACTCGTAGAAGTTATCAGAGGAATTGCAACAAGCCAGGAAACATTCGATGCTGTTAA AGAAACATCAATTGCAATCGGAAAAGACCCTGTCGAAGTTGCAGAAGCTCCTGGATTCGTA GTAAACAGAATCCTTATTCCAATGATCAATGAAGCTGTTGGAATCTTAGCCGAAGGAATTGC TTCAGTAGAAGACATCGACAAAGCAATGAAATTAGGTGCTAATCACCCTATGGGACCACTCG AATTAGGTGACTTCATCGGTTTAGATATTTGTCTTGCTATAATGGATGTTTTGTACAGCGAAA CCGGAGATTCAAAATACAGACCTCACACCTTATTAAAAAAATACGTTAGAGCTGGATGGTTG GGCAGAAAATCTGGCAAAGGATTTTACGACTACAGTAAATAAGTGATTTTATGTCACAAGCA TTAAAAAACCTCTTAACATTGTTGAATTTAGAAAAAATTGAGGAAGGTCTCTTTAGAGGTCAA TCAGA
MBpmcrB	CATGGGACGTCGACCTGAGGTAATTATAACCCGGGCCCTATATATGGATCCGCATGCTTCA TTTATCGGAGAACACAAAAGATTTAAGTACCTTCTAAACGAATGAGATTTCATTGGGAATAGT GGACACTCGAGTAGGTGACCAGTCCCAAAATGATTTTAATAAATTAAGGAGGAAATTCATAT GGCTGTTACTAATGTCGCTGAACTTAACGCACTCGTAGAGCGTG
MMCOECadhE 1	ACCTTCTAAACGAATGAGATTTCATTGGGAATAGTGGACACTCGAGTAGGTGACCAGTCCCA AAATGATTTTAATAAATTAAGGAGGAAATTCATATGGCAGTAACCAACGTTGCTGAGTTAAAC GCACTTGTTGAAAGAGTTAAAAAAGCACAGAGAGAATACGCTTCTTTTACTCAAGAACAAGT TGATAAAATATTCAGAGCTGCAGCTTTAGCAGCAGCAGACGCAAGAATTCCTTTAGCAAAGA TGGCAGTCGCAGAAAGTGGAATGGGAATTGTTGAAGACAAAGTTATAAAAAACCACTTCGCT AGCGAATATATTTACAATGCCTACAAAGATGAAAAAACATGCGGAGTATTGTCTGAAGACGA CACTTTCGGAACAATTACAATTGCAGAACCTATTGGCATTATCTGCGGTATTGTTCCAACCAC AAATCCTACAAGCACTGCAATTTTCAAATCATTGATTTCATTAAAAACTAGAAACGCAATCAT CTTTAGCCCTCACCCTAGAGCAAAAGACGCTACCAATAAAGCTGCTGACATTGTATTACAGG CTGCTATTGCAGCAGGCGCTCCTAAAGACCTCATTGGATGGATTGACCAACCATCCGTTGA ATTATCAAATGCACTCATGCACCACCCTGACATTAATTTAATCTTAGCAACAGGTGGACCAG GTATGGTTAAAGCAGCTTATTCATCAGGAAAACCAGCTATTGGCGTTGGAGCTGGAAATACT CCTGTTGTTATAGATGAAACAGCAGATATCAAAAGAGCAGTTGCATCAGTTTTAATGAGCAA AACCTTTGACAACGGTGTAATTTGTGCATCCGAACAGTCAGTTGTGGTAGTTGATAGCGTAT ATGACGCAGTTAGAGAAAGATTCGCTACACACGGAGGATACTTACTACAAGGAAAAGAATTG AAAGCAGTACAAGACGTAATTCTAAAAAACGGTGCTTTGAACGCAGCAATAGTTGGACAACC AGCATA
MMCOECadhE 2	ACGGTGCTTTGAACGCAGCAATAGTTGGACAACCAGCATACAAAATAGCAGAATTAGCTGGT TTTTCTGTACCAGAAAACACCAAAATTCTCATTGGCGAAGTGACAGTAGTTGACGAATCAGA ACCATTCGCGCACGAAAAATTATCCCCTACATTAGCTATGTATAGAGCAAAAGACTTTGAAG ATGCAGTTGAAAAAGCTGAAAAATTAGTAGCTATGGGAGGTATCGGTCACACTTCATGTCTT TACACAGATCAAGATAACCAACCAGCAAGAGTTTCATACTTTGGACAAAAAATGAAAACAGC AAGAATTTTAATCAACACTCCAGCGTCACAAGGAGGTATCGGTGATTTATACAACTTCAAATT AGCACCTTCATTAACATTAGGTTGCGGATCATGGGGTGGCAATTCAATCAGTGAAAATGTTG GTCCTAAACACTTAATTAACAAAAAAACTGTTGCAAAAAGAGCTGAAAACATGCTTTGGCACA AATTGCCTAAATCAATCTATTTCAGAAGAGGTTCATTACCTATCGCCCTCGATGAAGTTATCA CAGACGGACACAAAAGAGCATTAATAGTAACAGACAGATTCCTCTTCAATAACGGTTACGCA GACCAAATTACTTCTGTTTTAAAAGCTGCTGGAGTAGAAACCGAAGTTTTTTTTCGAAGTAGAA GCAGACCCTACATTATCCATTGTTAGAAAAGGAGCTGAATTAGCTAACTCATTTAAACCAGA CGTTATCATTGCACTCGGAGGTGGTTCACCAATGGATGCAGCAAAAATCATGTGGGTTATGT ACGAACACCCAGAAACACACTTTGAAGAATTAGCACTTAGATTCATGGATATCAGAAAAAGA ATCTACAAATTTCCTAAAATGGGAGTTAAAGCTAAAATGATCGCAGTAACAACTACTAGCGG CACAGGATCCGAAGTTACTCCTTTTGCAGTTGTAACAGATGATGCAACAGGTCAAAAATACC CTTT
MMCOECadhE 3	CAGTTGTAACAGATGATGCAACAGGTCAAAAATACCCTTTAGCTGATTACGCGCTTACACCT GACATGGCAATTGTTGATGCAAACTTAGTAATGGACATGCCAAAAAGTCTTTGTGCTTTTGG TGGATTAGACGCTGTTACTCATGCTATGGAAGCATACGTATCAGTATTAGCTAGCGAATTTTC AGATGGACAAGCATTACAGGCATTGAAATTATTAAAAGAATACTTACCTGCTAGTTACCACGA AGGATCAAAAAATCCAGTTGCTAGAGAAAGAGTACACTCAGCAGCAACTATCGCTGGTATCG CTTTTGCAAACGCATTTCTCGGAGTGTGTCACTCAATGGCTCACAAATTAGGATCTCAATTTC

ACATTCCACACGGACTCGCTAACGCTCTCTTAATTTGCAACGTTATCAGATACAACGCTAAC
GATAACCCTACAAAACAAACAGCATTTTCTCAGTACGACAGACCCCAGGCAAGAAGAAGATA
CGCTGAAATTGCTGACCATCTTGGTTTATCAGCACCAGGAGACAGAACCGCTGCTAAAATTG
AAAAATTATTAGCATGGCTTGAAACATTAAAAGCAGAGCTTGGAATCCCAAAATCTATCAGAG
AAGCAGGAGTTCAGGAAGCAGATTTCCTTGCTAACGTTGACAAACTCTCAGAAGACGCATTC
GATGATCAGTGCACTGGAGCAAATCCTAGATACCCATTAATCAGTGAATTAAAACAAATTTTA
TTAGATACTTACTATGGAAGAGACTATGTTGAAGGAGAAACAGCAGCAAAAAAAGAAGCAGC
ACCAGCAAAAGCAGAAAAAAAAGCAAAAAAGTCCGCAAGCGCCTGGAGCCATCCGCAGTTC
GAGAAGTAAATTATAAATTAAATTTAAATTGGTGAATTATTTTTCAGGTGAAATTTTGGATATA
AAACCTTCAAAAATAGTATGTGCTGGATTGAATTACAAAGACCATGCAGAAGAACTTAAAATG
A

ACCTTCTAAACGAATGAGATTTCATTGGGAATAGTGGACACTCGAGTAGGTGACCAGTCCCA
AAATGATTTTAATAAATTAAGGAGGAAATTCATATGACTGACGTTGTTATCGTTTCTGCTGCA
AGAACTGCAGTAGGTAAATTTGGAGGTAGTTTAGCAAAGATACCTGCTCCAGAACTCGGTG
CAGTAGTTATTAAAGCAGCTTTAGAAAGAGCTGGAGTAAAACCAGAACAGGTATCAGAAGTA
ATCATGGGACAGGTTCTTACAGCAGGATCAGGCCAAAACCCAGCAAGACAAGCTGCTATCA
AAGCTGGTTTGCCAGCTATGGTACCAGCAATGACTATTAACAAGGTATGTGGCTCAGGACTC
AAAGCAGTAATGTTAGCTGCAAACGCAATTATGGCAGGAGATGCAGAAATTGTTGTTGCAGG
TGGTCAAGAAAACATGAGTGCAGCTCCACACGTTTTACCAGGATCAAGAGATGGATTTAGAA
TGGGAGATGCTAAATTGGTAGACACAATGATTGTGGATGGATTATGGGATGTTTACAACCAG
TACCACATGGGTATTACAGCAGAAAACGTAGCAAAAGAATACGGAATCACAAGAGAAGCTCA
GGATGAATTCGCAGTAGGATCACAAAATAAAGCAGAAGCAGCACAGAAAGCTGGTAAATTT
GATGAAGAAATTGTTCCAGTATTAATTCCTCAGAGAAAAGGTGACCCTGTTGCATTCAAAAC
AGATGAATTTGTAAGACAAGGAGCAACCTTAGATTCCATGAGTGGACTAAAACCAGCTTTCG
ACAAAGCAGGAACCGTTACTGCAGCAAACGCATCAGGACTTAACGATGGCGCTGCTGCAGT
TGTAGTAATGTCAGCTGCAAAAGCTAAAGAATTGGGTCTCACACCATTAGCAACCATCAAAA
GCTACGCAAACGCAGGTGTTGATCCAAAGGTTATGGGAATGGGACCTGTACCTGCTTCAAA
AAGAGCATTATCAAGAGCTGAATGGACGCCTCAAGATCTCGATTTAATGGAAATTAACGAAG
CATTCGCTGCTCAGGCACTTGCAGTACACCAACAAATGGGTTGGGACACAAGCAAAGTTAA
TGTAAACGGTGGGGCAATTGCAATTGGACACCCTATCGGTGCTTCAGGATGTAGAATTTTAG
TTACATTACTTCACGAAATGAAAAGAAGAGACGCTAAAAAAGGTTTAGCTTCACTTTGCATCG
GAGGAGGAATGGGC

TGAAAAGAAGAGACGCTAAAAAAGGTTTAGCTTCACTTTGCATCGGAGGAGGAATGGGCGT
TGCTCTCGCAGTTGAAAGAAAATAAGGTAATAAACGATGACACAAAGAATTGCTTACGTAAC
TGGAGGAATGGGAGGTATCGGTACTGCTATTTGTCAGAGATTAGCTAAAGATGGTTTCAGA
GTAGTTGCTGGATGCGGCCCAAACTCACCTAGGAGAGAAAAATGGTTAGAACAACAAAAAG
CACTTGGCTTTGATTTCATCGCAAGCGAAGGTAACGTTGCTGATTGGGACAGTACAAAAACT
GCATTCGATAAAGTAAAAAGTGAGGTAGGTGAAGTAGACGTTCTTATTAACAACGCTGGAAT
TACAAGAGACGTGGTTTTCAGAAAAATGACAAGAGCTGACTGGGACGCTGTAATCGATACTA
ACCTTACGTCATTATTTAACGTAACAAAACAAGTTATAGACGGCATGGCTGATAGAGGTTGG
GGTAGAATCGTTAATATTTCTAGTGTTAATGGTCAGAAAGGACAATTCGGTCAGACTAATTAC
TCAACTGCAAAAGCTGGGTTACACGGTTTTACTATGGCATTAGCTCAGGAAGTTGCAACAAA
AGGAGTAACCGTAAACACCGTTTCACCAGGTTATATCGCAACTGACATGGTTAAAGCAATTA
GACAAGATGTATTAGACAAAATTGTAGCAACAATTCCAGTTAAAAGATTAGGATTACCTGAAG
AAATCGCATCAATTTGTGCATGGTTATCCTCCGAAGAAAGCGGATTTTCTACTGGAGCAGAC
TTTTCATTAAATGGTGGATTGCACATGGGTTAAGTGATTTTATGTCACAAGCATTAAAAAACC
TCTTAACATTGTTGAATTTAGAAAAAATTGAGGAAGGTCTCTTTAGAGGTCAATCAGAAGATT
TAGGTCTCAGACAGGTTTTCGGTGG

ATGGGACTATTATCGTTATTTTTTTGATAGGGGCGAAAACTTTATATAGTAAATAATCTATAGC
ATAGTTCACCCCTTAGAAGCAAGGGTATAATAACTAAAAGATCGGAAATAAATTTCCGAAAG
ACAACAATATATAGAGGCCTAAAAAATGGTAAGAAAAATCGCAATTTACGGAAAAGGTGGAA
TTGGAAAATCAACCACCACACAAAACA

CCTCTTAACATTGTTGAATTTAGAAAAAATTGAGGAAGGTCTCTTTAGAGGTCAATCAGAAGA
TTTAGGTCTCAGACAGGTTTTCGGTGGACAAGTAGTAGGCCAAGCATTATACGCTGCTAAAG
AAACAGTTCCGGAAGAAAGACTCGTACACAGCTTTCACAGCTACTTTTTAAGACCTGGAGAC
TCCAAAAAACCAATTATCTACGACGTGGAAACATTGAGAGACGGTAACAGCTTTTCAGCAAG
AAGAGTAGCTGCAATACAAAACGGTAAACCTATTTTCTACATGACCGCTTCATTCCAAGCTC
CAGAAGCTGGTTTTGAACACCAAAAAACAATGCCTTCAGCACCAGCACCAGATGGACTTCCA
AGTGAAACTCAAATTGCTCAGAGCTTAGCACACTTATTACCACCTGTATTAAAAGACAAATTT
ATCTGCGACAGACCTTTAGAAGTAAGACCAGTTGAATTCCACAACCCACTTAAAGGTCACGT
TGCTGAACCACACAGACAAGTTTGGATTAGAGCAAACGGAAGCGTACCTGATGACTTAAGA
GTACACCAATACTTATTAGGATACGCTTCAGACTTGAACTTTTTACCTGTTGCTTTACAGCCT
CACGGAATTGGTTTCTTAGAACCTGGAATTCAGATTGCAACAATCGACCACTCAATGTGGTT
CCACAGACCTTTCAATCTTAACGAATGGTTACTTTATTCAGTAGAAAGCACCTCAGCATCATC
AGCTAGAGGTTTCGTTAGAGGTGAATTTTACACTCAAGATGGAGTTCTTGTAGCATCAACTG
TACAAGAAGGAGTGATGAGAAACCACAACTAAATTATAAATTAAATTTAAATTGGTGAATTAT

TTTTCAGGTGAAATTTTGGATATAAAACCTTCAAAAATAGTATGTGCTGGATTGAATTACAAA
GACCATGCAGAAGAACTTAAAATGAAGTTACCAAAAG

C

Name	Sequence
adhE QF1	GATGCATTCGATGACCAGTGC
adhE QR1	CTTCGCTGCAGTTTCACCTTC
atpD QF1	GAAGAGTTAACGCTCTTGAATACGTTG
atpD QR1	CTTTAGCGTCCATTCTCGCTTTAATG
cofEQF	TTAACGACAGTATGGGCAGA
cofEQR	CTGCAATTCCAACCTCTGTT
ehbLQF	CCGCTTAACGATTCCTGAAA
ehbLQR	GAAGTGTCTCCAATTCACCC
flaB1 QF1	GATGCTGTAGCATTGATTGTTGACG
flaB1 QR1	CAAGTGTTGTTGTGTATGATGCAGG
hbd QF1	CTATGGGACCACTCGAATTAGG
hbd QR1	GAATCTCCGGTTTCGCTGTA
MMP0737QF	GAAGGAACGGTTTTTGATGC
MMP0737QR	TGCATTTGGATCTGCAATGA
MMP1349QF	TCCCACTTTTTCAGGAGGAA
MMP1349QR	CAAACTGACGAAGACGAACT
MMP1578QF	ACTGGAAATTCGCTCGTTAG
MMP1578QR	GAGATGTTCCCAAGCACTAC
nadAQF	GCAGATTGCGTCAGTTCTTA
nadAQR	TTATCGGAACAGAATGCGAC
nadCQF	CCGATATCAACAGAAGTGGC
nadCQR	AGCGGCGGAATAAATGAAAA
pac QF1	TCTCACCCGACCACCAG
pac QR1	GCGGAGGTCTCCAGGAA
phaA QF1	CACTTGCAGTACACCAACAAAT
phaA QR1	CTACATCCTGAAGCACCGATAG
phaB QF1	GAAAGGACAATTCGGTCAGACTA
phaB QR1	CGGTGTTTACGGTTACTCCTT
porEQF	GCTTGTTCGTCTCTTCCAAA
porEQR	CATTGGATGTGGACTCTGTG
tesB QF1	CATCAGCTAGAGGTTTCGTTAGAG
tesB QR1	TGTGGTTTCTCATCACTCCTTC